SUBMICRON AEROSOL FORMATION DURING COMBUSTION OF PULVERIZED COAL

Thesis by

Constance Lynn Senior

In Partial Fulfillment of the Requirements

for the Degree of

Doctor of Philosophy

California Institute of Technology

Pasadena, California

1984

(Submitted July 26, 1983)

"A man goes to knowledge as he goes to war, wide-awake, with fear, with respect, and with absolute assurance. Going to knowledge or going to war in any other manner is a mistake, and whoever makes it will live to regret his steps."

-Carlos Castaneda,
The Teachings of Don Juan

ACKNOWLEDGEMENTS

The first thank-you must go to fellow graduate student Jeff Gelles, who first asked the question, Why not look at a model system? (My immediate reply was, "No. Can't be done.") Jeff also provided much needed moral support throughout this work.

Financial support for this work was provided primarily by the National Science Foundation. I would also like to thank the Pasadena Lung Association and the Jesse Smith Noyes Foundation for providing partial support for me.

The experimental part of this work quickly grew beyond the scope of just one person and I would like to thank those who aided me. The combustion furnace and related paraphernalia were built in-house by Joe Fontana and Rich Eastvedt. Elton Daly supervised this effort and provided much valuable advice on all aspects of the design. Scanning electron microscopy work was done by Patrick Koen in the laboratory of Professor J. P. Revel. Some of the analytical work was performed for me by other students. Kathy Sheedy developed quick and easy techniques for particle density analysis in our laboratory. Thermogravimetric analysis of char samples was performed by Theresa Weston in the laboratory of Professor G. R. Gavalas. A. V. Anilkumar fixed many of the bugs in the coal feeding system and conducted the calibration experiments.

The theoretical part of this work was conducted with the guidance

and assistance of Professor R.C. Flagan. Discussions with Professor Gavalas on devolatilization and char combustion also provided much insight into the problem. Numerical simulation was performed on the PDP-11/60 in Keck laboratory. Some of the initial program development and debugging was done on a computer in the laboratory of Professor M.R. Hoffmann and I am grateful for the use of this machine. Moral and spiritual guidance for the theoretical part of this work was provided by The Elements of Programming Style by B. W. Kernighan and P. J. Plauger, a most invaluable reference.

The last thank-you goes to those persons who, by their advice and example, taught me how to do impossible things: my advisor, Richard C. Flagan and Cathy van Ingen.

ABSTRACT

A detailed investigation is conducted into the fundamental processes responsible for the formation of submicron aerosol during combustion of pulverized coal. To this end, both theoretical and experimental tools are developed.

The first part of the work consists of a numerical simulation of the vaporization of ash and formation of aerosol. The work combines a model of a single, burning coal particle with one of the formation of aerosol by nucleation and the growth of aerosol by coagulation. A quasi-steady approach is used to model combustion and aerosol formation and this is shown to be valid a posteriori. Calculations are performed for vaporization of refractory oxides during combustion. The effect of thermophoresis on the transport of aerosol around a burning coal particle is found to be small. For refractory species like silica, nucleation typically occurs within 4-5 particle radii from the surface of the coal particle. Thus, in this case, nucleation is controlled by the combustion process. The vaporization rate is found to be weakly dependent on the presence of aerosol in the gas.

The second part of this work is the development of an experimental system in which to study the aerosol formation processes. A new material is produced that is similar to coal in many respects, but is chemically simpler and more well-characterized. This makes it possible for the first time to study the fundamental aerosol formation processes

without interference from the complex chemistry of coal ash. Experiments in a laminar drop-tube furnace confirm that this material burns in a manner similar to coal and that combustion produces an aerosol from vaporization of ash.

CONTENTS (cont'd)

CONTENTS (cont'd)

CONTENTS (cont'd)

LIST OF FIGURES

FIGURES (cont'd)

FIGURES (cont'd)

FIGURES (cont'd)

LIST OF TABLES

CHAPTER 1

INTRODUCTION

1.1 Problem statement

Coal combustion is a major source of particulate emissions to the atmosphere. Gas cleaning equipment removes most of the mass of aerosol produced by combustion. But because gas cleaning devices have a minimum collection efficiency for particles in the size range 0.1 to 1.0 microns (McCain et al., 1980), large numbers of submicron particles are released to the atmosphere.

Considerable attention has been focused on the submicron mode of the ash aerosol primarily because of its environmental impact.

> Fine particulates are especially injurious because they more easily bypass the lung's defenses, are the principal carriers of trace metals in coal ash, including toxic compounds containing lead, cadmium, and arsenic, and act as a magnet for other air pollutants, providing them with a passageway to the lungs (Komanoff, 1980).

Considerable incentive exists, therefore, to understand the processes that form the submicron aerosol. Formation has been explained

qualitatively by vaporization of some of the ash during combustion followed by homogeneous nucleation and condensation (Flagan and Friedlander, 1978). Few measurements of the size distribution of the submicron aerosol (Markowski et al., 1980) or the chemical composition (Taylor, 1981) exist. The details of the formation process remain unknown. Greater knowledge of the fundamental physical and chemical processes is needed to design better control strategies for particlulate pollutants, particularly because of the increased reliance on coal as an energy source. The use of coal in new ways like liquefaction or solvent extraction requires some insight into pollutant formation in these new systems. This, of course, depends on an understanding of the fundamental aspects of aerosol formation.

1.2 Objective of the present work

This work proposes to examine the fundamental structure of the submicron aerosol formation processes during combustion of pulverized coal. Only after we understand the micro-scale chemistry and physics, can we successfully model aerosol formation in large-scale combustion systems. Therefore, the objective of this project is to develop theoretical and experimental tools with which to study aerosol formation from single burning coal particles. A novel and unique aspect of this work is the introduction of a model system in which significant features of the real system can be isolated for study. The first step in understanding aerosol formation in a chemically complex system like coal is often to understand the same process in a chemically less complicated

system.

The presentation of the work can be outlined briefly. Chapter 2 provides background information on the nature of coal and the combustion process. Previous work on the composition and formation of ash aerosol is discussed.

Chapter 3 presents a theoretical model for the combustion of a single coal particle. This model is an integral part of the theoretical portion of this work. Chapters 4 and 5 give birth to a model of the aerosol formation around a single burning coal particle. The interaction between the model and coal combustion experiments is explored in Chapter 6.

Chapter 7 introduces the idea of a model system for use in the experimental study of aerosol formation. The development of a material that models coal ("artificial coal") but which is chemically simpler than coal is outlined. The laboratory combustion furnace used for combustion experiments is detailed in Chapter 8. The model system is evaluated experimentally in Chapter 9 in which the results of combustion experiments are discussed. The major conclusions and suggestions for further study are outlined in Chapter 10.

CHAPTER 2

BACKGROUND

2.1 Combustion of pulverized coal

2.1.1 Composition of coal

Coal is a heterogeneous substance composed of organic and inorganic material that arises from the decay of plant debris. The original plant matter, through chemical and biological action, becomes peat. On the time-scale of millions of years, heat and pressure transform peat into coal.

The chemical composition and the physical structure varies greatly among coals. Coals are classified by rank, a measure of the degree of metamorphosis of peat from the most highly metamorphosized, anthracite, to the least, lignite. The carbon content and heating value are used to distinguish different ranks of coal.

Coal is composed of aromatic building blocks containing many different functional groups. The basic units of coal are planar and

many crosslinks exist between them, giving some coals a very open, porous structure. Hirsch (1954) performed an x-ray scattering study of coals and proposed three basic structures which describe most coals. Low rank coals containing up to 85% fixed carbon are characterized by an open structure. Individual layers are randomly oriented and there are many crosslinks. These coals are quite porous. A liquid structure is typical of coals containing 85-91% carbon, such as bituminous coals. Fewer crosslinks exist in this structure and the layers show more orientation. These coals contain little open pore structure. Finally, high rank coals with greater than 91% carbon have few crosslinks and a high degree of orientation among layers.

Measurements of the pore structure of coal confirm the preceding descriptions of coal structure. Gan et al. (1972) measured the pore size distributions of twelve coals of different rank. The low-rank coals containing less than 75% carbon contained mostly macropores (pore diameters greater than 30 nm), no transitional pores (30-1.2 nm), and some micropores (pore diameters less than 1.2 nm). High-rank coals containing greater than 85% carbon contain primarily micropores. Those coals with 75-85% carbon contained a range of pore sizes.

The inorganic material in coal can be introduced with the original plant remains (either as inorganic compounds in plant tissue or minerals in silt) or mixed in during the mining process. Inherent mineral matter, that derived from the original plant tissue, does not generally exceed 2% of the mineral matter in coal (Reid, 1971). The rest of the

inorganic material is labeled extraneous mineral matter. Microscopic analysis of coal reveals that the extraneous mineral matter is distributed as fine inclusions in the coal matrix (on the order of one micron or less) or as distinct particles (on the order of 10 microns). Sarofim, et al. (1977) measured mean diameters of 1.7 and 2.0 for the inclusions in a lignite and a bituminous coal, respectivley. Hamblen et al. (1980) measured the mean pyrite inclusion size for two coals and found it to be 1.5-2 μm.

The composition of the mineral matter is primarily that of silicate rocks. The major inorganic elements in coal are Si, Al, Fe, Ca, Mg, S. Almost all of the silicon, aluminum and iron are associated with extraneous mineral matter as aluminosilicates, calcites, and pyrites. Calcium, magnesium, and sulfur are associated with both the mineral inclusions and the organic matrix. In the study of Sarofim et al. (1977) individual inclusions were subjected to electron microprobe analysis. The mineral composition was found to vary greatly from inclusion to inclusion.

2.1.2 Macro-scale combustion

Pulverized coal-fired boilers burn coal that has been ground to a fine powder, typically 60 to 90% by weight less than 200 mesh (74 microns). The mass mean diameter is in the range 30 to 70 microns. The coal is entrained in a primary air stream (15 to 20% of the total combustion air) and injected into the furnace through many burners.

Preheated air (secondary air) is introduced coaxially with the primary air. Heat transfer from hot combustion gases in the furnace causes the incoming coal to ignite and burn. Heating rates on the order of 10^5 K/sec are common in large furnaces (Field et al., 1967). Peak flame temperatures are in the range 2500 to 1800 K. However, some particles may be exposed to substantially lower gas temperatures because mixing is slow within the furnace. Coal particles actually experience a broad spectrum of temperature and gas composition. Combustion of the coal occurs in the 1 to 2 second residence time in the furnace section.

Steam is generated by heat transfer to the furnace walls which are lined with many water-containing tubes. At the exit of the furnace section, the product gases are somewhat cooler (1300 to 1700 K). More heat transfer occurs in the convective section, where steam is superheated, and the following economizer section, where condensed water is preheated. At the inlet to the emission control equipment, the gas temperature is 300 to 700 K. Typically, wet scrubbing is used to remove SO_2 and electrostatic precipitation, to remove particulate matter.

2.1.3 Micro-scale combustion

As stated earlier, individual particles injected into the furnace are heated by hot combustion gases. Rapid decomposition occurs first, releasing hydrocarbons and tars into the gas phase where they burn. The devolatilization step is fast with respect to the residence time in the furnace: on the order of 10 to 100 milliseconds. The residual carbon

(char) burns more slowly, on the order of 0.1 to 1 seconds.

Although it is not possible to observe the combustion behavior of individual coal particles in large furnaces, studies done in laboratory furnaces can provide much of the needed information. Particle temperatures and burnout times have been measured in small, well-controlled combustion experiments. Most of the measurements have been of burnout time, from which the kinetics of the combustion reaction can be deduced (Field, 1969; Smith, 1971a, 1971b; Sergeant and Smith, 1973). A few measurements of particle temperature during combustion have also been made (Ayling and Smith, 1972; Mims et al., 1980; Mitchell and McClean, 1982).

2.2 Fate of mineral matter during coal combustion

2.2.1 Overview

Mineral matter in coal is, of course, the precursor of fly ash. The flyash or ash aerosol has a very characteristic bimodal size distribution. Most of the mass of the aerosol resides in a large particle mode often called the residual ash. The mass mean diameter of this aerosol is on the order of 10 μm and it is removed from the stack gases with better than 99% efficiency. A small percentage of the mass of ash ends up in the submicron aerosol mode, typically about 1% (Markowski et al.,1980). The mean size of this mode is on the order of 0.1 μm. Although the submicron aerosol does not represent much of the

total mass, it contains very large numbers of small particles, particles that are released to the atmosphere because of the lower collection efficiency of gas-cleaning devices for this size range.

Study of the fly ash from coal combustion has been primarily motivated by a desire to understand the nature of emissions from coal-fired power plants. Table 2.1 hightlights the areas of interest in the study of residual ash over the last two decades. The observation that submicron particles are enriched with certain toxic trace elements like arsenic and lead (see, for example, Davison et al., 1974) has promoted an interest in the submicron aerosol mode. However, most of the measurements of the submicron aerosol have been of the size distribution and not of the composition distribution. Table 2.2 traces the history of the observation of the submicron aerosol.

Based on the previous work in this area, there are some generally accepted mechanisms for the formation of ash aerosol (Flagan and Friedlander, 1978; Damle et al., 1982). Figure 2.1 depicts the processes of importance to aerosol formation. During combustion, particle temperatures are high enough to melt the inclusions. Coal ash begins to melt at 1200-1400°C (O'Gorman and Walker, 1973; Huffman et al., 1981); the melting behavior of ash varies greatly depending on the composition of the ash and of the surrounding gas. As combustion proceeds, the carbon is burned away and the molten inclusions come into contact. Due to the large contact angle between liquid ash and carbon (Raask, 1966), large drops of molten ash are probably found on the

TABLE 2.1: Studies of Residual Ash Particles

1965 1971 1974	Littlejohn O'Gorman & Walker Ruch et al.	Distribution of minerals in coal
1965 1968 1976 1977	Watt & Thorne Raask Fisher et al. Sarofim et al.	Ash bubbles & cenospheres
1969 1977	Ramsden Sarofim et al.	Melting and coalescence of mineral inclusions
1974 1975 1975 1975 1975	Davison et al Kaakinen et al. Lee at al. Klein et al. Ragaini & Ondov & numerous others	Observation of the enrichment of small particles with volatile species
1976 1980 1982	Linton et al. Biermann & Ondov Hock & Lichtman	Surface predominance of volatile species
1977	Sarofim et al.	Ash loss due to vaporization
1976	Flagan & Friedlander	Review of mechanisms relationship between sizes of coal and ash particles
1981	Haynes et al.	Chemical control of surface enrichment

TABLE 2.2: Studies of Submicron Ash - Observations

1952	Murphy et al.	Silica fume in stoker-fired boilers
1965	Raask & Wilkins	Silica volatilization
1975	McCain et al.	Particle size distribution measurements
1975	Schulz et al.	
1976	Schmidt et al.	
1979	Ensor et al.	
1980	Markowski et al.	
1981	Flagan & Taylor	
1981	Taylor & Flagan	Submicron ash aerosol composition distribution measurements
1979	Ensor et al.	Correlation between concentration of fine particles and NO
1980	Ensor	

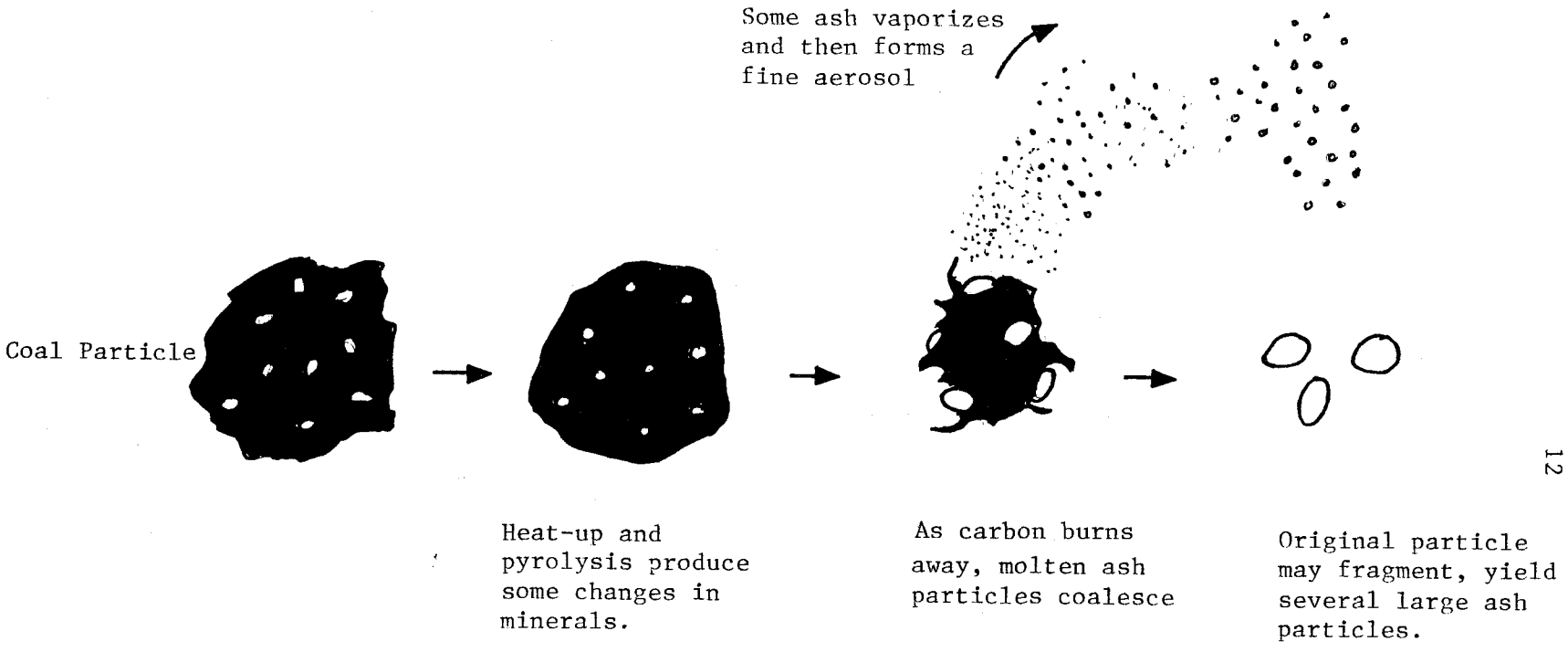

Figure 2.1 Mineral matter transformations during coal combustion.

carbon matrix. Finally, several residual ash particles are produced for every coal particle burned (because of fragmentation of the char particle in the final stages of combustion). Sarofim et al. (1977) observed that 3-5 ash particles were produced for every coal particle burned in a laboratory study of residual ash formation.

During combustion, temperatures are also high enough to vaporize some of the components in ash. The earliest and most dramatic demonstration of this was circa 1901, when it was observed that arsenic from coal could be introduced into hops dried over a malting kiln. (Wood Smith and Jenks, 1901). Several deaths occurred from drinking beer made in this way. Other chemical species in ash may also vaporize under combustion conditions. Raask and Wilkins (1965), for example, demonstrated the feasibility of silica volatilization based on thermodynamic considerations. The ash vapors condense, either heterogeneously on existing aerosol or homogeneously to form a fine fume. The latter can grow either by condensation or by coagulation. What results from these processes is the bimodal size distribution observed from combustion of coal. Most of the mass of the aerosol is contained in the residual ash but there are large numbers of submicron particles.

2.2.2 Formation of the submicron aerosol

Vaporization of ash followed by condensation is the mechanism by which the submicron aerosol is formed. Although this has been generally

agreed upon for some time (see, for example, Davison et al., 1974), confirmation of this and an understanding of the fundamentals of the process have been difficult to achieve. Table 2.3 outlines work in this area. Preliminary modeling efforts by Flagan and Friedlander (1978) and Desrosiers et al. (1978) were hampered by the lack of unambiguous data. The only data available at that time were taken from large-scale combustion systems. The complexity of both the starting material (coal) and the combustion process makes field data difficult to interpret.

In order to obtain better data on ash vaporization and submicron aerosol formation, several laboratory-scale combustion studies were initiated. Experiments performed by Taylor (1981) in a small-scale turbulent combustor provided the first size and composition distributions for the submicron aerosol. The work of Sarofim and co-workers (Mims et al., 1980; Neville et al., 1981; Quann and Sarofim, 1982) on combustion of coal in a small, laminar furnace have provided much data on the rate of vaporization of ash during combustion.

The first attempt to model the formation of the submicron aerosol (Flagan and Friedlander, 1978) was based on growth of an aerosol in the combustion gases in a boiler using the theory of self-preserving aerosol size distributions. This theory assumes that a certain fraction of the ash vaporizes and nucleates homogeneously during the combustion process; the aerosol then grows by coagulation. This approach has been somewhat successful in predicting size distributions from large-scale combustion systems, but it provides no insight into the physics and chemistry of

TABLE 2.3: Studies of Submicron Ash Particles - Mechanisms

1978 1978 1979 1980 1981	Flagan & Friedlander Desrosiers et al. Flagan Im and Chung McNallan et al.	Postulate fine particle formation by vapor nucleation and develop models to predict particle size
1981	Flagan & Taylor	Comparisons of size distribution prediction with laboratory data
1979	Smith et al.	Postulate fine particle formation by ash bubble or cenosphere bursting
1980 1981 1982	Mims et al. Neville et al. Quann & Sarofim	Studies of ash volatilization mechanisms and measurement of rates
1981	Taylor	Influence of combustor operating conditions on fine particles

nucleation and growth. Desrosiers et al. (1978) formulated a model to describe the transport of ash vapor away from a burning coal particle. The vapor was then assumed to nucleate somewhere in the combustion gases. A similar approach was adopted by Im and Chung (1980) to model the carryover of slag vapor in an MHD combustion system. This model consisted of a detailed look at nucleation in a one-dimensional plug flow reactor. McNallan et al. (1981) studied nucleation in conventional combustion systems. They also assumed that vapor condensed from the bulk combustion gases.

Theoretical work to date on ash vaporization and aerosol formation during combustion has focused on the bulk combustion environment and neglected the influence of local combustion conditions (i.e., conditions near a single burning coal particle). One notable exception to this is the recent work of Quann and Sarofim (1982) which is concerned with the effect of a porous, burning solid on the vaporization from individual mineral inclusions. From this work and from an understanding of the local combustion process, one sees that the local combustion environment is very different from that of the bulk gas. In the present work, the first attempt to model the local ash vaporization and aerosol formation is presented. It is hoped that this approach will yield needed insight into the processes that form the submicron aerosol.

CHAPTER 3

COAL COMBUSTION MODEL

3.1 Introduction

The present investigation is motivated by a desire to understand the fate of the mineral matter in coal during combustion of a single coal particle. This requires a good understanding of the particle's local gaseous environment and temperature field. Previous models have generally treated in detail either the gas-phase (Caram and Amundson, 1977; Libby and Blake, 1979) or the solid-phase (Gavalas, 1980), but not both. This study aims to combine the two approaches by modeling the local environment of a single coal particle through the entire combustion process.

Detailed information about the local gaseous environment during combustion can be obtained using a quasi-steady combustion model. This means that the behavior of the gas phase is modeled as a succession of steady states on the assumption that the response time of the gas is very much shorter than that of the solid. Ubhayakar and Williams (1976) used a quasi-steady model to predict extinction times of a burning

sphere in a cold environment. Radial convection and radiation were included in the particle energy balance. Gas-phase chemistry was assumed to be frozen. An iterative solution of the quasi-steady equations was used to find extinction times. Caram and Amundson (1977) have presented a careful treatment of the gas-phase chemistry during the combustion of a solid carbon sphere surrounded by a stagnant boundary layer. The quasi-steady model included the heterogeneous reactions of carbon with O_2 and CO_2 and the homogeneous oxidation of CO to CO_2. The effect of radiative heat transfer on the particle energy balance was included (Mon and Amundson, 1978). The state of the particle was explored as a function of various ambient conditions. Libby and Blake (1979) developed a quasi-steady model for the combustion of solid carbon in an infinite medium. The model included the reaction of carbon with O_2 and CO_2. Two limiting cases of gas-phase chemistry (frozen and equilibrium) were considered. Radiation and radial convection were included in the particle energy balance. Equations for the dynamic response of the particle were coupled with the gas-phase transport equations to give the particle temperature and radius as a function of time.

The preceding models used the quasi-steady approach to get detailed information about the gas-phase while neglecting aspects of the solid behavior that are relevant to coal combustion. Models that include more detail about the coal particle behavior during combustion have not generally treated the local gaseous environment in as much detail as those discussed above. Baum and Street (1971) presented a model for

coal combustion which includes the effects of devolatilization and swelling on the coal particle. However, the gas composition was assumed to be spatially homogeneous. The model of Stickler et al. (1979) contained a very thorough treatment of pyrolysis and char oxidation, but also assumed the gas to be locally homogeneous. Mass and energy transport in the gas were modeled as bulk processes. Radiative heat transfer was not included in the particle energy balance. These models are more applicable to the combustion of a large cloud of particles rather than a single particle.

Models of the solid-phase behavior during combustion for single particles have been developed (e.g., Gavalas, 1981; Simons, 1979). These analyses contain a detailed treatment of the pore structure of coal and its evolution throughout combustion. However, heat and mass transfer in the gas phase are either neglected or treated in a simplified fashion.

In this chapter, a model is developed for the combustion of a single coal particle. The particle is assumed to be immersed in an infinite quiescent medium. A quasi-steady treatment of the gas surrounding the particle is coupled with a dynamic particle energy balance as in the model of Libby and Blake. The gas-phase chemistry is assumed to be frozen. The model of Libby and Blake considered a solid carbon sphere burning via a surface reaction. We extend this to include the porous char combustion model of Gavalas (1981). Finite rate coal devolatilization is incorporated using the pyrolysis model of Stickler,

et al. (1979). The effect of mineral matter on the particle energy balance is also considered.

3.2 Gas-phase Transport and Chemistry

In this section the steady gas conservation equations will be derived and the details of the heterogeneous combustion reactions will be discussed. The crucial assumption in this analysis is that the thermal response time of the gas is very much shorter than that of the particle. In this case a quasi-steady combustion model can be used. That is, the gas field during combustion can be represented by a succession of steady states while the behavior of the particle is unsteady.

Several assumptions are made to allow a relatively simple analytic solution to the quasi-steady problem. The only gaseous species considered are O_2, N_2, CO_2, and CO; since these have similar molecular weights, a single gas diffusivity is used. The quantity ρD is assumed to be constant at any instant and equal to ρD for air at a mean temperature $(T_p T_\infty)^{1/2}$ where T_p and T_∞ are the particle and free stream temperatures, respectively. In effect, we assume that the radial temperature gradients are not very steep. The idealized coal particle is a sphere that is composed of carbon and discrete mineral inclusions. (The nature of the mineral matter will be discussed in more detail in a subsequent section.) The sphere is assumed to be at rest in an infinite medium and the flow field is assumed to be spherically

symmetric. There is a radial gas flow caused by the mass flux due to combustion

Radial coordinates are used in this analysis with the center of the particle located at r = 0. The instantaneous particle radius is r_p. The radial gas velocity due to combustion, V, is found from the steady-state mass balance:

$$\frac{d}{dr} (\rho r^2 V) = 0 \tag{3.1}$$

The solution is

$$\rho r^2 V = (\rho V)_p r_p^2 = m_p r_p^2 \tag{3.2}$$

where m_p is the mass flux from the surface and ρ is the mass density of the gas. The subscipt p denotes conditions at the particle's surface.

In deriving the conservation equations for gaseous species we follow the conventions of Libby and Blake (1979). The four species are O_2, CO_2, CO, and N_2 and the species mass fractions are denoted g_1 through g_4, respectively. The conservation equations are written in terms of the element mass fractions instead of species mass fractions. The elements considered are oxygen, carbon, and nitrogen and their mass fractions are

$$O_2: \quad \tilde{g}_1 = g_1 + \alpha_{12}g_2 + \alpha_{13}g_3$$

$$C: \quad \tilde{g}_2 = \alpha_{22}g_2 + \alpha_{23}g_3 \tag{3.3}$$

$$N_2: \quad \tilde{g}_3 = g_4 = 1 - g_1 - g_2 - g_3$$

where α_{ij} is the ratio of grams of element i to grams of species j. Some combinations of the α_{ij} that re-occur throughout the analysis are grouped together as

$$\bar{\alpha} = \alpha_{22}(\alpha_{12}/\alpha_{22} - \alpha_{13}/\alpha_{23}) \tag{3.4}$$

$$\tilde{\alpha} = \frac{\alpha_{13}}{\alpha_{23}}$$

The element conservation equation is

$$m_p r_p^2 \frac{d}{dr}(\tilde{g}_i) = \rho D \frac{d}{dr} r^2 \frac{d}{dr}(\tilde{g}_i), \quad i = 1,2 \tag{3.5}$$

To non-dimensionalize the equation a dimensionless radial coordinate $z = (r/r_p)$ and a dimensionless mass loss $K = (m_p r_p/\rho D)$ are used. Without yet specifying the boundary conditions, the solution to Equation 3.5 is

$$\tilde{g}_i = \frac{(\tilde{g}_{i\infty} - \tilde{g}_{ip})e^{-K/z} + (\tilde{g}_{ip} - \tilde{g}_{i\infty}e^{-K})}{1 - e^{-K}}, \quad i = 1,2 \tag{3.6}$$

The boundary conditions at infinity are fixed by the particular problem. The surface boundary conditions can be written as

$$\frac{d}{dz}(\tilde{g}_1) = K\tilde{g}_1$$

$$\frac{d}{dz}(\tilde{g}_2) = -K(1-\tilde{g}_2) \qquad (3.7)$$

There is no net flux of the element oxygen at the surface while the flux of element carbon at the surface equals the mass flux m_p. Applying Equation 3.6 to Equation 3.7 gives expressions for the instantaneous element mass fractions in the gas.

The relationship between elemental and species mass fractions depends on the rate of combustion and the gas-phase chemistry. In particlular, the distribution of the element oxygen among the species O_2, CO_2, and CO depends on the rate of oxidation of CO to CO_2. In their analysis, Libby and Blake (1979) considered two limiting cases in the gas-phase: frozen chemistry and equilibrium distribution of the species. If the behavior of the real system can be approximated by either of these cases, the analysis is greatly simplified. Libby and Blake developed an equation that represents the ratio of the chemical source term to the convection term in the conservation equation for O_2. This ratio can used to determine if either of the limiting cases applies. We restrict our analysis to particles in the pulverized size range (r_p < 50 micron) burning at one atmosphere total pressure. For these conditions the frozen chemistry limit is approached at the particle's surface and far away from the particle the equlibrium limit is approached. In the present work frozen chemistry is assumed in order to simplify the analysis. A more thorough treatment might include finite oxidation kinetics (e.g., Caram and Amundson, 1977), but it is

our intent to develop a simple and tractable model.

In order to determine the gas-phase composition, three mass fractions must be known. Element carbon and element oxygen are known from the solution to Equation 3.6. Since chemistry is frozen, the O_2 mass fraction can be found by substituting g_1 for $\tilde{g}_1$ in Equation 3.6. A boundary condition for O_2 at the surface is formulated from conservation of oxygen:

$$\frac{M_1 R_1}{M_c} = -2\left[m_p g_1 - \left(\rho D / r_p\right) \frac{dg_1}{dz}\right]_{z=1} \tag{3.8}$$

Equation 3.6 can be solved for the surface O_2 concentration as follows

$$g_{1p} = \frac{g_{1\infty} K e^{-K}}{K + A\tilde{\alpha}\left(1 - e^{-K}\right)} \tag{3.9}$$

The mass fractions of CO_2 and CO can be computed by solving Equation 3.3 given $\tilde{g}_1$, $\tilde{g}_2$, and g_1. The analysis cannot proceed further without an expression for the mass loss; this is taken up in the next section.

3.3 Solid-phase reactivity

3.3.1 Overview

The kinetics of pulverized coal combustion have been studied by many. For porous particles there are three regimes of combustion rate

control. Using the notation of Mulcahy and Smith (1969) these regimes are: Zone I in which the rate control is by chemical reaction, Zone II in which the rate control is by pore diffusion and chemical reaction, and Zone III in which the rate control is by diffusion to the outer surface of the particle. Based on experimental data, it is generally agreed (see, for example, Mulcahy and Smith, 1969) that, for typical combustion conditions, pulverized coal burns with some penetration of oxygen in the pores and that the rate is controlled by both pore diffusion and chemical rate (Zone II).

The activation energy of the first-order reaction between carbon and oxygen is approximately 40 kcal/mole (Smith, 1978). The theory of reaction between gases and porous solids predicts that for Zone II reaction control the observed activation energy should be half of the true activation energy. Smith (1971a) and Sergeant and Smith (1973) observed the combustion of pulverized coal particles and concluded that for high particle temperatures (particle temperatures above 1000 K) combustion proceeded with nearly constant density but decreasing radius. Activation energies for the rate based on external surface area were in the range 15-20 kcal/mole. These data are consistent with the penetration of a thin layer of the solid by oxidant since the observed activation energy is half the true activation energy but combustion occurs at constant density.

In this work, we present two different treatments of solid reactivity: a surface model and a pore model. The former uses

experimentally observed reaction rates based on the external surface area of the particle. The latter is a more fundamental treatment of reaction in a porous solid, but requires data which may not be readily available.

The surface model lumps all the details of the char combustion into a single, experimentally determined parameter. Since rate coefficients determined from actual coal combustion are used, the reactivity reflects the fact that some internal burning occurs during combustion. Aside from the fact that the surface model is not physically correct, it is less flexible than the pore model. Apparent surface reactivities have been measured for only a handful of coals. The surface reactivity is only applicable to the particular coal for which it was measured. Also, the observed rate may depend subtly on the combustion conditions under which it was measured. In contrast, the pore model requires data on char physical properties such as porosity and surface area that are not often measured in conjunction with combustion experiments.

The two treatments of solid reactivity complement each other. The surface model is a gross approximation to the actual physical process, but can be used for a limited number of systems where data exist.

3.3.2 Surface model

The particle combustion is modeled as a heterogeneous, first-order reaction between solid carbon and either O_2 or CO_2. For combustion

in air there is no CO_2 anywhere since chemistry is assumed to be frozen. There are cases when there exists a substantial amount of CO_2 in the free stream and therefore the reaction with CO_2 has been included for completeness. The two reactions are first order and given by

$$R_i = \frac{k_i p M_c}{M_i} m_{ip} \exp(-T_i/T_p) \tag{3.10}$$

The units of R_i are g/sec-cm^2. T_1, T_2, k_1, k_2 are the kinetic parameters for combustion. For the reaction of with oxygen the kinetic parameters of Smith (1971b) for semi-anthracite are used. The parameters for the reaction with carbon dioxide are taken from the work of Dobner (1976). These are

k_1=20.4 g/sec-cm^2-atm

T_1=9562 K

k_2=247 g/sec-cm^2-atm

T_2=21,060 K

The dimensionless mass loss due to combustion is written as the sum

$$K = Ag_{1p} + Bg_{2p} \tag{3.11}$$

where A and B, the dimensionless rate coefficients, are functions of pressure, particle radius, and particle temperature defined by

$$A = \frac{K_1 pr_p}{\rho D} e^{-T_1/T_p}$$

$$B = \frac{K_2 pr_p}{\rho D} e^{-T_2/T_p} \qquad (3.12)$$

To simplify the above equation it is assumed that $M_c/M_i \cong 1$. Considering the uncertainty in the determination of the kinetic parameters, this assumption does not significantly affect the results.

The distribution of chemical species in the gas-phase is finally expressed as a function of the parameter K alone. Once the dimensionless mass loss has been determined, the composition of the gas surrounding the coal particle is known. Substituting expressions for surface mass fractions into Equation 3.11 gives the following transcendental equation for K.

$$K = (A - B/\bar{\alpha}) \left[\frac{\tilde{g}_{1\infty} K e^{-K}}{K + A\tilde{\alpha}\left(1 - e^{-K}\right)} \right] + (B/\bar{\alpha}) \left[\tilde{g}_{1\infty} e^{-K} - \tilde{\alpha}\left(1 - (1 - \tilde{g}_{2\infty}) e^{-K}\right) \right] \qquad (3.13)$$

The equation can be solved iteratively for K using a Newton's method algorithm. For the special case when $K \ll 1$ a two term expansion may be substituted for the exponentials in Equation 3.13. The resulting equation is cumbersome but yields an explicit expression for K.

$$K = \frac{[A-B/\tilde{\alpha}]g_{1\infty}(1-A\tilde{\alpha})^{-1} + (B/\bar{\alpha})(g_{1\infty}-\tilde{\alpha}\tilde{g}_{2\infty})}{1 + [A-B/\bar{\alpha}]g_{1\infty}(1-A\tilde{\alpha})^{-1} + (B/\bar{\alpha})[g_{1\infty} + \tilde{\alpha}(1-g_{2\infty})]} \qquad (3.14)$$

This expression proves applicable during the initial phase of combustion and also gives a first guess for K in the iterative solution.

3.3.3 Pore model

Gavalas (1980) developed a random capillary model to simulate combustion in porous chars. The model has been applied to combustion both in Zone I (Gavalas, 1980) and in Zone II (Gavalas, 1981). As discussed earlier, pulverized coal combustion appears to take place in Zone II with only partial penetration by oxygen. The complete problem of Zone II combustion must be solved numerically, but Gavalas has shown that a semi-analytic solution exists for the case of combustion in a thin layer near the particle's surface (that is, numerical evaluation of integrals is still required). Evaluation of the complete solution under pulverized coal combustion conditions reveals that for most of the burning particle's history combustion does occur in a thin surface layer (Gavalas, 1981).

In this work, combustion is assumed to take place at constant density and decreasing particle radius. This assumption allows the use of an analytic solution for the char combustion problem. The theoretical framework that has been developed can be modified to include the random capillary model of porous char combustion. In this section

the relevant equations are presented. A detailed explanation of the theory will not be presented. The interested reader is referred to the work of Gavalas cited above.

The random capillary model allows calculation of the pore surface area and effective diffusivity as a function of local burnoff. These quantities are expressed in terms of a local conversion variable q(x,t) which is the length that the solid surface at location x has receded during the interval from zero to time t. As before, the particle is assumed to be isothermal. The only reaction considered is that between carbon and O_2.

Assuming reaction occurs in a thin zone which is small relative to the particle radius and neglecting curvature, the problem is formulated as one-dimensional combustion in a semi-infinite region. The variable x represents the distance from the original position of the boundary (i.e., particle's external surface). As before g_1 is the mass fraction of oxygen. The conservation equation for oxygen inside the char is

$$\frac{\partial}{\partial x}\left(\rho D_e \frac{\partial g_1}{\partial x}\right) = b\, R_{in}(g_1,T)\, S(q) \tag{3.15}$$

S is the local surface area and is related to the local porosity by

$$S(q) = \frac{d\,\varepsilon_T(q)}{dq} \tag{3.16}$$

$R_{in}(g_1,T)$ is the intrinsic reaction rate of oxygen with carbon in grams of carbon per unit surface area per unit time. It includes

reaction in micropores, those pores with radii less than 0.6 nm. b is a stoichiometric coefficient equal to 4/3.

Of interest is a psuedo-steady state where the velocity of the boundary, u, has reached a constant value. If the position of the boundary is given by $x^*(t)$, the problem can be reformulated in terms of a new independent variable $y = x - x^*(t)$, the distance from the instantaneous boundary. Assuming asymptotic steady state combustion, the new problem is

$$\frac{d}{dy}\left(\rho D_e \frac{dg_l}{dy}\right) = b R_{in}(g_l, T)\, S(q) \tag{3.17}$$

$$\frac{dq}{dy} = -\frac{1}{\rho_c u} R_{in}(g_l, T) \tag{3.18}$$

where u is the velocity of the boundary recession, i.e.,

$$u = \frac{dx^*}{dt} \tag{3.19}$$

The boundary conditions are

$$\begin{aligned} &y = 0: \quad q = q^* \text{ and } g_l = g_{lp} \\ &y \to \infty \ : \ g_l \to 0 \text{ and } q \to 0 \end{aligned} \tag{3.20}$$

These equations can be solved (Gavalas, 1981) to give a simple expression for u:

$$u = \frac{1}{\rho_c}\left(\frac{I(u)}{bJ}\right)^{1/2} \tag{3.21}$$

where

$$I(u) = \int_{o}^{g_{lp}} R_{in}(g,T)\, dg \tag{3.22}$$

$$J = \int_{o}^{q^*} \frac{\varepsilon_{T(q)} - \varepsilon_{To}}{D_e(q)}\, dq \tag{3.23}$$

In order to match the solution to the oxygen conservation equation inside the particle to that outside the particle, the surface oxygen mass fraction has been fixed in Eq. 3.20. It can be shown that the solution inside the particle satisfies the flux boundary condition for the outside solution, Eq. 3.8. Therefore, the flux and concentration of oxygen match at the particle's surface.

The quantity q^* is a critical value of the burnoff and serves as the upper limit for the integral in Eq. 3.23. When the surface porosity of a burning char particle reaches a critical value ε^*, disintegration begins; that is, the pore walls merge. Dutta and Wen (1977) concluded from experimental observations of char gasification that disintegration occurs for $\varepsilon_T = 0.8$. This value of the critical porosity will be used in the calculations presented here. Gavalas (1981) has shown that the model results are not very sensitive to the value of ε^*.

The quantity of interest is actually the combustion rate per unit external surface area, i.e.,

$$R_{es} = \rho_c(1 - \varepsilon_{To})u \tag{3.24}$$

To relate Eq. 3.24 to the results already derived for the gas-phase problem, the dimensionless mass loss can be written in terms of R_{es} as

$$K = \frac{R_{es} r_p}{\rho D} \tag{3.25}$$

The surface boundary condition for O_2 (Eq. 3.8) can be evalutated using Eq. 3.24 and 3.25 to give an equation for K which is the counterpart of Eq. 3.12.

$$g_{1p} = e^{-K}(g_{1\infty} - \tilde{\alpha}) - \tilde{\alpha} \tag{3.26}$$

This equation is simpler than Eq. 3.12 because only one reaction of carbon is involved, that with O_2. If the particle temperature is known, this equation can be solved iteratively for g_{1p} since K is a function of g_{1p}.

An outline of the pore model has been presented. Details of the actual implementation remain to be discussed. Two points are of particular importance and will now be examined: the porosity and effective diffusivity in the solid and the nature of the intrinsic reaction rate.

In formulating a model for combustion in a porous solid, it is assumed that the structure of the solid can be approximated by a discrete pore size distribution. There are n pore sizes; the ith pore size is characterized by a radius R_i and porosity ε_i. The initial values are R_{oi} and ε_{oi}. The binary diffusion coefficient in a

capillary of radius R is given by (Feng and Stewart, 1973):

$$\frac{1}{D(\tilde{R})} = \frac{1}{D} + \frac{1}{A_k \tilde{R}} \tag{3.27}$$

where D is the bulk diffusion coefficent and $A_k\tilde{R}$ is the Knudsen diffusion coefficient in a pore of radius $\tilde{R}$. One can approximate the effective diffusivity in a solid by

$$D_e(q) = \frac{1}{\zeta} \int \varepsilon(R,q)\ D(R)\ dR \tag{3.28}$$

ζ is the tortuosity of the pores. A value of 2 is used after Smith and Tyler (1972). For a discrete pore size distribution the effective diffusivity is

$$D_e(q) = \frac{1}{\zeta} \sum_{i=1}^{n} \varepsilon_i(q)\ D(R_i) \tag{3.29}$$

In order to calulate the integral quantity J, one must also know the porosity as a function of q, the local burnoff. The following equations give the porosity in each size.

$$1 - \varepsilon_n = \left(1 - \varepsilon_{on}\right)^{\gamma_n^2} \tag{3.30}$$

$$\frac{1 - \sum_{j=i}^{n} \varepsilon_j}{1 - \sum_{j=i+1}^{n} \varepsilon_j} = \left[\frac{1 - \sum_{j=i}^{n} \varepsilon_{oj}}{1 - \sum_{j=i+1}^{n} \varepsilon_{oj}}\right]^{\gamma_i^2}, \quad i = 1,\ldots n-1 \tag{3.31}$$

The quantity γ_i is a function of q and R_{oi} given by

$$\gamma_i = 1 + q/R_{oi} \tag{3.32}$$

Equations 3.29 through 3.32 are substituted into the expression for J, Eq. 3.23.

Calculation of the external surface reaction rate now requires evaluation of the integral I, Eq. 3.22. All that is needed is the reaction rate R_{in}. Even though many of the complicated or misleading aspects of the combustion problem (e.g., pore structure) have been removed from consideration, this is not a simple task.

> In drawing attention to the obtrusiveness of the C + O_2 reaction-it has so far defied any efforts to unify it with other gasification reactions-we proceed well into the area of theoretical, if not experimental, uncertainty. This reaction is of rabbinical complexity (Thomas, 1970).

Although there is much to be learned about the details of the reaction between carbon and oxygen, there is some general agreement about the process. Smith (1978) studied the reactivity of many different carbons from diamonds and graphite to soot and coal. When corrected for the effects of pore structure, all had remarkably similar reactivities. The activation energy was calculated to be 42 kcal/mole. However, most of the carbon in this investigation was reacting at temperatures below about 2000 K. It has been observed by Nagle and Strickland-Constable (1962), Walls and Strickland-Constable (1964), and Park and Appleton (1973) that carbon has a reactivity maximum for temperatures near 2000 K. This phenomenon is explained by the presence of two types of

reaction sites, one of which is more reactive than the other. At high temperatures the char undergoes an annealing process in which the more reactive type site is converted to the less reactive causing the maximum in the reaction rate with temperature.

Nagle and Strickland-Constable (1962) proposed a semi-empirical rate equation for this mechanism.

$$R_{in} = \left(\frac{k_A Po_2}{1 + k_z Po_2}\right) \chi + k_B Po_2 (1 - \chi) \tag{3.33}$$

where

$$\chi = \left[1 + k_T/(k_B Po_2)\right]^{-1} \tag{3.34}$$

The Nagle-Strickland-Constable rate equation is used in this work, although the values of the rate coefficients have been modified slightly so that it coincides with the formula of Smith (1978) at low temperatures. Figure 3.1 compares these rates. In part b of Fig. 3.1 the rate expressions are compared with data on carbon black reactivity from shock tube studies done by Park and Appleton (1973). The kinetic constants actually used in this work are given in Table 3.1. In applying these kinetics to the combustion model, oxygen mass fraction has been used in place of oxygen partial pressure. All the calculations in this work are performed at 1 atmosphere total pressure and the mean molecular weight of the gas is approximately constant. Given the uncertainty in the kinetic parameters, this is a reasonable assumption.

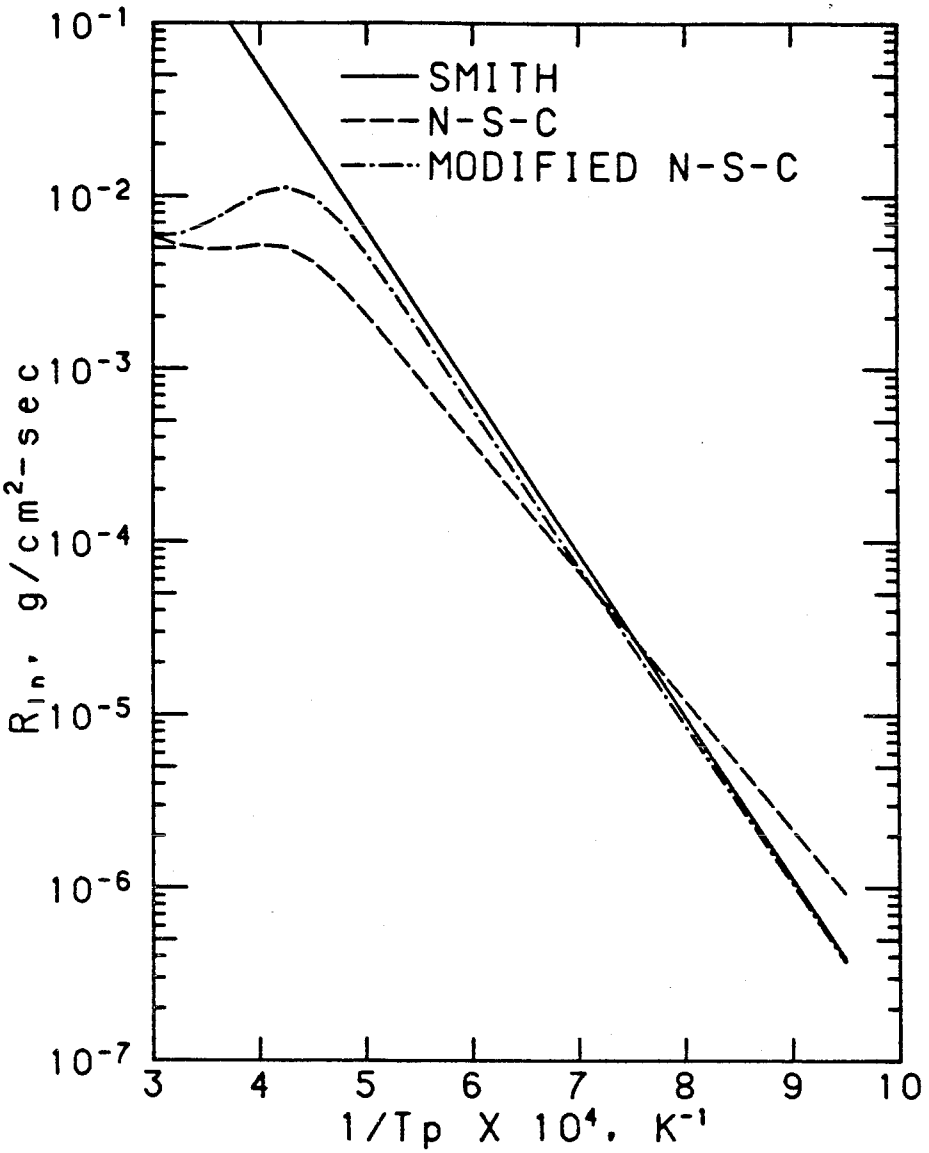

Figure 3.1a Intrinsic reactivity of carbon to oxygen: comparison of kinetic mechanisms (at 1 atm partial pressure).

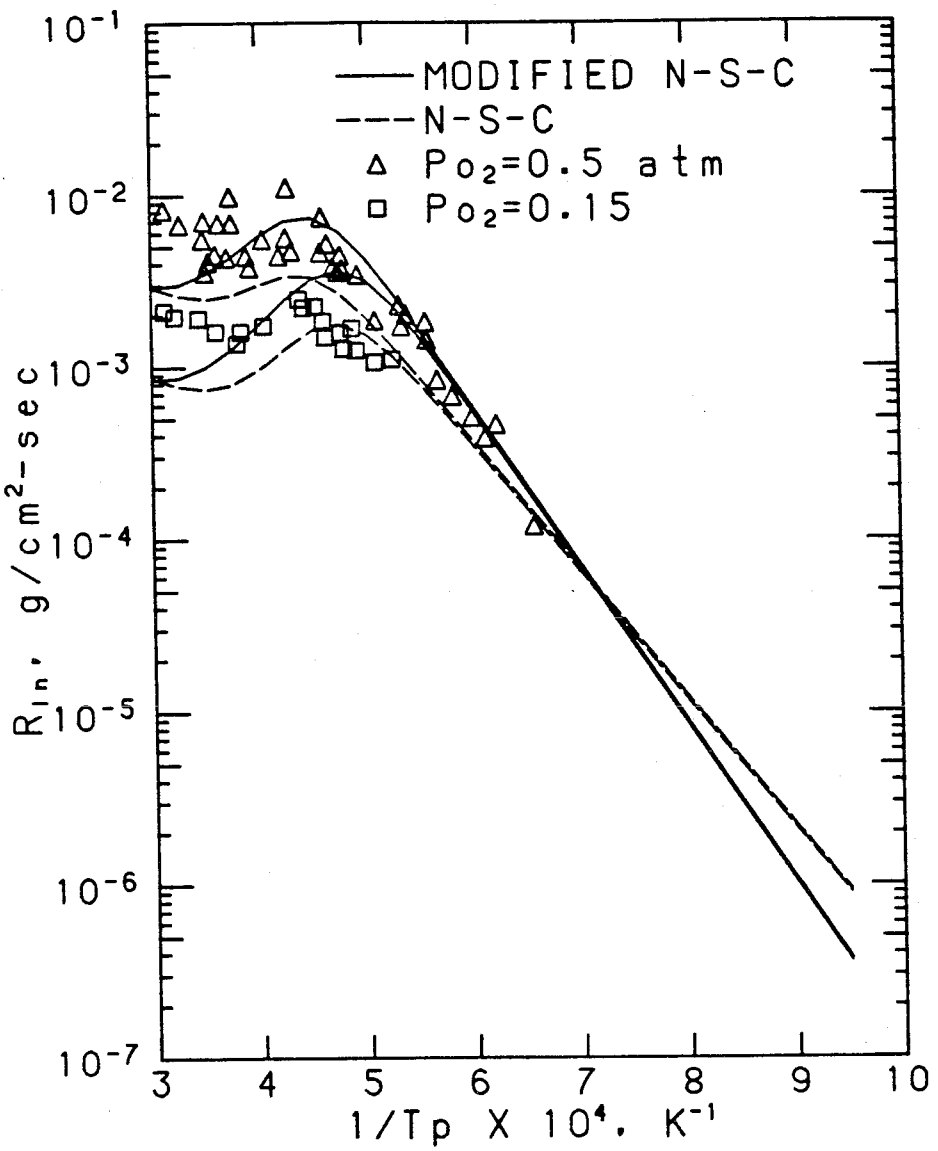

Figure 3.1b Intrinsic reactivity of carbon to oxygen: Comparison with data of Park and Appleton (1973).

TABLE 3.1: INTRINSIC REACTION RATE FOR CARBON

$$R_{in} = 12 \left[\left(\frac{k_A P_{o2}}{1 + k_z P} \right) \chi + k_B P (1 - \chi) \right] , \ g/cm^2\text{-sec}$$

where $\chi = \left[1 + k_T / (k_B P) \right]^{-1}$

and $k_i = A \exp(E/T)$

CONSTANT	A	E
k_A	325	-19,000
k_B	4.46×10^{-3}	-8,500
k_T	1.51×10	-48,800
k_z	21.3	2060

3.4 Mineral Matter

Coal is composed of organic and inorganic material; the majority of the inorganic elements are found in discrete mineral inclusions (Sarofim et al., 1977). Microscopic examination of coal reveals that there are many small inclusions in the range 1-5 microns distributed throughout (Sarofim et al., 1977; Hamblen et al., 1980). As coal burns, the carbonaceous material disappears and inclusions are brought to the surface. Figure 3.2 shows a partially burned coal particle. Mineral matter on the surface appears lighter in color than the bulk coal in this photograph. The mineral matter also appears to have been molten and fused at some time. Fusion of mineral matter in coal begins at temperatures in the range 1200-1600 K (Raask, 1969; O'Gorman and Walker, 1973). During combustion the inclusions coalesce on the surface when they come in contact. This molten mineral matter or ash accumulates on the particle's surface as it burns.

One consequence of the behavior described above is that a portion of the carbon surface is covered with ash and therefore is not in contact with the gas phase. This ash coverage may affect the reactivity of the particle. In terms of the present model, in which combustion is modeled as occuring only on the surface, the surface reaction rate is simply scaled by the exposed area of carbon. To assess the importance of this phenomenon it is necessary to calculate the surface ash coverage as a function of burnout. A Monte Carlo simulation is used to explore ash coalescence during combustion. Inclusions are randomly distributed

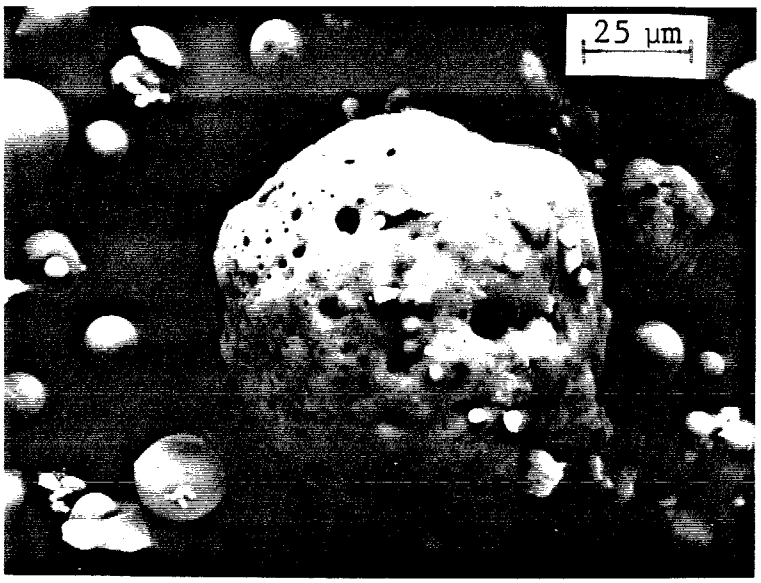

Figure 3.2 Partially burned coal particle.

throughout the volume of a sphere. The motion and coalescence of the inclusions are followed as the sphere 'burns.' The coal particle radius is decreased in increments; at each increment the number and position of all inclusions on the surface are calculated. If the distance between the centers of any two inclusions is less than the sum of their radii, they are assumed to coalesce. The area that each inclusion occupies on the particle's surface is calculated given the contact angle between the ash and carbon. This contact angle has been experimentally determined (Raask, 1966). The calculation is repeated many times to give an average surface ash coverage as a function of burnout. The averaging is possible because the inclusion size (2.5 microns) is so much smaller than the particle size (50-80 microns). Figure 3.3 shows some typical calculations which are carried out to 95% burnout. It is apparent that very little surface area is occluded by ash up to 95% burnout. Therefore the mineral inclusions don't occupy much area on the surface, and the effect of surface ash on combustion rate is not large. The volume fraction of ash in coal does, however, have an effect on the combustion rate as will be seen in a later section.

3.5 Devolatilization

Devolatilization has a great influence on the combustion history of a particle. Models of solid carbon combustion (Caram and Amundson, 1977; Libby and Blake, 1979), while adequate for modeling char combustion, neglect the effects of devolatilization. Particle temperature is affected because pyrolysis reactions are endothermic and

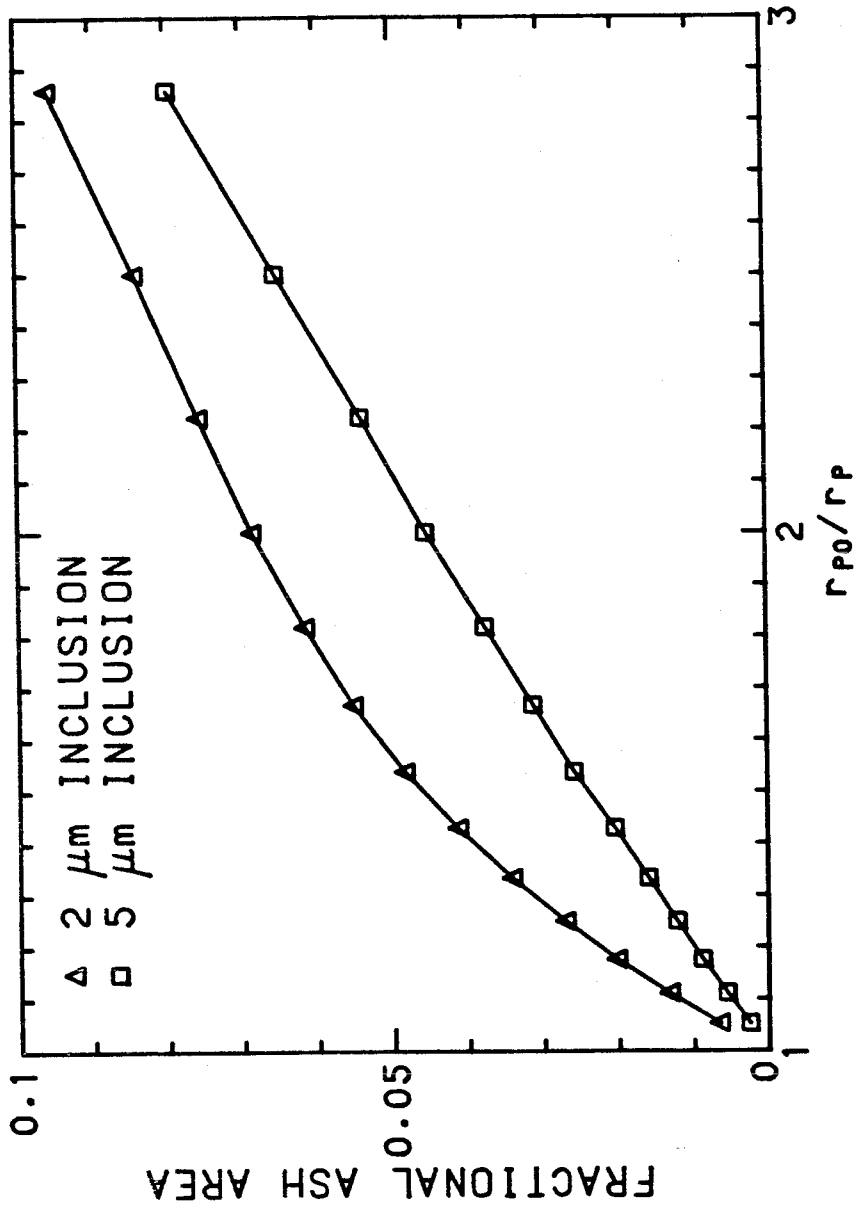

Figure 3.3 Fraction of surface covered by ash as a function of coal particle radius during combustion.

consequently it slows down the particle heat-up. The burnout time is also affected because the time required for the relatively slow char combustion is reduced if there is substantial loss of volatiles. There have been some attempts to include devolatilization in dynamic combustion models (Baum and Street, 1977; Stickler et al., 1979), but these models have made extreme simplifications in treating heat transfer in the surrounding gas.

The pyrolysis is treated with an empirical model of two competing reactions as proposed by Kobayashi et al. (1976) and Stickler et al. (1979). There are two first order reactions in parallel; each converts coal to residual char (r_1 and r_2) and volatiles (v_1 and v_2). The reaction scheme is as follows:

$$\text{daf coal} \xrightarrow{K_1} (1-\beta_1)\, r_1 + \beta_1 v_1$$

$$\text{daf coal} \xrightarrow{K_2} (1-\beta_2)\, r_2 + \beta_2 v_2$$

where β_i is the mass fraction converted and the rate constants K_i are in an Arrhenius form:

$$K_i = B_i \exp(-E_i/RT_p) \qquad i = 1,2 \qquad (3.35)$$

The first reaction has a low activation energy and dominates at low temperatures while the second has a high activation energy. In general, β_i is chosen so that the first reaction alone gives a volatile yield equal to the proximate analysis volatile yield. We use the values of Stickler et al. (1979) in this work (Table 3.2) although when the

proximate analysis of a particular coal is known, the volatile matter content may be used for β_i.

The mass of undegraded coal is denoted by m_{cu} and the mass of coal plus char by m_c. The rate of production of volatiles is therefore

$$\dot{m}_v = \beta_1 m_{cu}(t)K_1 + \beta_2 m_{cu}(t)K_2 \tag{3.36}$$

Integrating this equation gives the instaneous mass of undegraded coal:

$$m_{cu}(t) = m_{co} - \int_o^t \left[m_{cu}(t)K_1 + m_{cu}(t)K_2\right] dt \tag{3.37}$$

where m_{co} is the initial daf mass of coal. The total daf mass at any time is given by

$$m_c(t) = m_{co} - \int_o^t \left[\beta_1 m_{cu}(t)K_1 + \beta_2 m_{cu}(t)K_2\right] dt \tag{3.38}$$

3.6 Dynamic Particle Response

Results of the previous sections are now used to formulate a model of the response of a cold particle in a hot reactive gas. A thermodynamic analysis of the particle is combined with previously-derived material to give equations of change for the particle temperature, radius, and carbon density during devolatilization.

The particle is assumed to be at rest in an infinite gas. The

particle is initially near room temperature (300 K) while the gas is at the free stream temperature, T_∞ . The particle temperature increases due to radiation and gas-phase conduction. Volatiles begin to evolve at a rate which can be computed as described in the previous section. The volatiles mix with the gas and burn far away from the particle. For a dilute suspension of particles, it is reasonable to assume that combustion of the volatiles does not affect the free stream gas composition, nor does the associated heat release affect the particle heat balance. These two assumptions are made to simplify the analysis and are representative of drop tube combustion studies, e.g., Mims et al. (1980) and Chapter 9 of this work. Devolatilization is assumed to proceed at constant particle radius; in order to model this process, the carbon density ρ_c is assumed to change during devolatilization. When devolatilization is complete, char combustion on the surface of the particle begins. Calculations are carried out to approximately 95% burnout. Beyond this point the clumps of residual ash may become about the same size as the remaining coal particle and the model breaks down.

The starting point of the analysis is an unsteady energy balance on the coal particle. The total energy of the particle is given by

$$E = U(m_c + m_a) \tag{3.39}$$

where U is the specific internal energy and m_c and m_a are the masses of carbon and ash, respectively. Carbon and ash are assumed to have the same heat capacity which allows U to apply to both the carbon and the ash mass. In addition, the solid internal energy is taken to be equal

to the solid enthalpy which is a linear function of temperature. The unsteady energy balance on the particle is

$$\frac{dE}{dt} + 4\pi r_p^2 \Sigma \rho_i V_i H_i = \dot{Q}_R + Q_c \tag{3.40}$$

The terms on the left-hand side of the equation are the rate of change of particle energy and the flux of energy by convection of gaseous species away from the particle. The particle temperature is assumed to be uniform.

The terms on the right-hand side of Equation 3.39 are the energy fluxes due to radiation and gas-phase conduction. These are:

$$\begin{aligned} \dot{Q}_R &= 4\pi r_p^2 \sigma(T_p^4 - T_w^4) \\ \dot{Q}_c &= 4\pi r_p^2 k\left(\frac{T_\infty - T_p}{r_p}\right) \end{aligned} \tag{3.41}$$

where σ is the Stefan-Boltzmann constant and k is the thermal conductivity of the gas. The gas is assumed to be transparent to radiation and the particle is assumed to have an emissivity of one. The wall temperature for radiation is equal to the free stream temperature. This latter assumption is adequate for modeling combustion in small laboratory furnaces where the walls and gas are at the same temperature.

There are two distinct phases in the combustion history. The first is devolatilization which is characterized by constant particle radius and changing carbon density. The second is char combustion which is characterized by constant carbon density and shrinking particle radius.

The equations of change which pertain to each phase will be examined separately.

The analysis begins with differentiation of Equation 3.39 to give

$$\frac{dE}{dt} = U \frac{dm_c}{dt} + (m_c + m_a)\, c_{ps} \frac{dT_p}{dt} \tag{3.42}$$

where c_{ps} is the solid heat capacity. During devolatilization Equation 3.36 specifies the rate of change of mass of carbon, dm_c/dt, or the mass flux of volatiles away from the particle. Therefore the expression in Eq. 3.36 is used in the convective flux term in the energy balance:

$$4\pi r_p^2 \Sigma \rho_i V_i H_i = \beta_1 K_1 m_{cu} H_1 + \beta_2 K_2 m_{cu} H_2 \tag{3.43}$$

where H_1 and H_2 are the enthalpies of the volatile species. As with the enthalpies of other gas species, it is assumed that the enthalpy is a linear function of temperature, $H_i = c_p T + \Delta H_i$. The heat capacity is the same as that used for the combustion gas species. Since very little thermodynamic data about the volatile species exist, the ΔH_i are chosen to be the heats of formation of volatiles given by Stickler et al.

Equations 3.41 through 3.43 are substituted into Equation 3.40 to give the rate of change of particle temperature during devolatilization:

$$\frac{dT_p}{dt} = \frac{1}{(m_c + m_a)c_{ps}} \left\{ -H_c \frac{dm_c}{dt} + 4\pi r_p^2 \left[\frac{k(T_\infty - T_p)}{r_p} - \sigma(T_p^4 - T_\infty^4) \right] \right.$$

$$\left. - \left[\beta_1 K_1 m_{cu} H_1 + \beta_2 K_2 m_{cu} H_2 \right] \right\} \qquad (3.44)$$

To solve the system, the following dimensionless variables are introduced:

$$\theta = T_p / T_\infty$$

$$R = r_p / r_{po}$$

$$M_u = m_{cu} / m_{co}$$

$$R = \rho_c / \rho_{co}$$

$$\tau = \frac{(\rho D)_o t}{r_{po}^2 \rho_{co}}$$

where ρ_{co} is the initial carbon density and $(\rho D)_o$ is the product of the gas density and diffusivity at the free stream temperature. A dimensionless radiation term $Q_R = \left(\sigma r_{po} (T_p^4 - T_\infty^4) / (\rho D)_o c_{ps} T_\infty \right)$ is also defined. The dimensionless temperature change during the devolatilization phase is given by

$$\frac{d\theta}{d\tau} = \frac{3R}{\left(R R^3(1-\alpha) + \alpha\rho_s/\rho_{co}\right)} \left\{-Q_R R + \left(\frac{c_p}{c_{ps}}\right) \frac{\rho D}{(\rho D)_o} \frac{1-\theta}{Le} \right.$$

$$\left. - \frac{(1-\alpha)M_u}{3} \left[\beta_1 K_1' (\tilde{H}_1 - \tilde{H}_c) + \beta_2 K_2' (\tilde{H}_2 - \tilde{H}_c)\right]\right\} \tag{3.45}$$

where α is the volume fraction of ash and Le is the gas-phase Lewis number which is assumed to be constant and near unity. A tilde over enthalpy represents division by $c_{ps}T_\infty$. The dimensionless frequency factors are $K_i' = (K_i r_{Po}^2 \rho_{co}/(\rho D)_o)$ Equation 3.45 is coupled with two other rate equations

$$\frac{dM_u}{d\tau} = -M_u(K_1' + K_2') \tag{3.46}$$

and

$$\frac{dR}{d\tau} = -M_u(\beta_1 K_1' + \beta_2 K_2') \tag{3.47}$$

The preceding three equations represent the behavior of the particle during the first phase, that is, until M_u=0. When devolatilization is over, the second phase begins.

During char combustion the carbon density ρ remains constant and the particle radius decreases. The rate of mass loss of carbon is given by

$$\frac{dm_c}{dt} = -4\pi r_p^2 m_p \tag{3.48}$$

The flux of gaseous species away from the particle is proportional to the rate of the heterogeneous reactions. For example the mass flux of oxygen (species 1) is written as

$$\rho_1 V_1 = -R_1\left(\frac{M_1}{2M_c}\right) \tag{3.49}$$

where M_1 and M_c are the molecular weights of oxygen and carbon. The convective flux term in the energy balance is written therefore in terms of the reaction rate based on external surface area:

$$\begin{aligned}\Sigma \rho_i V_i H_i = R_1 &\left[-\left(\frac{Mo_2}{2M_c}\right) Ho_2 + \left(\frac{M_{co}}{M_c}\right) H_{co}\right] \\ &+ R_2\left[-\left(\frac{M_{co_2}}{M_c}\right) H_{co_2} + \left(\frac{2M_{co}}{M_c}\right) H_{co}\right]\end{aligned} \tag{3.50}$$

This equation applies to either the pore model or the surface model, although in the case of the pore model R_2 is not defined ($R_2 = 0$). The same energy balance (Equation 3.40) is used for both combustion and devolatilization. Equations 3.41, 3.42, 3.48, and 3.50 are substituted into the energy balance and it is rearranged to give the rate of change of particle temperature:

$$\begin{aligned}\frac{dT_p}{dt} = \frac{4\pi r_p^2}{(m_c + m_a)c_{ps}} \Bigg\{ &-\sigma\left(T_p^4 - T_\infty^4\right) + \frac{d(T_\infty - T_p)}{r_p} \\ &- R_1 \Delta H_{R_1} - R_2 \Delta H_{R_2} \Bigg\}\end{aligned} \tag{3.51}$$

where the ΔH_{ri} are the enthalpies of reaction. For example, the enthalpy for reaction 1 (oxygen and carbon) is given by

$$H_{R1} = \left(\frac{M_{co}}{M_c}\right) H_{co} - \left(\frac{Mo_2}{2M_c}\right) Ho_2 - H_c \tag{3.52}$$

The corresponding dimensionless equation is obtained by manipulating Equation 3.51 to give

$$\frac{d\theta}{d\tau} = \frac{3R}{\left(R\bar{R}^3(1-\alpha) + \rho\alpha_a/\rho_{co}\right)} \left\{ -Q_R R + \left(\frac{c_p}{c_{ps}}\right) \frac{\rho D}{(\rho D)_o} \frac{1-\theta}{Le} \right.$$
$$\left. - \frac{\rho D}{(\rho D)_o} \left[Ag_{1p} \Delta\tilde{H}_{R1} + Bg_{2p} \Delta\tilde{H}_{R2} \right] \right\} \tag{3.53}$$

The other differential equation required for the combustion phase is the rate of change of the particle radius. This can be obtained from Equation 3.48 if it is recognized that the mass of carbon

$m_c = 4/3\pi r_p^3 (1 - \alpha)\rho_c$ is related to the particle radius. In terms of the appropriate dimensionless quantities, the rate of change of particle radius is

$$\frac{dR}{d\tau} = \frac{\rho D}{(\rho D)_o} \frac{K}{(1-\alpha)R\bar{R}} \tag{3.54}$$

Equations 3.53 and 3.54 describe the behavior of the particle when char combustion occurs. Both equations depend on the mass loss parameter K and on the gas composition. The quasi-steady nature of the combustion allows the calculation of mass loss and gas composition at every time step in the manner outlined in a previous section.

TABLE 3.2: PYROLYSIS CONSTANTS

Frequency Factors	B_1	$3.7 \times 10^5\ s^{-1}$
	B_2	$1.46 \times 10^{13}\ s^{-1}$
Activation Energies	E_1	17.6 kcal/mole
	E_2	60.0 kcal/mole
Mass Coefficients	β_1	0.38
	β_2	0.8
Heats of Formation	ΔH_1	-400 cal/g
	ΔH_2	-200 cal/g

TABLE 3.3 PHYSICAL PROPERTIES FOR CHAR COMBUSTION

Enthalpies: $H_i = c_p T + \Delta_i$

Solid Carbon:	
Heat Capacity, c_{ps}	0.48 cal/g K
Δ_i	-140 cal/g
Gases:	
Heat Capacity, c_p	0.28 cal/g
Δ_1	0
Δ_2	-2172 cal/g
Δ_3	-956 cal/g
Δ_4	0
Densities	
Ash, ρ_a	2.5 g/cm^3
Unburned Carbon, ρ_{co}	1.3 g/cm^3

The system is solved using a modified fourth order Runge-Kutta routine (Fehlberg, 1969). Equations 3.45 through 3.47 are integrated until devolatilization is complete; then Equation 3.53 and 3.54 are integrated until 95% burnout is reached. For the most part the thermodynamic data used for the calculation are those chosen by Libby and Blake (1979) except as noted. Tables 3.2 and 3.3 list the constants that are used in the calculations.

3.7 Discussion of Results

The dynamic coal combustion model has been introduced and several effects that were not present in other quasi-steady models have been described. Numerical results of calculations using the model are presented in this section. First, we examine the sensitivity of the model to assumptions about gas properties, ash content, and devolatilization. Then, particle temperatures and lifetimes are compared with the available data from coal combustion experiments.

A test case is considered in some detail to illustrate the behavior of the model. For this example, semi-anthracite kinetics are used with the surface model to calculate the reaction rate as indicated in the text. A coal particle with a 40 micron initial radius burns in air at one atmosphere pressure; the gas temperature is 1750 K and the particle contains 5 % ash by volume distributed as 2.5 micron inclusions.

This work represents major changes in the model of Libby and Blake.

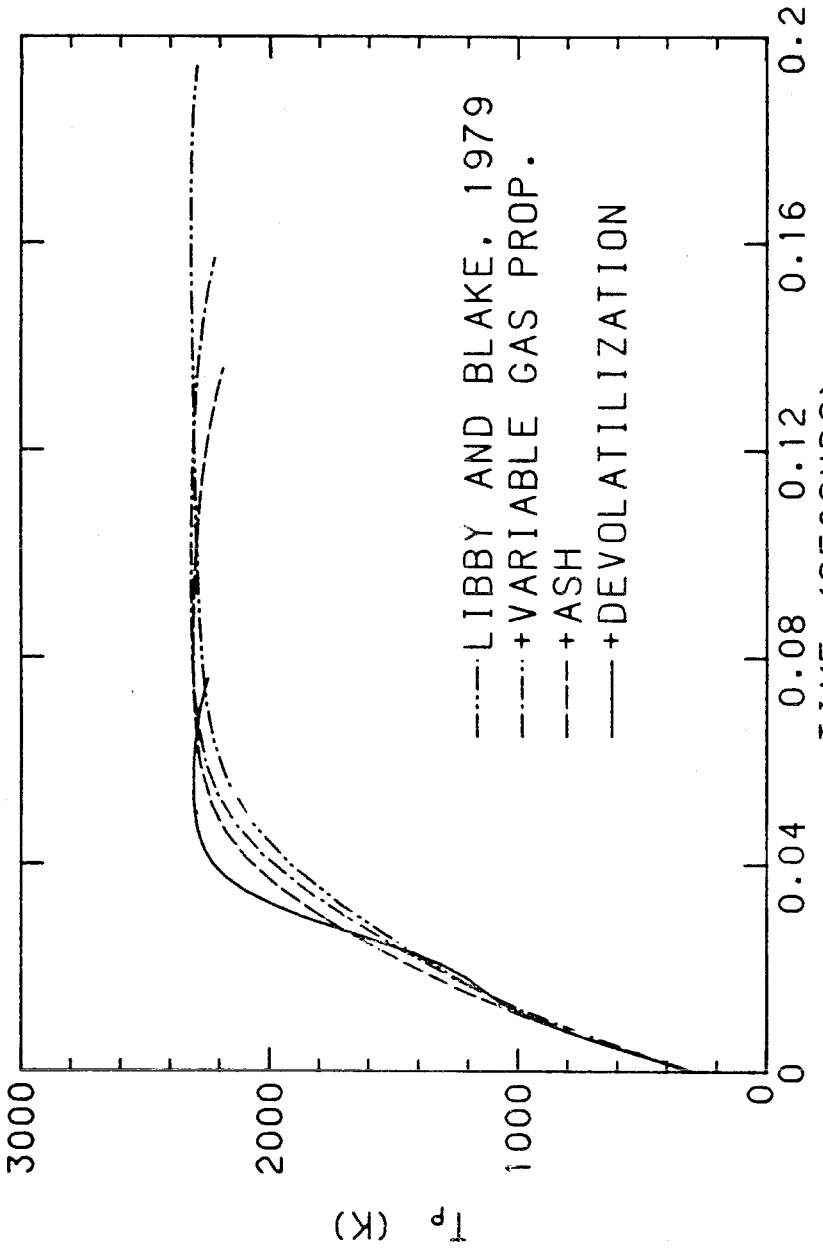

Figure 3.4a Evolution of the combustion model: particle temperature during combustion.

Successive additions to their model are shown in Figure 3.4: variable gas properties, i.e., computing diffusivity based on a geometric mean temperature and using constant Lewis number; ash, including the ash volume in the particle energy balance; surface ash, allowing ash to cover part of the surface; devolatilization. The solid curve therefore represents the full model as derived in the previous sections.

The gas properties have the greatest effect on particle temperature. Allowing the gas properties to vary with particle temperature causes the temperature during char combustion to be less than in the Libby and Blake model. The temperature is lower because the gas-phase conduction is increased. Devolatilization kinetics lead to a much steeper initial temperature increase than is predicted for the combustion of pure carbon. The other features which have been added to the model do not have as large an effect on particle temperatures during combustion.

Figure 3.4b shows the radius history for the various versions of the model. All calculations are carried out up to 95% burnout. Allowance for variable gas properties in Libby and Blake's model produces a shorter burnout time. When mineral inclusions are also considered, the burnout time shortens considerably because there is now less carbon to burn in the same particle volume. The volume of ash in the particle greatly affects the total burnout time, even though surface occlusion by the ash has little effect on the apparent reaction rate. By far the greatest influence on the burnout time results from the

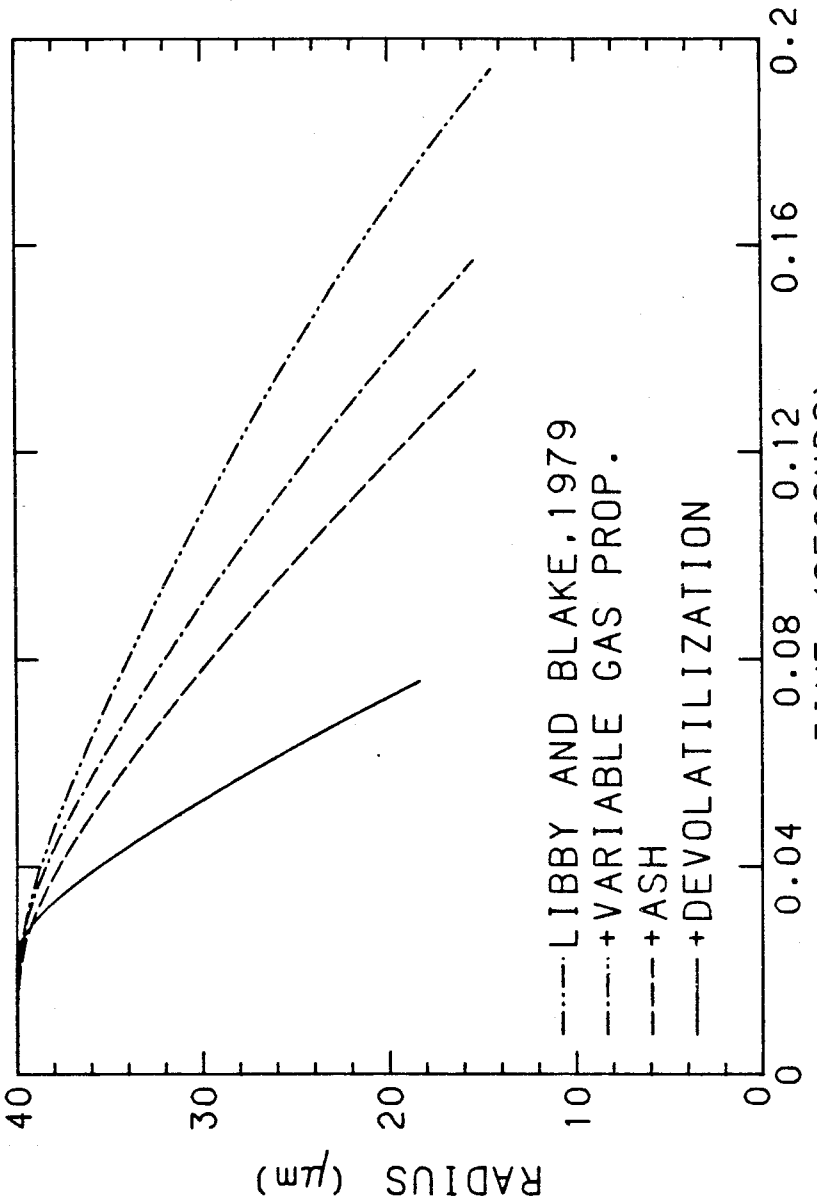

Figure 3.4b Evolution of the combustion model: particle radius during combustion.

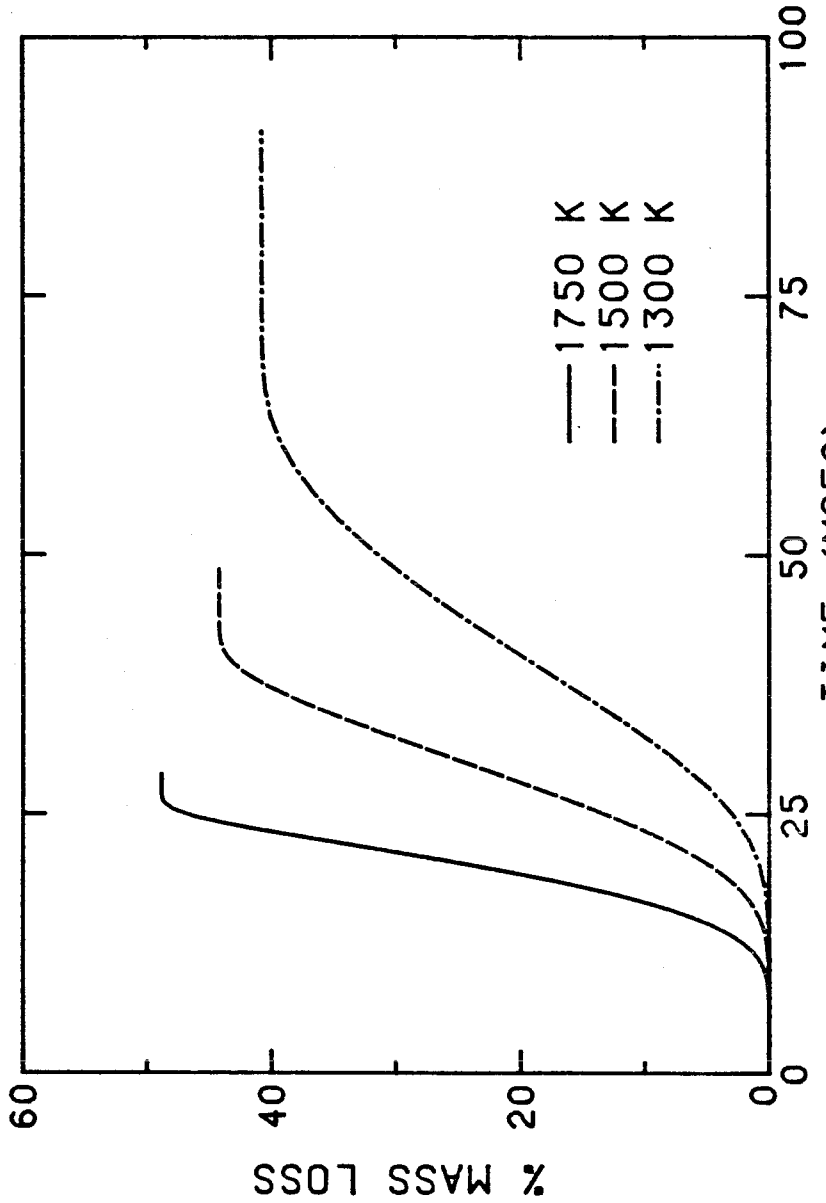

Figure 3.5 Effect of gas temperature on devolatilization. Combustion of 40 μm coal particle in air.

addition of devolatilization to the model. Approximately one-half of the carbon mass is lost during devolatilization, decreasing the time necessary for char combustion. Figure 3.5 shows the behavior of the 40 micron particle for various free stream temperatures. As the temperature increases, the devolatilization rate and the total mass loss increase. This agrees qualitatively with what has been observed in experiments on coal (Kobayashi, et al., 1979).

As previously observed (Mulcahy and Smith, 1969), the rate of combustion of coal in the pulverized fuel size range is limited by the rate of surface reaction rather than external transport processes. This is illustrated in Figure 3.6 by the variation of the dimensionless mass loss parameter K with time. The value of K corresponding to diffusion-limited combustion is shown by the broken line. At no time during combustion does the mass loss approach the diffusion limit. Only for much larger particles or higher gas temperatues will mass transfer limit combustion.

As shown in Figure 3.4, the assumptions incorporated into the coal combustion model have only minor influence on the maximum particle temperature but yield widely disparate particle burn times. Thus, the time required for combustion of the particle is a much more sensitive test of the model validity than the particle temperature. Data obtained from the combustion of coal under well-controlled conditions are scarce. Smith (1971a, 1971b) and Field (1970), for example, provided good kinetic data but did not measure particle temperature. Baum and Street

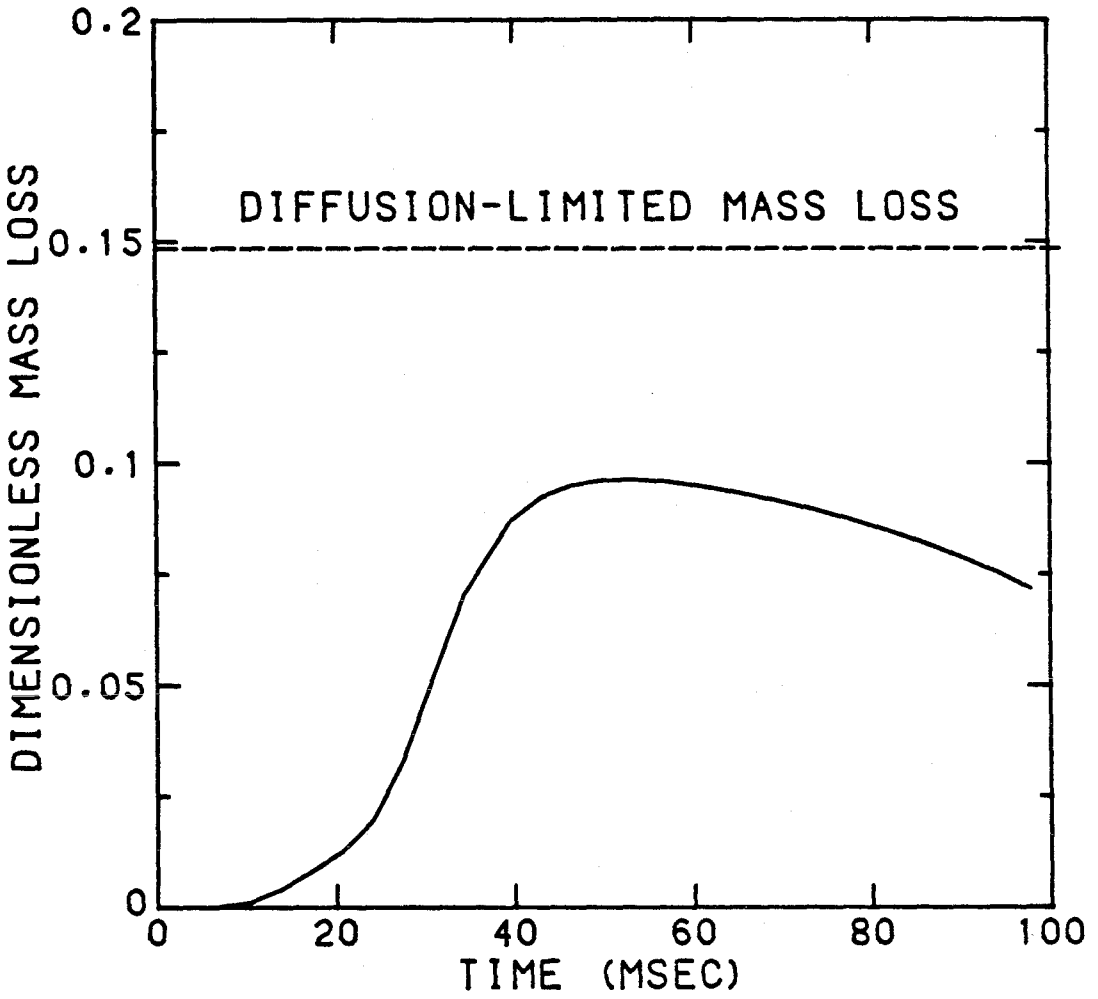

Figure 3.6 Dimensionless mass loss during combustion for combustion of 40 μm coal particle at 1750 K.

(1971) presented data on carbon burnout versus time during coal combustion but made no direct measurement of particle temperatue. Measurements of both particle temperature and lifetime have been made by Sarofim and co-workers (Neville et al., 1981; Mims et al., 1981) for one coal, a Montana lignite, having a mean particle radius of 42 micron and burning at 1750 K. A time-averaged particle temperature was measured by optical pyrometry and the burning time, by photography.

The model can be used to predict burnout times and particle temperatures. To illustrate the use of the pore model, it will be used to calculate reaction rate. The pore model requires as input data quantities which have not been measured in these experiments: char density and porosity. In this case, the needed data will be estimated from existing data on other lignites. Jenkins et al. (1973) measured surface area and open pore volume for several different coal chars, including a lignite. The coal char pore structure is strongly affected by the temperature at which devolatilization takes place. The surface area, pore volume, and reactivity of most chars have a maximum value for a devolatilization temperature of about 600°C. The experimental data correspond to devolatilization temperatures under 1000°C so the pore structure will be estimated for devolatilization at a higher temperature.

For this calculation, two pore sizes are considered: $\varepsilon_{o1} = 0.01$, $R_{o1} = 0.25$ mm and $\varepsilon_{o2} = 0.05$, $R_{o2} = 25$ mm. The apparent particle density is 1.36 g/cc. The coal is assumed to have

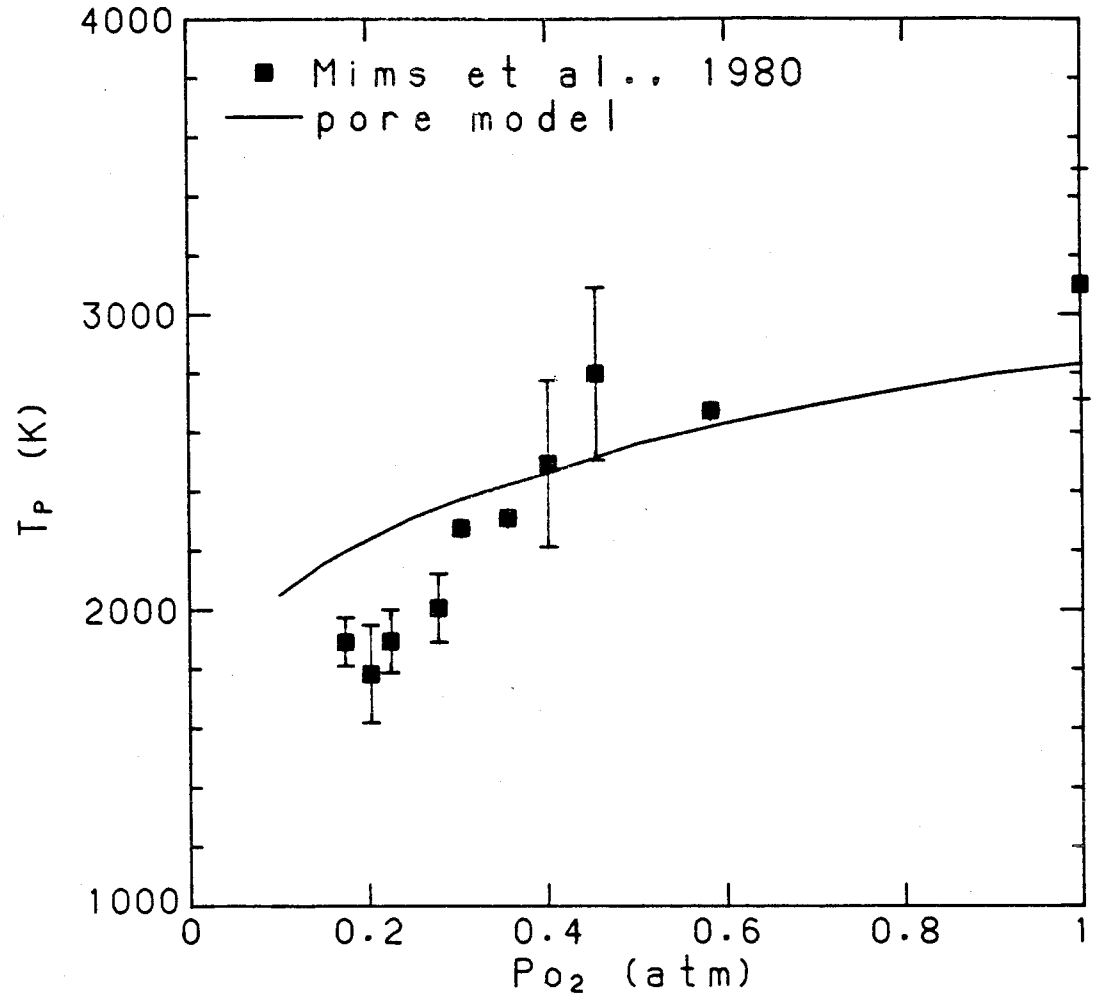

Figure 3.7 Comparison of combustion model with data: mean particle temperature as a function of oxygen partial pressure.

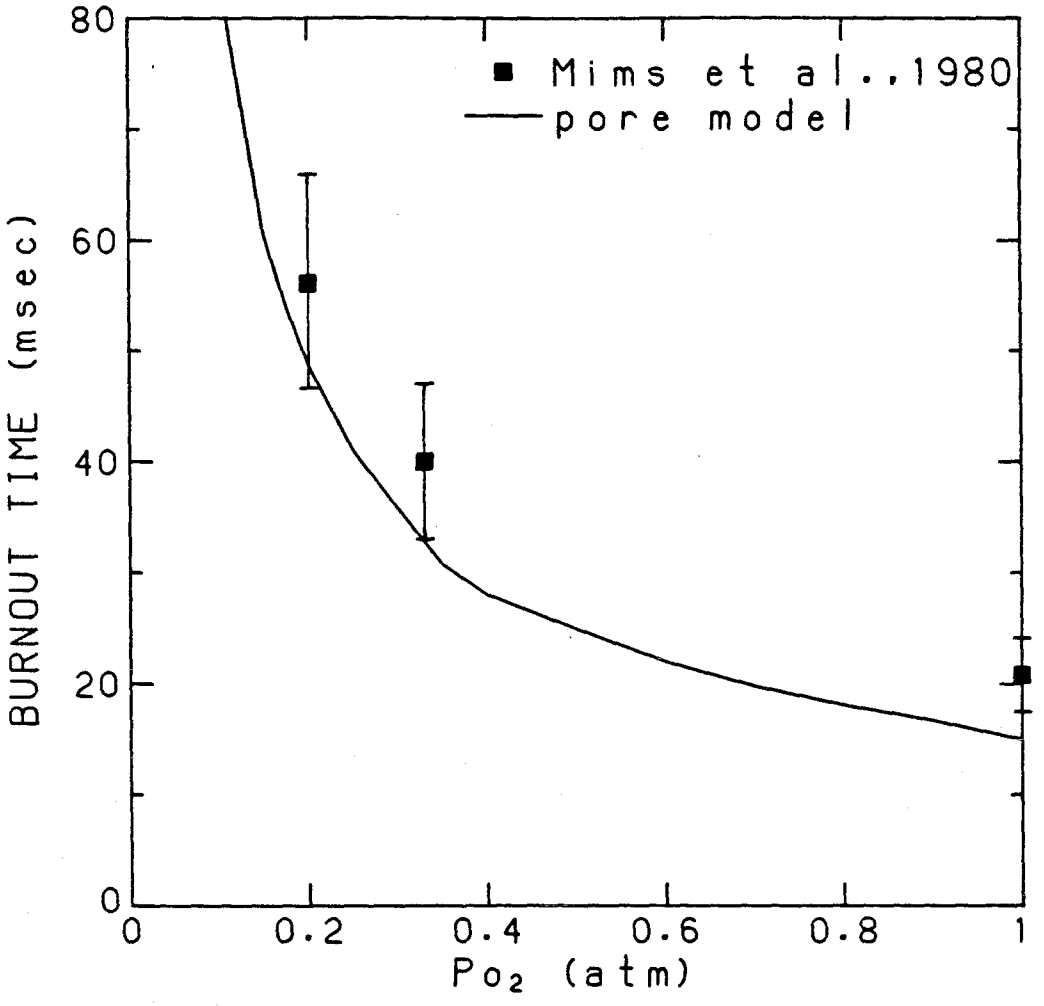

Figure 3.8 Comparison of combustion model with data: burnout time as a function of oxygen partial pressure. (Note: calculated values are time to reach 95% burnout.)

8.2% ash by weight and 40% volatile matter by weight. Figure 3.7 shows the mean temperature versus oxygen partial pressure. There is good agreement between the model and the data especially for partial pressures in the range 0.2-0.5 atmospheres. A complementary set of measurements of particle lifetimes are shown in Figure 3.8 together with the results of the model calculation (to 95% burnout). Despite the fact that the degree of burnout of the experimental points is unknown, the model predicts the data quite well. Figures 3.7 and 3.8 taken together show that the model can simulate both particle temperature and particle lifetime based on fundamental char structure and reactivity models alone.

3.8 Conclusions

We develop a theoretical model of a single coal particle burning in an infinite quiescent medium. The combustion is assumed to be quasi-steady and several features are incorporated into the model which are not present in previous quasi-steady models. The effects of devolatilization kinetics and mineral matter on combustion rate are studied. The following factors are found to have a significant effect on the combustion rate: the kinetics of the char combustion reactions, since the combustion is not mass transfer-limited; the volume fraction of ash in the coal, although the inclusion size does not have a great effect on rate; the kinetics of devolatilization; the gas properties in the vicinity of the particle. Particle temperature is a weak function of the above, while burnout time is very strongly affected.

Comparison of both predicted particle temperatures and burnout times with experimental data yields good agreement.

Two different models for calculating char reactivity are used for the combustion model, a surface model and a pore model. The former is conceptually simpler but not as fundamentally correct as the latter. Both formulations require input data that have not always been available in previous work. In the surface model, the reaction rate as a function of particle temperature is needed. This involves measuring the carbon consumed during combustion as a function of time as well as the particle temperature. Carbon consumption can be measured by either monitoring CO_2 in the gas (Smith, 1971a) or measuring the weight loss of partially burned char (Field, 1969). The particle temperature is usually measured optically. The pore model requires data on the char pore structure as a function of pore radius. The particle density must also be known. These quantities can be obtained directly from conventional porosimetry techniques or can be estimated from surface area measurements.

NOMENCLATURE

A	Dimensionless reaction coefficient
A_k	Knudsen diffusion coefficient (cm/s); see Eq. 3.27
B	Dimensionless reaction coefficient
B_i	Rate coefficient for devolatilization (s^{-1})
b	Stoichiometric coefficient (= 4/3)
C_p	Heat capacity (cal/g - K)
D	Diffusivity (cm^2/s)
E	Total energy (cal/g)
E_i	Activation energy for devolatilization (kcal/mole)
g_i	Mass fraction of gaseous species
H_i	Enthalpy (cal/g)
I	Defined by Eq. 3.22
J	Defined by Eq. 3.23
K	Dimensionless mass loss during combustion
K_i	Rate constant for devolatilization (s^{-1})
k	Thermal conductivity
k_i	Rate coefficient for char combustion ($g/cm^2 - s - atm$)
M_i	Molecular weight (g/mole)
M_u	Dimensionless mass of carbon
m	Mass (g)
m_p	Mass flux from combustion (g/s)
Q_R	Dimensionless radiation flux
$\dot{Q}$	Heat flux ($cal/cm^2 - s$)
q	Local burnoff (cm)
R	Dimensionless radius

R_{es}	Reactivity per unit external surface area ($g/cm^2 - s$)
R_{in}	Intrinsic reactivity of carbon ($g/cm^2 - s$)
R_{oi}	Initial pore radius for i^{th} size (cm)
R	Dimensionless carbon density
r	Radial position
r_i	Residual char converted during devolatilization
T	Temperature (K)
U	Internal energy (cal/g)
u	Char boundary velocity (cm/s)
V	Gas velocity (cm/s)
v_i	Volatiles produced during devolatilization
x	Position in char (cm)
y	Position in char (cm)
z	Dimensionless radial position

Superscripts

*	Denotes conditions at external char surface

Subscripts

a	Ash
C	Conduction
c	carbon
e	Denotes effective diffusivity
o	Initial value
p	Denotes conditions at particles surface
R	Radiation

s	Solid
u	Unburned
v	Volatiles
∞	Denotes conditions at infinity

Greek symbols

α	Defined by Eq. 3.3 and Eq. 3.4
β	Fraction volatilized during devolatilization
γ_i	Defined by Eq. 3.32
ε_i	Porosity of i^{th} pore size
ε_T	Total porosity
θ	Dimensionless particle temperature
ρ	Density (g/cm^3)
σ	Boltzmann constant
τ	Dimensionless time
ζ	Tortuosity
χ	Defined by Eq. 3.34

CHAPTER 4

AEROSOL MODEL: DEVELOPMENT

4.1 Introduction

To date there have been few theoretical studies of the formation of submicron aerosol from coal combustion. Desrosiers et al. (1978) modeled the diffusive transport of vapor away from a burning coal particle. Ash vapor concentrations near the particle's surface were calculated from consideration of liquid-vapor equilibrium and the vapor was assumed to nucleate and grow in the combustion gases far from the burning coal particles. McNallan et al. (1981) modeled the homogeneous nucleation of silicon, sodium, and lead as the products of combustion cooled, assuming that the ash vapors were uniformly distributed in the product gases and that the gas temperature was uniform. Both of the analyses neglected the influence of the local combustion environment on aerosol formation and growth. This approach may be valid for species such as As, Na, and Pb which remain volatile long after combustion is complete. However, the fate of refractory species such as Si, Ca, and Mg may be determined very near the burning coal particle, long before the product gases cool significantly. There is evidence that conditions

surrounding the burning coal particle are very different from those in the bulk product gases.

The combustion process affects the transport of vapor and the growth of aerosol in two important ways. First, the mass flux due to combustion induces a bulk motion away from the coal particle. This radial convection enhances the transport of vapor from the particle's surface. Second, the combustion process alters the local gas composition and temperature. Because char combustion is exothermic, the particle temperature may be higher than that of the surrounding gas as shown in Chapter 3. For combustion of coal in air, particle temperatures several hundred degrees greater than the gas temperature have been measured by Mims et al. (1980) and by Mitchell and McClean (1982). In addition to a temperature gradient around a burning coal particle, there is a gas composition gradient. The combustion reaction consumes oxygen in the neighborhood of the coal particle. The gas near the particle's surface is, therefore, more reducing than the bulk gas.

Radial transport and local temperature and composition gradients can enhance the vaporization of ash. In a reducing environment, metal oxides can be reduced to the more volatile suboxide or metal species. In a study of the vaporization of silica during coal gasification and combustion, Raask and Wilkins (1965) concluded that the amount of silica vaporized could not be explained by direct vaporization, but must be due to the reduction of silica to silicon monoxide in the char. Aerosol formation and growth can be affected by the local combustion

environment, too. As vapor moves away from the coal particle, it becomes supersaturated because of the gas temperature and composition gradients; this provides a strong driving force for condensation, either homogeneous or heterogeneous.

In this chapter, we introduce the conceptual framework for the model of aerosol formation around a single burning coal particle. A mathematical model is developed to account for transport of vapor, formation of aerosol by homogeneous nucleation, and growth of aerosol by condensation. An extended example is presented to illustrate the kinds of information that this model can offer and the importance of various parameters in the problem. Silica is used to represent the ash in these calculations. It is a major component of both the bulk ash and, in some cases, the submicron aerosol. Furthermore, because of its refractory nature, it is more likely to be affected by the local combustion environment than some of the more volatile species found in ash.

4.2 Theoretical Analysis

The steady diffusion of vapor from a single sphere is considered in this analysis. The vapor problem is superimposed on the solution to the quasi-steady combustion of a single burning coal particle, which provides values for the radial convective velocity and gas composition and temperature profiles around the particle at any instant. The gas is assumed to contain only trace amounts of the vapor so the presence of vapor (and the subsequent aerosol) may be assumed to have no effect on

the combustion process.

4.2.1 Coal Combustion Model

The aerosol calculation requires the following information about the combustion process and the environment around a burning coal particle: the combustion rate, the instantaneous gas composition profile, and the instantaneous gas temperature profile. The combustion model outlined in Chapter 3 based on the work of Libby and Blake (1979) provides this information. For the purpose of illustration, a simple model of combustion via a surface reaction will be used in the example calculation. The important features of coal combustion are retained in the example without requiring much detailed information about the coal char.

The local gaseous environment during combustion is described by a quasi-steady combustion model. The behavior of the gas phase is modeled as a succession of steady states, assuming that the response time of the gas is much shorter than that of the coal particle. In this way, the local environment of a single coal particle is characterized throughout the entire combustion process. A spherical coal particle is assumed to be immersed in an infinite, quiescent medium. The quasi-steady treatment of the gas phase is coupled with a dynamic particle energy balance. The chemistry of the combustion gases is assumed to be frozen. The effect of devolatilization and bulk ash on combustion are also included in the combustion model.

Radial coordinates centered on the particle are used in the analysis (Fig. 4.1). A radial convective velocity is caused by the bulk gas motion due to combustion. At typical pulverized coal combustion conditions, the important combustion reaction is $2C + O_2 \rightarrow 2CO$ (Mulcahy and Smith, 1969). For every oxygen molecule that moves toward the surface, two carbon monoxide molecules move away from the surface. The convective velocity u is proportional to the combustion rate R.

$$u = \frac{R}{4\pi r^2 c} \tag{4.1}$$

where r is radial position (in centimeters) and c is gas concentration in moles per cubic centimeter. R has units of moles per unit time.

4.2.2 Conservation Equations

Vapor is transported away from the particle's surface by convection and diffusion. Vapor is lost by both homogeneous and heterogeneous condensation. Particles formed by vapor condensation are transported away from the burning coal particle primarily by convection since the particle diffusivities are much less than that of the vapor. Vapor condensation represents a sink for vapor and a source for aerosol. Assuming the transport and growth processes to be much faster than combustion, a quasi-steady conservation equation can be written for the total volatilized ash. It will be shown later that the quasi-steady formulation is justified. The conservation equation is written in terms of y, the vapor species mole fraction, and M, the moles of aerosol per mole of gas, as

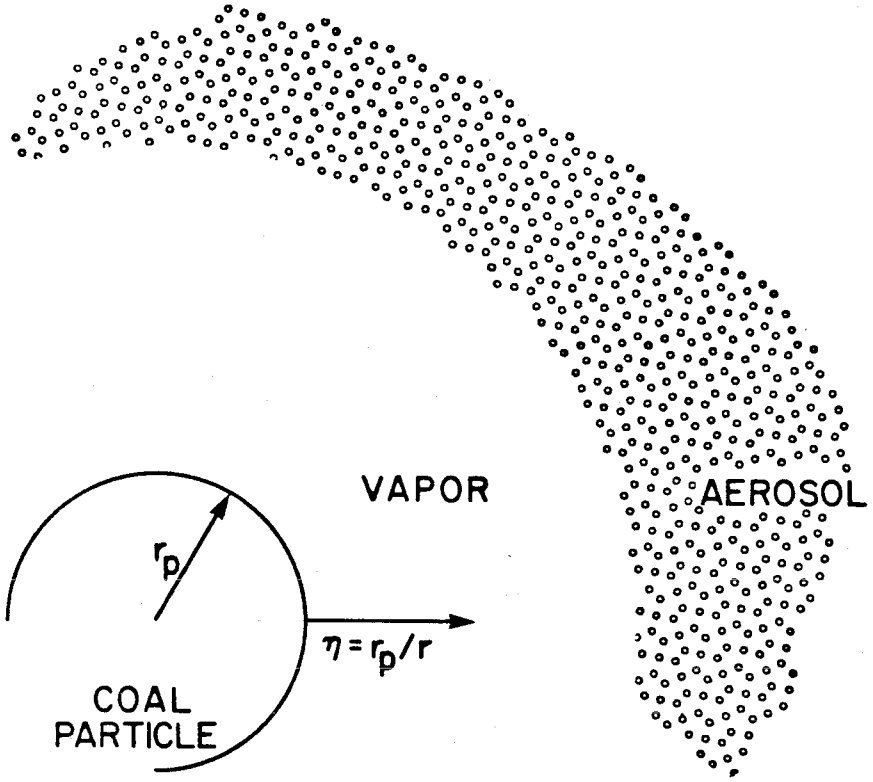

Figure 4.1 The local environment around a burning coal particle.

$$R \frac{d}{dr} (y + M) = \frac{d}{dr} (4\pi r^2 c\mathcal{D} \frac{dy}{dr}) \tag{4.2}$$

subject to

$$y = y_p \text{ at } r = r_p$$

$$y = 0 \text{ as } r \to \infty$$

$$M = 0 \text{ at } r = r_p$$

The quantity cD is assumed to be constant in the region surrounding the coal particle. It has been calculated at a temperature which is the geometric mean of the particle temperature and the free stream gas temperature. For the sake of simplicity we calculate the surface partial pressure by assuming that the vapor species is in equilibrium with liquid at the particle's surface. More complicated models for the surface boundary condition (e.g., Quann and Sarofim, 1982) could be used in the framework of this analysis.

Equation 4.2 can be solved if the aerosol mole fraction M is known. (In fact, the case of no particle formation (M = 0) has a simple analytic solution.) The aerosol mole fraction, which is proportional to the total volume of aerosol at any radial position, can be obtained by integrating the aerosol size distribution function as follows:

$$M = \frac{\rho}{M_w} \int_0^\infty \frac{\pi}{6} D^3 n(D,r) dD \tag{4.3}$$

where ρ and M_w are the species density and molecular weight. The aerosol size distribution function n has units of number per centimeter per mole of gas. D is the particle diameter.

The aerosol size distribution function is determined using an aerosol growth equation. The change in number of particles with position and particle size is expressed by three terms: convection (diffusion of particles is neglected), growth by condensation, and formation of new particles by nucleation.

$$R \frac{\partial n}{\partial r} + 4\pi r^2 c \frac{\partial (n\dot{D})}{\partial D} = 4\pi r^2 I \delta(D - D_*) \tag{4.4}$$

Particle growth by coagulation is neglected in the present analysis. The condensation growth law D is calculated for particles in the free molecule range, neglecting the Kelvin effect. Thus, the growth law becomes (Friedlander, 1977)

$$\dot{D} = \frac{2v_m(p - p_e)}{(2\pi mkT)^{1/2}} \tag{4.5}$$

v_m and m are the molecular volume and mass of the liquid state, k is the Boltzmann constant and p is species vapor pressure. The subscript e denotes equilibrium conditions.

Equation 4.4 can be solved easily because the growth rate (Eq. 4.5) is a function of radial position but not particle size. Later in the paper we discuss the validity of the assumptions that allow such a simple form for the particle growth law. The term on the right-hand of Eq. 4.4 represents the addition of new particles to the aerosol via nucleation. We assume that new particles are formed with a diameter D_* (hence the use of the delta function). The critical diameter, D_*, is a function of local temperature and saturation ratio. An average critical diameter which is independent of radial position is

used in this analysis. This is calculated as the number-average critical diameter over all space.

The nucleation rate I (in units of number per cubic centimeter per second) is given by Friedlander (1977) as

$$I = 2\alpha_c \left[\frac{p}{(2\pi mkT)^{1/2}} \right] \frac{p}{kT} v_m^{2/3} \left[\frac{\sigma v_m^{2/3}}{kT} \right]^{1/2} \exp \left[\frac{-16\pi\sigma^3 v_m^2}{3(kT)^3 \ln^2(p/p_e)} \right] \quad (4.6)$$

where σ is the surface tension of the liquid species and is assumed to be constant for a given calculation. The accommodation coefficient α_c is assumed to be unity.

4.2.3 Method of Solution

In order to transform the problem from an infinite domain to a finite one, the conservation equations are rewritten in terms of a new independent variable $\eta = r_p/r$. The method of characteristics is applied to the aerosol growth equation to derive an explicit expression for the aerosol mole fraction M. Finally, the ash conservation equation is solved numerically using a shooting method.

With this transformation the aerosol growth equation becomes

$$\frac{-R}{r_p} \eta^2 \frac{\partial n}{\partial \eta} + \frac{4\pi r_p^2}{\eta^2} c\dot{D} \frac{\partial n}{\partial D} = \frac{4\pi r_p^2}{\eta^2} I\delta(D-D_*) \quad (4.7)$$

subject to the boundary conditions

$$n(D,1) = 0$$

$$n(D_*,\eta) = 0$$

Equation 4.7 is to be solved using the method of characteristics. The solution is found along trajectories of the size distribution function, n; these trajectories are called characteristics and depend on initial conditions. Along a characteristic the dependent and independent variables are related by

$$\frac{-d\eta}{R\eta^2/r_p} = \frac{dD}{4\pi r_p^2 c\dot{D}/\eta^2} = \frac{dn}{4\pi r_p^2 I\delta(D-D_*)/\eta^2} \tag{4.8}$$

This equation can be rearranged to obtain two ordinary differential equations for $dD/d\eta$ and $dn/d\eta$. Noting that $\delta(D-D_*)dD = \delta(\eta-\eta_*)d\eta$, the size distribution in Equation 4.8 can be evaluated explicitly in terms of η_* instead of D, yielding

$$n(D,\eta) = \frac{I(\eta_*)}{c\dot{D}(\eta_*)} \tag{4.9}$$

where η_* is defined as the position where a particle must nucleate in order to grow to a diameter D at a radial position η. The relationship between η, η_*, D, and D_* is known along a characteristic from the solution to Eq. 4.8.

The integral of the aerosol size distribution function must be evaluated to solve Eq. 4.2. Substituting Eq. 4.9 into the integral (Eq. 4.3) and changing the integration variable from D to η_*, we find

$$M = -\frac{4\pi r_p^3 \rho}{RM_w}\int_1^{\eta} \frac{\pi}{6} \frac{D^3(\eta_*)I(\eta_*)}{\eta_*^4} d\eta_* \tag{4.10}$$

Thus the total amount of aerosol at any radial position is related simply to the nucleation rate and the growth rate. In order to obtain Eq. 4.10, the lower limit of the integral in Eq. 4.3 has been changed to D_*. For the conditions we will consider, the critical nucleus is only a few molecules so this change has little affect on the final numerical answer.

The method of characteristics provides an expression for the aerosol mole fraction which can be evaluated at any radial position. To complete the solution, the ash conservation equation is integrated once which gives

$$4\pi r_p c\mathcal{D} \frac{dy}{dr} = R(y + M) - R_v \tag{4.11}$$

R_v is an unknown constant of integration equal to the rate of vaporization at the particle's surface. Equation 4.11 is transformed to inverse radial coordinates to give the following:

$$\frac{d\tilde{y}}{d\eta} = -Pe\ (\tilde{y} + \tilde{M} - R_v/y_p R) \tag{4.12}$$

subject to

$$\tilde{y}\ (1) = 1$$

A tilde over a variable means that it has been normalized with respect to y_p. The Peclet number at the particle's surface is defined as

$$Pe = \frac{R}{4\pi r_p c\mathcal{D}} \tag{4.13}$$

Equations 4.10 and 4.12 can be integrated from the surface of the coal particle (η =1) to infinite radius (η =0). A shooting method is

employed to solve the system. Beginning with an initial estimate for the vaporization rate R_v, the properties at $\eta=0$ are evaluated. The system is integrated using a modified fourth-order Runge-Kutta scheme developed by Fehlberg (1969). If the correct value for R_v has been used, the mole fraction of vapor will be zero at the boundary $\eta=0$. If not, a new value of R_v is chosen and the calculation is repeated.

4.3 Results

In order to examine the behavior of the model and its sensitivity to parameter variation, an example is discussed in which the ash is represented by single species. Two aspects of the solution are important: the character of the aerosol produced and the rate of vaporization of the ash species. The influence of the ash properties and the local combustion environment on the aerosol size distribution and vaporization rate will be examined.

4.3.1 Example: Silica Vaporization During Combustion

Silica is chosen to represent the ash for several reasons. First, it is found in significant quantities in both the bulk ash and in the submicron aerosol (Neville et al., 1981) produced from coal combustion. Silica is representative of a class of compounds found in ash, often called refractory oxides, which have a relatively low volatility at temperatures below 2000 K and yet are found to be major constituents of the submicron aerosol. Calcium oxide and magnesium oxide are two other

TABLE 4.1: CONDITIONS FOR EXAMPLE CALCULATIONS

COAL COMBUSTION	
Particle radius, micron	40
Volume fraction ash	0.05
Inclusion diameter, micron	2.5
Free stream gas temperature, K	1750
Free stream gas	Air
ASH	
Surface tension, dynes/cm	300
Liquid density g/cm^3	2.2
Molecular weight, g/mole	60.9
Diffusivity: $c\mathcal{D} = aT + b$	
a, mole/cm-sec-K	9.11×10^{-9}
b, mole/cm-sec	7.363×10^{-6}

compounds in this class. Finally, the requisite physical and thermodynamic properties for silica can be found in the literature. The latter point is not a trivial one. The present model requires equilibrium vapor pressure, liquid density, surface tension, and gaseous diffusivity for the compound of interest. Values for these properties are often difficult to obtain for high temperature oxides.

For the present work we assume that liquid oxide on the particle's surface is in equilibrium with vapor. In a high temperature environment such as that surrounding a burning char particle, the reduction of silica (SiO_2) to form gaseous silicon monoxide (SiO) determines the vapor pressure of silicon-containing species (Schick, 1960). We assume that the equilibrium vaporization reaction may be written as

$$SiO_{2(\ell)} + CO \rightleftharpoons SiO_{(g)} + CO_2$$

The primary product of carbon combustion at high temperatures is carbon monoxide (Mulcahy and Smith, 1969). If the subsequent oxidation to carbon dioxide occurs far from the particle, the only source of CO_2 near the particle is the SiO_2 reaction. The CO_2 partial pressure is, therefore, assumed to be equal to the SiO partial pressure. The equilibrium vapor pressure of silicon monoxide is given by

$$P_{SiO} = (Ka_\ell P_{CO})^{1/2} \qquad (4.14)$$

K is the equlibrium constant calculated from the JANAF Tables (Dow Chemical Company, 1971) and a_1 is the activity of the liquid silica (assumed to equal one). Equation 4.14 is used to calculate the SiO

partial pressure at the coal particle surface and to calculate the equilibrium pressure needed to evaluate the condensation flux (Eq. 4.5). Hence we assume that SiO vapor is oxidized to SiO_2 which then condenses as liquid.

Consider a bituminous coal particle with 40 micron inital radius burning in air which has been heated to 1750 K. Figure 4.2 shows the temperature and gas composition at the particle's surface as a function of burnout for this coal particle. (Burnout is defined as the volume fraction of carbon which has been lost by devolatilization or combustion.) During devolatilization (burnout less than about 50%) the particle temperature is less than the gas temperature. Char combustion becomes important for burnout greater than 50%. Due to the exothermicity of the char combustion reaction, there is a rapid rise in particle temperature to 400-500 degrees above the gas temperature. Figure 4.2 also shows the oxygen and carbon monoxide partial pressure at the surface. For combustion in air there is no carbon dioxide in the gas, since the gas-phase chemistry is frozen. During devolatilization the oxygen partial pressure at the surface remains relatively constant, but it drops sharply when char combustion becomes important. At this point the carbon monoxide concentration increases due to combustion.

The quantities needed for the aerosol calculation are the instantaneous radial profiles of gas composition and temperature. Figure 4.3 shows these profiles evaluated at 64% burnout. The significant feature of these curves is that both temperature and carbon

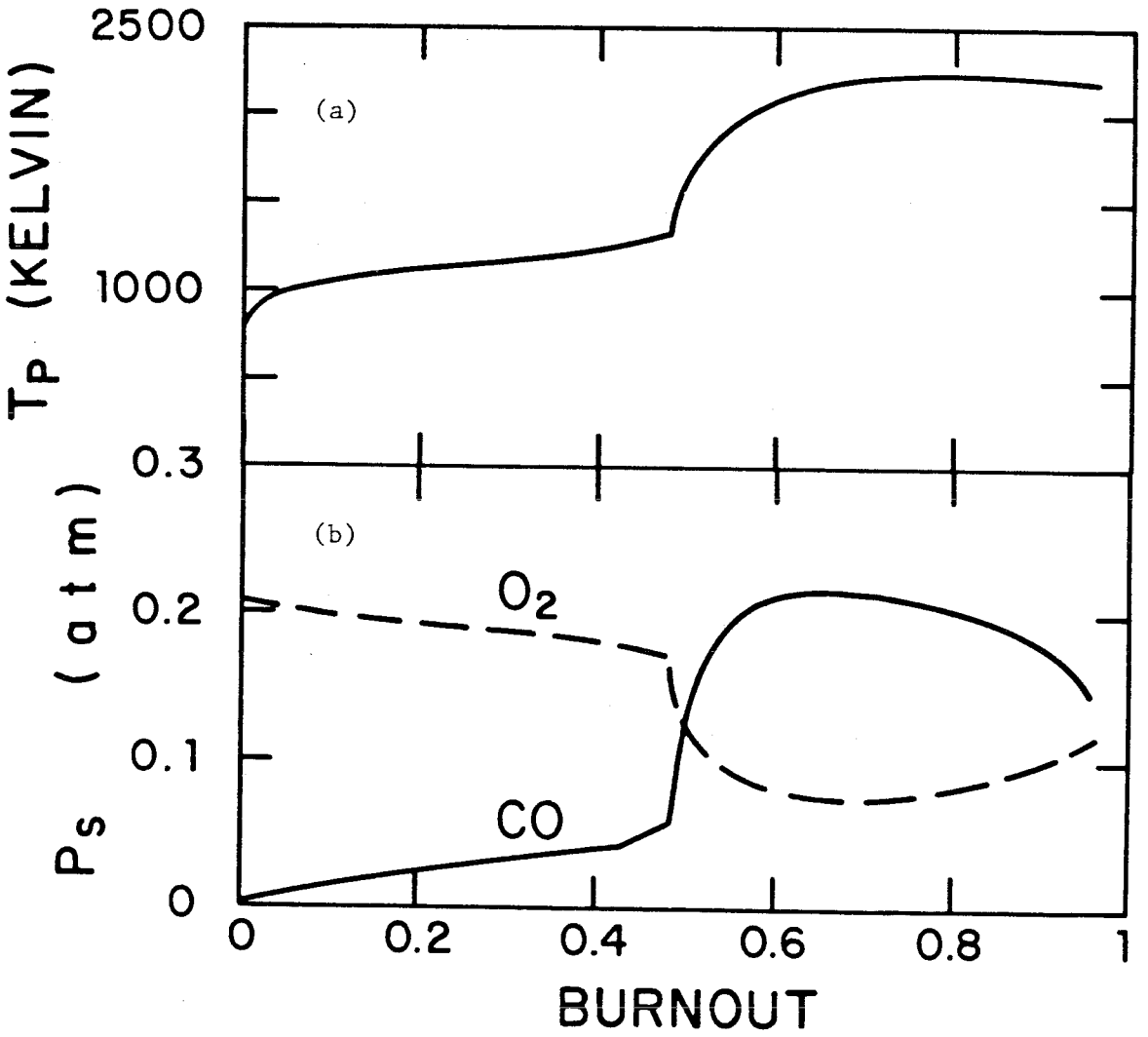

Figure 4.2 Particle temperature and gas composition at the surface of a bituminous coal particle (40 micron initial radius) burning in air with a gas temperature of 1750 K. (a) particle temperature in degrees Kelvin. (b) gas composition at the surface. ——— CO partial pressure. – – – – O_2 partial pressure.

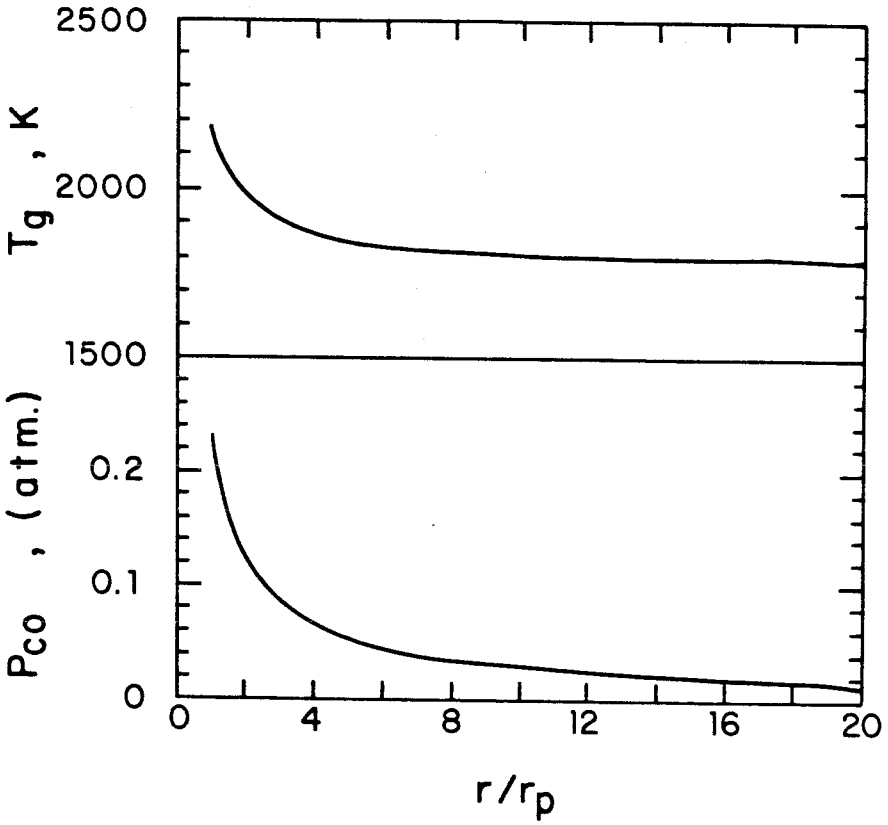

Figure 4.3 Profiles of gas temperature and carbon monoxide around a burning coal particle at 64% burnout.

monoxide partial pressure drop sharply within about three particle radii from the surface. This results in a rapid decrease in the equilibrium vapor pressure with increasing radius, since the vapor pressure depends strongly on temperature and carbon monoxide partial pressure.

4.3.2 Aerosol Formation

The size distribution function (Eq. 4.9) is inversely proportional to the condensation rate and proportional to the nucleation rate. Since the nucleation rate varies exponentially with the parameters in the system,i.e.,

$$I \sim \frac{y^2}{T} \frac{(\sigma M_w)}{\rho}^{1/2} \exp\left[-\left(\frac{M_w}{\rho}\right)^2 \left(\frac{\sigma}{T}\right)^3 \frac{1}{\ell n^2 S}\right] \qquad (4.15)$$

where $S = p/p_e$ is the saturation ratio, it should have the larger influence on the aerosol size distribution. Both the ash properties (molecular weight, density, and surface tension) and the local combustion environment strongly influence nucleation rate and the resulting aerosol. The saturation ratio is a function of both local gas temperature and local gas composition as described in Eq. 4.14. In the aerosol calculation, we shall use constant values for the physical properties of silica (Kingery, 1959; Smithells, 1976). In the next section the effect of the variation of physical properties is discussed.

Figure 4.4 shows the results of the aerosol calculation at 64% burnout. Plotted are the radial profiles of saturation ratio and logarithms of nucleation rate, total number concentration, and average

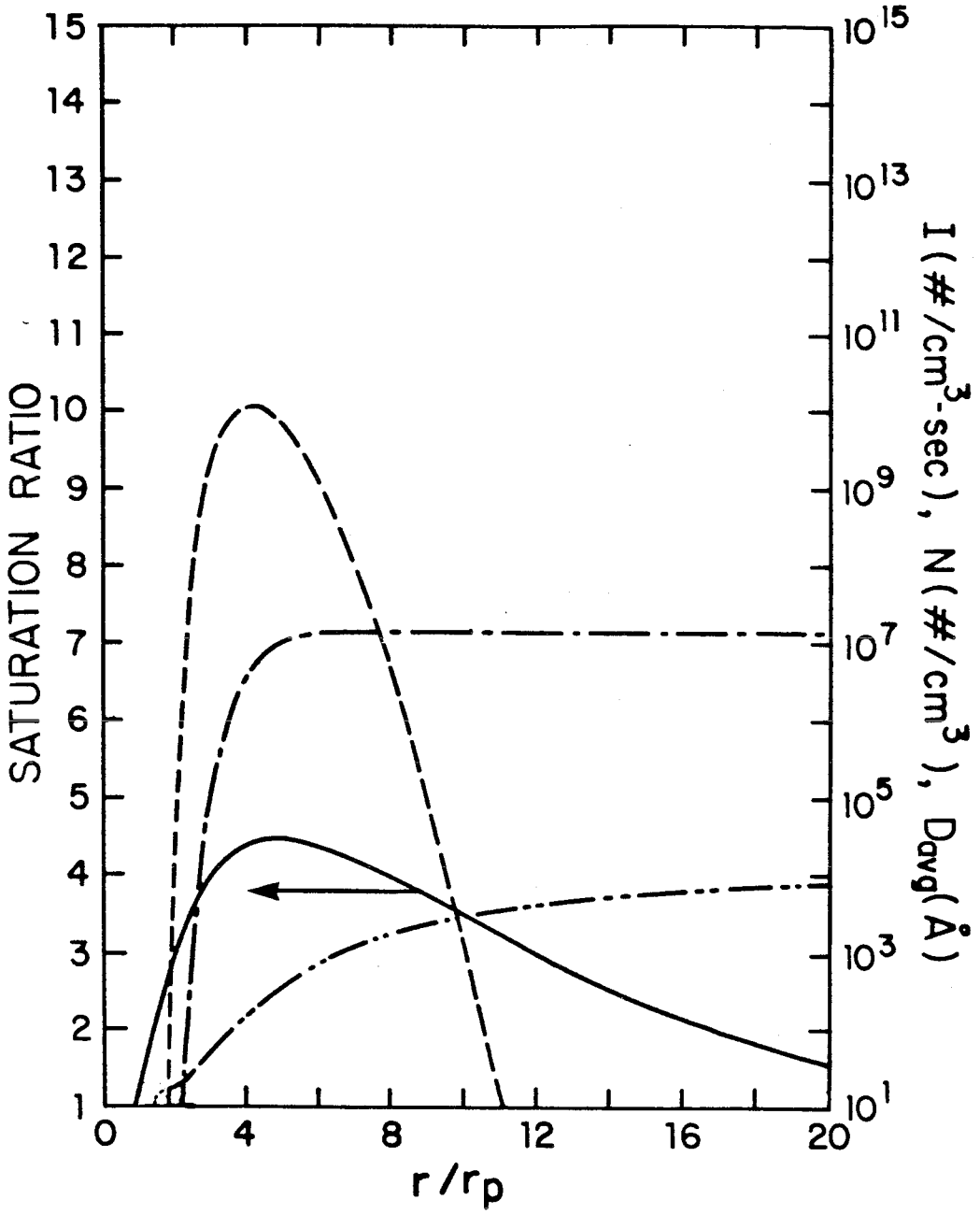

Figure 4.4 Results of the aerosol calculation for silica at 64% burnout.

——— Saturation ratio. — — — Nucleation rate, #/cm^3-sec. —·—·— Number density, #/cm^3. —·—·—·— Average diameter, Angstrom.

diameter. The saturation ratio rises very sharply with radial position and peaks three radii from the particle's surface. It is in this region that both the gas temperature and the carbon monoxide partial pressure are rapidly decreasing (Fig. 4.3). The saturation ratio decreases slowly beyond three radii due, for the most part, to depletion of vapor by condensation. As the saturation ratio increases, so does the nucleation rate. The number concentration also grows rapidly within three particle radii. But farther away from the particle the number concentration is constant because the nucleation rate becomes too small to change the total number significantly. The average diameter increases slowly with radial position due to condensation; it is still increasing at large radial positions.

The preceding discussion applies to a single instant in the combustion history. Local conditions change dramatically throughout the combustion as was shown in Fig. 4.2. In order to consider the influence of local combustion environment on the aerosol, we shall perform the aerosol calculation at various points in the sample combustion history. Figure 4.5 gives aerosol number concentration, mass loading, and average diameter as a function of burnout for several different radial positions. It is evident from all three parts of this figure that there is no vaporization or aerosol formation during devolatilization.

The number concentration (Fig. 4.5a) increases dramatically one to three particle radii from the particle's surface. For radial positions greater than this, there is almost no change in the total number of

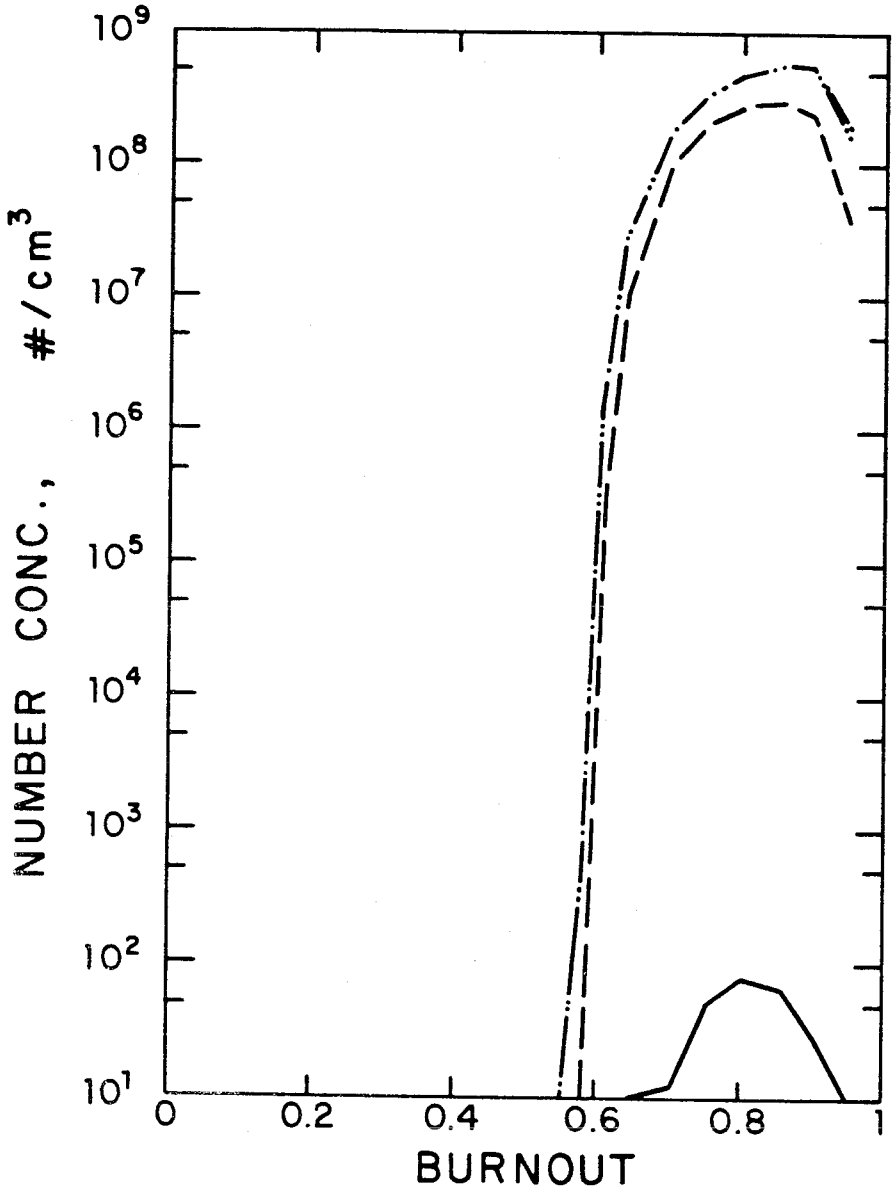

Figure 4.5a Number concentration of the aerosol as a function of burnout. —— 1 particle radius from the surface. — — — 3 particle radii from the surface. —·—·— 5 particle radii from the surface. —·—·—·— 8 particle radii from the surface.

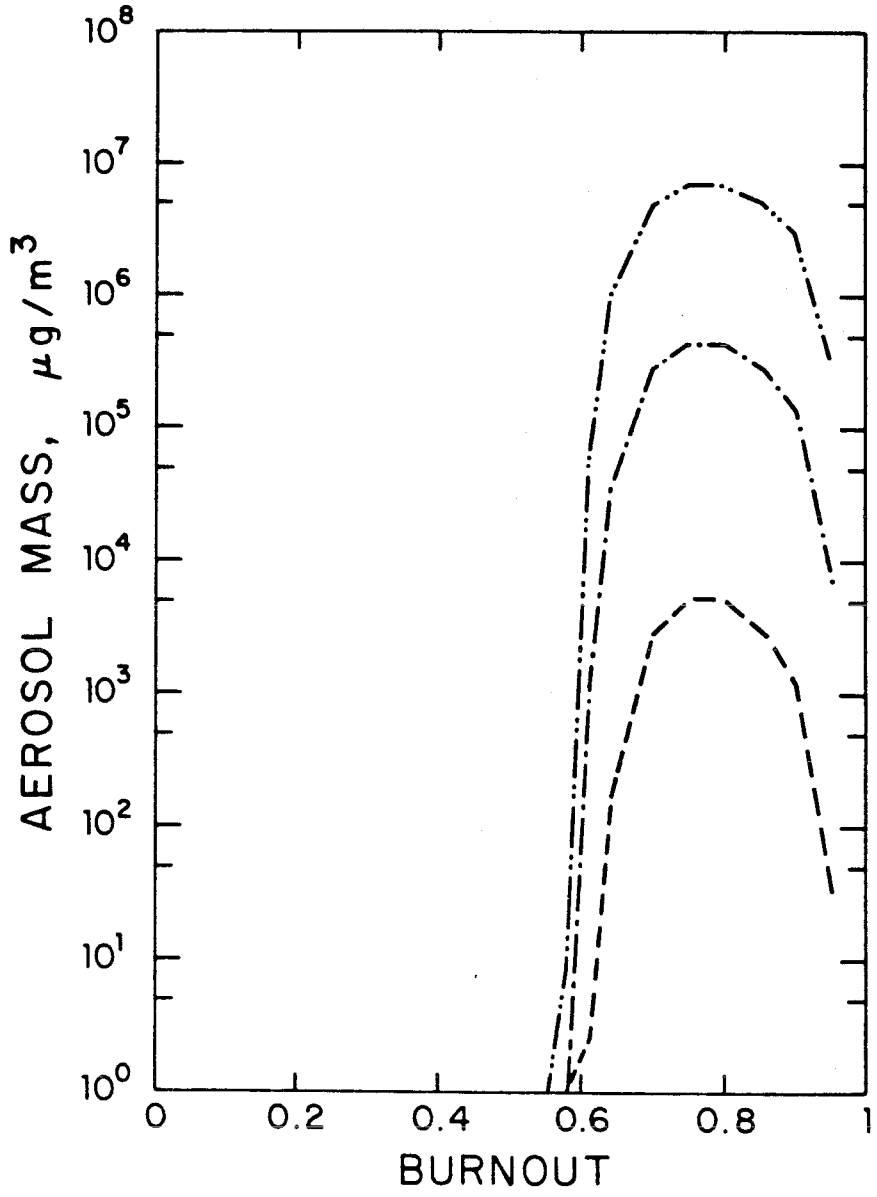

Figure 4.5b Mass loading of the aerosol as a function of burnout.

——— 1 particle radius from the surface. — — — 3 particle radii from the surface. —·—·— 5 particle radii from the surface. —·—·—·— 8 particle radii from the surface.

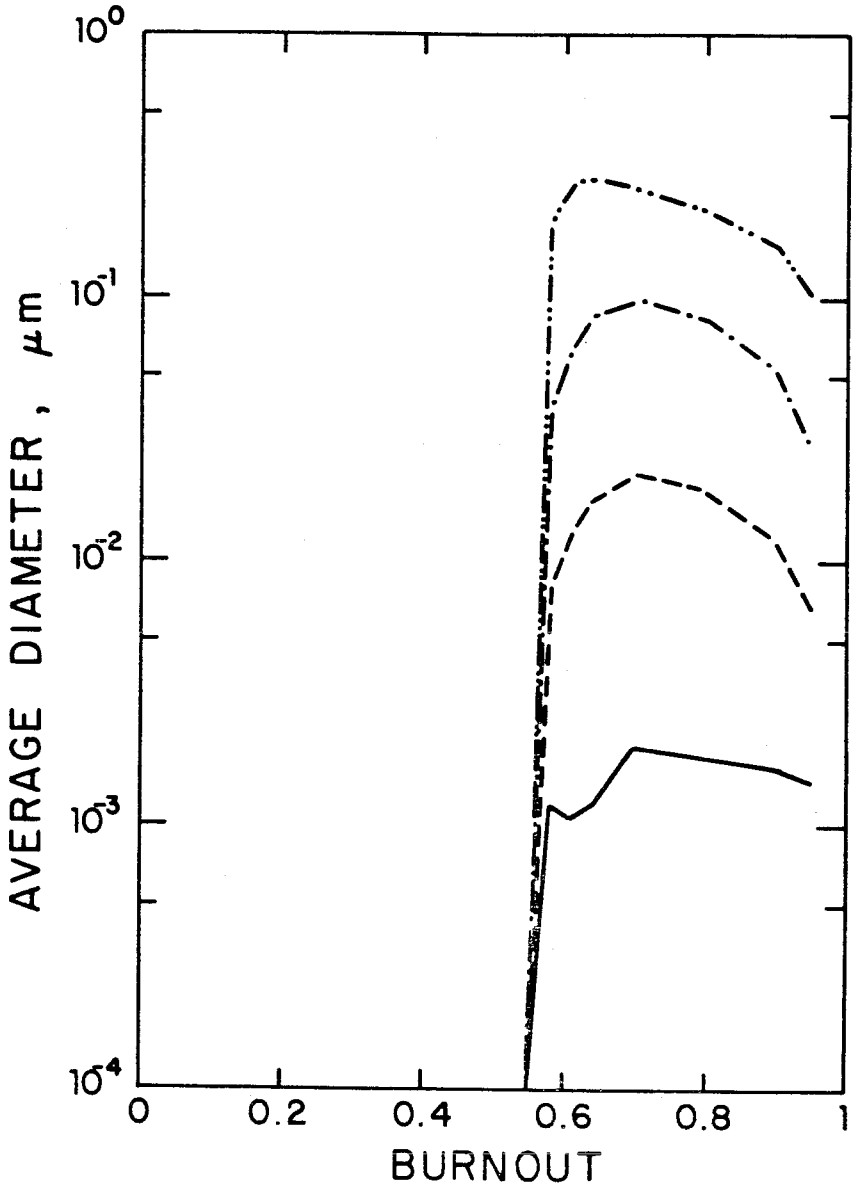

Figure 4.5c Average particle diameter of the aerosol as a function of burnout.

—— 1 particle radius from the surface.
– – – 3 particle radii from the surface.
—·—·— 5 particle radii from the surface.
—··—··— 8 particle radii from the surface.

particles. The mass loading (Fig. 4.5b), however, steadily increases with radial position after the total number has stopped changing, due to the growth of aerosol by condensation. Within eight particle radii of the surface, the mass loading reaches very high values. The effect of condensation can also be seen in Fig. 4.5c where the average aerosol diameter is plotted versus burnout. In this example, the average diameter grows larger than 0.1 micron within eight particle radii from the surface.

Finally, we consider the variation of vaporization rate with combustion conditions in order to quantify the effects of local conditions and aerosol formation on vaporization. If there is no aerosol in the gas, the vaporization rate, R_{vo}, is

$$R_{vo} = \frac{Ry_p}{1-e^{-Pe}} \tag{4.16}$$

Figure 4.6 shows the vaporization rate calculated for various values of burnout plotted against the corresponding value of R_{vo}. The formation and growth of the aerosol increases vaporization by less than ten percent for the sample combustion history. The Peclet number at the particle's surface is near one for these calculations and, therefore, some of the transport of vapor from the particle's surface is by convection. The influence of the vapor concentration gradient on vaporization is somewhat damped by convection.

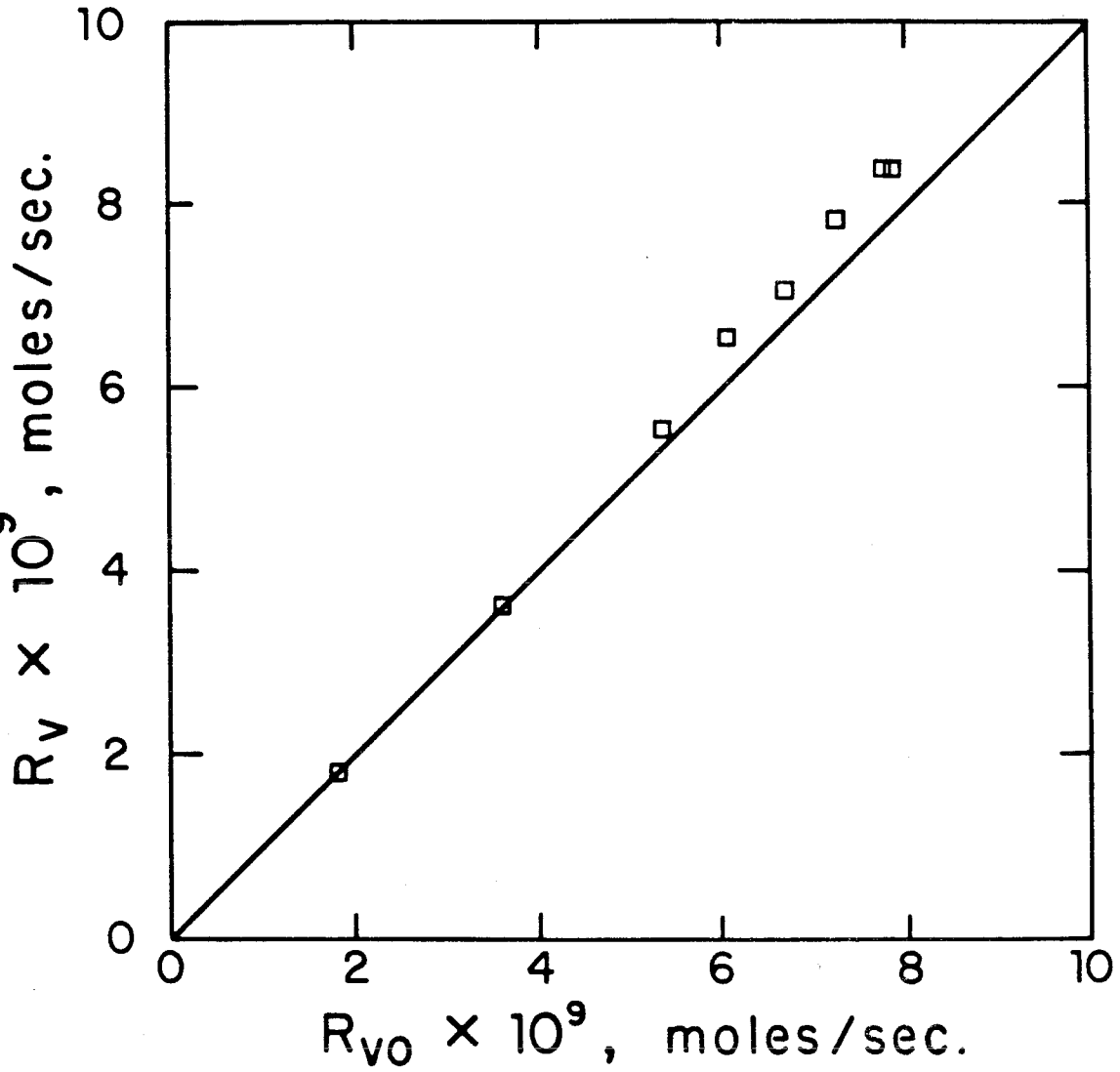

Figure 4.6 Effect of aerosol formation and growth on the vaporization rate.

4.3.3 Effect of Physical Properties

The effects of ash properties on aerosol formation may be examined by considering the influence of surface tension variation. Equation 4.15 shows which other physical properties, e.g., molecular weight and density, will have similar effects on the aerosol size distribution. The local temperature and composition profiles used are those given in Fig. 4.3. The value of the surface tension of silica used in the previous calculation was 300 dynes per centimeter; this value corresponds to that measured by Kingery (1959) at a temperature of 1900 K. Due to temperature variations with radial position, the surface tension of silica actually varies from 310 to 295 dynes per centimeter.

Decreasing the surface tension produces a higher nucleation rate and number concentation. Fig. 4.7a shows the calculation with a surface tension of 250 dynes per centimeter. The peak nucleation rate and the final number concentration have increased by two orders of magnitude with only a 17% decrease in surface tension. In parts b and c the surface tension has been increased to 350 and 400 dynes per centimeter, respectively. High values of the surface tension suppress nucleation. A 14% increase in surface tension (Figure 4.7b) causes the peak nucleation rate to decrease by four orders of magnitude. At even higher values of the surface tension nucleation ceases entirely and there are essentially no particles formed.

The value of the surface tension has a profound effect on the character of the aerosol because the nucleation rate is such a strong

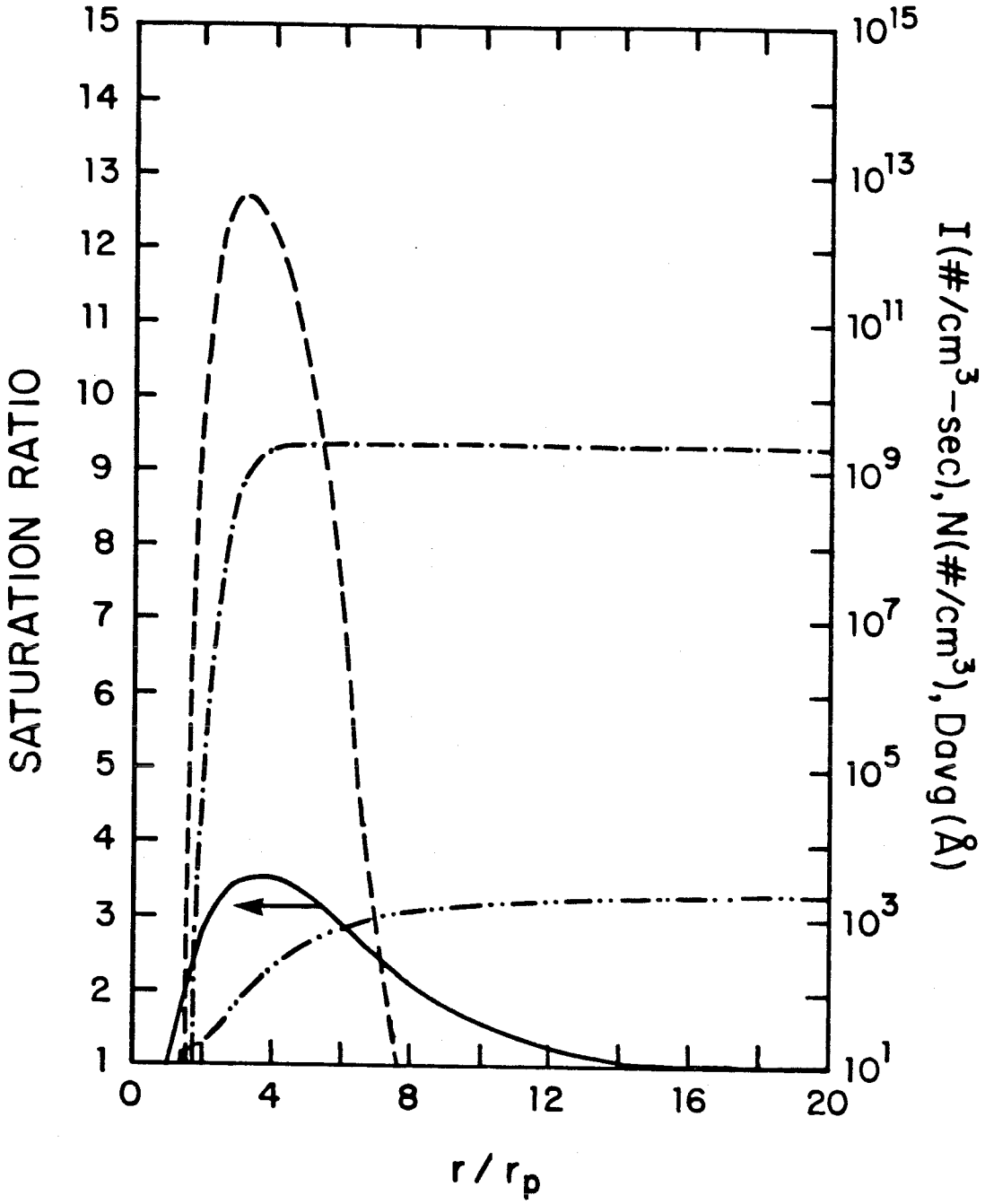

Figure 4.7a Characteristics of the aerosol as a function of surface tension: 250 dynes per centimeter.

——— Saturation ratio. — — — Nucleation rate, #/cm³-sec. —.—.— Number density, #/cm³. —..—..— Average diameter, Angstrom.

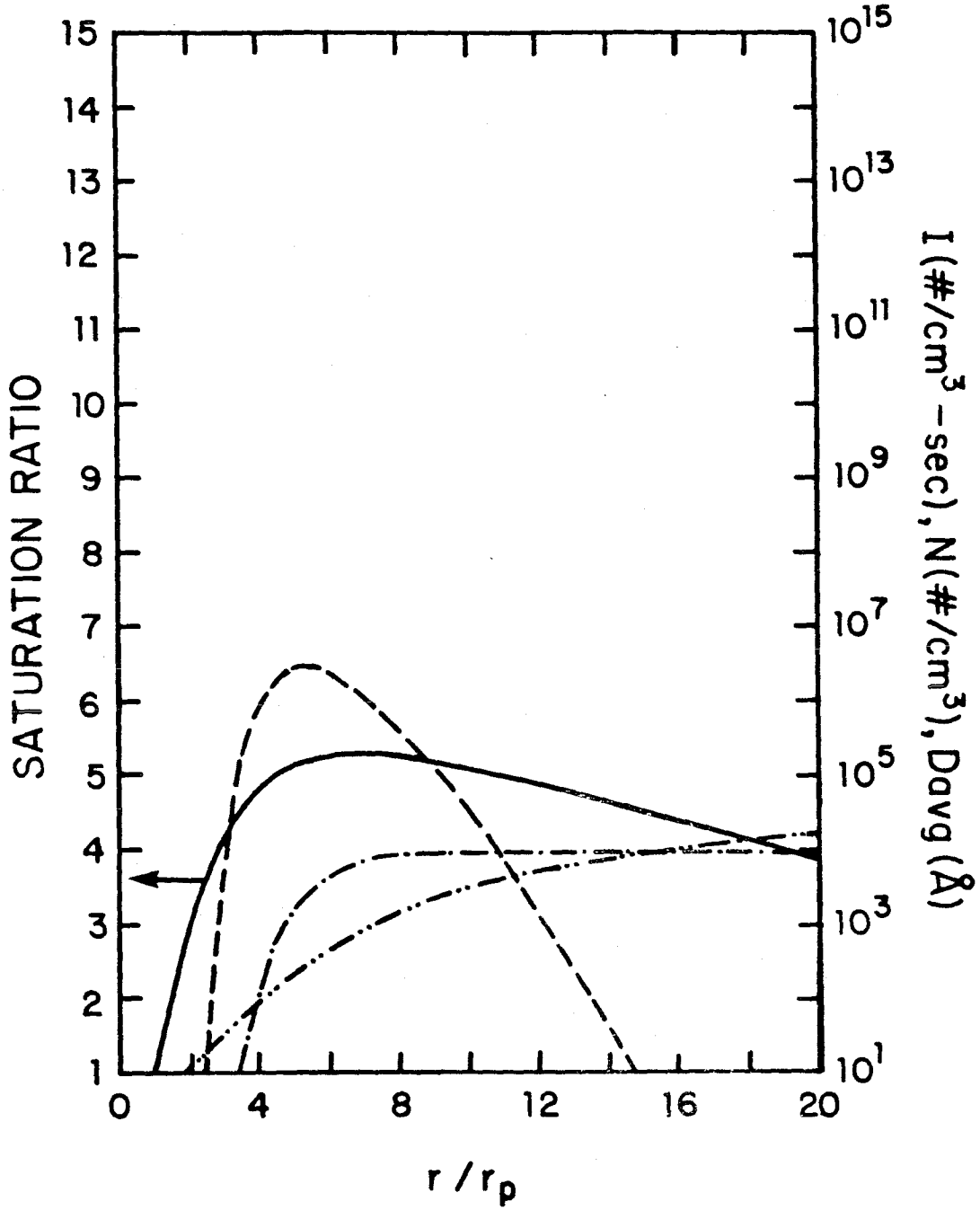

Figure 4.7b Characteristics of the aerosol as a function of surface tension: 350 dynes per centimeter.

——— Saturation ratio. — — — Nucleation rate, #/cm³-sec. —.—.— Number density, #/cm³. —.._..— Average diameter, Angstrom.

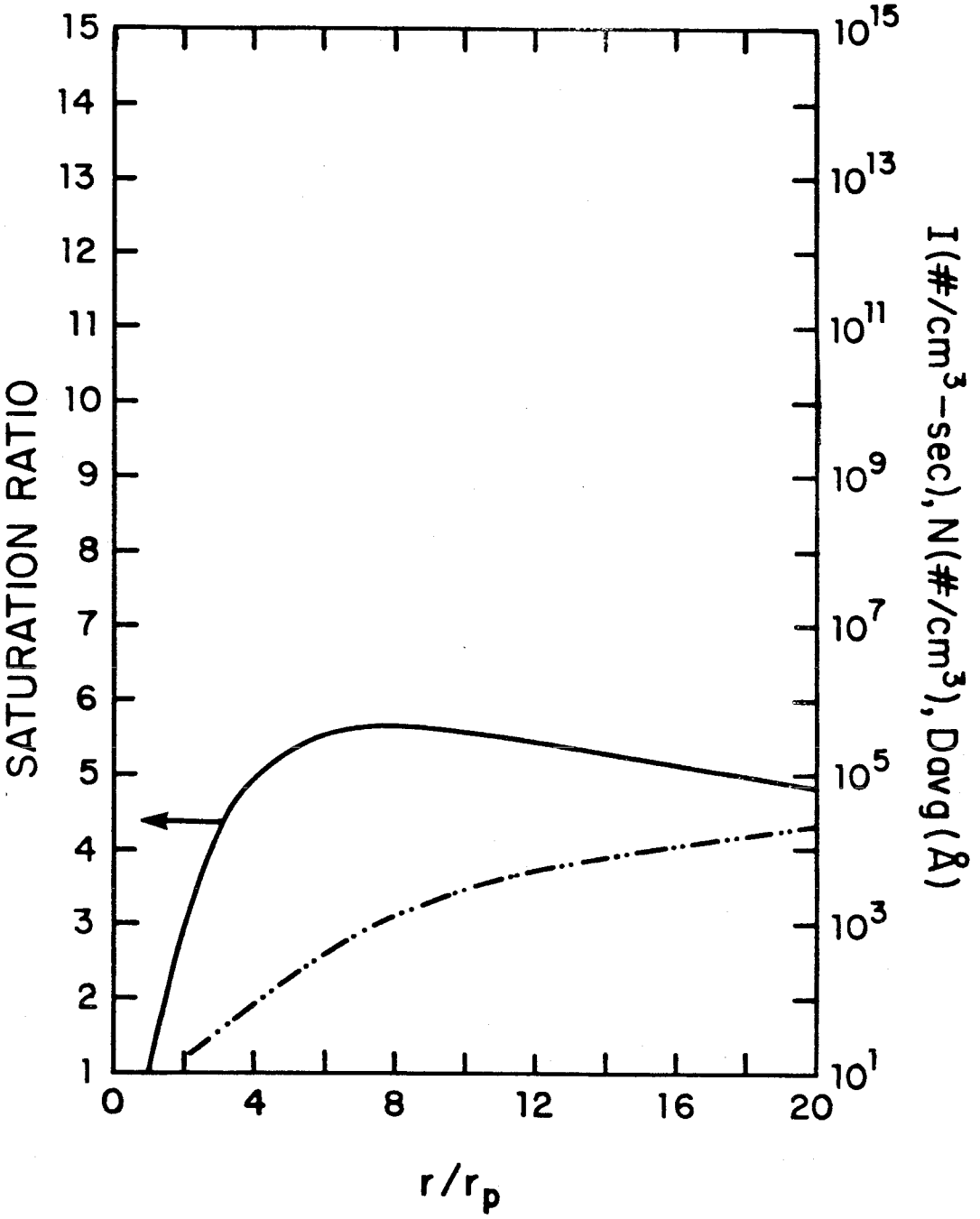

Figure 4.7c Characteristics of the aerosol as a function of surface tension: 400 dynes per centimeter.

——— Saturation ratio. — — — Nucleation rate, #/cm³-sec. —.—.— Number density, #/cm³. —.—.—.— Average diameter, Angstrom.

function of surface tension. However, the vaporization rate is not strongly affected by ash properties. For the preceding cases there is only a five percent variation in vaporization rate even though the amount and size of the aerosol varies over many orders of magnitude.

4.4 Validity of assumptions

Now that the results of a sample calculation have been presented, we shall examine the validity of the major assumptions that have been made in the formulation of the model. A steady conservation equation for the transport of ash (Eq. 4.2) has been superimposed on the solution to the combustion problem. In order to employ this method, the time scales for transport and aerosol growth must be much shorter than the combustion time scale. The expression for the nucleation rate (Eq. 4.6) is derived assuming the existence of a quasi-steady state for the distribution of molecular clusters. For the theory to be valid, there must be sufficient time for the establishment of this steady state. Coagulation has been omitted from the aerosol growth equation (Eq. 4.4) in order to simplify the analysis. We have assumed implicitly that the coagulation process is much slower than the transport and aerosol growth processes. The validity of these assumptions can be judged by comparing the time scales of various processes: combustion, convection, vapor diffusion, nucleation, and coagulation. Finally, we have used an aerosol growth law (Eq. 4.5) for particles in the free molecule regime (neglecting the Kelvin effect) and we shall assess the qualitative effects of this approximation on the aerosol size distribution.

The characteristic times of the relevant processes are shown in Fig. 4.8 at a representative point in the combustion history (64% burnout). Since convective velocity, vapor concentration, and aerosol number concentration change with radial position, the characteristic times are calculated as functions of radial position. The length scale used in calculating the characteristic times is the coal particle radius. The nucleation time represents the time required to establish a quasi-steady distribution of molecular clusters as proposed by Wakeshima (1954). A range of characteristic times for coagulation is estimated from the total aerosol number and the Brownian coagulation coefficient (Gelbard, 1978) calculated for collision between a particle of the critical size (one nanometer) and representative-sized particle . The lower bound on the characteristic time represents collision with a one micron particle and the upper bound, with a particle of the average diameter.

The combustion time scale is much slower than any of the transport or growth time scales. Within at least 10-20 particle radii of the coal particle, the vapor and aerosol are always in steady state with respect to combustion. The time required to establish a steady state for nucleation is at least an order of magnitude less than the characteristic convection time for $r/r_p > 2$. At smaller radial positions the nucleation rate is too small to be significant. The calculation of the nucleation rate (Eq. 4.6) assumes that there is a steady state distribution of molecular clusters. This assumption is justified in the regions where nucleation is important.

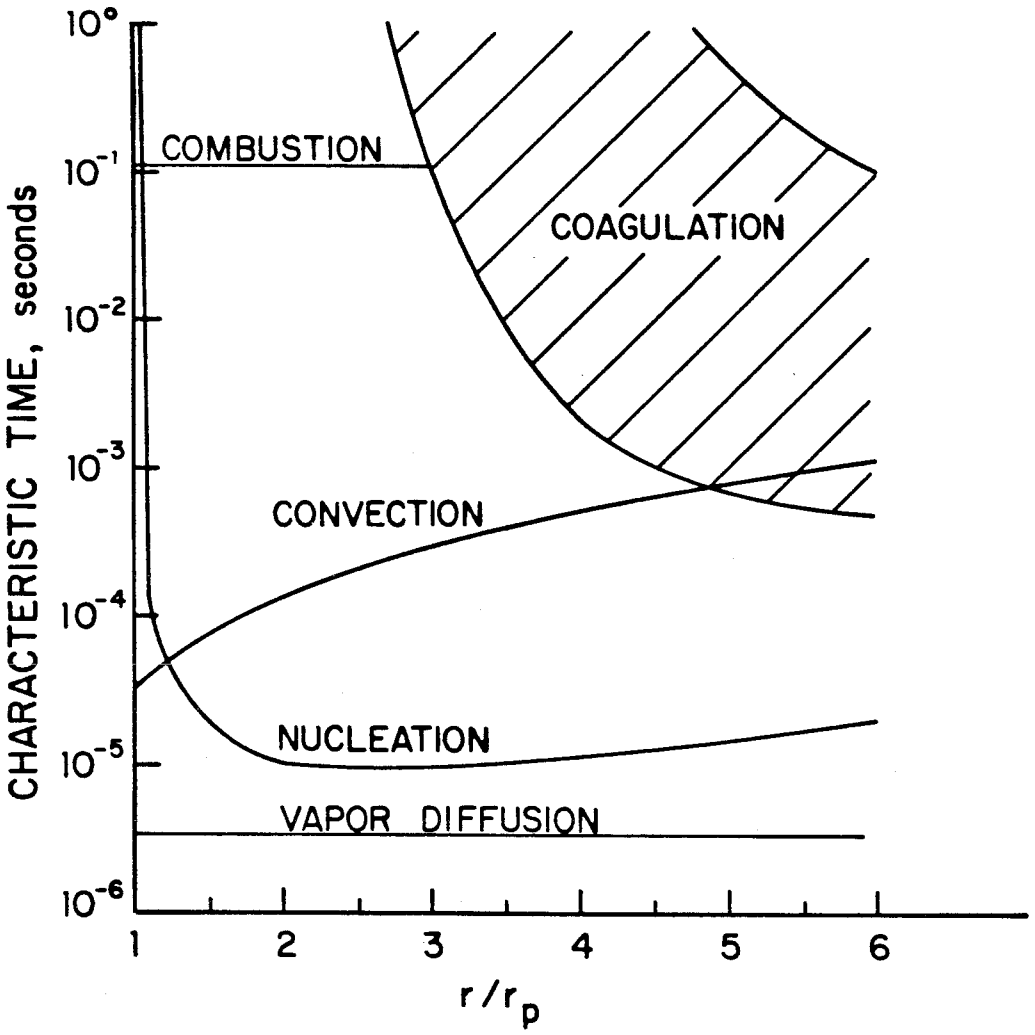

Figure 4.8 Characteristic times as a function of radial position at 64% burnout.

In the region where nucleation is important coagulation is too slow to have any effect on the aerosol size distribution. Figure 4.8 suggests that coagulation may become significant at 5-10 radii from the coal particle. However, addition of coagulation to the model would not alter the qualitative results: early nucleation of vapor followed by slow growth as the aerosol moves far from the particle's surface.

At the gas temperatures in the sample calculation the mean free path in the gas is on the order of 0.5 micron. Near the coal particle, the results suggest that the aerosol is much smaller than the mean free path and therefore the use of the growth law in the free molecule regime is correct. For radial positions greater than about ten particle radii, the average aerosol diameter approaches the mean free path length. In this region, the free molecule growth law overpredicts the growth rate of aerosol particles. Therefore if the transition from free molecule to continuum growth were included in the growth rate, the particles would not grow as fast as indicated by the calculations far away from the coal particle's surface.

At conditions typical of the sample calculation, the Kelvin effect is important for aerosol particles in the range of one to five nanometers. By neglecting the Kelvin effect, we are overpredicting the growth rate for particles in this size range. Including the Kelvin effect would make the aerosol smaller on average, while increasing the nucleation rate. That is, there would be less depletion of vapor by particles near the critical size and therefore more nucleation.

4.5 Conclusions

A mathematical model has been developed to describe the vaporization and condensation of ash in coal during combustion. The behavior of a single particle is studied in order to evaluate the influence of the local combustion environment on aerosol formation. A steady-state solution to the problem of aerosol transport and growth can be superimposed on the quasi-steady combustion problem both because the time scales of the relevant processes are much shorter than the combustion time scale and because the concentration of vapor and aerosol is too small to affect combustion.

The local combustion environment has a large influence on both vaporization and aerosol formation. The radial convective velocity enhances the transport of vapor. Higher temperatures and a locally more reducing atmosphere increase the amount of ash vaporized. The steep gas temperature and composition gradients near the coal particle provide a strong driving force for nucleation and condensation. Certain properties of the ash strongly influence the nucleation rate and the aerosol size distribution. Therefore, the present, relatively unsophisticated calculation can be used to identify combustion conditions or ash species which are likely to produce a particular kind of aerosol.

The vaporization rate of ash is only weakly dependent on the presence of the aerosol in the gas, partly because of the convective

transport (due to combustion) at the particle's surface. Detailed knowledge of the aerosol formation or growth processes is, therefore, not needed for the calculation of ash vaporization rates.

For refractory species like silica, nucleation occurs during combustion and takes place very near the coal particle. Nucleation is, therefore, controlled by the combustion process rather than by heat transfer from the combustion gases or other processes which follow combustion. Calculations indicate that coagulation may be neglected within 5-10 radii from the coal particle. It does not become important until virtually all the nucleation has taken place.

Further work is needed to elucidate the relative importance of coagulation and condensation as mechanisms for ash particle growth. This study also reveals a need for better characterization of the high-temperature physical properties of ash and a better understanding of the factors which govern ash vaporization.

NOMENCLATURE

a_1	Species activity in solution
c	Molar gas concentration, mole/cm^3
D	Aerosol diameter
$\mathcal{D}$	Gas diffusivity, cm^2/sec
I	Nucleation rate, #/cm^3-sec
K	Equilibrium constant
m	Species molecular weight, g/molecule
M	Aerosol mole fraction
M_w	Species molecular weight, g/mole
n	Aerosol Distribution Function, #/mole-cm
P	Pressure, atm
r	Radial position, cm
R	Combustion rate, mole/sec
R_v	Vaporization rate, mole/sec
S	Saturation ratio
T	Temperature
u	Radial velocity, cm/sec
v_m	Species molecular volume, cm^3/molecule
y	Species gas mole fraction

Greek Letters

α_c	Accommodation coefficient
η	Dimensionless inverse radius, r_p/r
ρ	Species density, g/cm^3
σ	Surface tension, dynes/cm

Superscripts

$\sim$	Denotes division by y_p

Subscripts

e	Equilibrium value
p	Conditions at particle's surface
*	Denotes critical condition

CHAPTER 5

AEROSOL MODEL: THERMOPHORESIS

5.1 Thermophoretic force on a free molecule-size aerosol

Small particles suspended in a temperature gradient experience a force in the direction opposite to that of the gradient. This phenomenon, thermophoresis, can be observed by holding a cool plate above a flame. Soot particles will be driven from the hot region near the flame to the cooler region near the plate.

Thermophoretic forces arise from unequal momentum transfer to a particle from the gas. Molecules arriving at the particle's surface have more momentum if they come from the hot part of the gas than from the cool part of the gas. Thus more momentum is transferred to the particle on its "hot" side. This inequality in momentum transfer produces a force on the particle; The direction of this force is opposite to the direction of the temperature gradient in the gas.

From the preceding chapter, it is obvious that pronounced temperature gradients exist around a burning coal particle.

Thermophoresis may be important to the transport of aerosol away from the burning coal particle. In this chapter, the equations are presented for the force balance on a particle in the free molecule size range. An approximate solution for the thermophoretic velocity in this system is developed and applied to the existing theoretical framework.

Consider a particle moving relative to a stationary gas. If there is no net acceleration on the particle the thermophoretic force is balanced by drag:

$$F_V + F_T = 0 \tag{5.1}$$

The thermophoretic velocity for the limit $Kn \to \infty$ (and assuming complete thermal accomodation) is given by Waldman (1959):

$$\lim_{Kn\to\infty} F_T = F_{T_\infty} = -2\pi\nu\mu \frac{R^2}{\lambda} \frac{(\nabla T)_r}{T} \tag{5.2}$$

Kn is the Knudsen number, equal to λ/R. λ is the mean free path of gas molecules and R is the particle radius. μ and ν are the viscosity and kinematic viscosity, respectively. F_V can be calculated from the Millikan drag formula:

$$F_V = \frac{6\pi\mu VR}{1 + \lambda/R(A + Be^{-CR/\lambda})} \tag{5.3}$$

where A = 1.2, B = 0.41, and C = 0.88. With the inclusion of these terms the force balance becomes

$$\frac{3V_T}{R/\lambda + A + Be^{-CR/\lambda}} - \frac{\nu(\nabla T)_r}{T} = 0 \tag{5.4}$$

Rearranging Eq. 5.4 and taking the free molecule limit, $Kn \to \infty$ gives and expression for the thermophoretic velocity:

$$V_{T_\infty} = - \frac{(A+B)}{3} \nu \frac{(\nabla T)_r}{T} \tag{5.5}$$

5.2 Application to the aerosol model

The expression for thermophoretic velocity can be evaluated explicitly if the local temperature gradient is known. The model discussed in Chapter 3 provides the local gas temperature at each instant during combustion. A linear relationship between temperature and enthalpy has been used in the combustion model. Therefore the local gas enthalpy is

$$h = c_p T + \Sigma \Delta_i g_i \tag{5.6}$$

c_p and Δ_i, the gas heat capacity and heat of formation, are as stated in Table 3.3. The dependence of enthalpy on radial position is the same as that of species mass fractions, g_i, which are given in Eq. 3.6. In the notation of Chapter 3 the gas enthalpy is

$$h = \frac{(h_\infty - h_p) e^{-Kr_p/r} + (h_p - h_\infty e^{-K})}{1 - e^{-K}} \tag{5.7}$$

The temperature derivative is obtained by differentiating Eq. 5.6 with substitution of the appropriate equations for h and g_i. The result is

$$\frac{dT}{dr} = (\nabla T)_r = \frac{k}{c_p}\frac{r_p}{r^2}\left(\frac{h_\infty - h_p}{1 - e^{-K}}\right)e^{-Kr_p/r} - \frac{k}{c_p}\frac{r_p}{r^2}\left(\frac{\left(\Sigma \Delta_i g_i\right)_\infty - \left(\Sigma \Delta_i g_i\right)_p}{1 - e^{-K}}\right)e^{-Kr_p/r} \tag{5.8}$$

Using the definition of h (Eq. 5.6) gives an exact expression for the local gas temperature gradient around a burning coal particle:

$$(\nabla T)_r = \frac{1}{r^2}\frac{kr_p}{c_p}\left(\frac{c_pT_\infty - c_pT_p}{1 - e^{-K}}\right)e^{-Kr_p/r} \tag{5.9}$$

Now the thermophoretic velocity can be evaluated. The total velocity field experienced by the aerosol in the combustion system is the sum of the thermophoretic velocity and the convective velocity. In dimensional terms this quantity is

$$V_c + V_{T_\infty} = \frac{1}{r^2}\left(\frac{R}{4\pi c} - \frac{1.61}{3}\frac{\nu}{T}\left(\frac{R}{4\pi r_p c\mathcal{D}}\right)\frac{r_p}{c_p}\frac{(c_pT_\infty - c_pT_p)}{1 - e^{-K}}\ e^{-Kr_p/r}\right) \tag{5.10}$$

In the notation of Chapter 4, a more convenient expression is

$$V_c + V_{T_\infty} = \frac{R}{4\pi r^2 c}\left(1 - \frac{1.61}{3}\frac{\nu}{D}\left(\frac{1 - \theta_p}{1 - e^{-K}}\right)\frac{e^{-K/z}}{\theta}\right) \tag{5.11}$$

is the local temperature divided by the bulk gas temperature T_∞. From this equation, the thermophoretic velocity is seen to have a form similar to that of the convective velocity. To make this analogy even more obvious, define the thermophoretic coefficient R_T by

$$R_T = -\frac{1.61}{3}\frac{\nu}{D}\ \frac{1 - \theta_p}{1 - e^{-K}}\left(\frac{e^{-K/z}}{\theta}\right) \tag{5.12}$$

The total velocity field is now

$$V_c + V_{T_\infty} = \frac{R + R_T}{4\pi r^2 c} \tag{5.13}$$

If the thermophoretic coefficient were independent of radial position, the thermophoretic velocity could be substituted directly into the equations derived in Chapter 4., However, the term ($e^{-K/z}/\theta$) is a function of radial position. This quantity represents the ratio of two functions of radial position. Therefore it might be only a weak function of radial position in which case the thermophoretic velocity might be approximated by a constant value.

To test the constancy of the term ($e^{-K/z}/\theta$) it is calculated as a function of radial position for the example in the previous chapter. Figure 5.1 shows this calculation at several points in the combustion history. This quantity varies approximately 20% with radial position; most of the variation takes place within about 2 particle radii from the surface. Its value is nearly constant for radial positions greater than about 10 particle radii. The example has shown that most of the nucleation takes place in the region $2 < r_p < 10$.

In order to retain the simplicity of the solution to the aerosol problem an approximation is made concerning the thermophoretic coefficient. A weighted average of the quantity ($e^{-K/z}/\theta$) will be used to give a constant value of R_T. This average value is shown by the dashed line on Fig. 5.1 and corresponds to the sum of the values at $r/r_p = 1$ and $r/r_p = \infty$ weighted by 0.25 and 0.75, respectively. For the case illustrated in Fig. 5.1 this approximation results in a

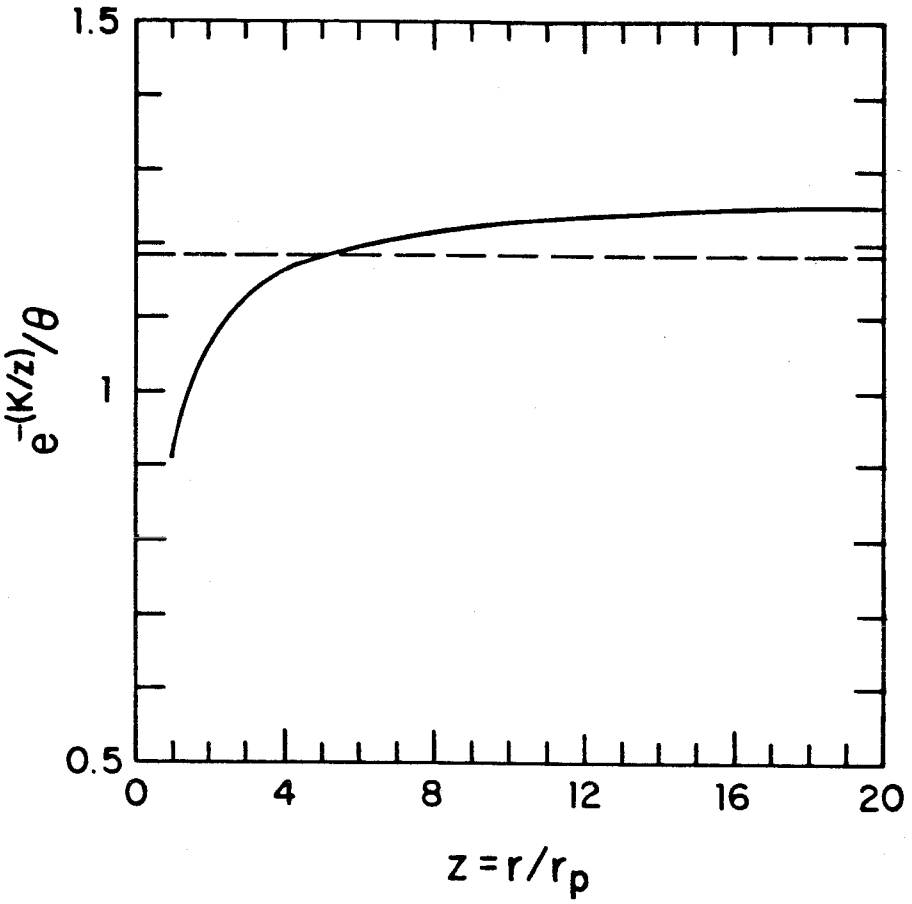

Figure 5.1b Variation of thermophoretic coefficient with radial position (75% burnout).

maximumm error of 10% in the region where nucleation is occuring and an error of about 5% far away from the particle.

Including the thermophoretic velocity changes the ash conservation and aerosol growth equations of Chapter 4 slightly. It is assumed that vapor is transported by convection, aerosol by convection and thermophoresis. The ash conservation equation (Eq. 4.2) becomes (in the notation of Chapter 4)

$$\frac{d\tilde{y}}{d\eta} = -Pe\left(\tilde{y} + (1 + R_T/R)\tilde{M} - R_V/y_s R\right) \tag{5.14}$$

Pe, the ash species Peclet number, is defined by Eq. 4.13. The aerosol growth equation (Eq. 4.4) becomes

$$(R + R_T)\frac{\partial n}{\partial r} + 4\pi r^2 c\dot{D}\frac{\partial n}{\partial D} = 4\pi r^2 I\delta(D - D_*) \tag{5.15}$$

The boundary conditions and method of solution of this system remain unchanged from Chapter 4.

5.3 Effect on solution

The effect of thermophoresis on the solution to the aerosol problem is illustrated by recalculating the example of Chapter 4. The conditions for this calculation have been stated already. Figure 5.2 reproduces the solution from Fig. 4.4 (solid line) and shows the solution including thermophoresis (dashed line).

Including thermophoresis in the model produces a larger number of

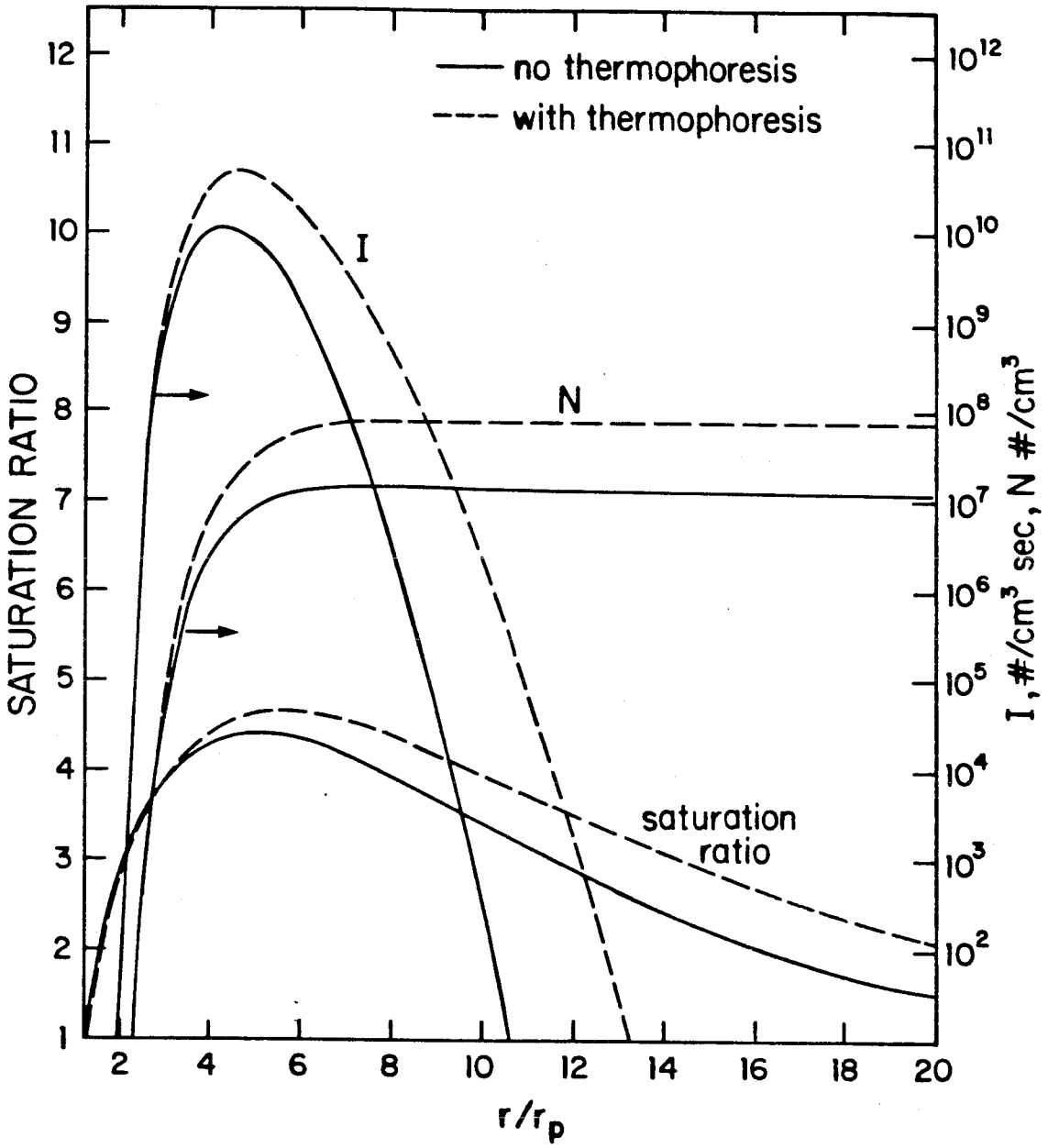

Figure 5.2 Effect of thermophoresis on aerosol calculations.

nuclei and broadens the nucleation peak. Aerosol moves outward more rapidly because of thermophoresis. This decreases the local condensation and increases the nucleation rate. The total number is higher becaused of the increased nucleation rate.

Nucleation still begins 1-2 particle radii from the surface and peaks at about 3 radii from the surface. Adding thermophoresis to the model produces quantitative differences in the solution, but its qualitative nature remains unchanged. The numerical effect is such that thermophoresis cannot be neglected in these calculations; subsequent calculations will include it.

CHAPTER 6

AEROSOL MODEL: APPLICATION TO COAL COMBUSTION

6.1 Ash vaporization during combustion

6.1.1 Calculation of vaporization rates

The last several chapters have introduced a large and complex theoretical structure for modeling aerosol formation during coal combustion. Detailed consideration of a sample combustion history reveals two important conclusions about modeling this process. The local combustion conditions determine the fate of the ash that vaporizes during combustion. While a substantial amount of aerosol is produced near the burning coal particle (for refractory species like silica), the presence of this aerosol has little influence on the vaporization rate.

The overall vaporization rate during combustion can be measured unambiguously and can be calculated as well. This provides an opportunity to compare the model with experiment and illustrates ways in which the model can be applied to real combustion systems.

Very few measurements of the ash vaporization during combustion exist. Sarofim and co-workers (Mims et al. (1980); Quann and Sarofim, 1982) have made the only comprehensive measurements of combustion aerosol under well-controlled combustion conditions. Burning a dilute suspension of coal in a small, laminar-flow furnace, both coal particle temperatures and burnout time have been measured (as discussed in Chapter 3). The composition of the ash aerosol has also been measured, giving the percentage of various components that end up in the submicron aerosol.

In this chapter effective vaporization rates will be calculated. The vaporization rate in the case of no aerosol formation can be calculated at each point in the combustion history of a single burning coal particle. Integrating the vaporization rate over the burnout time gives the amount of ash vaporized. When normalized with respect to the initial amount of ash in the particle and divided by the burnout time, the resultant quantity is the effective vaporization rate (in seconds^{-1}):

$$\phi_v = f_v/t_b = \frac{3M_a}{4\pi\alpha\rho_a r_{Po}^3 t_b} \int_o^{t_b} R_{vo}\, dt \qquad (6.1)$$

R_{vo} is defined in Equation 4.16. α is the volume fraction of ash. M_a and ρ_a are the ash molecular weight and density. The burnout time t_b can be calculated as it was in Chapter 3.

Two species are considered in these calculations, SiO_2 and Al_2O_3. Quann and Sarofim (1982) provide effective vaporization

rates for SiO_2 from the combustion of lignite particles having an initial diameter of 61 μm burning at 1500 K and 1750 K. Mims, et al. (1980) give effective vaporization rates for Al_2O_3 from the combustion of a lignite having an initial diameter of 75-90 μm at a furnace temperature of 1750 K. The combustion model from Chapter 3 is used to compute the local combustion conditions as well as burnout times. The pore structure used in Chapter 3 is used again in these calculations.

6.1.2 Effect of aerosol on vaporization rate

The sample calculation in Chapter 4 indicate that the ash vaporization rate during combustion at a relatively low particle temperature is enhanced by a maximum of 5% due to the presence of aerosol. It has been shown (Chapter 3) that for combustion in pure oxygen the average particle temperature approaches 3000 K. To test the enhancement of the vaporization rate at other combustion conditions, the full aerosol calculation is performed at many different combustion conditions. By varying the oxygen concentration, the particle temperature can be varied. Using oxygen partial pressures varying from 0.1 to 1.0 and the conditions outlined in Table 6.1, the effective vaporization rate for silica has been calculated. The results are shown in Figure 6.1 as the vaporization rate enhancement versus oxygen partial pressure. The maximum vaporization rate enhancement is 40% and it remains nearly constant throughout combustion; that is, the values calculated at two different points in the combustion history, 75% and

TABLE 6.1: CONDITIONS FOR CALCULATIONS

	SiO_2 Case	Al_2O_3 Case
r_{Po}, μm	30.5	37.5 and 45
T_∞, K	1500 and 1750	1750
$Po_{2\infty}$, atm	0.1 - 1.0	0.1 - 1.0
Weight percent ash	9.8	8.2
Initial particle density, g/cm^3	1.36	1.36
Weight percent volatile matter	40	40
Pore Structure		
ε_{01}	0.01	0.01
ε_{02}	0.05	0.05
R_{01}, nm	0.25	0.25
R_{02}, nm	25	25

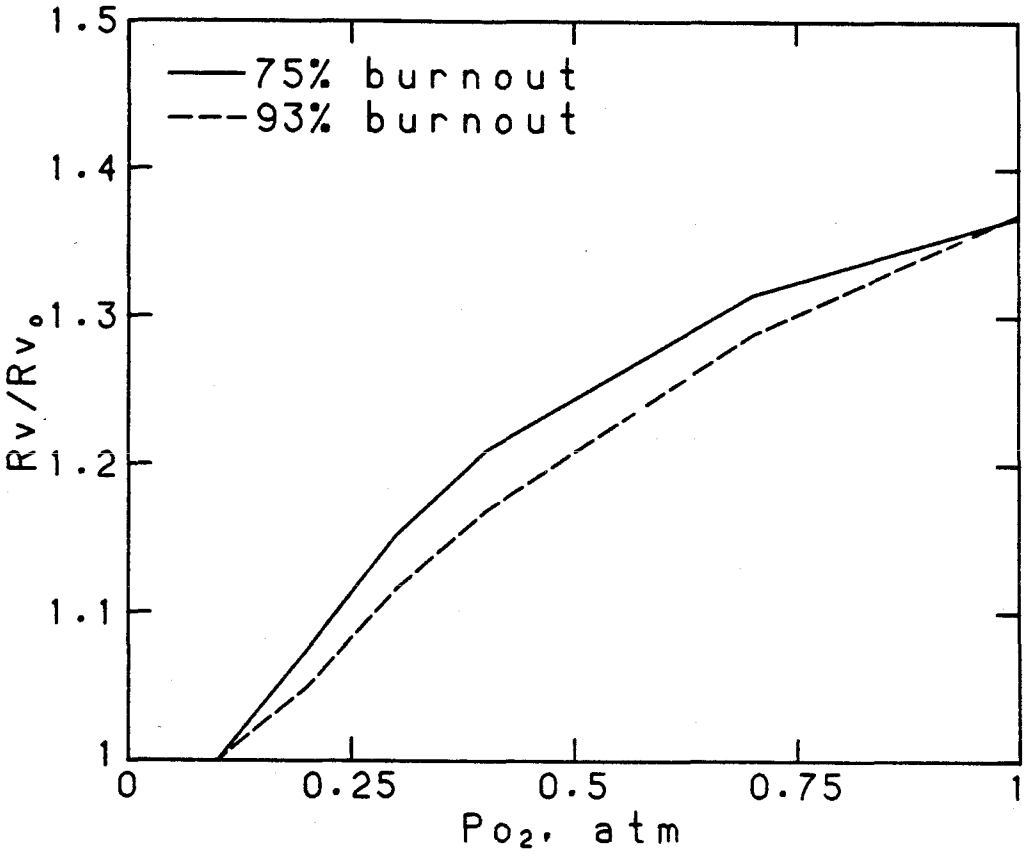

Figure 6.1 Vaporization rate enhancement due to aerosol.

93% burnout, are not too different.

Figure 6.2 shows the effect of the aerosol on the effective vaporization rate. The effective vaporization rate has been calculated from Equation 6.1 (solid line) and this value has been multiplied by the average rate enhancement (dashed line) and plotted against the inverse mean particle temperature. These calculations use a gas temperature of 1750 K only although the data are for combustion in both 1750 K and 1500 K. Also included in this figure are the data of Quann and Sarofim (1982). Two things are immediately obvious. The rate enhancement due to the presence of aerosol is not large when compared with the scatter of the data. However, the calculated rate is much lower than the reported experimental values. It is clear from this figure that the enhancement of vaporization rate cannot account for this difference. In subsequent sections this discrepancy will be analyzed further.

6.1.3 Effect of nonideal liquid solutions

Equation 4.14 demonstrates the dependence of the silica activity coefficient on the equilibrium partial pressure. In the preceding calculation, it is assumed that the activity of silica in solution is unity. An examination of the bulk composition of ash might convince one that a molten ash solution is not an ideal solution.

No one has measured the activity of the various components of molten coal ash at high temperatures. (This would be quite a task!)

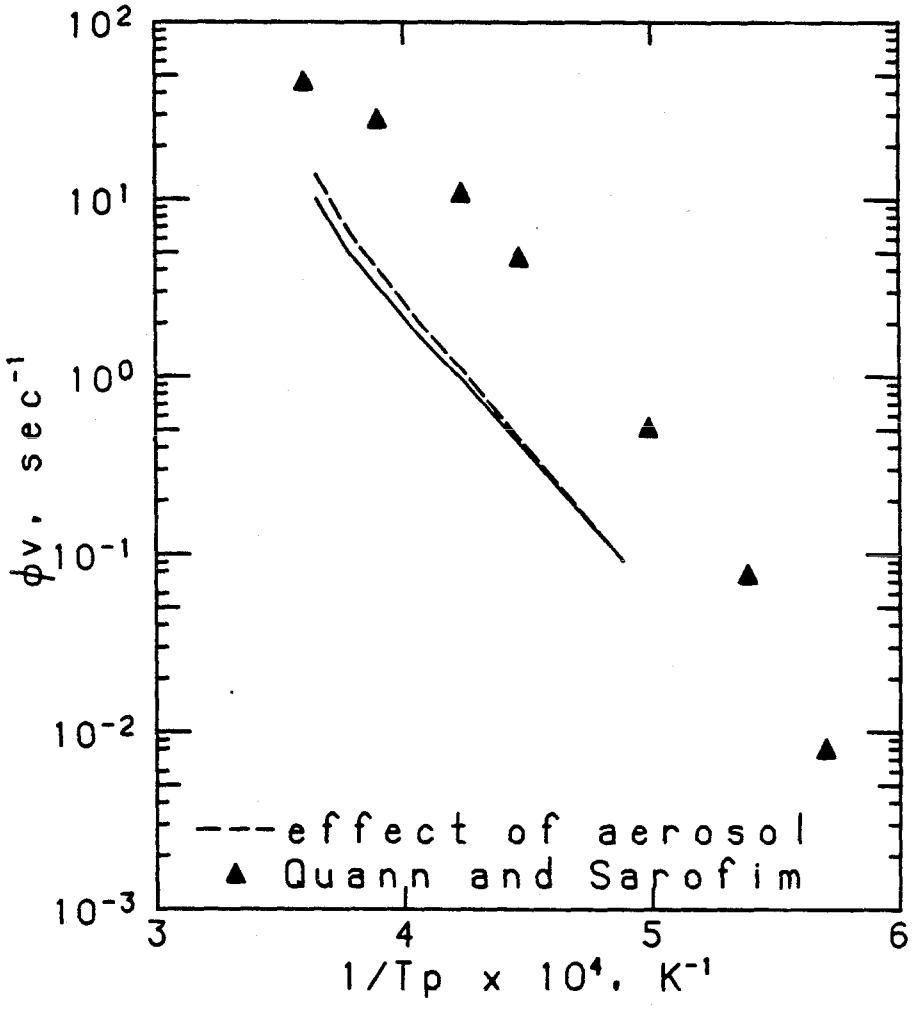

Figure 6.2 Effect of aerosol on the effective vaporization rate for silica. Combustion of 61 μm particles at a gas temperature of 1750 K.

However, measurements have been made of the activity in synthetic slag mixtures. Rein and Chipman (1965) measured activities in the SiO_2-CaO-MgO-Al_2O_3 system at 1600°C. Henderson and Taylor (1966) measured activities in the CaO-MgO-SiO_2 and MgO-Al_2O_3-SiO_2 systems. Based on these works and a knowledge of the range of silica content in coal, the activity of silica in coal should be in the range 0.01 to 0.7.

The calculation of silica vaporization rate is repeated for two different activities, 0.05 and 1 and at two different gas temperatures, 1500 K and 1750 K, to give a wider range of particle temperatures. The results are shown in Figure 6.3. Activity is seen to have a tremendous effect on the vaporization rate although, in this case, decreasing the activity only serves to widen the gap between data and theoretical prediction.

6.1.4 Effect of particle size

Even in small and well controlled combustion systems a range of coal particle sizes are burned. Since particle size affects the ash vaporization rate, it is logical to explore this possibility next. Data from Mims, et al. (1980) are reported for the combustion of a lignite with particle diameters in the range 75-90 μm. The rate calculation is repeated for alumina instead of silica since there is no reported silica data for these conditions.

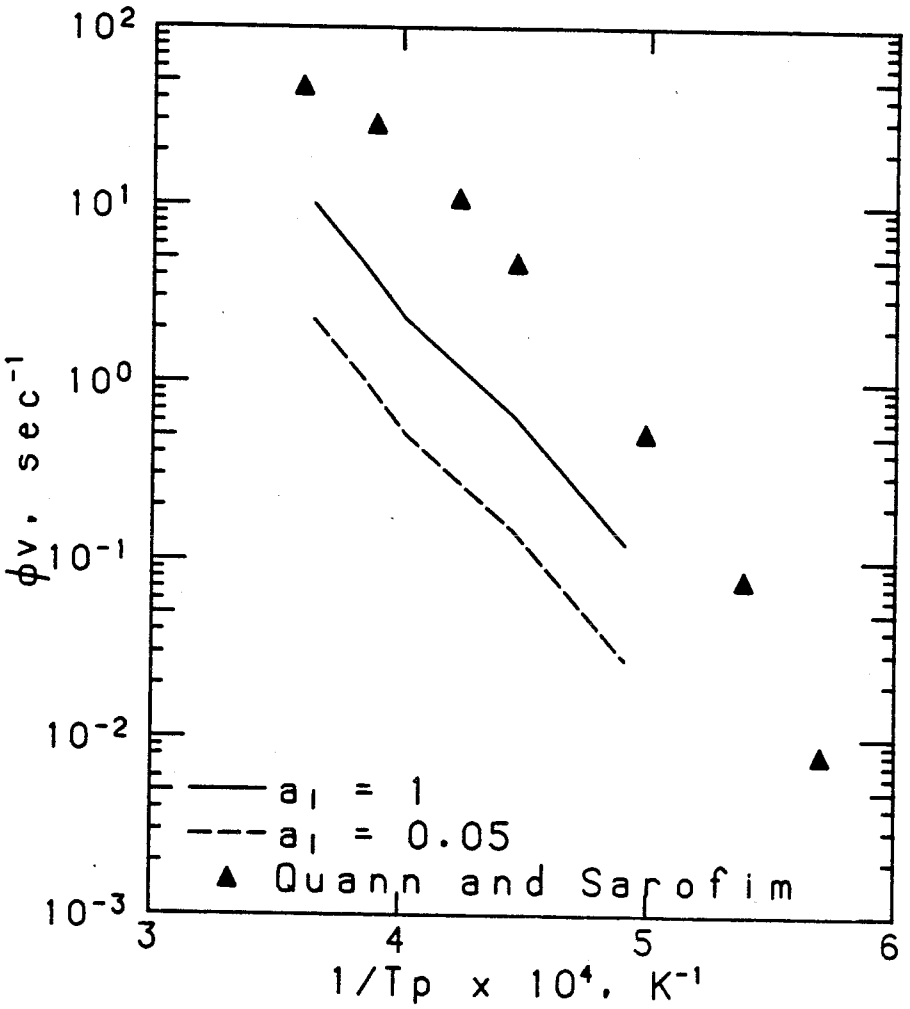

Figure 6.3 Effect of liquid activity coefficient on effective vaporization rate for silica. Combustion of 61 μm particles in gas temperatures of 1500 K and 1750 K.

An equilibrium between liquid and vapor is assumed for the alumina system in a fashion analogous to the silica system. Brewer (1953) states that under reducing conditions the stable gaseous oxide is Al_2O. The following equilibrium relationship is assumed:

$$Al_2O_{3(\ell)} + 2CO \rightleftarrows Al_2O_{(g)} + 2CO_2$$

The equilibrium vapor pressure is given therefore by

$$P_{Al_2O} = (a_\ell P_{CO}^2)^{1/3} \qquad (6.2)$$

The conditions described in Table 6.1 are used to calculate the effective vaporization rate and the fraction of alumina vaporized.

Figure 6.4 shows the results of these calculations assuming an activity of unity in the liquid. In this case, the effect on vaporization of burning a range of particle sizes is small. However, these calculations do not account for fragmentation of the char during combustion. Because of this, it is possible that particles smaller than the initial particle size will be burning, resulting in more uncertainty in the experimental data.

6.2 Discussion

Calculations of effective vaporization rate have been performed for two different ash species, silica and alumina. In both cases the computed vaporization rate was about seven times lower than the reported data. This difference is potentially much greater if the nonideality of

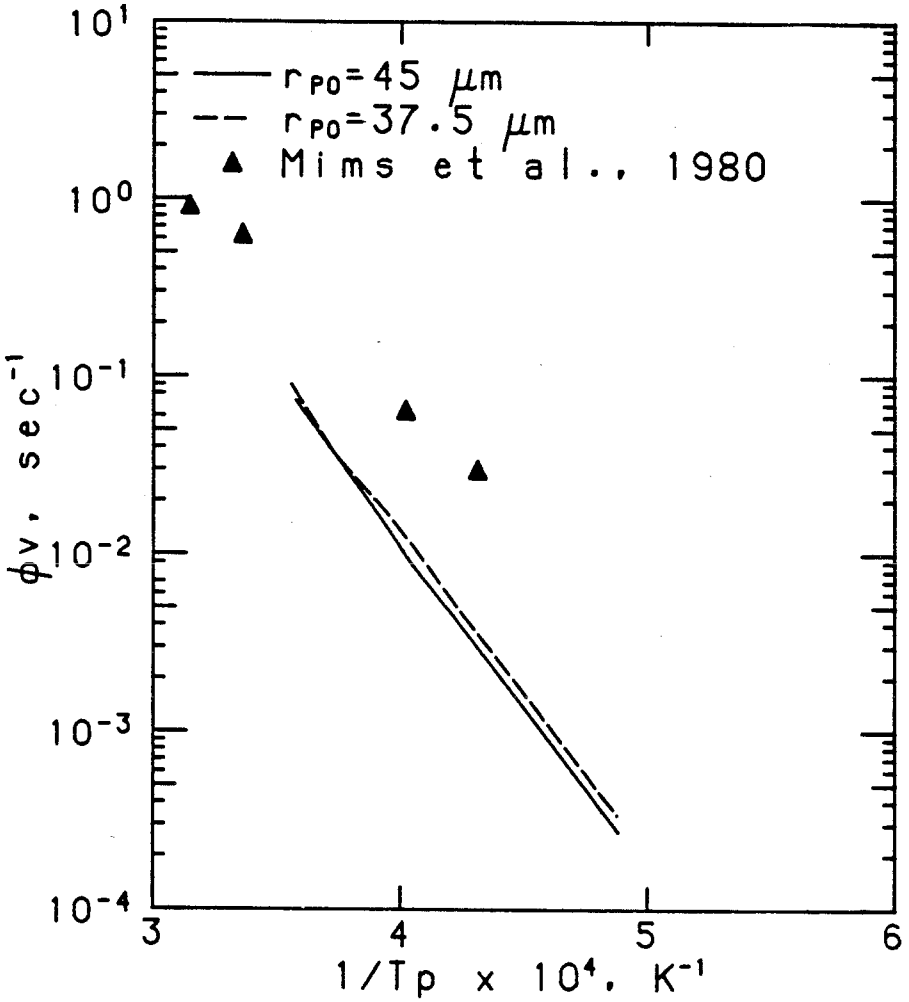

Figure 6.4a Effect of initial particle radius on effective vaporization rate of alumina. Combustion at a gas temperature of 1750 K.

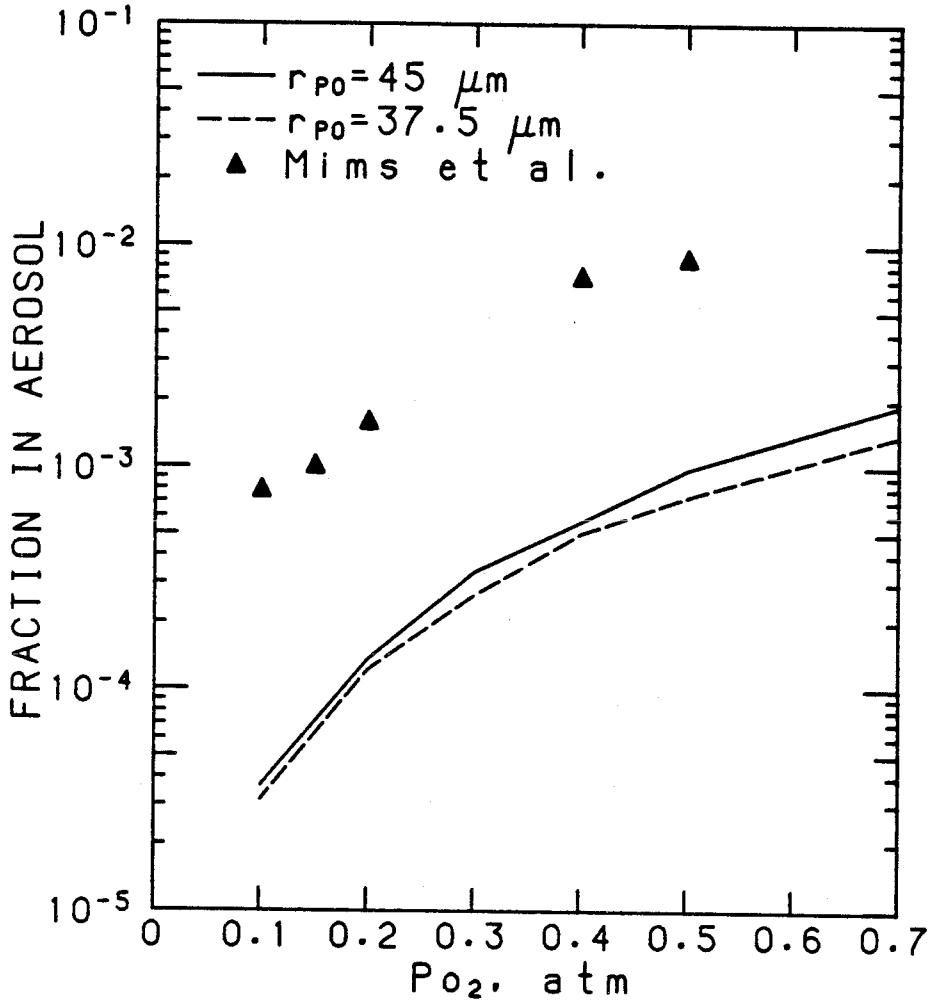

Figure 6.4b Effect of initial particle size on fraction of alumina vaporized. Combustion at a gas temperature of 1750 K.

the liquid solutions is taken into account. Neither the presence of aerosol in the gas nor the range of initial coal particle sizes can explain this difference.

The fact that this discrepancy is observed for two different species having very different volatilities is significant. It points to some common problem and not, for example, to the use of incorrect chemical data for alumina or silica. One possible problem, incorrect combustion kinetics, can be eliminated also. If the combustion model overpredicted the combustion temperature, for example, the vaporization rate would increase. The result would be to shift the vaporization rate along the curve of rate versus 1/T without changing the shape of this curve.

More likely, some process that effects the vaporization process has not been considered in the model. The major physical feature that has not been included in the model is the vaporization of ash within the coal particle. Vaporization has been assumed to occur only on the surface of the particle even though the particle itself is porous. The interior of the particle represents a larger source for vapor than the surface alone. In addition, conditions inside the particle are more reducing than those at the surface. The equilibrium vapor pressure in the interior of the particle would be expected to be higher than that at the surface for this reason alone.

Quann and Sarofim (1982) modeled the vaporization of inclusions

inside a burning coal particle based on an analysis of a spray of vaporizing droplets. The diffusion equation inside the particle was solved in the standard way for diffusion and reaction in a porous catalyst. Reasonably good agreement was obtained between theory and experiment although the nonideality of the liquid was not considered and combustion was assumed to be diffusion-limited.

6.3 Conclusions

The models developed in this study can be used to predict the effective vaporization rate of ash and the fraction vaporized. At present there exits only a limited amount of experimental data with which to compare the model. Comparison with measured vaporization rates shows that, while the effective activation energy (the slope of the vaporization curve) can be predicted well, the rate is at least an order or magnitude too low. The effect of vaporization within the entire porous solid has not been included in this analysis; this is a very important physical feature of the system that should be examined in detail.

Interpretation of the results is clouded by uncertainty in the ash chemistry. It is clear that the molten ash represents a nonideal liquid solution of unknown properties. A better understanding of the vaporization process will require a more detailed knowledge of the ash chemistry. In addition, the present model considers a very simple vaporization mechanism. During combustion the molten ash is not a

simple system and needs to be represented by a more complex equilibrium model.

CHAPTER 7

MODEL SYSTEM: ARTIFICIAL COAL

7.1 Introduction

In the preceding chapters, models have been developed that contain most of the important physical features of the combustion and aerosol formation processes. However, models are only as good as their input data. This principle becomes especially relevant in a system as physically and chemically complex as coal.

The lack of data on the physical structure of coal char and the physical and thermodynamic properties of coal ash makes verification of models difficult. More importantly, the chemical complexity of coal ash may mask important features of aerosol formation and growth. How can the fundamental physics and chemistry of aerosol formation be studied in such a complicated and ill-defined system?

One way out of this predicament is to find a simpler system in which to study the problem. The first step in understanding aerosol formation in a chemically complex system like coal is often to

understand the same process in a chemically less complicated system. To this end, a model compound will be developed to be used as a tool in the study of aerosol formation during combustion. This does not mean that the study of coal has been abandoned. Instead we will try to gather insight into the workings of the process of interest in a model compound ("artificial coal") with the aim of applying this knowledge to coal.

The most important requirement for artificial coal is that it preserve the important features of coal combustion without being unnecessarily complex. Since the local heat and mass transfer during combustion are so important to ash vaporization and aerosol formation, these phenomena must be reproduced during the combustion of the model compound. The model compound must contain finely divided inclusions of mineral matter of known composition. In addition, we would like to control the pore structure of artifical coal since char pore structure is an important feature of coal.

This chapter presents the procedures used to make and characterize artificial coal. The nature of the material produced and the effect of the curing process on it is also discussed. Directions for further study are discussed.

7.2 Production of artificial coal

Interest in the production of carbonaceous solids extends over the last several decades. Polymeric resins have been used to make a variety

of carbon-containing solids: chemically resistant cements, structural carbon and graphite, and catalyst supports. The basic process for all of these products begins with an organic compound (e.g., furfuryl alcohol, vinyl chloride) that is polymerized with a suitable catalyst, cast into a mold, and heated in an inert atmosphere. Heating to low (ca. 600 C) temperatures produces a material that is often called glassy carbon.

One property of glassy carbon that has aroused interest is its lack of pores in the macro and transitional size ranges. Glassy carbon contains only micropores with diameters less than about 1.5 nm (Schmitt, 1970; Marsh and Campbell, 1971). Schmitt and co-workers (1976) claim to have produced 15 nm pores by adding 12 nm carbon black particles to the polymer. It appears possible to control the pore size distribution with the amount and size of carbon black particles added to the polymer carbon.

The chemistry of furfuryl alcohol polymerization and glassy carbon formation is quite complex. Fortunately, these materials have been studied extensively so the details of the chemistry will not be discussed here. Dunlop and Peters (1953), Riesz and Susman (1960), Conley and Metil (1963), and Wewerka (1968) studied polymerization of furfuryl alcohol. Formation of glassy carbon has been the subject of many investigations; the interested reader is referred to the work of Nakamura and Atlas (1960), O'Neill et al. (1963), Dollimore and Heal (1967), Wewerka et al. (1969), Fitzer et al. (1969), and Fitzer and

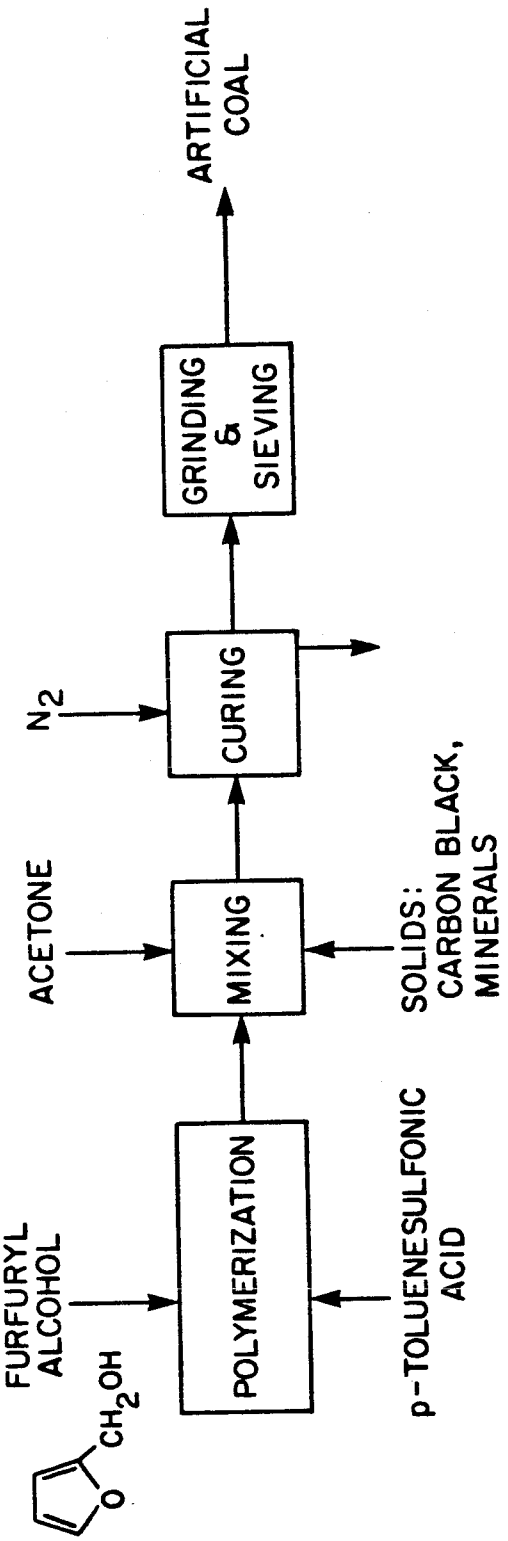

Figure 7.1 Procedure for production of artificial coal.

Schaefer (1970).

The procedure used in this work to produce synthetic char is outlined below and diagrammed in Figure 7.1. Furfuryl alcohol is polymerized with the aid of an acid catalyst. The resulting thick polymer is thinned with acetone. Solids are mixed into the polymer and the resulting material is baked in nitrogen as outlined by Schmitt (1970). Two types of solids are added: carbon black, having a primary particle size of 22 mm and silica, in the form of 1-5 micron quartz particles. Grinding and sieving the resulting solid carbon gives the desired product, artificial coal.

7.2.1 Polymerization

For a given sample, only as much polymer as could be cured at one time was produced. This meant starting with 30-40 ml of furfuryl alcohol monomer. The monomer was combined with the catalyst, p-toluenesulfonic acid (PTSA), in a 200 ml boiling flask. The amount of catalyst used was always 0.5 % (by weight) of monmomer and it was added in a water solution (0.0451 g/ml).

Following the addition of the catalyst, the boiling flask was fitted with a water-cooled condenser and set in a water bath at 70-73°C for ten minutes with constant stirring. The amber-colored liquid turned dark brown over a period of minutes and began to evolve water violently. After several minutes more, visible bubbling in the solution ceased and

a distinct aqueous phase was observed in the flask.

The contents of the flask were poured into a 125 ml separatory funnel and left undisturbed for at least one hour but not more than one and a half hour. The long separation time was required because of the high viscosity of the polymer phase. The polymer was poured into a 150 ml beaker that had been previously weighed. The beaker was covered with plastic wrap and weighed again.

7.2.2 Addition of solids

The procedure diverges at this point, depending on whether or not the desired char is to contain carbon black. The two cases are discussed separately.

For samples without carbon black, 40 ml of monomer was used as starting material and this usually yielded about 36 g of polymer. After weighing the beaker which contained the polymer, 12 ml of acetone were added and it was covered and put in an ultrasonic bath. The purpose of the acetone was to decrease the viscosity of the polymer in order to mix the solids effectively. The mineral matter was weighed and added to the beaker while it was in the bath. The mixture was blended for 15 minutes using a stirring rod in an overhead stirrer. The stirring was vigorous (2000 rpm) enough to cause formation of acetone bubbles throughout the solution. The resulting mixture was poured into four ceramic boats with dimensions 100 by 20 by 13 mm (manufactured by Coors Porcelain). The

boats were placed in a vacuum desiccator and were aspirated (using water) for 4 1/2 hours.

To produce samples containing carbon black, the starting material was 30 ml of monomer, yielding about 26 g of polymer. After it was weighed, the beaker containing the polymer was placed in the ultrasonic bath. 70 ml of acetone were added to it and it was covered. Carbon black and minerals were weighed and added separately to the acetone-polymer mixture. For all samples containing carbon black, the ratio of polymer to carbon black was 3:1. The mixture was stirred at 2000 rpm for 20 minutes. At this time, it was poured into boats and aspirated for four hours.

7.2.3 Curing

The apparatus used to cure the samples is shown schematically in Figure 7.2. A 60 mm quartz tube is placed horizontally in a tube furnace which has a two foot long hot zone. A cold trap downstream of the furnace condenses most of the vapors in the exhaust gases. A chromel-alumel thermocouple measures the temperature in the furnace.

In order to cure the samples, the boats were placed in the furnace which was then purged with high purity nitrogen for 25 minutes. The furnace was heated to 125°C at about 4° C per minute. This temperature was held for six hours. The furnace was heated to 200°C at about 3°C per minute and held at this temperature for ten hours. Then the

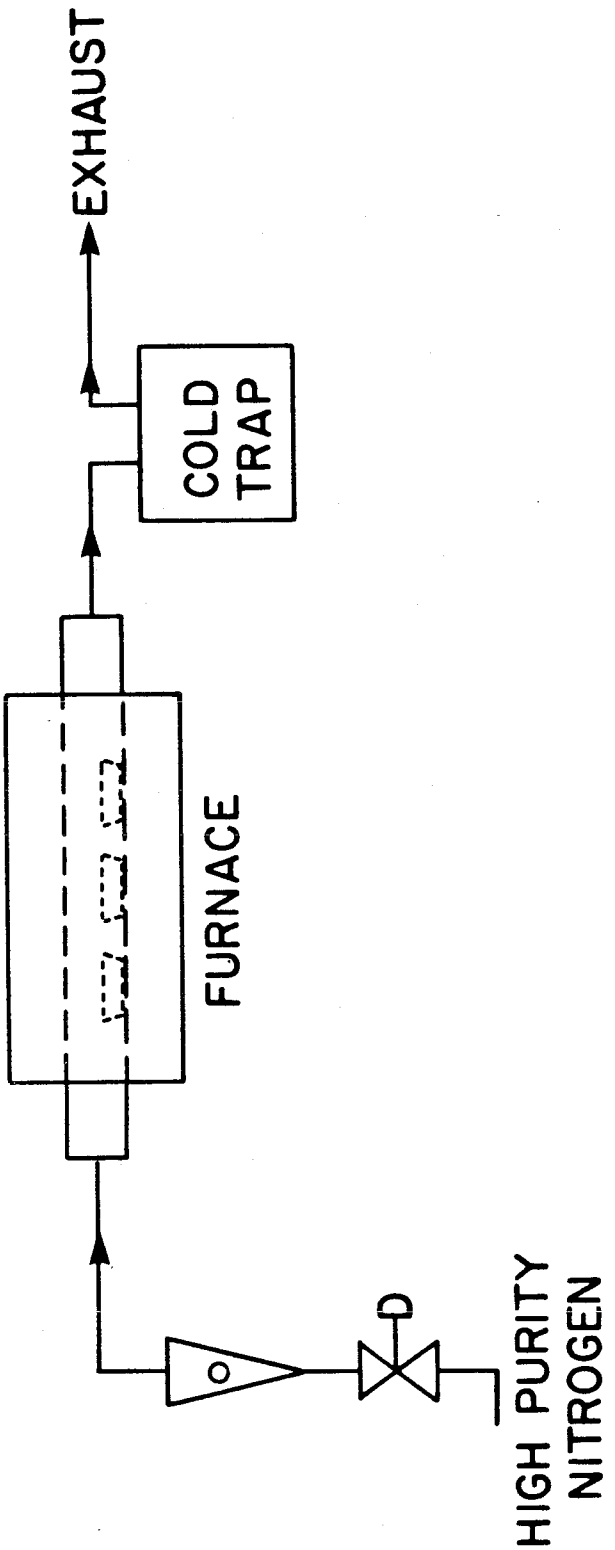

Figure 7.2 System for curing artificial coal.

temperature was increased at a rate of 4-5°C per minute until the soak temperature was reached; it was maintained at this temperature for one hour. The boats were cooled in flowing nitrogen.

The char produced was in the form of large pieces (ca. 20 mm). Grinding by hand with a mortar and pestle reduced the size to less than about 5 mm. Then the char was ground in a mechanized mortar and pestle (manufactured by Retsch) for 3-4 minutes. The +100 mesh portion of the char was ground for an additional 3-4 minutes. The char was sieved for 30 minutes using a mechanical shaker. Samples containing carbon black were sieved twice: after the first sieving the -400 mesh material was removed and the material sieved for another 30 minutes. All samples were dried at 105°C for at least 12 hours and stored in a desiccator until ready for combustion.

7.2.4 Materials

Furfuryl alcohol monomer was supplied by the Quaker Oats Company. Reagent grade acetone was obtained from Mallinckdrodt. The p-toluenesulfonic acid was sold by Sigma Chemical Company. Carbon black was obtained from Continental Carbon Company, Houston, Texas; the primary particle size was 22 nm, the specific surface area, approximately 119 m^2/g. The crystalline silica used has the trade name Min-u-sil 5 and was produced by Pennsylvania Glass Sand Corporation. Figure 7.3 shows a particle size distribution for this material (Lawler, 1979).

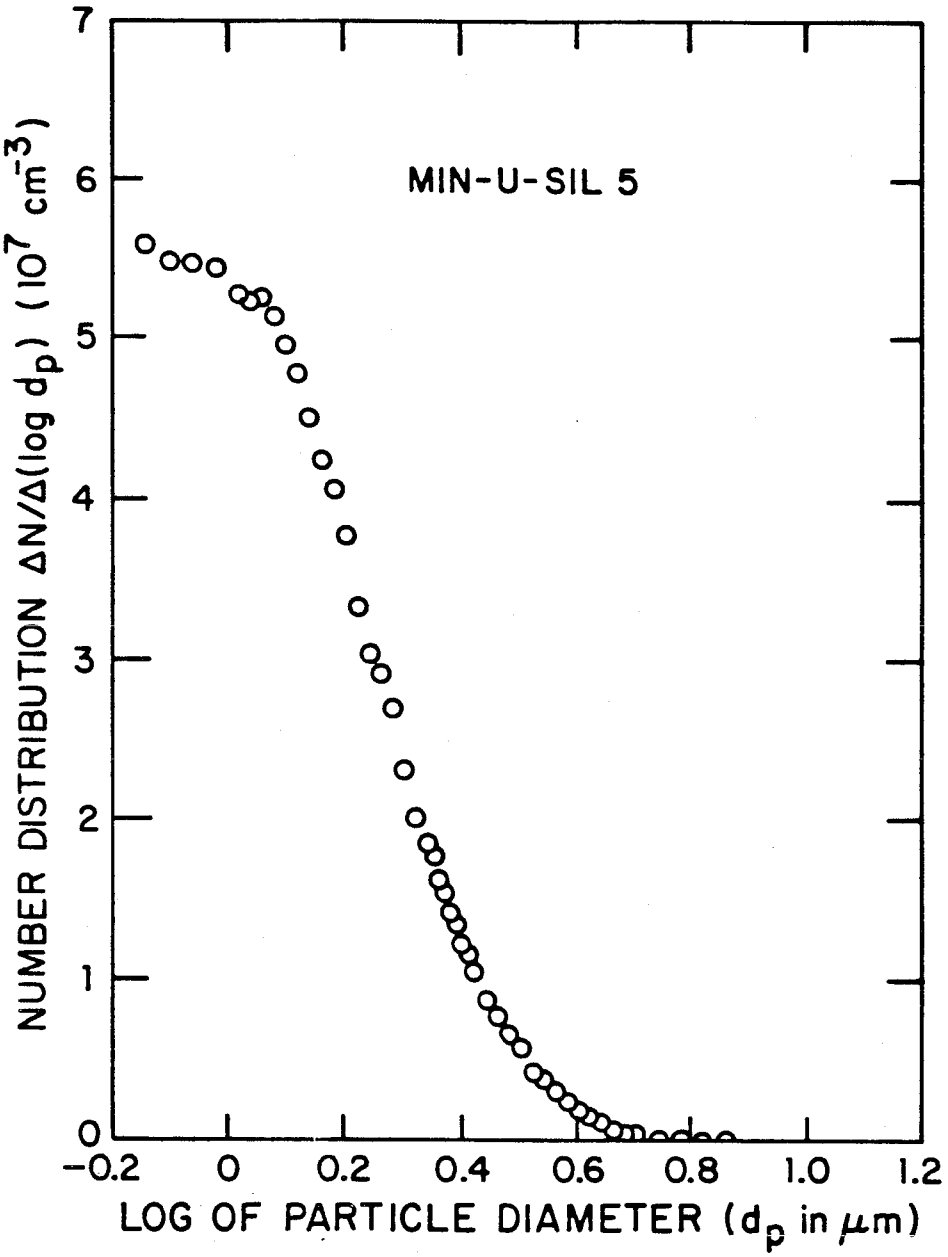

Figure 7.3a Number distribution for MIN-U-SIL 5 (source: Lawler, 1979).

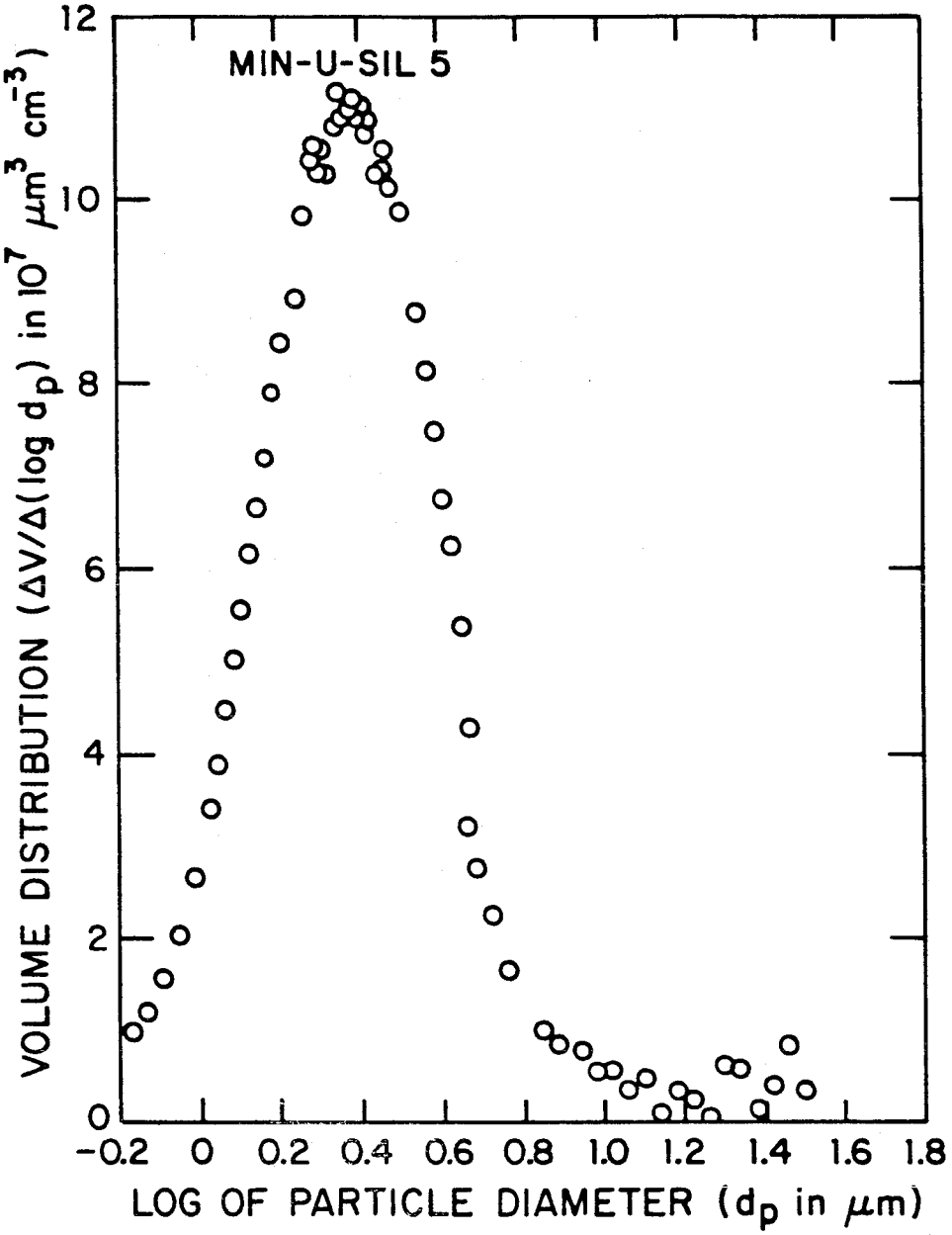

Figure 7.3b Volume distribution for MIN-U-SIL 5 (source: Lawler, 1979).

7.3 Characterization of chars

The synthetic chars produced for this study have been characterized both chemically and physically. There are two important reasons for this characterization. First, there must be some way to test the reproducibility of the production process. Second, characterization data are needed to predict combustion behavior. This section introduces the methods for characterization; the next goes into more detail concerning the results of these tests.

7.3.1 Chemical characterization

Elemental analysis was performed in the Caltech Chemistry department. It was possible to analyze for carbon, hydrogen, and nitrogen. Special samples of glassy carbon that contained no ash were prepared for elemental analysis. This glassy carbon was polymerized and cured in the same way the other chars were, but no acetone was added to the polymer and the mixing step was omitted.

The ash content of the char samples was measured using a procedure based on the ASTM D3174 standard. The difference between the standard and the procedure in this work is the amount of char used for each test. The standard requires about 1 g of material; in this study, 0.1 to 0.25 g is used for each determination. The test proved reproducible with these small quantities. This test gives the ash content from which one calculates the total weight loss of polymer during production (using the

ash as a tracer) and the carbon black content of the char.

Porcelain crucibles approximately 27 mm deep and 30 mm in diameter were used for the test. One test consisted of duplicate samples of about 0.1 to 0.25 g each. The char was placed in the crucible and dried for at least 12 hours at 105°C. The crucible was stored in a desiccator until cool enough to weigh. Immediately after weighing, the crucible was placed in a cold muffle furnace. The furnace was turned on and the temperature raised to about 725°C. This usually took 30 minutes. The samples were burned until no more char was present; the time required for this was 45 minutes to 1 hour. The sample was placed in a desiccator and weighed when cool.

Reactivity of the sample was measured with a thermogravimetric analyzer (TGA) manufactured by Dupont (Model 951). The measurement was made in a mixture of 17.4% O_2 in N_2 at 500°C. A small amount of the char (ca. 10 mg) was placed in the balance pan and the balance was tared. Using a gas flow rate of about 100 cc/min the sample was purged with nitrogen and heated (at 1-2°C/sec) up to 500°C. The sample was held at 500°C in nitrogen to allow thermal equilibration to occur. A mixture of 80% air and 20% N_2 was admitted to the balance and the weight and derivative were recorded continuously.

7.3.2 Physical characterization

The char samples were analyzed by Micromeritics Instrument

Corporation of Norcross, Georgia in order to characterize the physical structure of the char. True density, also called helium density, was measured by helium displacement. Specific surface area was measured by a static adsorption technique employing either nitrogen or krypton at 77 K. The surface area was calculated from BET theory (Lowell, 1979)

Mercury porosimetry was used to measure the pore size distribution. This technique is based on the intrusion of mercury into the pores (Lowell, 1979) and gives the pore volume as a function of pore diameter. The maximum intrusion pressure was 60,000 psi which corresponds theoretically to penetration of all pores greater than 3 nm (a contact angle of 130 degrees is assumed).

7.4 Discussion

7.4.1 Effect of curing temperature

Many factors influence the choice of conditions for the production of artificial coal. The choice of monomer has some small effect since different monomers have different amounts of weight loss during curing (Riesz and Susman, 1960). However, the structure of glassy carbon is essentially independent of the starting material (Fitzer et al., 1969).

Past work on the pyrolysis of polymers in inert atmospheres guides the choice of soak temperature. The temperature should be high enough so that most of the mass evolution that occurs during pyrolysis has

already occurred. If there is a high rate of mass loss at or near the curing temperature, the final product will be very sensitive to changes in process temperature. Differential thermal analysis studies of this process (Dollimore and Heal, 1967; Wewerka et al., 1969; Nakamura and Atlas, 1960; Fitzer et al., 1969) reveal two temperature regions associated with exothermic reactions and high rates of mass loss. The highest rate of mass loss occurs near 350°C; at 450°C there is also significant mass loss. Based on these data, the minimum temperature considered for curing is 500–550°C.

A second factor in choosing the soak temperature is the effect of temperature on the mineral matter contained in the artificial coal. The soak temperature must be low enough so that the mineral matter does not decompose or lose mass by vaporization. The mineral matter used in the current work, silica, boils at 2500 K. However, future work on this system will include other inorganic compounds that are not so inert. For example, calcium and magnesium carbonates decompose below about 600°C and many naturally occurring arsenic compounds boil below 600°C. In order to render the results of this work useful to future studies, a soak temperature of 550°C is used.

The effect of temperature on composition and mass loss is shown in the next three figures. As the soak temperature increases, the carbon content increases and the mass yield and atomic H/C ratio decrease. Figures 7.4 and 7.6 show that at 550°C the carbon content and yield are leveling off. The atomic hydrogen to carbon ratio (Fig. 7.5) is still

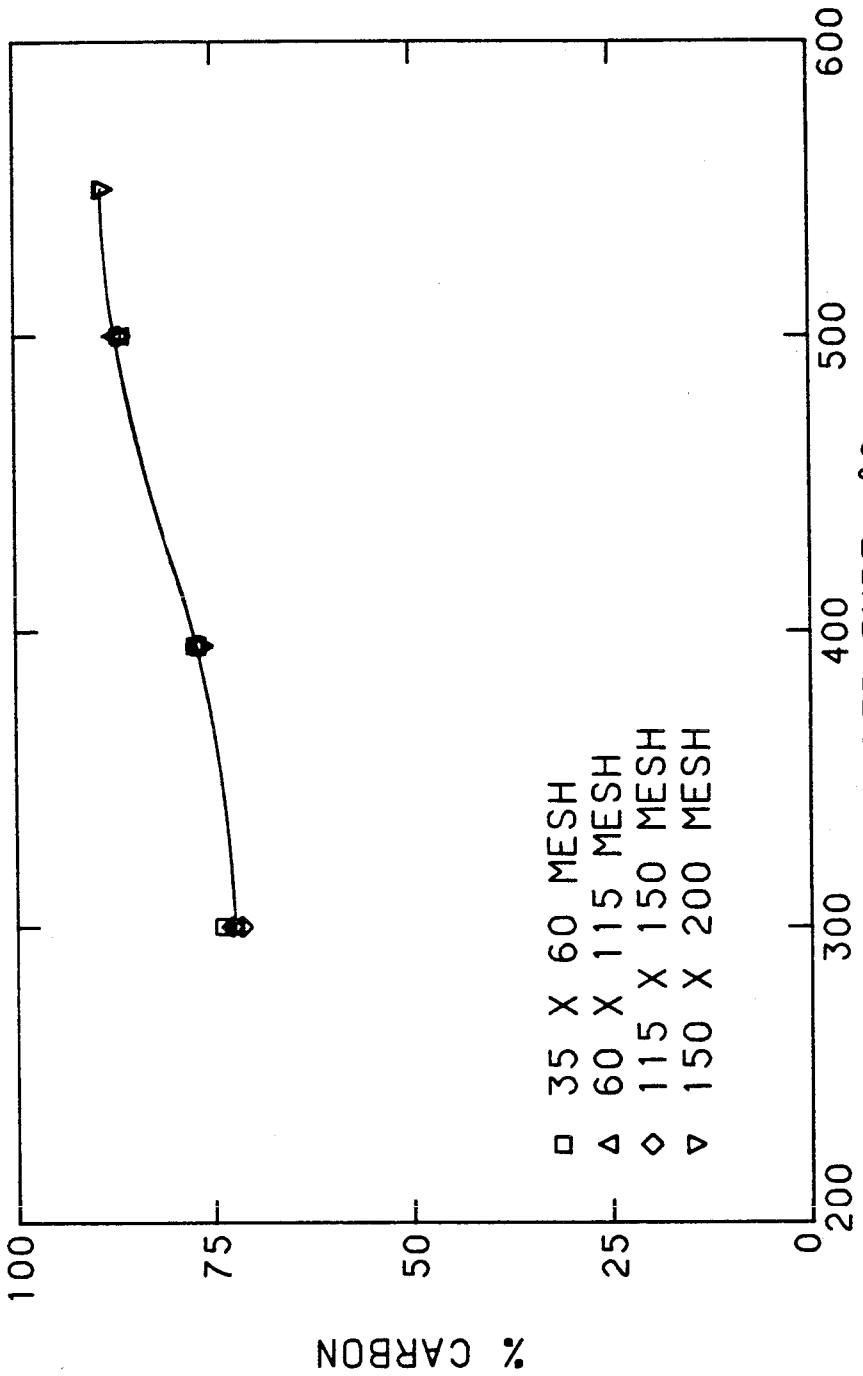

Figure 7.4 Carbon content of glassy carbon as a function of curing temperature.

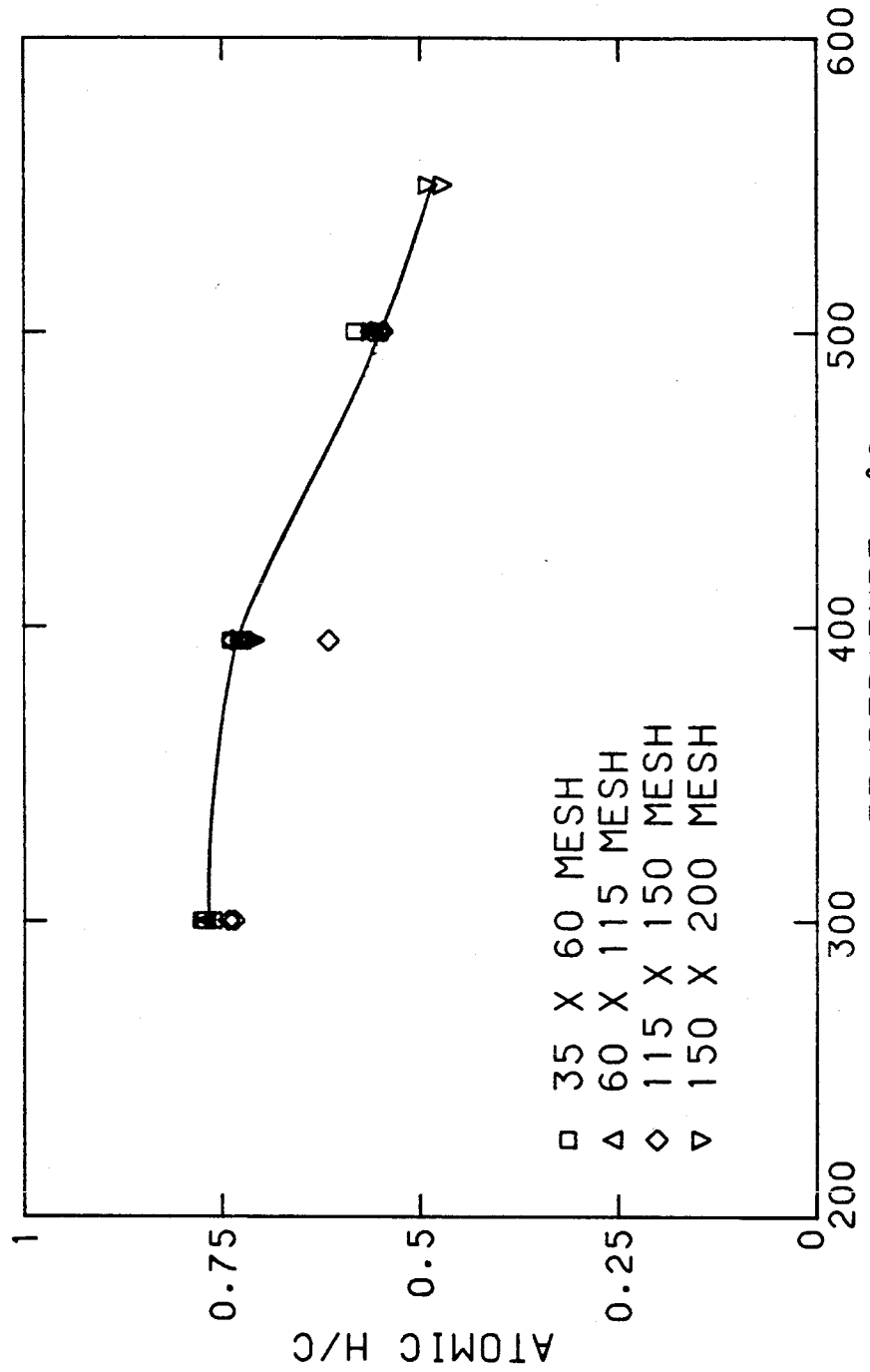

Figure 7.5 Atomic H/C ratio of glassy carbon as a function of curing temperature.

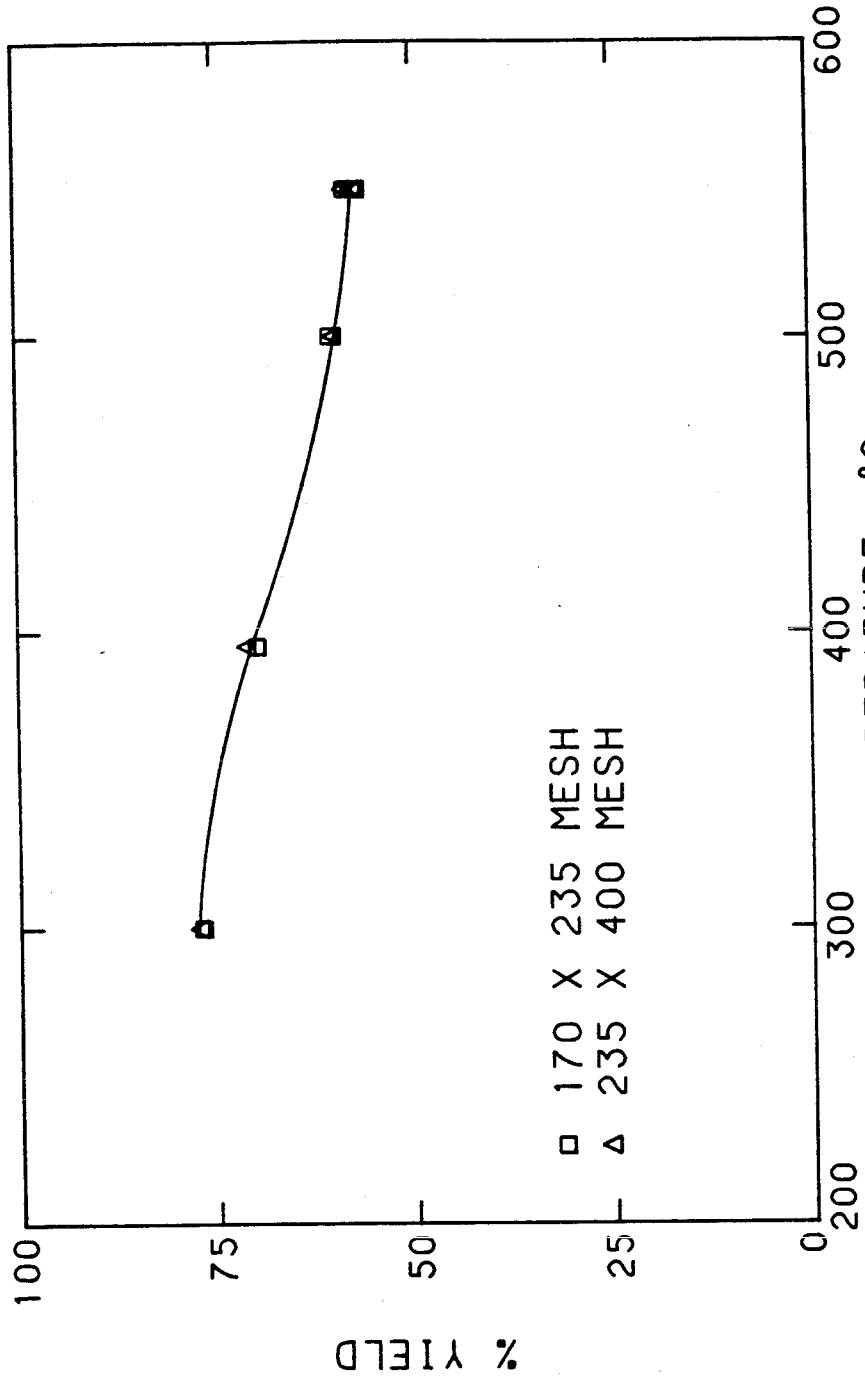

Figure 7.6 Mass yield on artificial coal (non-porous carbon) as a function of curing temperature.

decreasing rapidly at 550°C. At this temperature, the major gaseous products evolving are CH_4 and H_2 (O'Neill et al., 1963).

Table 7.1 gives the composition of the samples made in this work. Two different materials are considered for a preliminary evaluation of artificial coal in the study of aerosol vaporization and aerosol formation. As mentioned earlier, Schmitt et al. (1976) produced glassy carbon containing transitional pores by adding carbon black. (Note: transitional pores are usually identified as those for which $0.6 < d_p < 30$ nm). For this reason, the materials are identified as "non-porous" and "porous". The porous carbon contains 37.7% carbon black by weight in the form of 22 nm particles. In the following sections further characteristics of the two materials will be explored.

7.4.2 Pore structure

Table 7.2 gives data about the physical characteristics of the two carbons. The apparent density is calculated from mercury intrusion data and is based on the volume of solid and pores with diameter less than 3 micron (i.e., an intrusion pressure of 60 psia). The total porosity is calculated from the helium and apparent densities.

The porous carbon is denser than the non-porous carbon because of the carbon black that it contains. The porosity of the two materials is similar: both are about 15% porous. The two materials have very similar pore size distributions for pores in the range $3 < d_p < 1000$

TABLE 7.1: COMPOSITION OF ARTIFICIAL COAL

Elemental Analysis (Wt. %, Ash-Free)	"Non-Porous"	"Porous"
C	88.6	92.3 (est.)
H	3.5	-
O (by difference)	7.9	-
Carbon Black Content	0	37.7
Ash Content, Wt. %	8.6	8.9

TABLE 7.2: PHYSICAL STRUCTURE OF ARTIFICIAL COAL

	"NON-POROUS"		"POROUS"	
	mmcb[1]	mmfb[2]	mmcb	mmfb
Helium density, g/cm^3	1.440	1.380	1.598	1.536
Apparent density, g/cm^3	1.207	1.148	1.372	1.310
Total Porosity	0.154	0.161	0.155	0.152
N_2 Surface Area, m^2/g	1.8	1.97	182.0	199.8

[1] mineral matter containing basis

[2] mineral matter free basis

nm. However, their surface areas are quite disparate.

Pore size distributions for the two materials (by mercury porosimetry) are shown in Figure 7.7. As expected, the non-porous carbon (Fig. 7.7a) has few pores larger than about 10 nm. Surprisingly, the porous carbon (Fig. 7.7b) has very few transitional pores. Examining the pore size distributions in more detail, one finds subtle differences between the two. The non-porous carbon evidences some structure in the size range $100 < d_p < 1000$ nm. But the porous carbon has no pores at all in this range. This structure in the former carbon may be the result of microcracks associated with the mineral matter. Since the mineral matter is 1-5 microns in size, these cracks are of order one-tenth of the size of the silica particles. The structure of the porous carbon should contain microcracks associated with the carbon black that dominate the solid structure. Based on the evidence of the non-porous carbon, one expects these to be 1-2 nm in size. Pores of this size are too small to be seen by mercury porosimetry. However, the presence of a large number of such pores could explain the very high surface area of porous carbon.

The next series of figures are scanning electron mirographs of the carbons produced for this study. They provide qualitative information about these materials. Figure 7.8 shows glassy carbon that has been cured at 500°C. This material is true to its name: the surface appears smooth and impervious.

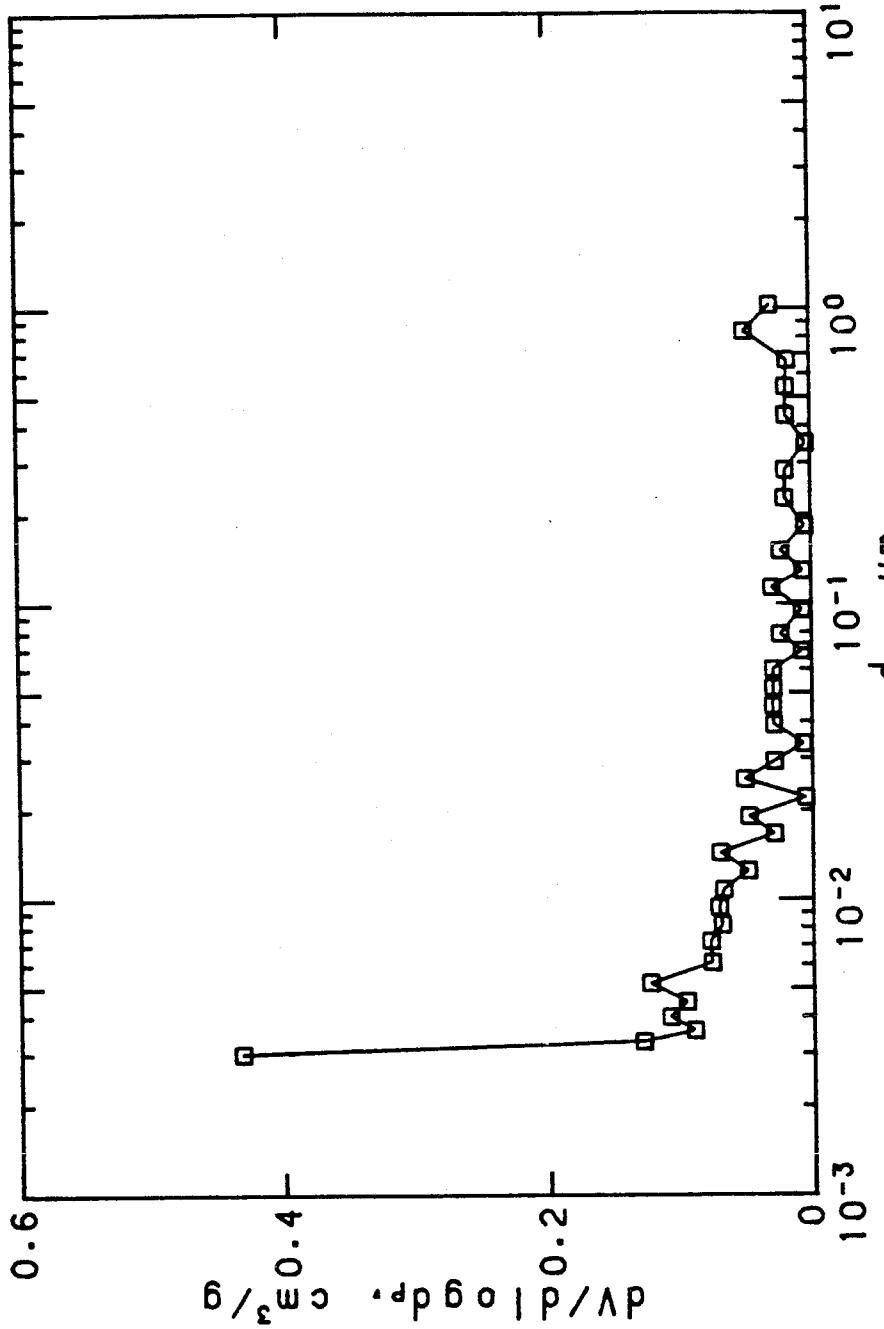

Figure 7.7a Pore size distribution of non-porous carbon by mercury porosimetry.

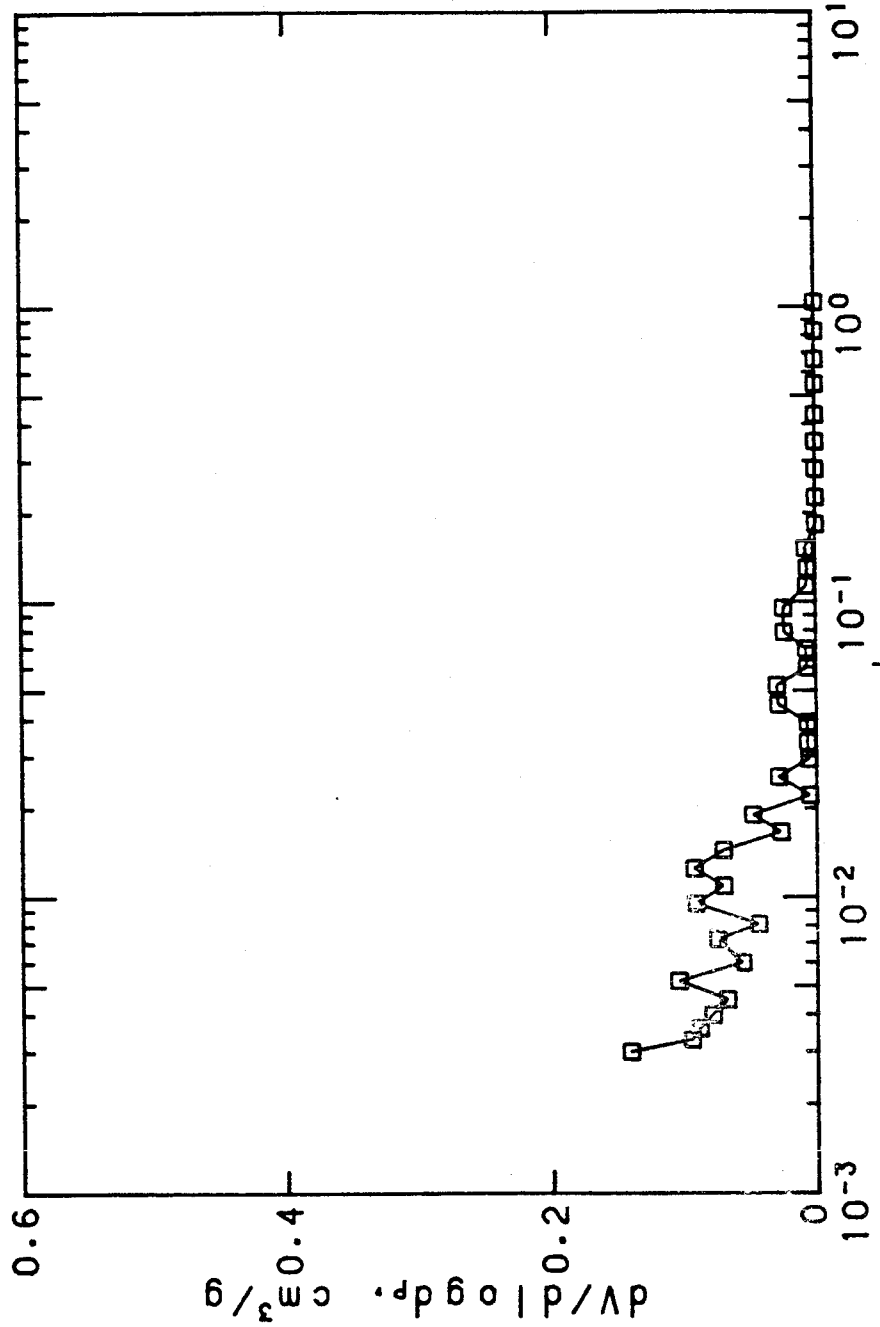

Figure 7.7b Pore size distribution of porous carbon by mercury porosimetry.

Figure 7.9 shows non-porous and porous carbon magnified about 2000 times. The mineral inclusions are homogeneously distributed in both materials. This indicates that the production process is adequately combining the polymer and the solids. The carbon black also appears evenly distributed in the solid of the porous carbon.

The non-porous carbon (Fig. 7.9a) consists of glassy carbon plus inclusions of silica. Like that of glassy carbon, the surface appears smooth. Quartz particles are seen studding the surface. Some depressions are also visible; these are caused by embedded inclusions that are torn loose during grinding. Figure 7.9b shows porous carbon at the same magnification; its gross structure resembles that of non-porous carbon but the surface appears rougher.

The differences between the two materials are preserved on a finer scale as Figure 7.10 illustrates. The non-porous carbon (Fig. 7.10a) appears quite smooth when maginified 7000 times. (The "track" across the surface is thought to be from abrasion during grinding.) On the other hand, the porous sample (Fig. 7.10b) has a rough, grainy surface. At even higher magnification, more of the surface features of porous carbon can be seen. At 20,000 times magnification (Fig. 7.11) individual lumps on the surface are visible. The primary particle size of the carbon black is 22 nm so one does not expect to resolve indiviual carbon black particles at this magnification. However, the effect of the carbon black on the structure can be seen. This photograph also confirms the homogeneity of the carbon black in the solid.

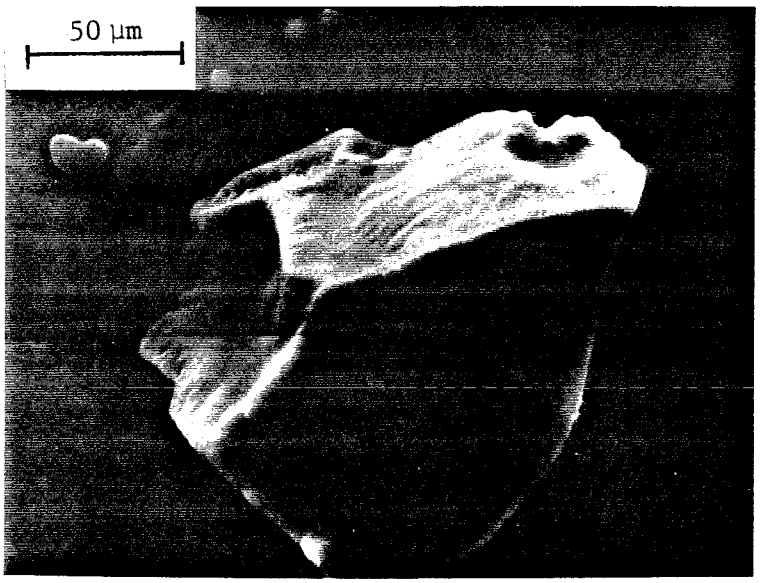

Figure 7.8 Glassy carbon (magnified 700 times).

Figure 7.9 b Porous carbon (magnified 2000 times).

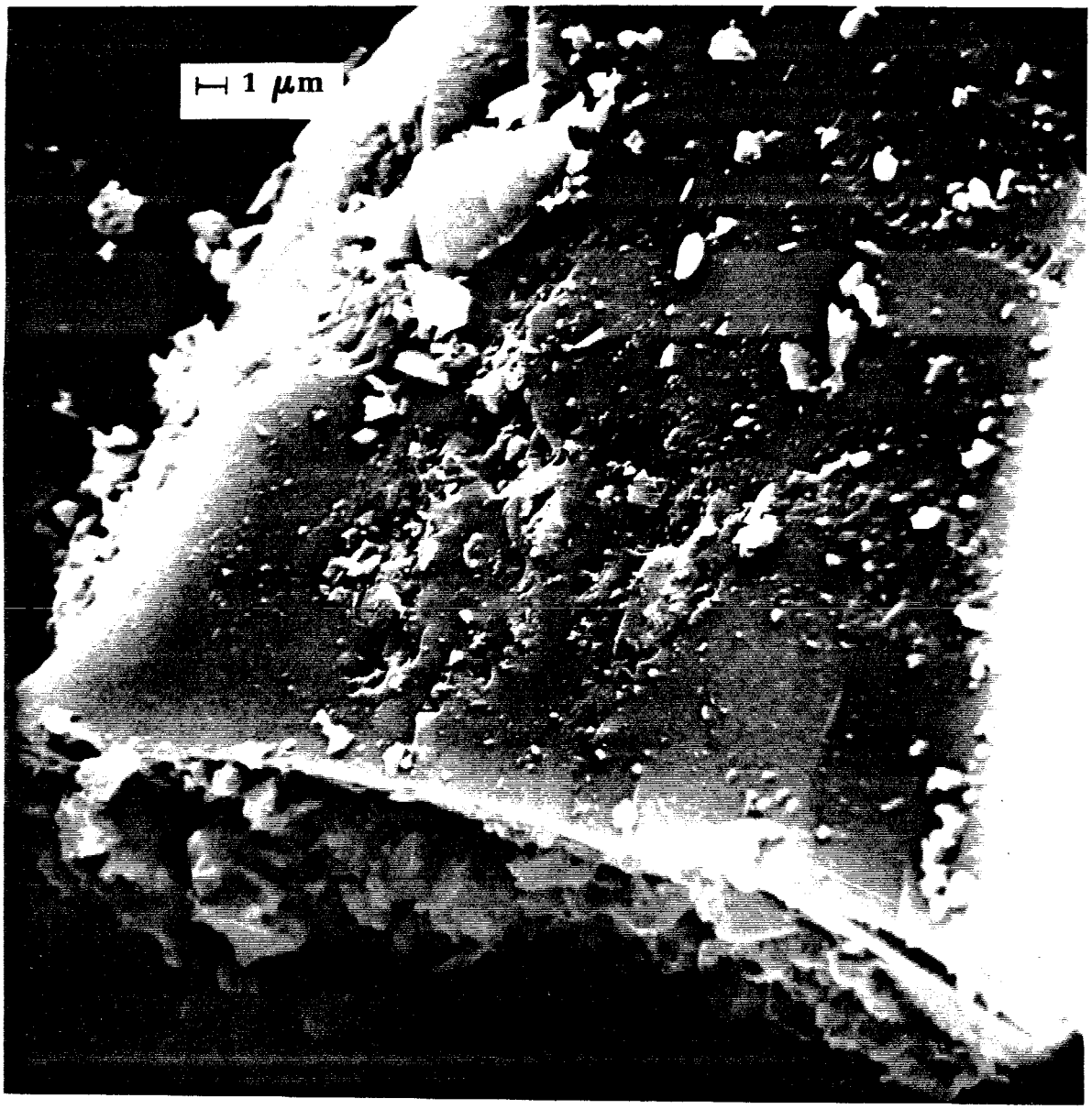

Figure 7.9a Non-porous carbon (magnified 2000 time).

Figure 7.10a Non-porous carbon (magnified 700 times).

Figure 7.10b Porous carbon (magnified 6000 times).

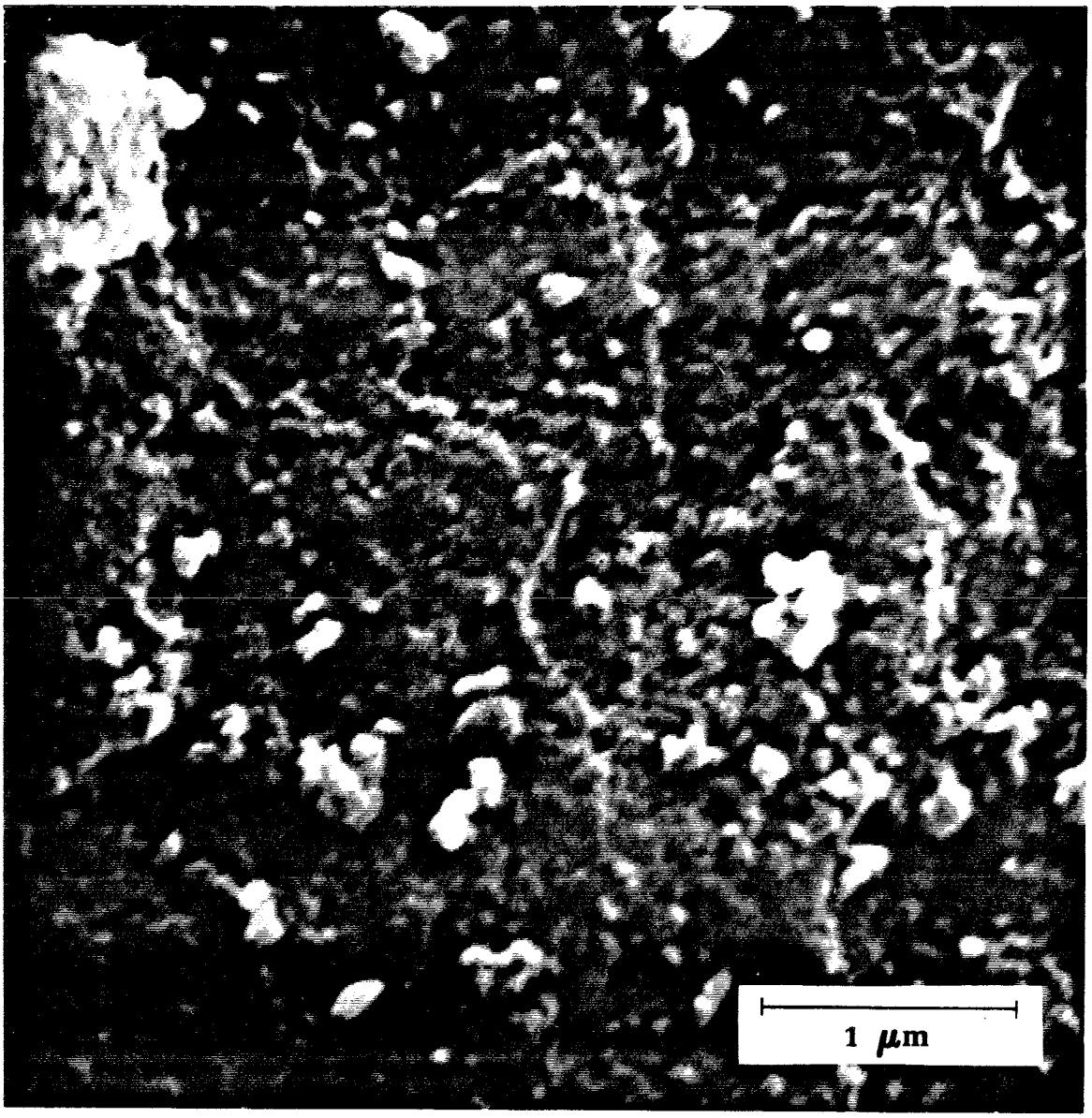

Figure 7.11 Porous carbon (magnified 20,000 times).

These photographs, when considered with the data on the physical structure, give an understanding of the nature of the solid. The process used to manufacture artificial coal produces a relatively homogeneous material containing finely divided mineral inclusions.

7.4.3 Reactivity

The reactivity of porous and non-porous carbon was measured at 500°C as previously described. A sample of the carbon black used in production of porous carbon was also tested. Thermogravimetric analysis (TGA) produces records of the sample weight (normalized to 100%) and the derivative with time.

Figure 7.12 shows results of the reactivity measurement of non-porous carbon. A small amount of mass (2.3%) is lost during heating in nitrogen. The maximum value of the derivative occurs at 14.6% mass loss. The rate changes during the course of the measurement because the surface area changes with reaction.

The reactivity of porous carbon under the same conditions is shown in Figure 7.13. The sample lost only 1.5% of its mass during heat-up because the carbon black contains less volatile matter than glassy carbon (this fact is confirmed in Fig. 7.14). The first part of the TGA record of porous carbon resembles that of non-porous carbon: the maximum rate (3.4 mg/hr-mg) occurs at 11% mass loss and is less than that for non-porous carbon (4.9 mg/hr-mg). After approximately 58% of

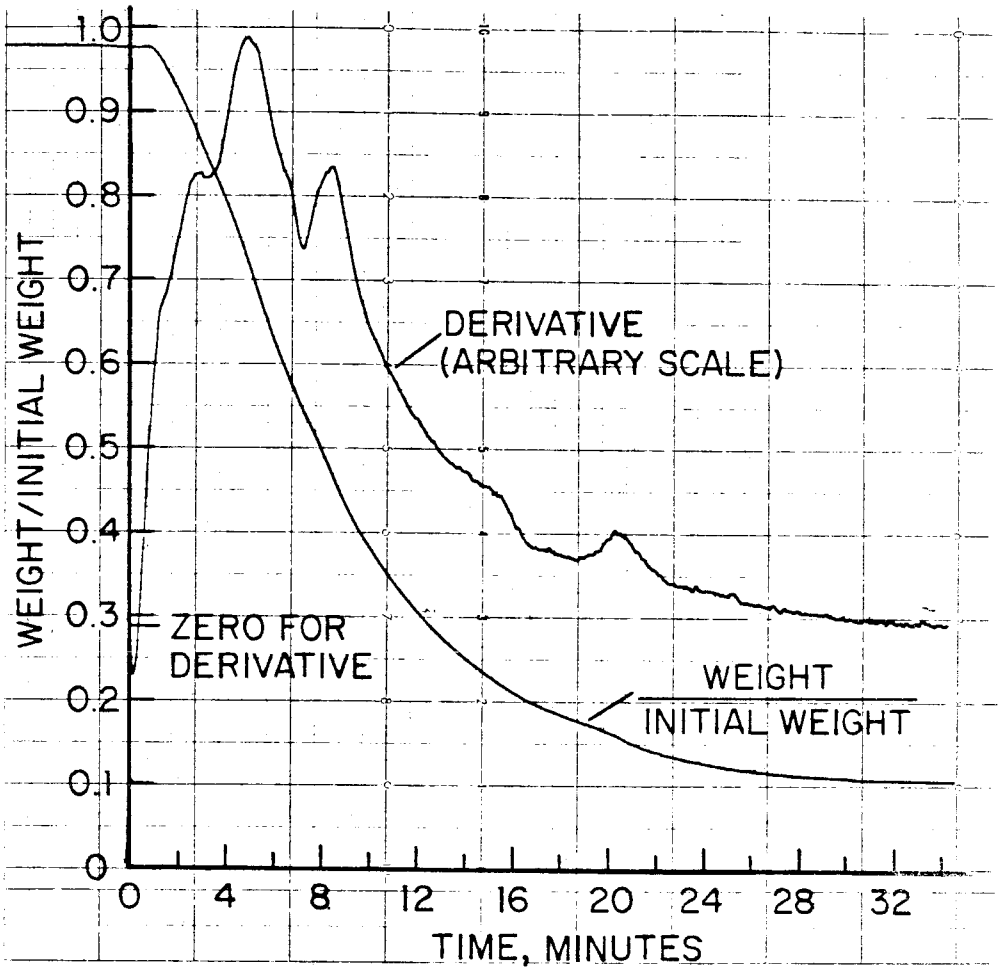

Figure 7.12 TGA record of non-porous carbon ractivity in 17.4% oxygen at 500°C.

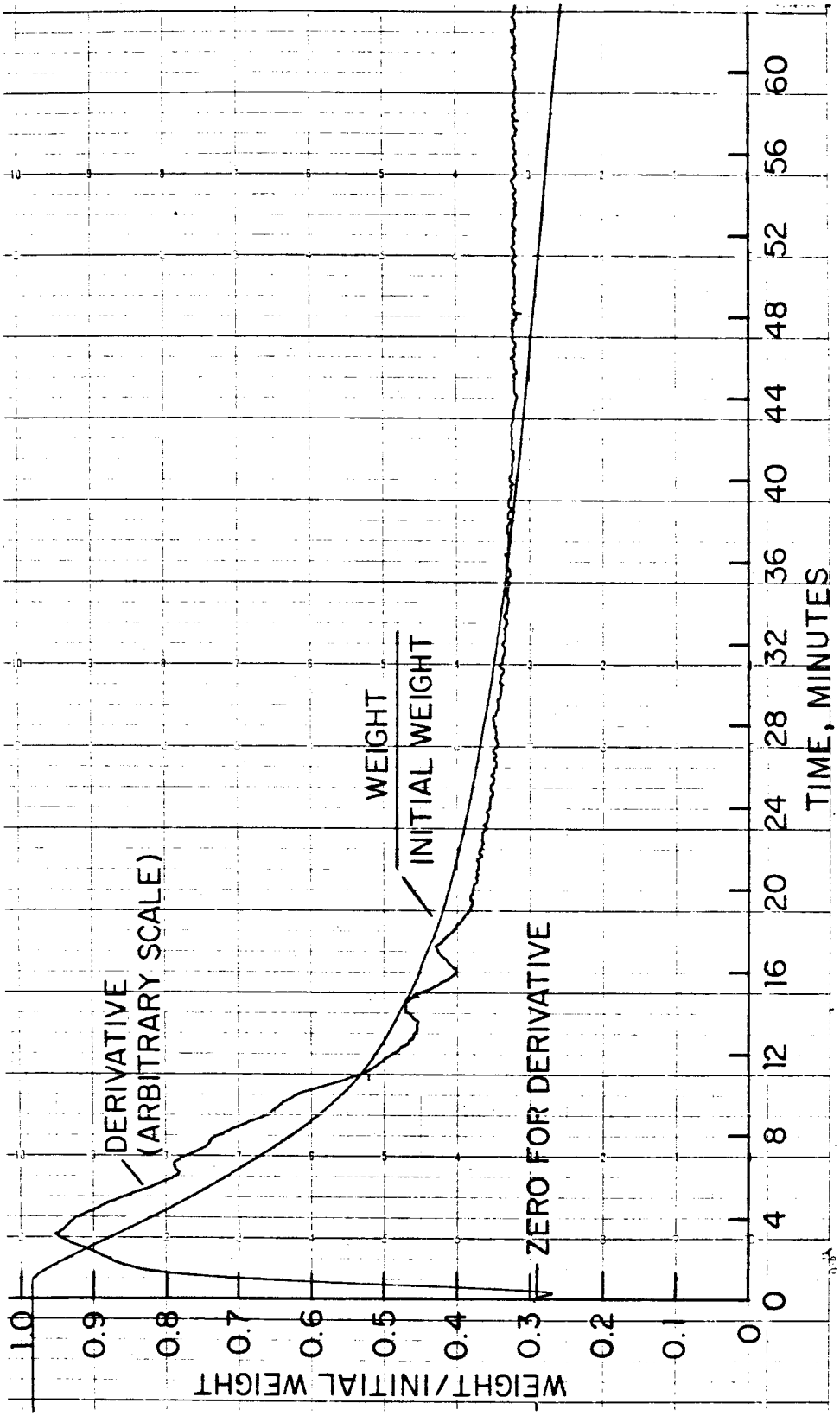

Figure 7.13 TGA record of porous carbon reactivity in 17.4% oxygen at 500°C.

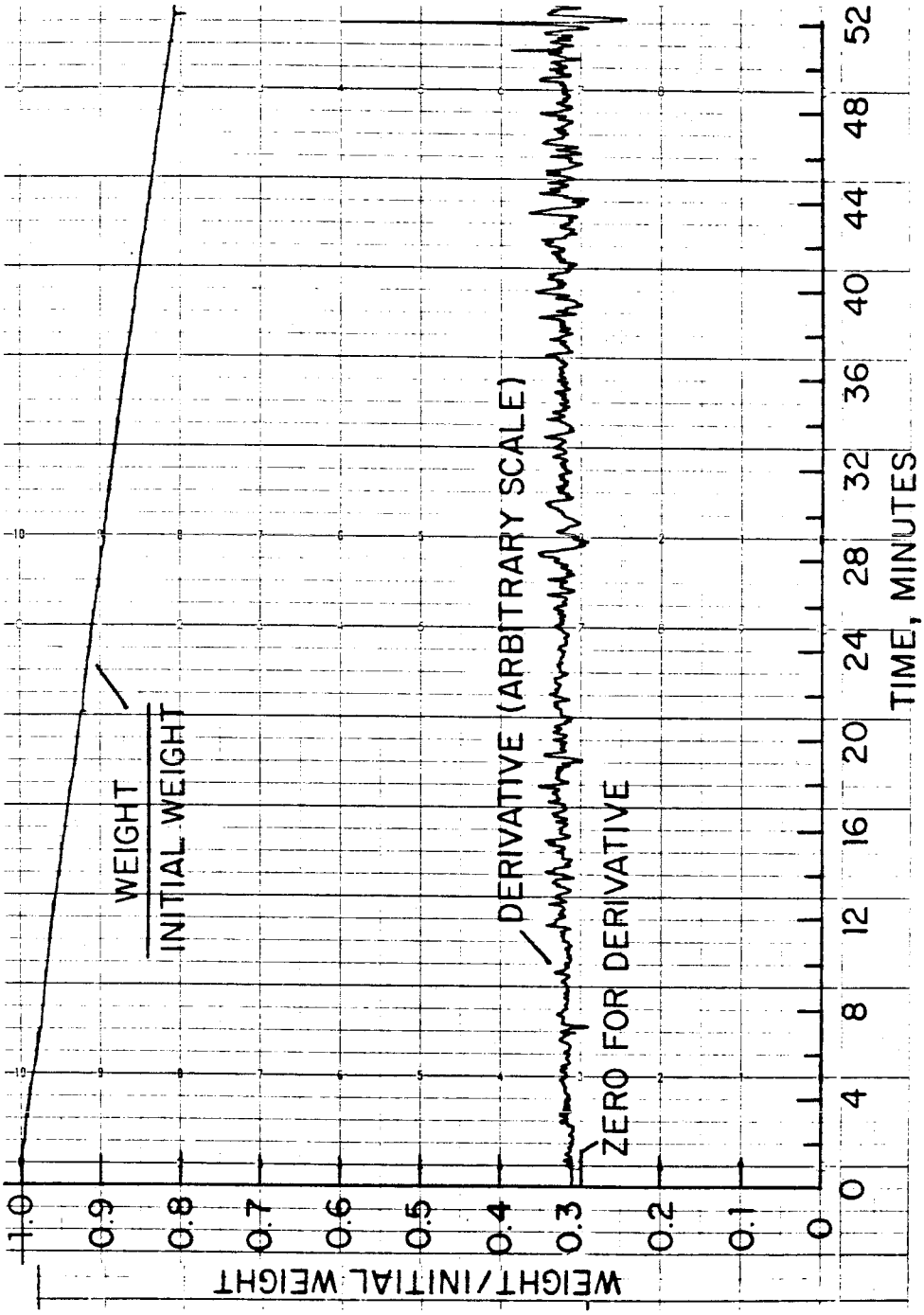

Figure 7.14 TGA record of carbon black reactivity in 17.4% oxygen at 500°C.

the mass is lost, the behavior changes. The rate is much lower in this later portion of the record. The difference between the reactivities of the two samples is explained by considering Figure 7.14, the TGA curve for carbon black. The rate of carbon black oxidation is very close to the rate of oxidation of porous carbon in the later stage of the process. Thus, the reactivities of porous and non-porous carbon are very different because the reactivity of glassy carbon is much higher than the reactivity of carbon black.

These preliminary results indicate that the two kinds of carbon have different reactivities, but cannot be applied directly to high temperature combustion conditions. Raising the carbon to a high temperature may cause devolatilization reactions that change the reactivity of the solid. Glassy carbon is more likely to be affected by heating to high temperatures than is the carbon black which has already undergone high temperature treatment. Devolatilization may decrease the reactivity of glassy carbon, decreasing the diffference between it and the reactivity of carbon black. For the same reason, these reactivity measurements cannot be compared directly with reactivity measurements of coal char. These measurements are usually made on coal that has been devolatilized at about 1000°C (Jenkins et al., 1973).

7.5 Conclusions

A material that serves as a model compound for coal has been made reproducibly. This artificial coal contains finely divided inclusions

of silica. The distribution of mineral matter in the solid has been shown to be homogeneous on the scale of a pulverized fuel particle.

Two types of artificial coal are produced in order to evaluate the material's utility. One type consists of glassy carbon containing mineral matter, the other of glassy carbon containing mineral matter and carbon black. The two materials are designated non-porous and porous carbon, respectively. Analysis of the pore structure by mercury porosimetry shows that both materials have virtually no transitional pores. The porous sample seems to have many more fine pores (below 3 nm) than non-porous carbon because the former's surface area is so high.

Low temperature reactivity measurements reveal that glassy carbon is substantially more reactive than carbon black at 500° C. The porous carbon, which contains carbon black, is consequently less reactive than the non-porous carbon. However, it is not possible to predict the reactivity difference at high combustion temperatures since the effect of devolatilization and heating on the carbon samples is not known.

This work is an attempt to develop a system in which aerosol formation and growth can be studied. The logical extension of the present work demands a more quanitative look at artificial coal. The fine pore structure of artificial coal must be characterized. This can be done using a nitrogen adsorption technique which gives pore volumes for pores in the range $1.2 < d_p < 60$ nm. Reactivity measurements must be made on the devolatilized char, i.e., char that has been heated to

the high temperature combustion temperature.

Preliminary work with this material indicates that it has much promise in the study of ash vaporization and aerosol formation from combustion of pulverized coal.

CHAPTER 8

LABORATORY COMBUSTION SYSTEM

8.1 Objectives

In developing a system to study the combustion of artificial coal, one must have somewhere to burn it. The second half of the experimental work in this study concerns itself with design of a small-scale combustion system. The overall objective is to build a small combustor in which to study single particle combustion and aerosol formation under reproducible and well-controlled conditions. This general objective dictates a set of more specific requirements. After a discussion of these requirements, details of the furnace and its workings are presented.

Combustion of a dilute suspension of particles requires the ability to feed very small amounts of material into the furnace. It is desired to measure the number and volume of aerosol produced during combustion. Therefore, the feed rate of solid must be determined precisely. The preceding two requirements imply the need for a coal feeder that can deliver minute quantities of coal reproducibly.

Since combustion of a dilute suspension of particles is not self-sustaining, the furnace must be externally heated. A study of the fundamental processes occurring during combustion requires that the local combustion environment be well characterized. The combustion and aerosol models developed are for conditions of combustion in a quiescent gas. This approach removes some potentially confusing fluid mechannics from consideration in order to study the micro-scale chemistry and physics with as little ambiguity as possible. Therefore to attain nearly quiescent conditions for single particles, the Reynolds number in the furnace must be low. In addition, the gas composition in the furnace must be variable from one experiment to the next. Chapters 4 and 6 illustrate the utility of varying the gas composition in the study of vaporization and aerosol formation.

The principal measured quantity in this system is the combustion aerosol. The volume of aerosol as a function of size can be measured with commercially available instruments but somehow the aerosol must get to these instruments. The flow system must be designed to minimize the loss of aerosol. Of equal importance is a means of diluting the aerosol-containing gases. Even when burning dilute suspensions of coal, the combustion gases contain aerosol concentrations far in excess of what most conventional aerosol-sizing intruments tolerate.

This chapter devotes itself to a description of the combustion and aerosol measurement systems. First the coal feeding system is presented. The furnace design and operating parameters are discussed.

The chapter closes with a discussion of the aerosol dilution and sampling system.

8.2 Coal feeder

8.2.1 Design

Taking into consideration many factors (such as the furnace size and the desired residence time) the combustion system requires a steady coal feed rate of 0.25-0.5 g/hr (70-140 μg/sec). This rate is too low to be obtained with a fluidized bed feeder as has been done for other small combustion systems (Hamor and Smith, 1971). A different approach to feeding coal has been developed for use with a small laminar-flow furnace (Mims et al., 1980). This design, with some modifications, is used in the present work.

Figure 8.1 shows the coal feeder used here. The heart of the feeder is a small test tube (10 mm diameter) containing a bed of coal. A needle extends down to the bed's surface. The end of the needle is a large cylinder with a hole in the center center of 0.061 cm diameter. The outer diameter of the cylinder itself is 0.635 cm. There is a smooth, conical inlet to the needle on the underside of the cylinder. Gas passes around the tip and is forced up through the needle. Coal is entrained with the gas. The feed is made stable over long periods of time by mounting the test tube on a syringe pump. An o-ring seal between the test tube and the body of the feeder allows the tube to move

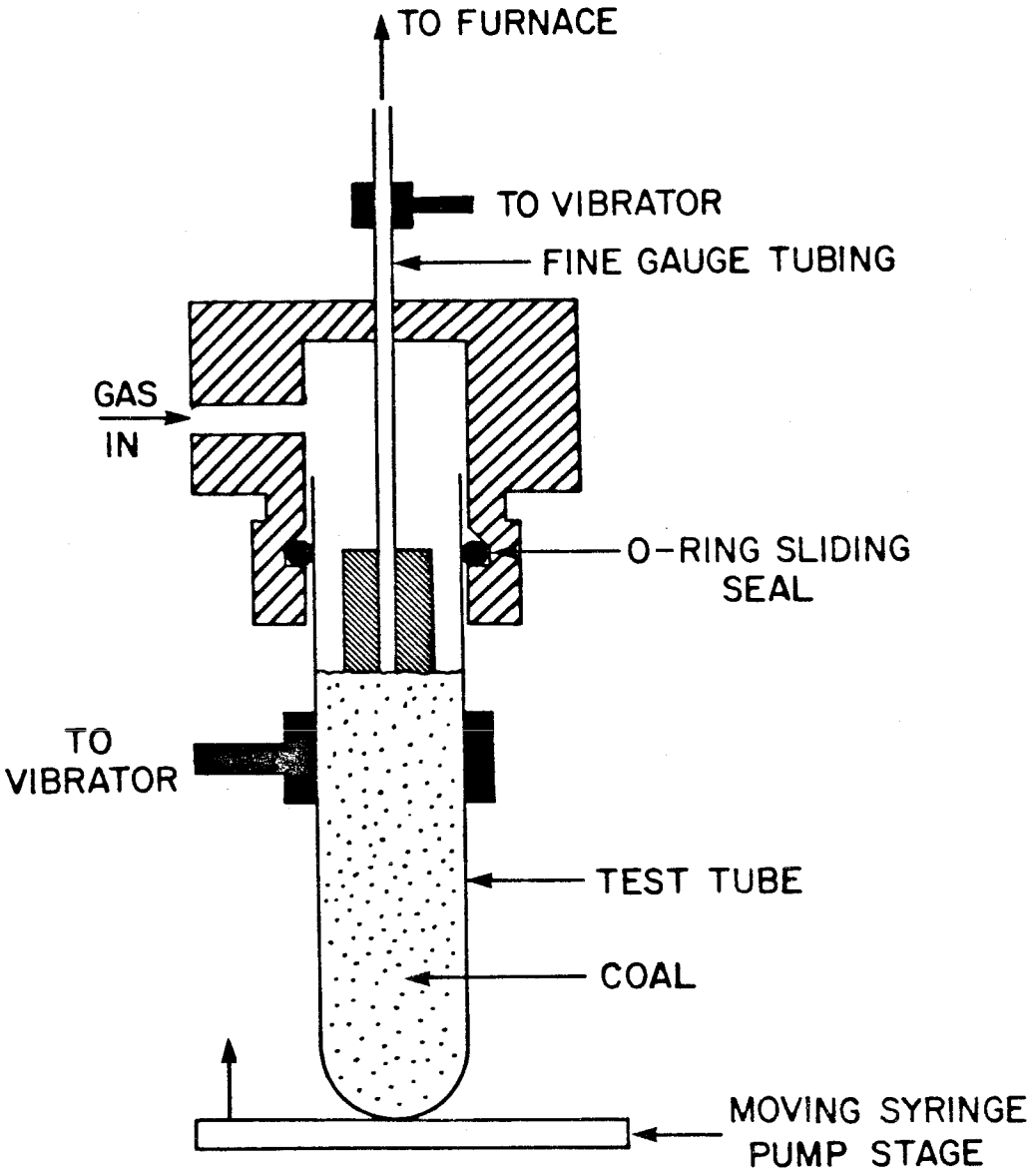

Figure 8.1 Coal feeder
(not to scale).

relative to the needle. The syringe pump moves the test tube up at a constant rate. Thus the needle "sees" a constant level of coal in the tube. The rather large, cylindrical tip causes the gas to flow across a large area of the bed before entering the needle and reduces channelization through the bed.

Problems with buildup of particles along the sides of the test tube and in the needle necessitate the use of mechanical vibration in the feeder. Vibration is accomplished with two engraving pencils which are loosely coupled to parts of the feeder. One is attached to the tube and another to the needle.

8.2.2 Calibration

The feed rate is determined by the syringe pump rate. It is independent of the gas flow rate so long as the gas velocity in the needle is somewhat higher than the terminal settling velocity for the particles. For example, the settling velocity for 50 micron coal particles corresponds to a gas flow rate of about 2 cm^3/min.

Calibration of the instrument is accomplished using an electronic balance (Mettler Model HL52) which is interfaced to a computer. Coal is fed through the needle into a 125 ml weighing boat. For the tests that will be discussed here, a sample of non-porous carbon that has been sized to 235 x 400 mesh (nominal diameter 61-38 microns) is used. For the calibration experiments, the feeder is run as during normal

operations but the coal is fed into a boat on the balance. The weight is recorded every 1 or 2 seconds using a PDP-11 minicomputer. The derivative of the weight record, the feed rate, is calculated by fitting a quadratic equation to the data locally (five points are used). The derivative is calculated from the quadratic coefficients.

The results of two calibration tests are shown in Figure 8.2. To summarize the conditions for the test, 235 x 400 mesh non-porous carbon is used; the gas flow rate is 47.5 cm^3/min.; the linear syringe pump rate is 0.792 cm/hr. The record in part a is the result of sampling at 1 Hz; part b is the calculated derivative. Parts c and d of Figure 8.2 show the results of another test under the same conditions at a sample rate of 0.5 Hz. Both records begin at the time the syringe pump is turned on. Initially, the feed rate is about 0.15 g/hr. After 10-15 minutes the rate is 0.25 g/hr. The average standard deviation of the rate is 30% ($\pm$ 0.075 g/hr.) It has been observed that this rate is maintained for 20-25 minutes with little change. After this time period, the feed rate increases, possibly due to bed compaction.

Some of the noise in the records may be caused by fluctuations in the balance output. Figure 8.3 shows the weight record for the case that no coal is being fed. Fluctuations in mass are due to noise from the balance. The noise component of the rate (Fig. 8.3b) is a significant contributor to the noise in the rates in Fig. 8.2. However, not all the fluctuations in rate can be accounted for by balance noise; some component must be due to short time fluctuations in the coal feeder

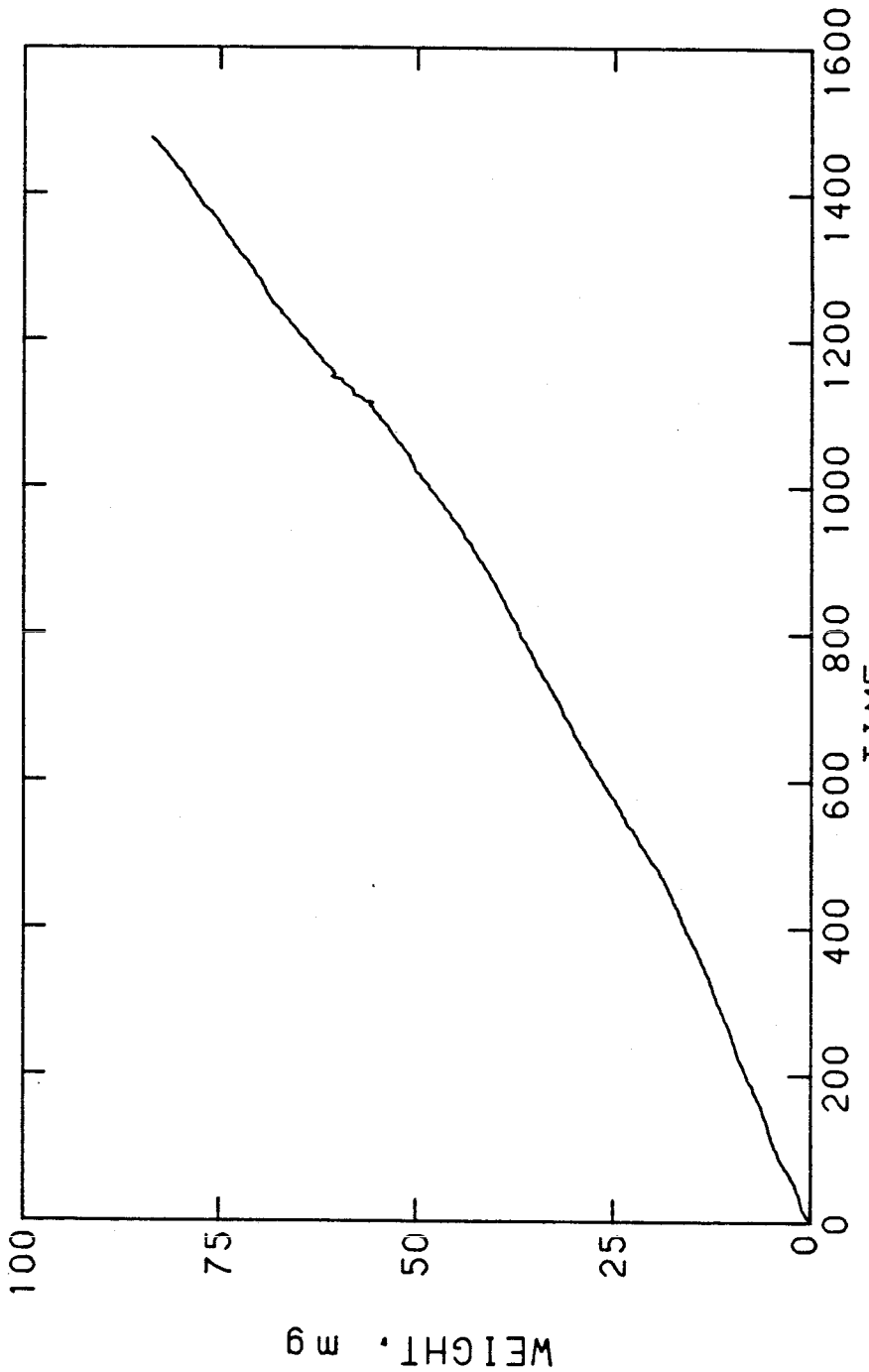

Figure 8.2a Coal feeder calibration test: weight vs. time.

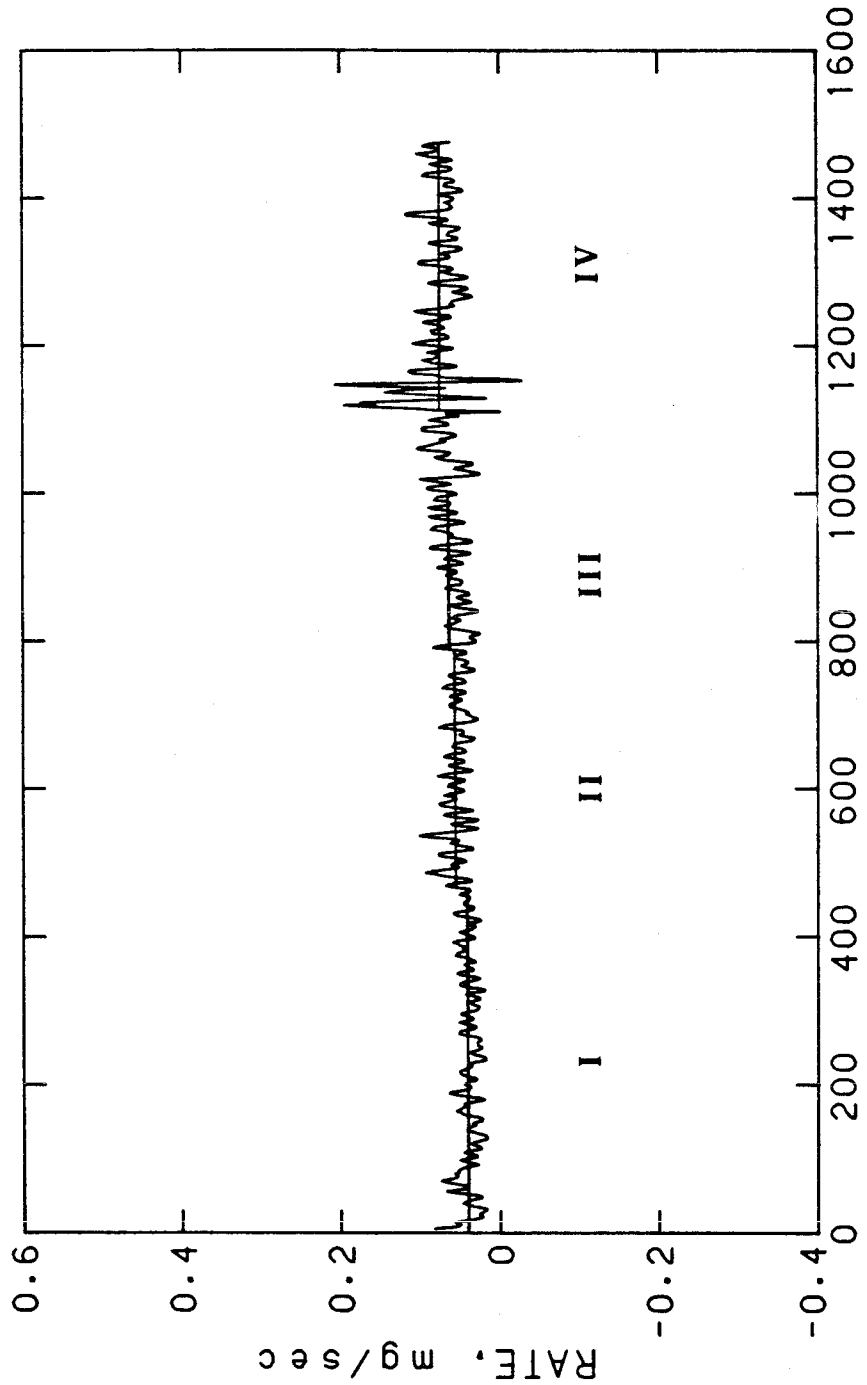

Figure 8.2b Coal feeder calibration test: calculated feed rates;
I. 0.145 g/hr; II. 0.194 g/hr; III. 0.219 g/hr; IV. 0.259 g/hr.

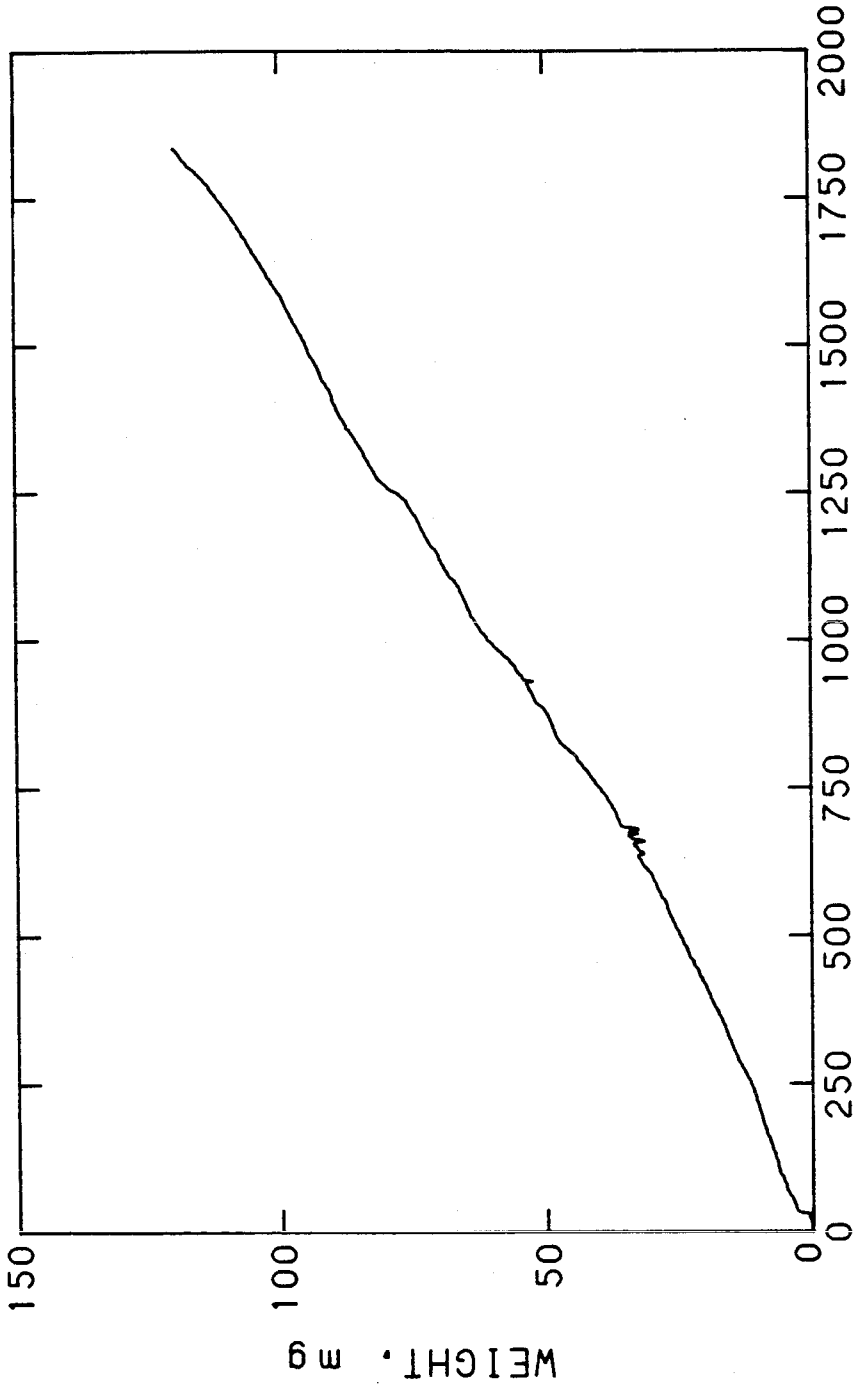

Figure 8.2c Coal feeder calibration test: weight vs. time.

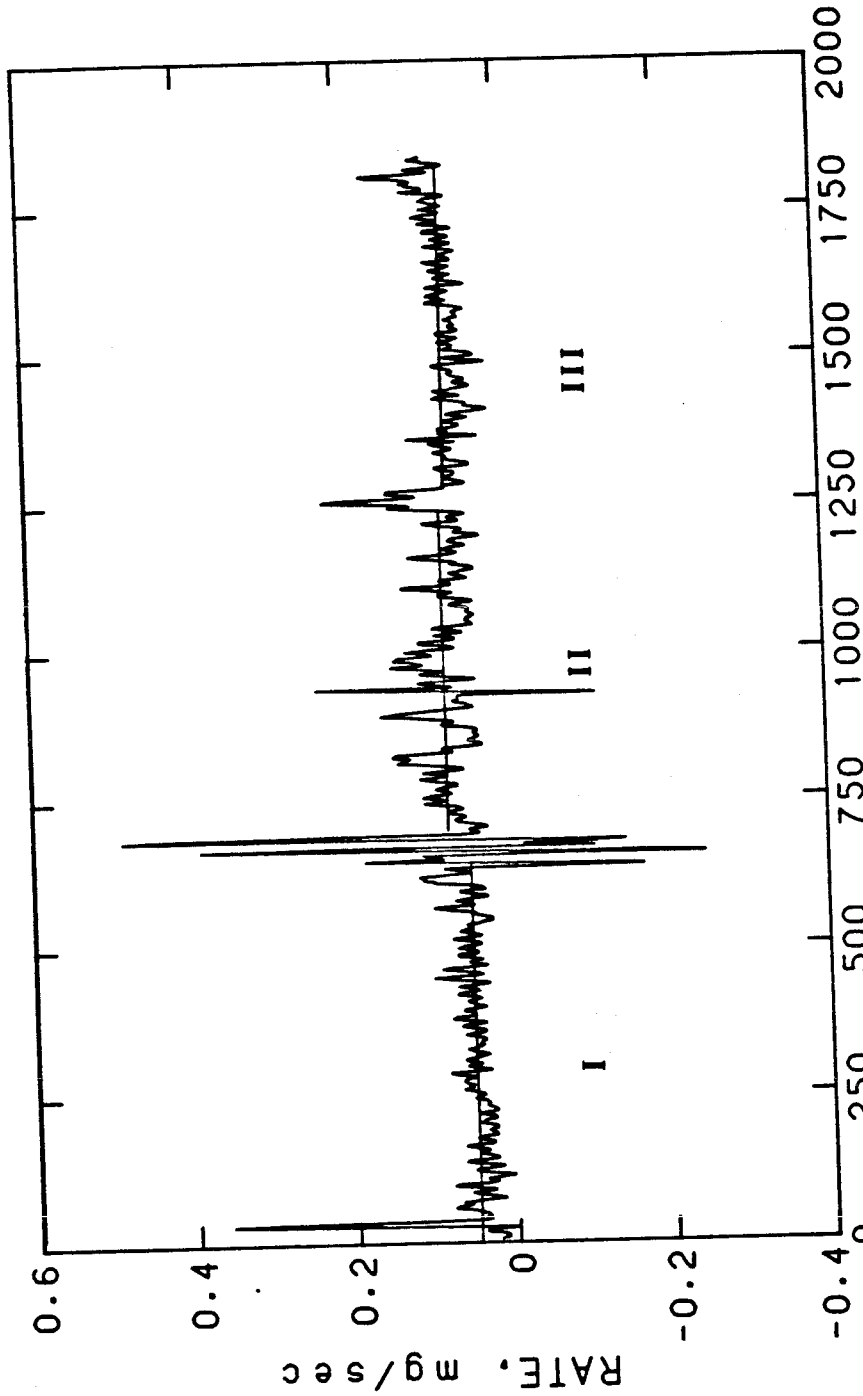

Figure 8.2d Coal feeder calibration test: calculated feed rates;
I. 0.173 g/hr; II. 0.265 g/hr; III. 0.250 g/hr.

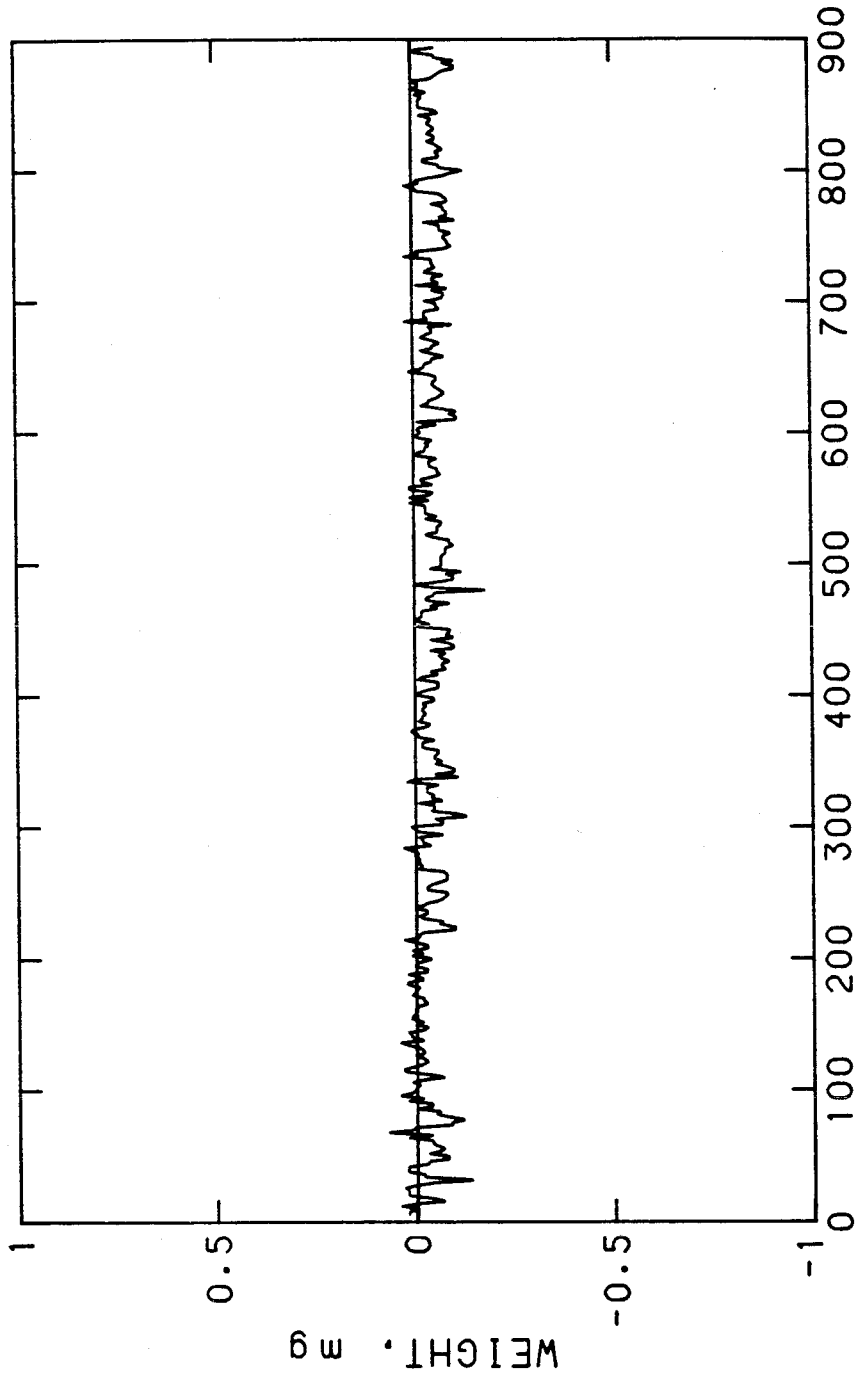

Figure 8.3a Coal feeder calibration test: weight vs. time with no coal flow.

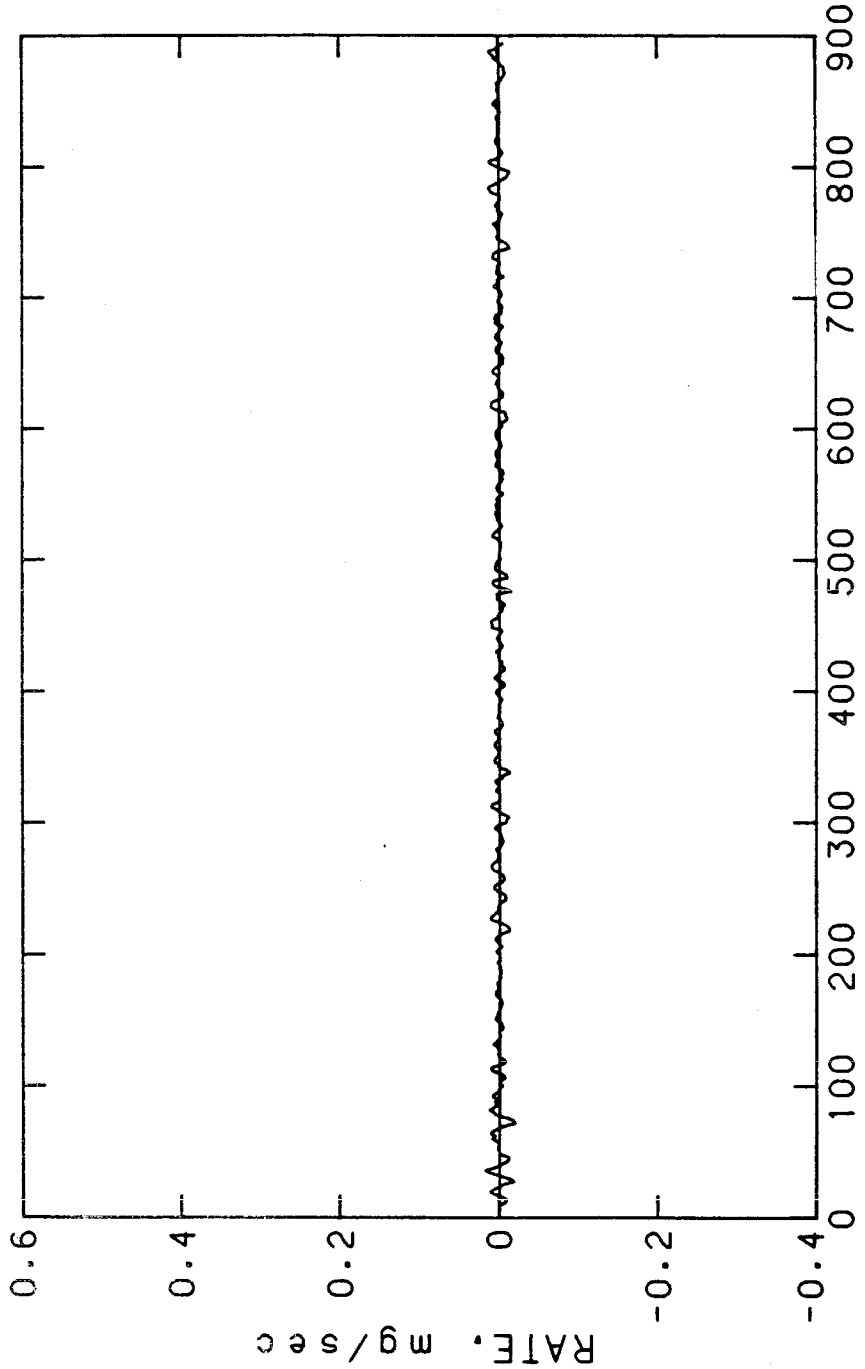

Figure 8.3b Coal feeder calibration test: calculated feed rate with no coal flow.

operation. In summary, the feed rate for these conditions is 0.25 g/hr. (± 0.075 g/hr.). This rate is reached after 10-15 minutes of operation and is maintained for 20-25 minutes.

It should be noted at this point that the fluctuations in the feed rate do not alter the oxygen concentrations in the furnace significantly. For example, the worst-case estimate of the effect of feed rate fluctuations on oxygen concentration is the case of combustion of non-porous carbon in air at a flow rate of 2 liters per minute. Using composition data (Table 7.1), one calculates that 0.25 g/hr. consumes 1.8% of the oxygen in the gas, reducing the oxygen partial pressure from 0.209 to 0.205. A 30% fluctuation in the feed rate causes only a 0.5% fluctuation in the oxygen concentration. At higher oxygen concentrations, the char consumes less of the total oxygen and this effect is reduced. Therefore, operation of the furnace under the conditions discussed produces a very stable gaseous environment during combustion.

8.3 Combustion furnace

8.3.1 Design

A schematic drawing of the combustion furnace is shown in Fig. 8.4. The heart of the furnace is an alumina tube that sits in a radiation cavity. The tube is heated externally by electric resistance heating elements.

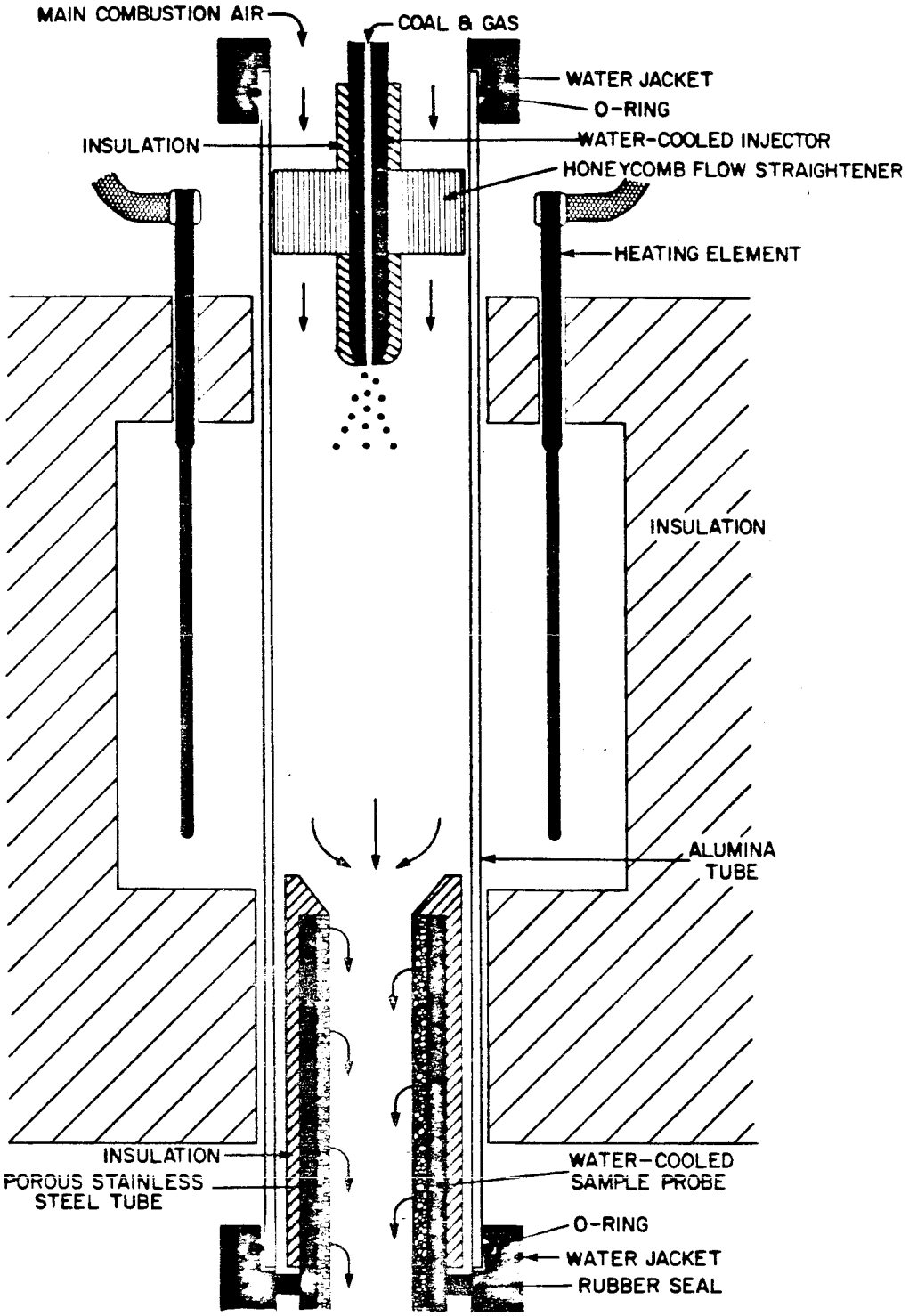

Figure 8.4 Combustion furnace (not to scale).

The furnace tube is made of high purity alumina and measures approximately 60 cm in length. The inner diameter is 5 cm and the outer diameter is 5.7 cm. The hot zone, the portion of the tube that is in the radiation cavity, is 20 cm long. Six thermocouples are attached to the outer surface of the alumina tube to measure the vertical temperature profile. The radiation cavity is formed from low density zirconia and alumina insulation manufactured by Zircar, Inc. The heating elements are made of a low resistance glass, molybdenum disilicide, and are manufactured by the Kanthal Corp. The U-shaped heating elements hang vertically from the top of the insulation; there are six elements that surround the alumina tube.

The alumina tube is secured at both ends to the rest of the furnace by o-rings. The o-rings are housed in stainless steel water jackets to ensure that the ends of the tube remain cool enough to make a good seal. The bottom water jacket is rigidly attached to the frame. The top water jackets is floating: it is restrained from side-to-side motion but can rise upward if the alumina tube thermally expands.

Coal enters the furnace through a water-cooled injector which extends down into the furnace 2 cm above the hot zone. A small fraction of the total gas flow enters through the injector; most of the gas enters around the injector in the annular region between it and the inner wall. A ceramic honeycomb placed 4 cm above the injector tip serves as a flow straightener. The tip of the injector is insulated with a 0.3 cm thick layer of low density zirconia.

From the bottom of the furnace an insulated and water-cooled sample collection probe extends up into the furnace. The inlet is 9 cm below the end of the hot zone. The probe collects all of the gas passing through the furnace. It is sealed to the bottom water jacket with a rubber gasket. The inner surface of the sample probe is made of porous stainless steel tube. The incoming gas is diluted with dried, filtered air through the walls of the probe. This prevents aerosol deposition to the walls and simultaneously cools and dilutes the combustion gases. The sample probe is connected to the dilution system that will be discussed in a later section.

The flow system is diagrammed in Figure 8.5. Gas flow into the furnace is metered by two rotometers, one for the feed stream and another for the main combustion gas stream. During normal operation, the combustion gas is either air (from a cylinder of compressed air) or some mixture of O_2 and N_2. The composition of the gas is controlled upstream of the metering rotometers by another set of rotometers. Cylinders of high-purity compressed O_2 and N_2 are used for the mixtures. The primary dilution air, that flowing through the sample probe, is from the building's compressed air supply and is dried, filtered, and metered by another rotometer.

8.3.2 Temperature and flow fields

The temperature of the furnace tube is monitored by thermocouples on its outer surface. The thermocouples are type S (platinum

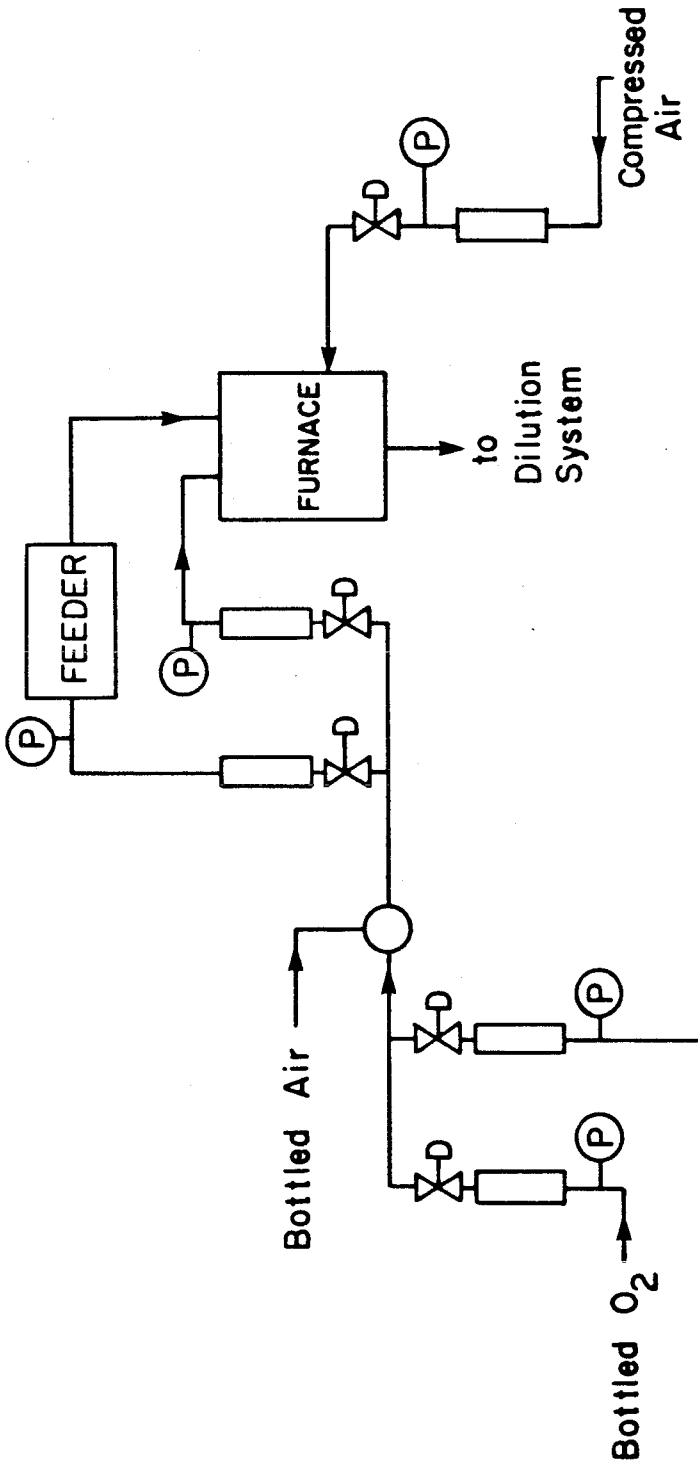

Figure 8.5 Flow system for combustion furnace.

vs. platinum-10% rhodium). They run through alumina feed-throughs of 0.08 cm diameter which are attached to the outside of the furnace tube with alumina cement. The bead of each thermocouple is embedded in cement so it does not see radiation from the heating elements. Placement of the six thermocouples is illustrated in Figure 8.6. All thermocouples are read with a digital voltmeter. At the position of thermocouple 3 there are actually two thermocouples. The second of these is connected to the temperature controller that regulates the furnace power supply. A proportioning controller manufactured by Love Controls (Model 52) is used for this function.

For the experimental work in this study, a maximum outer wall temperature of 1600 K is used. Figure 8.7 shows the measured temperature profile under these conditions. The profile is very flat in most of the hot zone. The inside wall temperature in the hot zone can be estimated from the heat flux to the outer surface and the wall temperature. The power consumed by the heating elements is measured and the heating element resistance as a function of element temperature has been supplied by the manufacturer. From this one calculates the heating element temperature and the radiant heat flux to the outer wall. A simple heat balance on the tube shows that the inner wall temperature is 25 K below the outer surface temperature. If one takes into account the losses through the insulation, the calculated inner wall temperature is slightly higher. Losses through the shell reduce the heat flux to the furnace tube and decrease the temperature drop across the tube walls. The loss of heat through the insulation is estimated to be about 15-20%

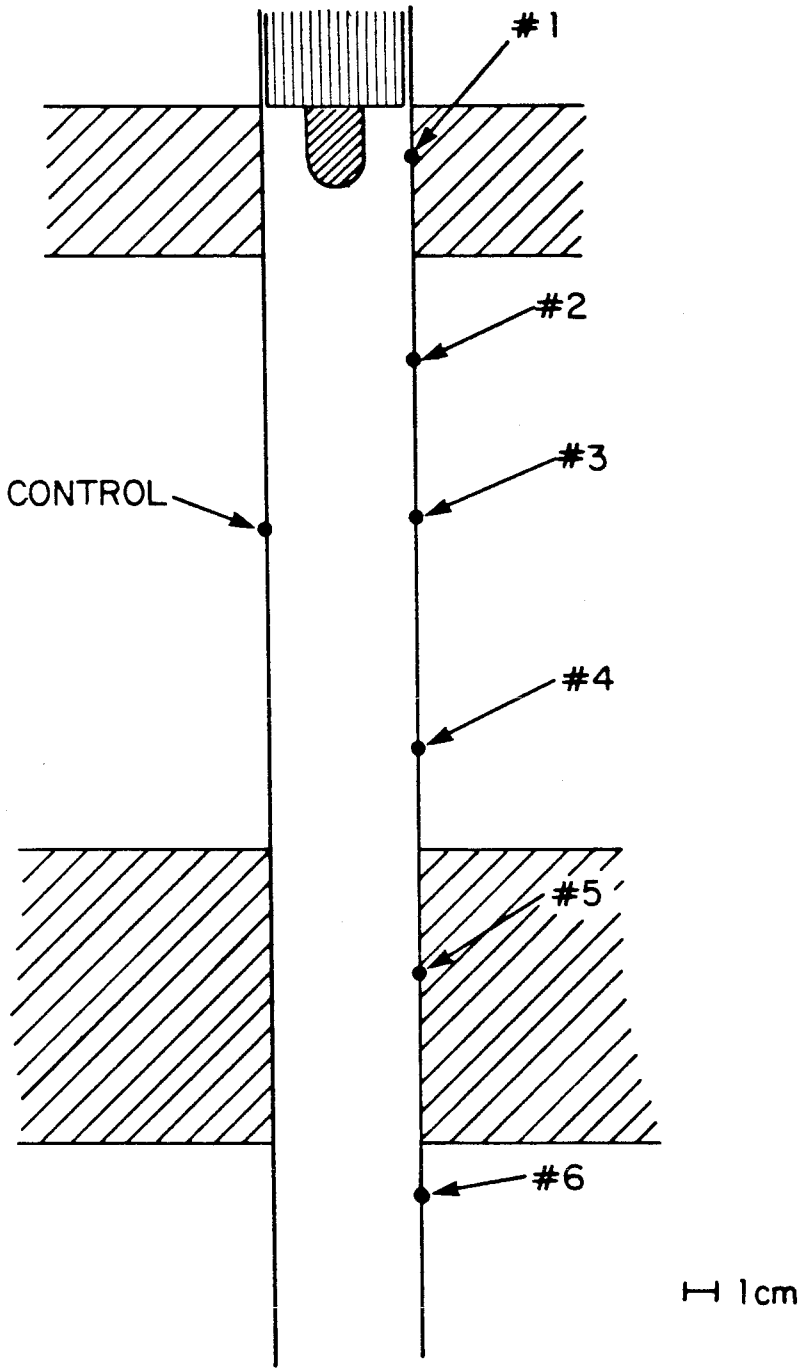

Figure 8.6 Placement of thermocouples (to scale).

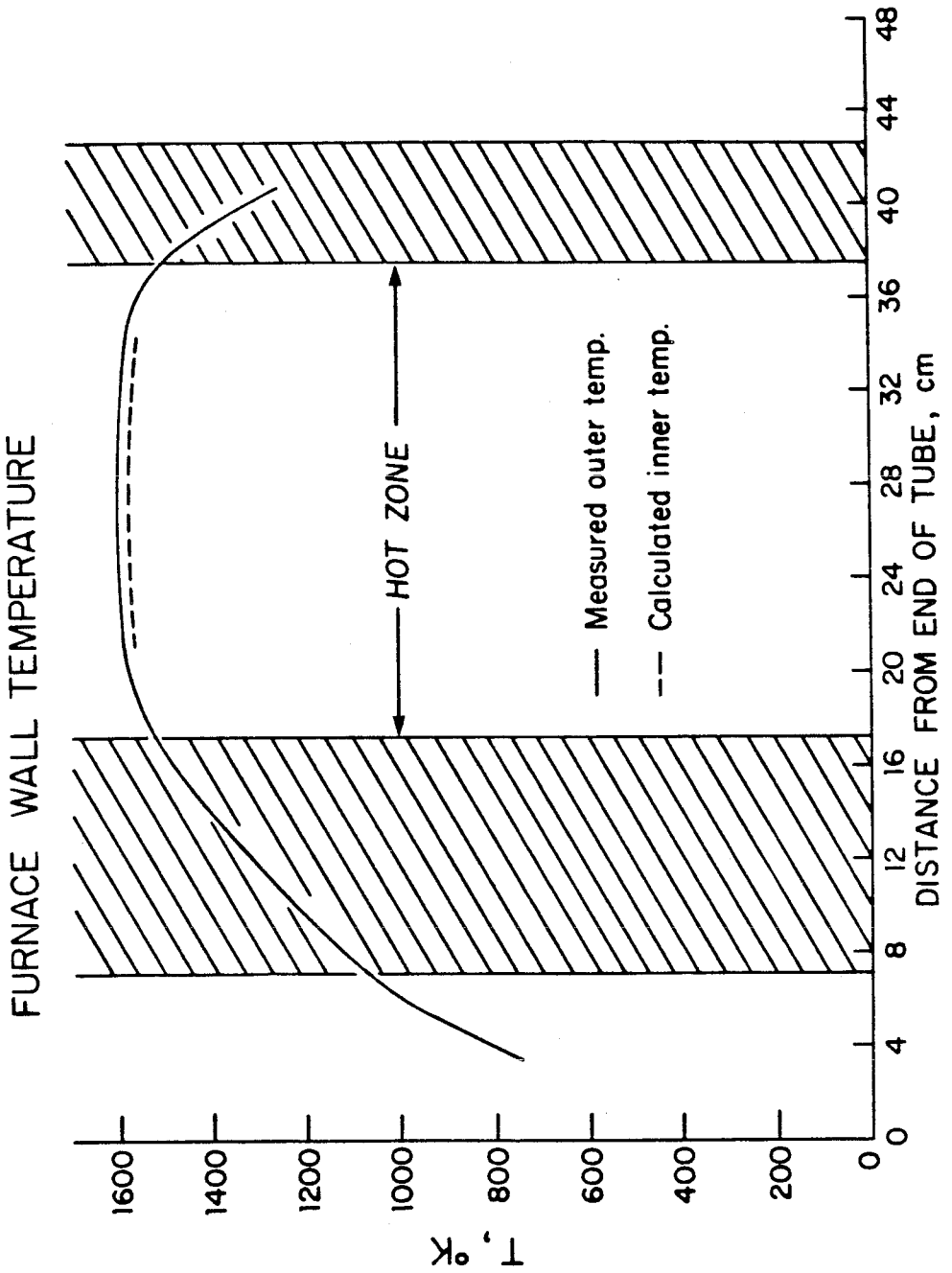

Figure 8.7 Temperature profile in the furnace (64% burnout).

of the total flux, reducing the temperature drop through the furnace tube to approximately 20 K.

As mentioned earlier, the gas flow rate through the feeder is 47.5 cm^3/min. for all experiments. This flow is above the minimum calculated flow rate in order to prevent sedimentation and the resultant blockage of the coal feed line. For most of the combustion experiments to be discussed the main combustion gas flow is 2 lpm. This rather low rate ensures that the residence time in the furnace is sufficient to burn out the char. The result is that there exists a mismatch of the inlet velocities: the initial velocity of the feed stream is about 50 times higher than the velocity of the main combustion gas stream. The furnace Reynolds number at combustion temperature is 20. The jet Reynolds number for the feed stream is 125. Therefore, the entrance of the gas into the furnace through the coal injector can be approximated as a laminar jet flowing into a stagnant gas. This gives an approximate solution that can be used to assess the impact of the inlet jet on the furnace flow field.

Schlichting (1960) developed an analytic solution for the axisymmetric three-dimensional laminar jet. This solution can be applied to the case under discussion if several assumptions are made. The nature of the assumptions preclude an exact solution, but this analysis provides a qualitative picture of the inlet conditions. It is assumed that the bulk gas temperature is constant at some average temperature. The effect of the furnace walls is not taken into account

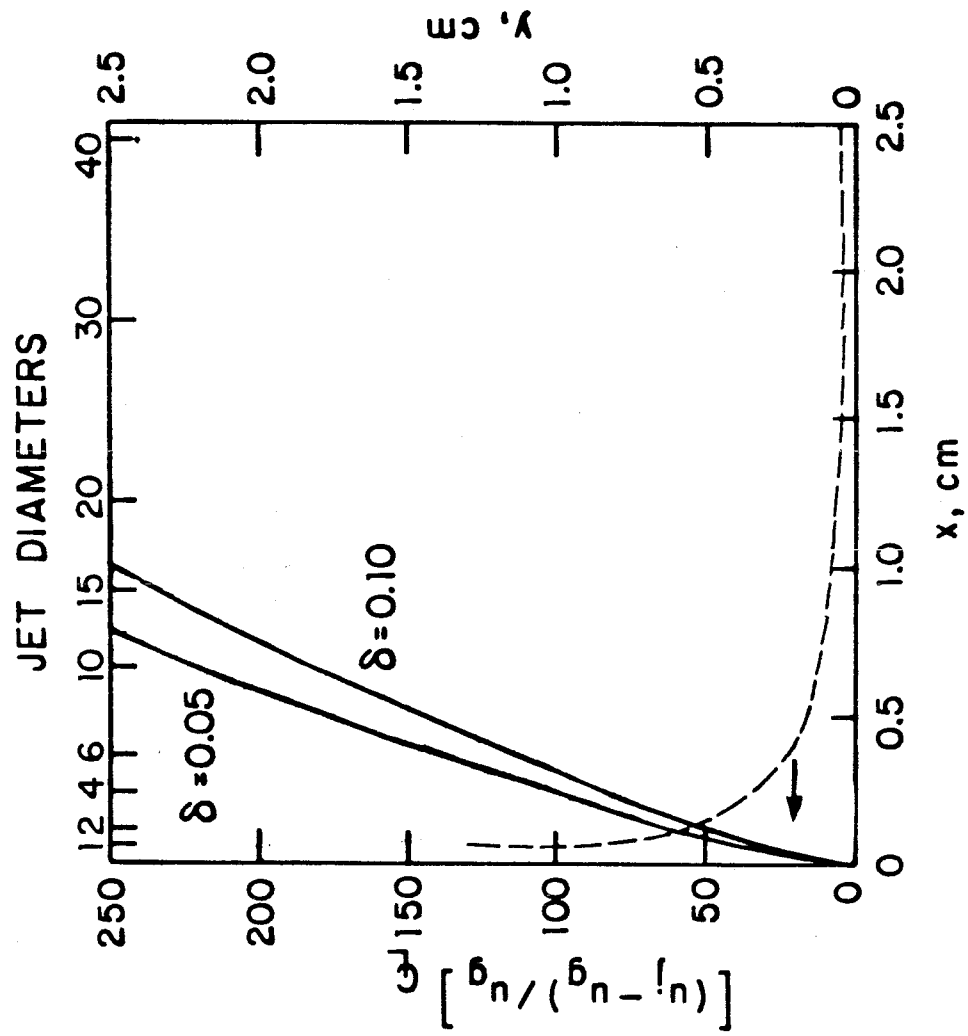

Figure 8.8 Results of laminar jet calculations (note: $\delta = (u_j - u_g)/u_g$).

and any recirculating flow around the tip of the injector is neglected. Figure 8.8 show the results of the laminar jet calculation. The jet centerline velocity, relative to the bulk gas velocity, is plotted as a function of distance from the injector tip (x = 0). The jet velocity rapidly decays and by the time the hot zone is reached (x = 2 cm), the centerline velocity has been reduced by at least an order of magnitude. Also plotted on this curve is the approximate jet width, the position corresponding to a value of the jet velocity that is 5% or 10% greater than the bulk gas velocity. These curves indicate that the jet width approaches the tube radius (2.5 cm) within about 30 jet diameters, or about 2 cm.

The preceding calculations are only approximate but the results indicate that the gas jet from the injector disappears as the hot zone is reached. Therefore the char particles are immersed in the bulk gas when they enter the hot zone of the furnace.

8.4 Aerosol sampling system

8.4.1 Dilution system

In order to measure the aerosol produced during combustion, the combustion gases must be diluted. Reasons for this are twofold. First, even the concentrations of aerosol produced in very dilute combustion are too high for conventional aerosol-sizing instruments to measure. Second, the aerosol must be dilute enough so that coagulation in the

sample lines does not alter the size distribution before it reaches the sampling instruments. In this system, the stream is diluted once in the sample probe. Under the conditions that will be described shortly, this amounts to a dilution ratio of about 3:1.

A second stage of dilution is used and the system is shown in Figure 8.9. On leaving the sample probe, the stream enters an isokinetic flow splitter which consists of two concentric tubes. Flow through the outer tube is filtered and exhausted to the room. The two flow rates, inner and outer, are adjusted so that their velocities are nearly equal at the inlet to the inner tube. The stream that flows through the small tube enters a 45.5 l mixing flask along with additional dilution air. The flask accomplishes two things: aerosol laden gas has time to mix with dilution air and, in its capacity as a continuous stirred tank reactor (CSTR), the flask damps out some of the aerosol concentration fluctuations in time. Most of the output stream is exhausted. A portion of the flask output is withdrawn for on-line aerosol concentration measurements. The analysis stream passes through a flow splitter to partition the flow appropriately. Two instruments are used to measure aerosol size distributions: the Electrical Aerosol Analyzer (EAA) and the Optical Particle Counter (OPC). The former is manufactured by Thermal Systems, Inc. and measures aerosol in the size range 0.01 to 1.0 micron. The latter is made by Royco and measures aerosol in the range 0.12 to 6 micron.

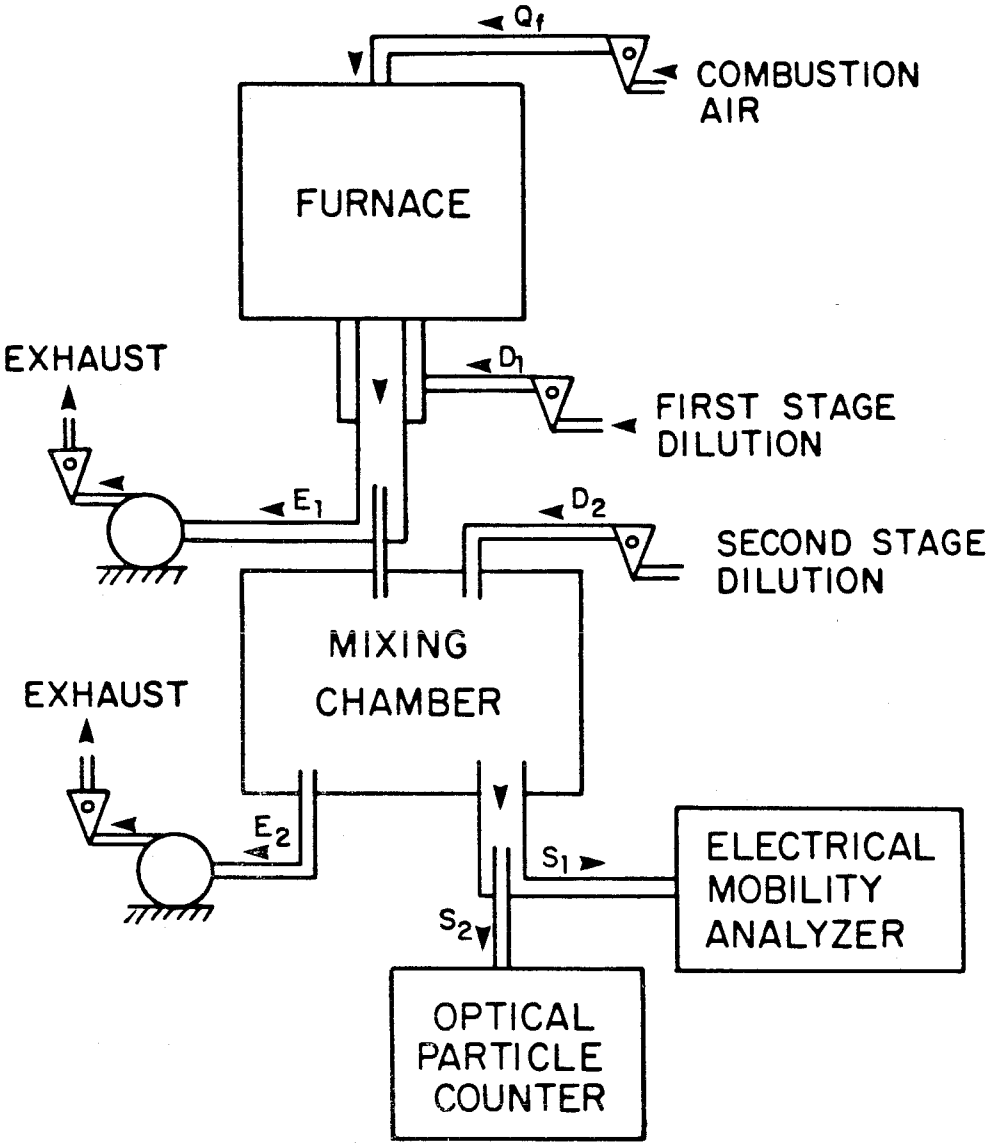

Figure 8.9 Dilution and sampling system.

8.4.2 Calibration of dilution system

Obtaining sufficient dilution means using many different pumps and flowmeters at the same time. The combined uncertainty in their settings necessitates some way of obtaining the dilution ratio other than by merely summing the flow rates. Two different methods are used to calibrate the dilution system; both give similar results. One method uses known concentrations of NO and an NO-NO_2 analyzer; the other uses aerosol-sizing instruments to measure the room aerosol. In both procedures, the quantities of interest are measured with and without the dilution system upstream of the measuring instrument.

The flows of interest have been labeled in Fig. 8.9 and the flow conditions for two different calibration tests are given in Table 8.1 The first method is used to obtain an overall dilution under the conditions of Case 1 in Table 8.1. The furnace combustion gas is taken from a precalibrated cylinder of N_2 containing 206 ppm NO. The dilution system is set up as under normal operations except that the EAA and OPC are replaced by a chemiluminescent NO-NO_2 analyzer manufactured by ThermoElectron Corp. The NO concentration at the outlet of the dilution system is measured as 5.2 ppm, giving an overall dilution of 39.6.

An alternate way to calibrate the dilution system is to use the aerosol found in room air. This is always amounts to a significant number of particles. This method is used to calibrate only the second stage of dilution. Room air is drawn into the mixing flask as the

TABLE 8.1: CONDITIONS FOR OPERATING DILUTION SYSTEM

FLOW (ℓ/min)	CASE 1	CASE 2
Q_f	1.98 ± 0.03	1.98 ± 0.03
D_1	3.4 ± 0.2	3.2 ± 0.2
D_2	22.0 ± 0.4	24.1 ± 0.4
E_1	5.0 ± 0.2	5.0 ± 0.2
E_2	19.3 ± 0.5	19.2 ± 0.5
S_1	4.0 ± 0.2	4.0 ± 0.2
S_2	0.3 ± 0.01	0.3 ± 0.01

combustion gases would be during normal operation. The EAA is not useful for this measurement because of the very small numbers of submicron particles in the room air. The OPC is very much more sensitive to low concentrations than the EAA. Tests have been made using flow conditions corresponding to both Case 1 and Case 2. The OPC readings have been corrected for losses in the CSTR using a method developed by Crump (1983). By comparing the total number concentration with and without the dilution system in place, the second stage dilution is calculated. The first stage dilution is calculated from measured flow rates. The aerosol method gives an overall dilution of 36.2 for Case 1 conditions; this value is in good agreement with that measured using NO. The dilution for Case 2 conditions is 130.

8.5 Suggestions for future work

A small laminar-flow combustor has been designed and built for the purpose of studying aerosol formation from coal combustion under well-characterized conditions. As with any system, there is room for improvement. The first design of any apparatus always brings to mind many ideas for the next generation. Some suggestions for further design and study are discussed in this section.

The feeder performs very well at delivering minute amounts of coal over periods of 10-20 minutes. However, there is much fluctuation in the feed rate over very short time scales, on the order of 10-20 seconds. These fast fluctuations pose a problem for aerosol sampling

instruments that require a stable aerosol concentrations for periods of many seconds; the EAA is one of these instruments. It measures the cumulative size distribution over a period of about one minute. If the aerosol concentration is not stable (because the feed is not stable), the measurement can be in error. In this work, a CSTR is used to damp out fluctuations in the aerosol concentration. In the future, redesign of the feeder should be studied to determine if more stability can be obtained. The lower practical limit for gas flow in the feeder should be probed also. If the feeder gas flow rate were lower, the furnace inlet velocities would be better matched.

The present work concerns itself with aerosol formation, but in the future the system could be used for the study of micro-scale char combustion. The sample collection system in the furnace could be redesigned so that the probe extends up into the hot zone. This would make possible the collection of partially burned char particles, "snapshots" of the combustion process. In this case, it would be valuable to measure the particle temperature during combustion. This has already been done in other small-scale combustion systems.

Finally, some of the uncertainty in the concentration measurements could be removed by redesign of the dilution system. This is perhaps the most troublesome part of any system that deals with aerosols. One possible improvement is the metering of exhaust flows by critical orifices instead of valves and rotometers.

CHAPTER 9

LABORATORY COMBUSTION STUDIES

9.1 Conditions for combustion

The preceding two chapters introduce an overall system for studying aerosol formation processes: combustion of artificial coal. This chapter contains preliminary experimental work; the aim here is to determine the utility of artificial coal for the purpose for which it was intended. Since this system is designed as a model for coal combustion, perhaps the most important question to answer is does it burn like coal? A related issue is whether or not the aerosol formation and growth processes are taking place in the model system as they are in the real system.

Two kinds of data are discussed in this chapter; both are from experimental studies of the combustion of the artificial coal that has been developed. A qualitative investigation of the char combustion process is carried out by examining partially burned char particles with a scanning electron microscope. A great deal of insight into the char combustion process can be gained in this way. Second, results of a

quantitative study of the effect of particle temperature and char structure on aerosol formation are discussed.

All combustion experiments are performed at a single furnace temperature. As mentioned in the previous chapter, the inner wall temperature in the hot zone is 1575 K. The temperature profile in Figure 8.7 applies to the combustion experiments discussed in this chapter. For the photographic study of devolatilized or partially burned char, the total gas flow rate through the furnace is 4-5 lpm. At the furnace temperature, this corresponds to a gas residence time in the hot zone of 0.45-0.6 seconds. (The particle residence time is expected to be shorter than the gas residence time due to initial particle momentum from the injector jet and the effect of gravitational settling in the furnace.)

For the studies of aerosol formation during combustion, a lower gas flow rate is used so that the residence time is sufficient for complete combustion. The total gas flow rate in this case is 2 lpm, corresponding to a gas residence time on the hot zone of 1.2 seconds. The furnace Reynolds number is about 20; the particle Reynolds number is less than 0.01. As indicated in the previous chapter, the sample must be diluted to make the aerosol measurements. The dilution system configuration is as discussed in Chapter 8 and the overall dilution ratio is 130 to 1 (Case 2 of Table 8.1).

9.2 Qualitative study of artificial coal combustion

Visual observation of char particles strengthens the understanding of the combustion process. Both non-porous and porous carbon (see Tables 3.1 and 3.2) have been burned in air. The partially burned particles are collected on an aluminum stub as they exit the furnace. The stub is sputter-coated with gold and viewed with a scanning electron microscope (SEM).

Rapid heating of coal particles to high temperatures induces chemical and physical changes in the solid. To assess the effect of rapid heating in artificial coal, the non-porous carbon is fed into the furnace at 1575 K in an atmosphere of pure nitrogen. The char undergoes devolatilization but no combustion in these experiments. Figure 9.1 shows two views of the devolatilized non-porous carbon. These can be directly compared with the raw material, Figure 7.9a. The heat-treated material retains the smooth and impenetrable surface of the raw material. The only observable change between the two materials is the presence of large ridges and cracks in the heat-treated material. Figure 9.1b shows a crack that is more than 5 microns long. It is probably brought about by thermally induced stress in the solid. Large cracks do not alter the specific surface area significantly and therefore should not have a big effect on the combustion behavior of the solid. Indeed, rapid heating of non-porous carbon does not appear to change the solid very much.

Figure 9.1 a Non-porous carbon devolatilized in N_2 at 1575 K (magnified 2000 times).

Figure 9.1 b Non-porous carbon devolatilized in N_2 at 1575 K (magnified 2000 times).

In the first combustion experiment, glassy carbon is burned in air. A partially reacted glassy carbon particle is shown in Figure 9.2. Part a, at lower magnification, resembles raw glassy carbon, Figure 7.8, except that its surface has smooth, shallow depressions. Presumably combustion is occurring on the surface only, resulting in it being eaten away. At higher magnification (Fig. 9.2b) the surface still appears as smooth and glasslike as that of the raw glassy carbon (and non-porous carbon). Thus, combustion of glassy carbon appears to proceed via a smooth, receding surface. This is expected since glassy carbon and non-porous carbon have been demonstrated to have no transitional pores and no macropores.

Partially burned non-porous carbon is shown in Figure 9.3. Large holes, on the order 5 microns, cover the surface of this char. At higher magnification (Fig. 9.3b) the holes appear shallow. The surface of the material is still very smooth and, at this magnification, is identical to the raw non-porous carbon and the burned glassy carbon. The fact that many of the holes in the burned non-porous carbon contain mineral inclusions suggests that the mineral matter has a catalytic effect on the reaction of carbon or at least that cracks surrounding the inclusions provide increased surface area for combustion. Overall, though, non-porous carbon appears to burn via a receding surface of carbon much as the glassy carbon does.

Examination of partially burned porous carbon, reveals a very different material than the previous two. Figure 9.4 shows at last why

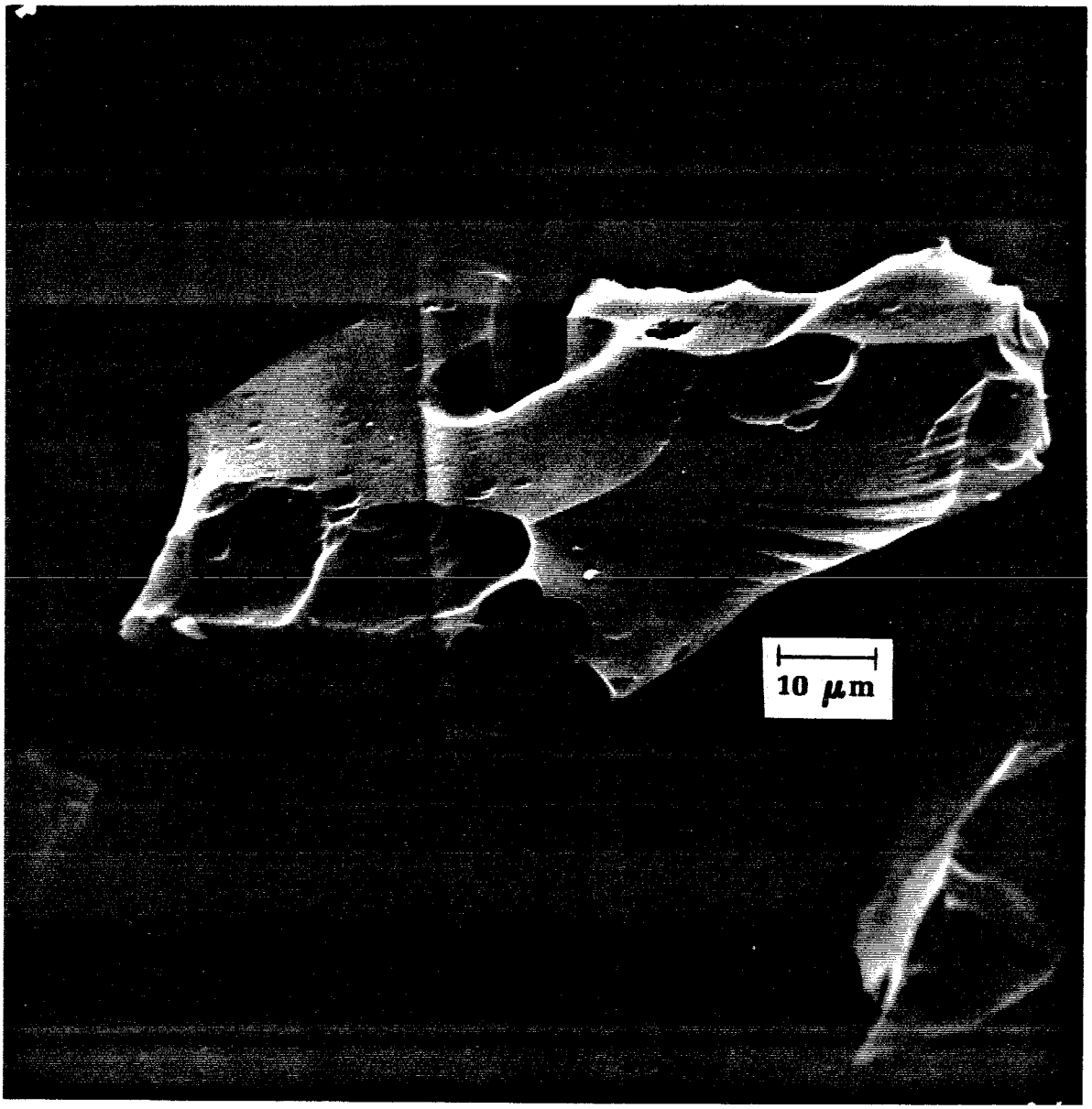

Figure 9.2a Partially burned glassy carbon (magnified 700 times).

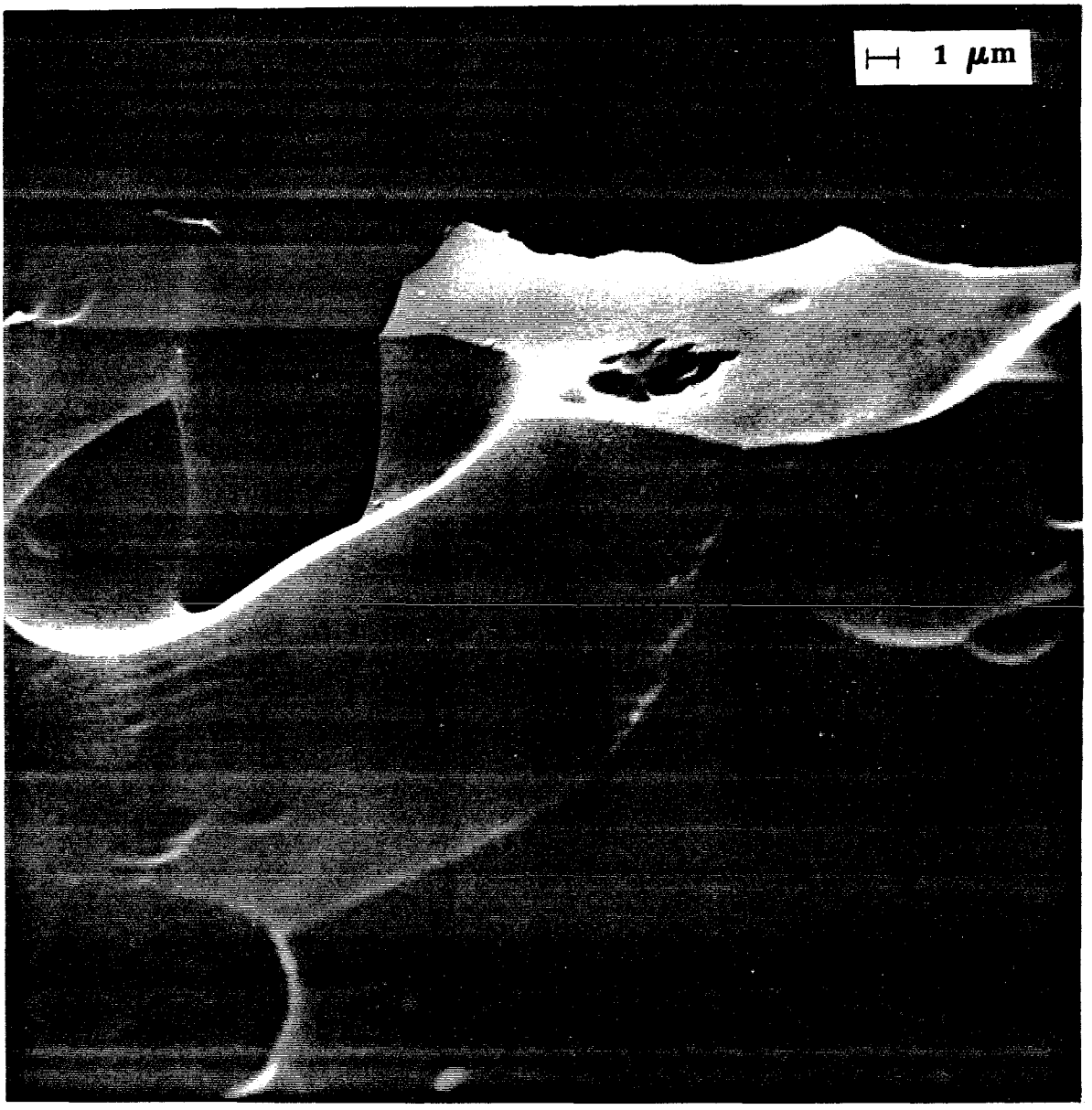

Figure 9.2b Partially burned glassy carbon (magnified 2000 times).

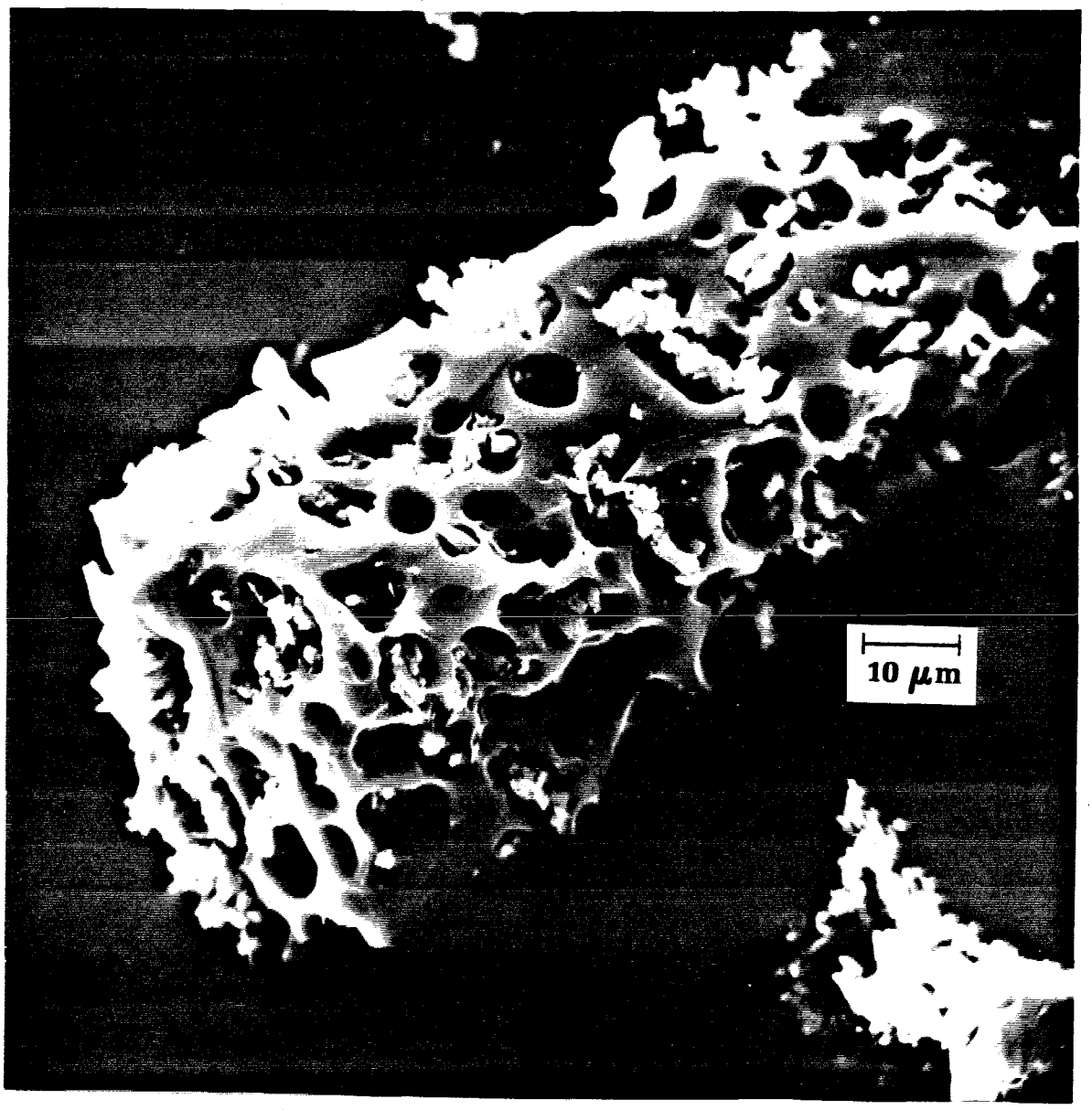

Figure 9.3a Partially burned non-porous carbon (magnified 700 times).

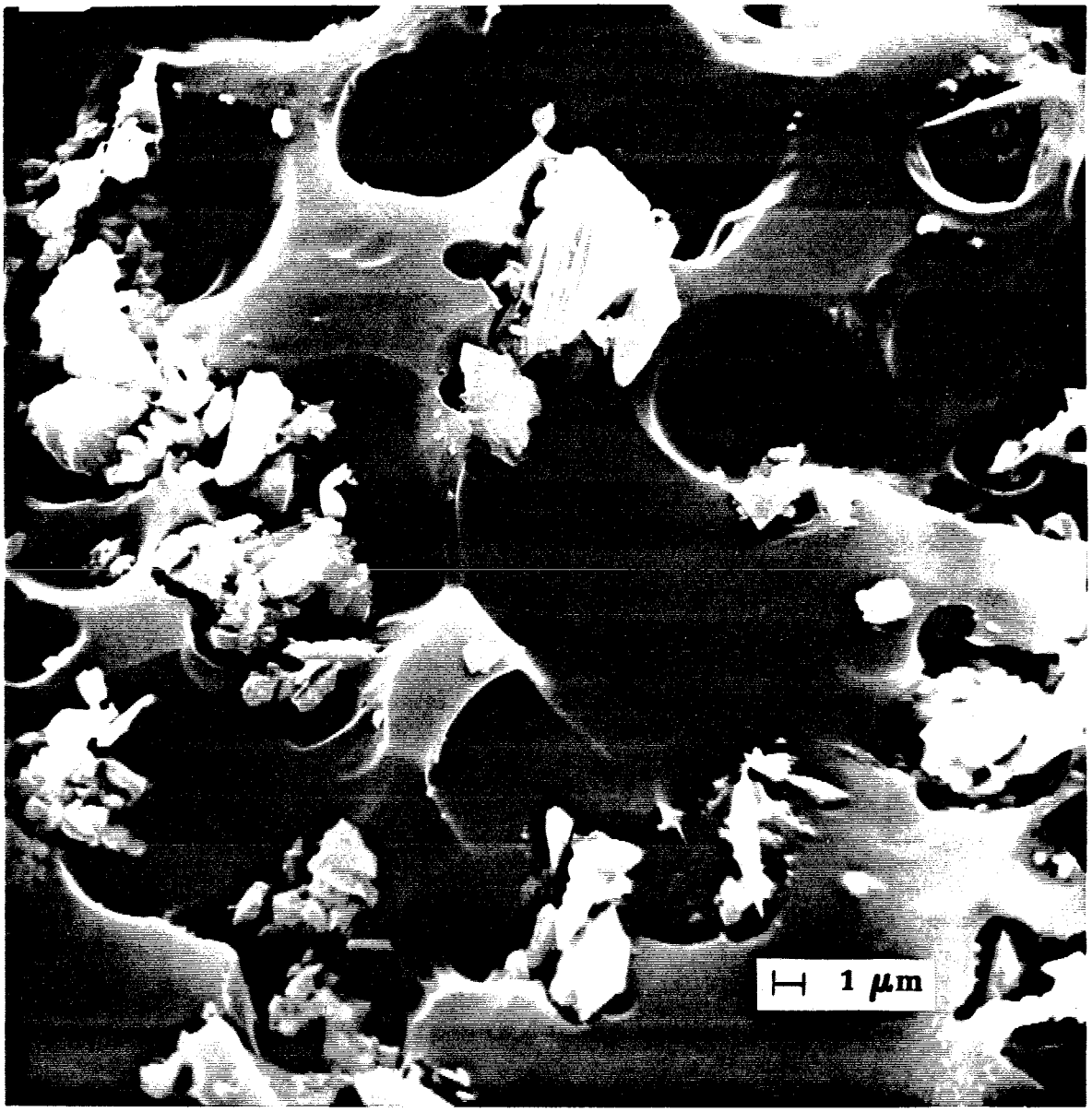

Figure 9.3 b Partially burned non-porous carbon (magnified 2000 times).

this material is labeled porous. Even at low magnification (Fig. 9.4a) porous carbon char is very different from non-porous or glassy carbon char. The surface is covered with smaller pores; none are larger than 2 microns and many pores one-tenth that size are visible. At higher magnification (parts b and c) the large pores do not appear as shallow as those of non-porous carbon. Finer pores in the size range 50-100 nm are visible; no such pores were observed in non-porous carbon char.

The reason for the differences in the appearance of the non-porous and porous chars may lie in the differences between glassy carbon and carbon black. Low temperature reactivity measurements on the raw (not heat treated) materials show that glassy carbon is considerably more reactive than carbon black. If this reactivity difference is preserved under high temperature combustion, one might expect the glassy carbon to burn out more rapidly than the carbon black. This would result in a fine network of carbon; recall that the primary particle size of the carbon black is 22 nm. The porous carbon appears to burn with substantial penetration of the solid by oxygen; the non-porous carbon, on the other hand, burns almost exclusively on its external surface. Since the porous carbon presents a much higher surface area for reaction, it may in fact have a higher combustion rate per unit volume in spite of the reactivity differences between glassy carbon and carbon black. This implies that the particle temperature of the porous carbon during combustion may be higher than that of the non-porous carbon.

Figure 9.4a Partially burned porous carbon (magnified 1700 times).

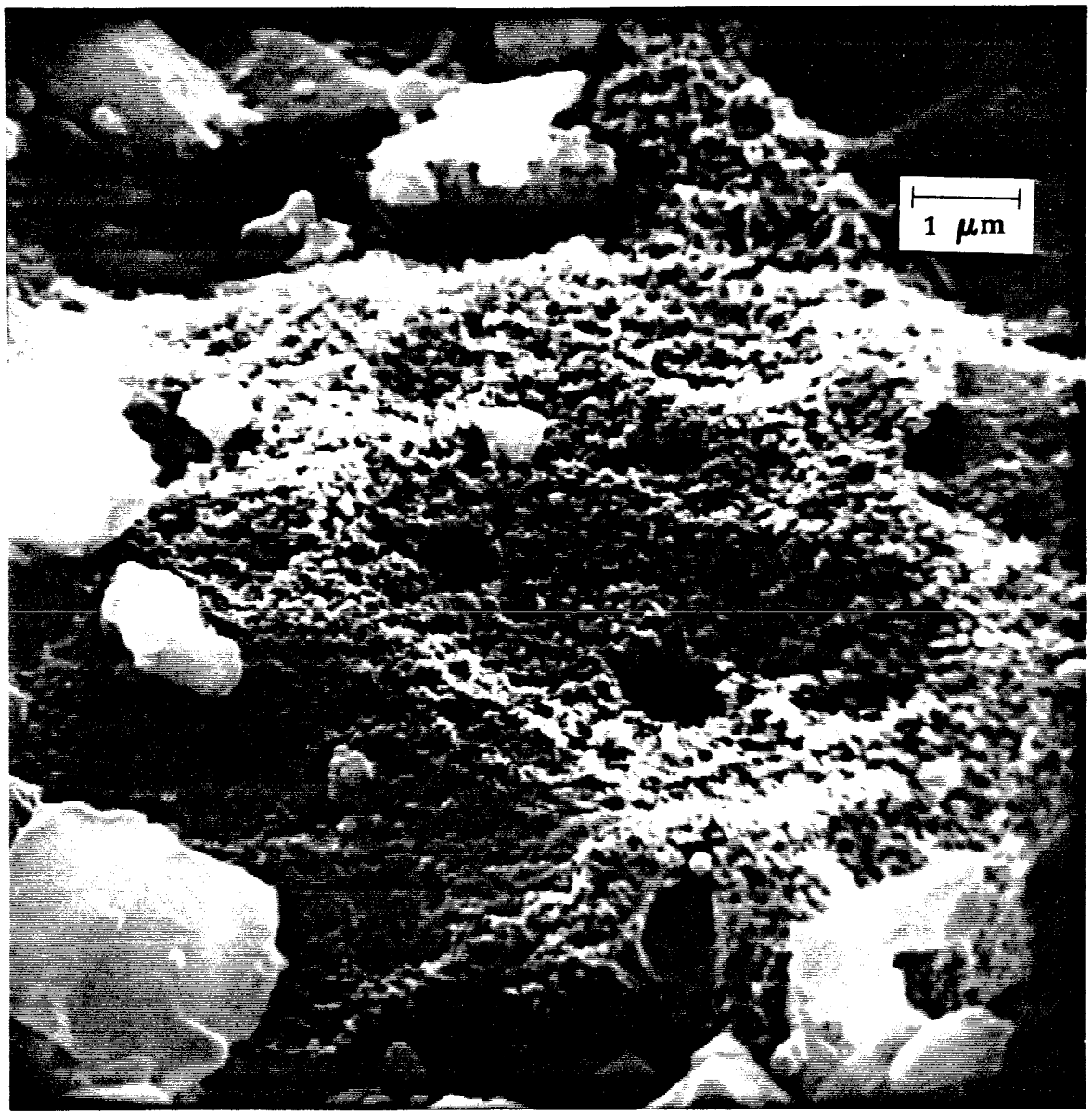

Figure 9.4b Partially burned porous carbon (magnified 8000 times).

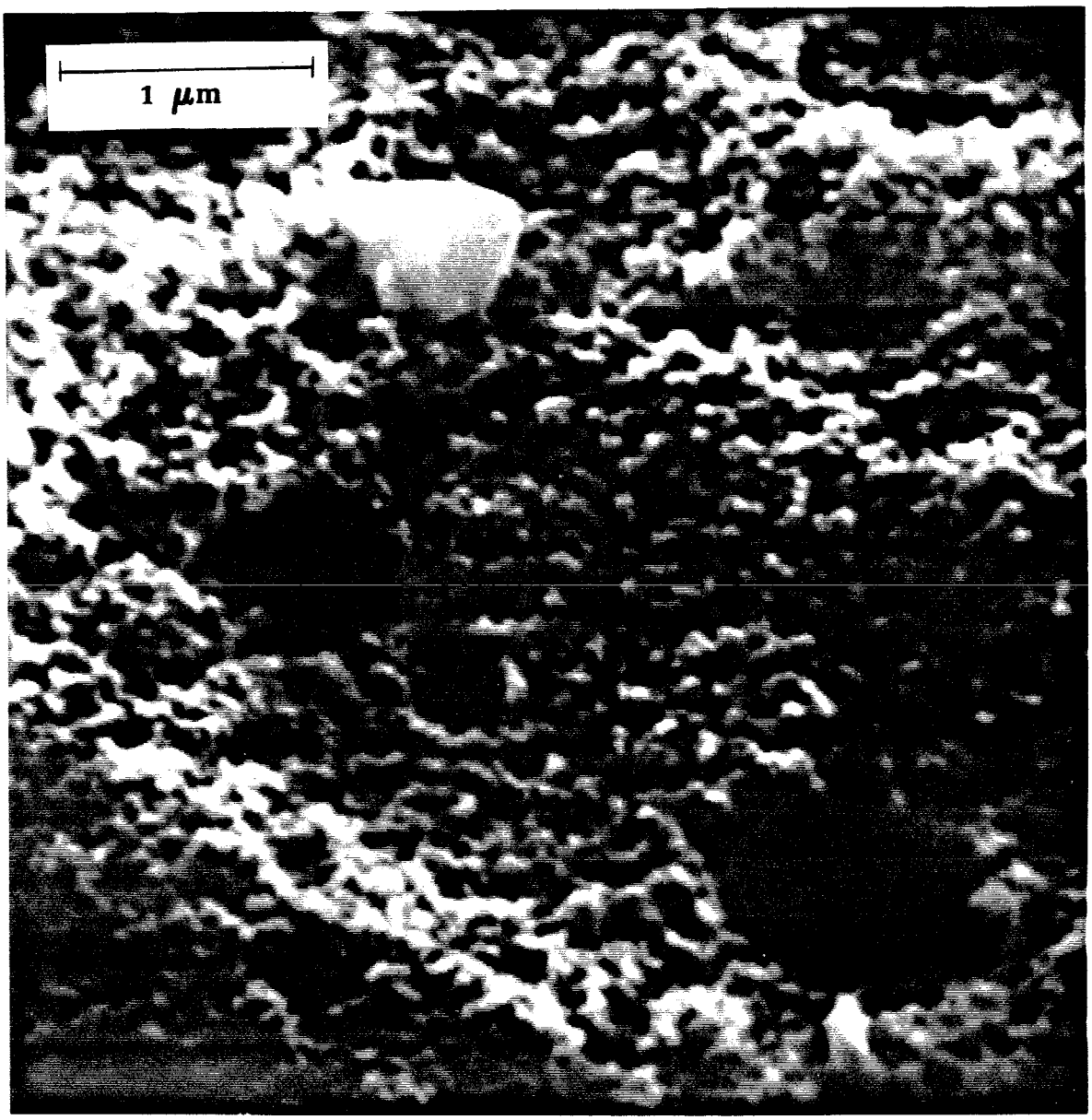

Figure 9.4c Partially burned porous carbon (magnified 20,000 times).

9.3 Aerosol production during combustion

The evaluation of artificial coal as a model system continues with a discussion of the results of a series of preliminary combustion experiments with artificial coal. Both porous and non-porous carbon are burned at 1575 K in mixtures of oxygen and nitrogen. The furnace gas and wall temperatures and the gas flow rate are kept constant. Thus only the local combustion conditions are changing.

As discussed in the previous chapter, both the EAA and OPC are used to make on-line aerosol measurements. Appendix B contains tables of the EAA and OPC readings for the measurements under discussion. These readings represent average values. The OPC reading is the average of two measurements made in the space of two minutes. The EAA reading is made during the same period. From these readings aerosol number and volume distributions are generated. The data are corrected for the loss of aerosol in the CSTR using equations developed by Crump (1983). Concentrations are also corrected for dilution and should be understood to be the aerosol concentration in the furnace. The EAA data are further reduced using a data inversion routine also developed by Crump (1983).

The use of a data inversion routine for EAA data is illustrated in Figure 9.5. The aerosol volume distribution in $(\mu m)^3/cm^3$ is shown as a function of particle diameter (note: $(\mu m)^3/cm^3$ is equal in magnitude to $\mu g/m^3$ at unit particle density). The figure corresponds

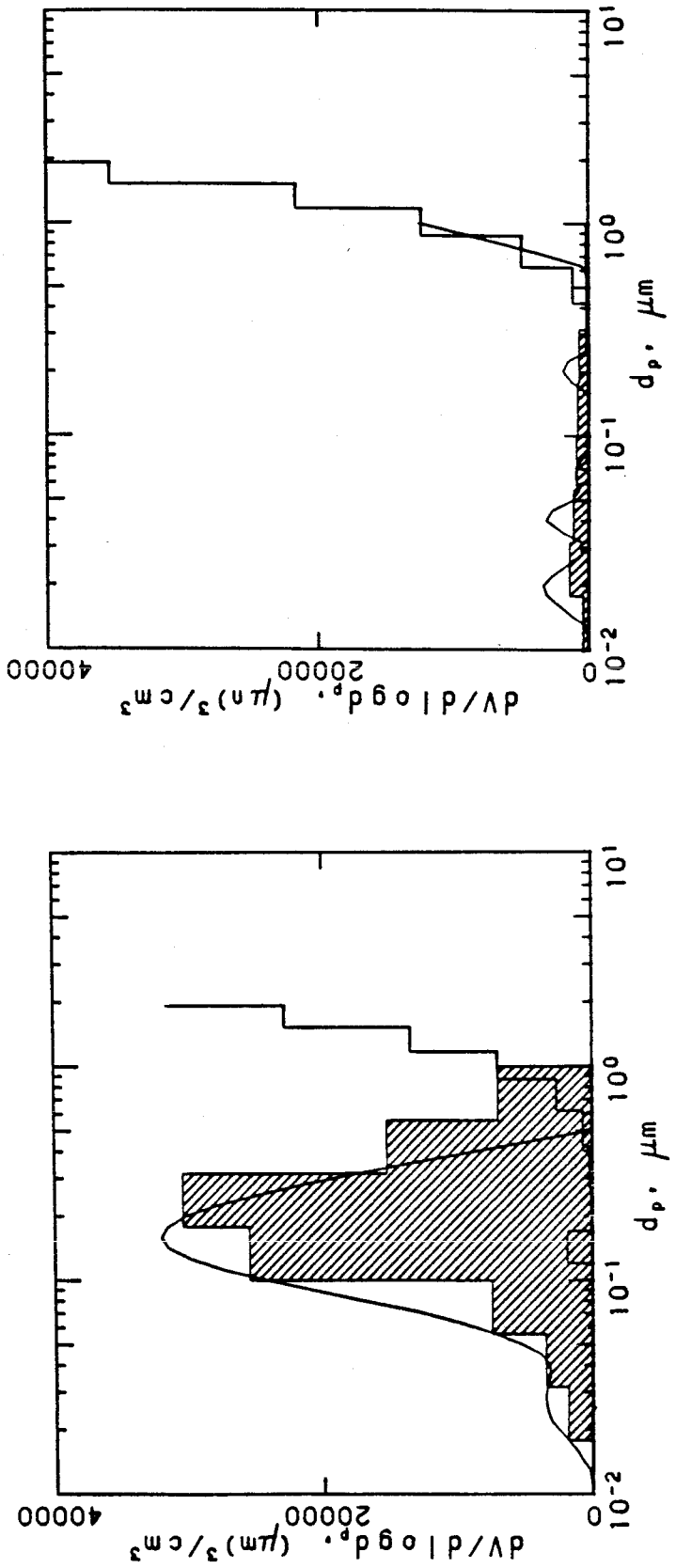

Figure 9.5 Effect of inverting EAA data. Aerosol volume distributions from EAA and OPC (shaded region is un-inverted EAA distribution).

(a) Combustion of porous carbon in 100% oxygen at 1575 K.

(b) Combustion of porous carbon in 51.4% oxygen at 1575 K.

to combustion of porous carbon in two different gas compositions, 100% and 51.5% oxygen in nitrogen. The solid lines represent the EAA (0.01-1.0 μm) and OPC (0.12-2.0 μm) volumes. The shaded regions are the EAA data before application of the inversion algorithm. The data inversion algorithm generally reveals more fine structure in the EAA data although the total volume remains about the same.

Figure 9.5 illustrates a very important point concerning the simultaneous use of the EAA and OPC. The EAA is less sensitive to aerosol concentration than the OPC. The latter cannot tolerate very high number concentrations. When the OPC is exposed to very high number concentraions, it becomes saturated. There is a large discrepancy between the EAA and OPC in their region of overlap (0.12-1.0 μm) in part a that is not found in part b. This is because the OPC is saturated for the case of combustion in 100% oxygen: there is simply too much aerosol for the instrument to measure. For combustion in 51.5% oxygen, however, both instruments agree very well. Part b also illustrates the utility of the EAA data inversion algorithm. The OPC data show that the aerosol volume rises sharply for diameters greater than 0.5 μm. The un-inverted EAA data do not show this increase in volume, but the inverted size distribution does. In fact, it agrees very well with the OPC data.

Both size distributions in Figure 9.5 show a small volume peak at a diameter of approximately 0.02 μm. This is probably background aerosol: aerosol somehow generated in the furnace but not associated

with combustion. It is not known at this time what the source of this aerosol is, but it may be caused by minute amounts of some of the furnace materials being vaporized. Figure 9.6 shows aerosol measurements made with and without coal feeding into the furnace. The dilution system was configured as in Case 1 for these measurements. Both measurements were made at a furnace temperature of 1575 K and with 2 lpm of gas flowing through the furnace. Both distributions have a large number of particles with mean size of about 0.02 μm and a small number of particles of about 0.2 μm in size. The presence of this background aerosol must be taken into account when interpreting the data. The combustion aerosol can be seen in part b of Figure 9.6 as a number peak at 0.05 μm diameter.

The effect of oxygen partial pressure on aerosol formation is illustrated in the next series of figures. Porous carbon has been burned in several different oxygen concentrations. As demonatrated in the theoretical treatment of a single burning coal particle, as the oxygen partial pressure increases, so does the particle temperature. Figure 9.7 shows aerosol number distributions, Figure 9.8, volume distributions. Both show the definite presence of some kind of background aerosol. The 0.02 μm mode changes very little in number or in volume even though the combustion conditions have changed dramatically. This indicates that this mode is not associated with combustion in the furnace. The 0.2 μm mode may also be due to background aerosol although it is observed to increase in number as the oxygen concentration increases. It appears, as in Figure 9.6b, that

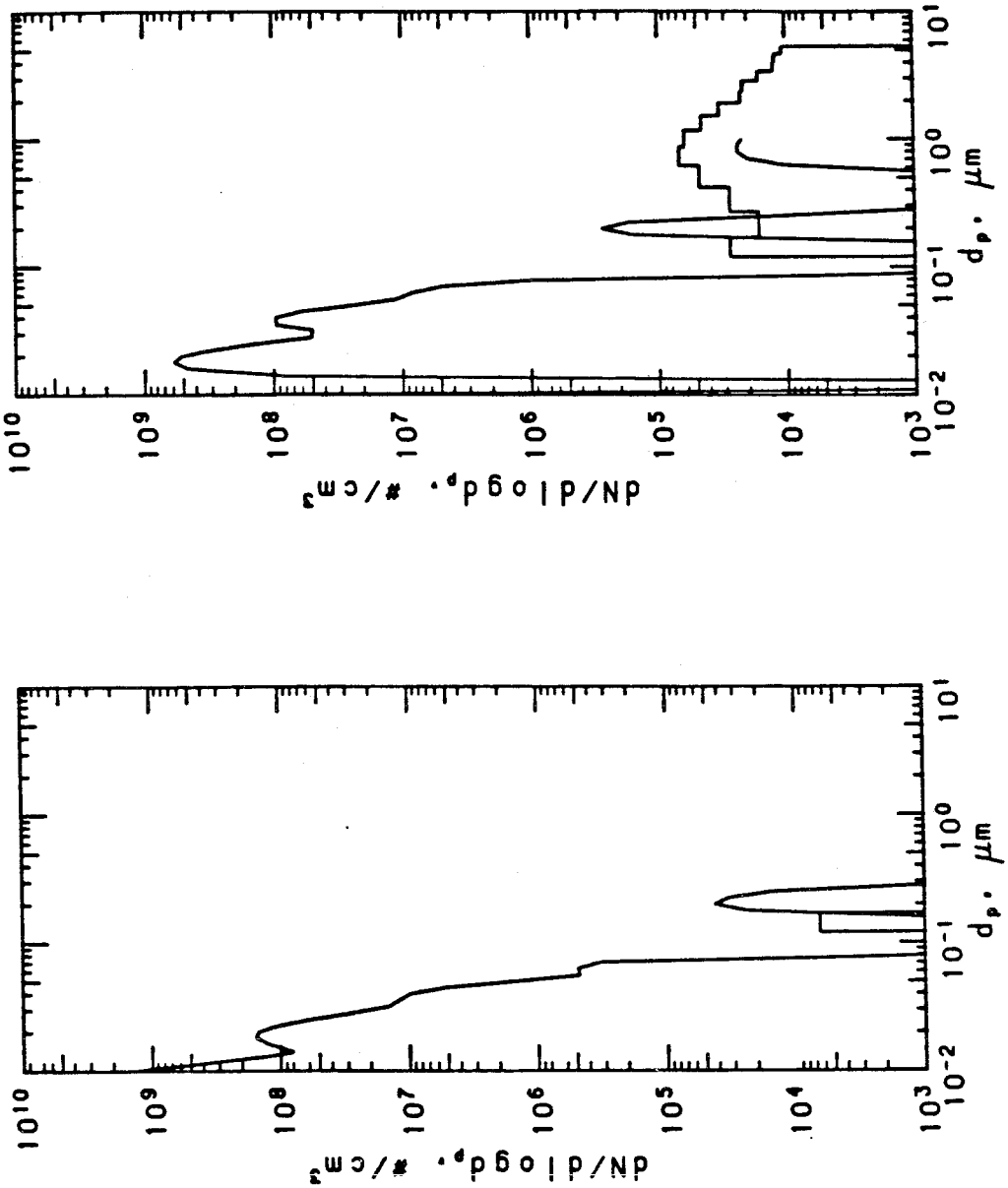

Figure 9.6 EAA and OPC volume distributions from combustion at 1575 K. (a) No feed. (b) Porous carbon in 40% oxygen.

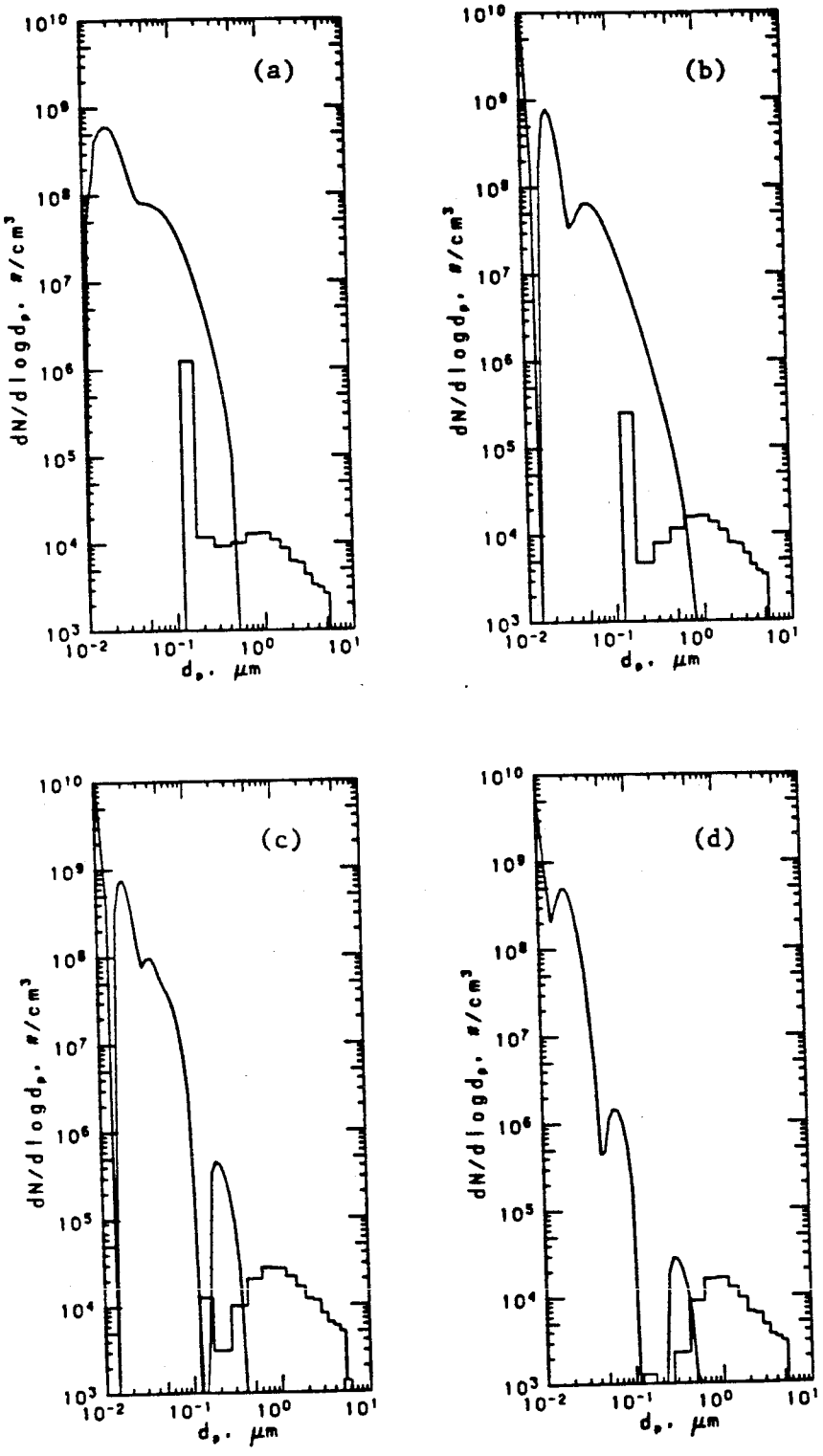

Figure 9.7 Effect of oxygen concentration on aerosol number distributions for combustion of porous carbon at 1575 K.

(a) 100 O_2 (c) 61.4% O_2
(b) 80% O_2 (d) 39.8% O_2

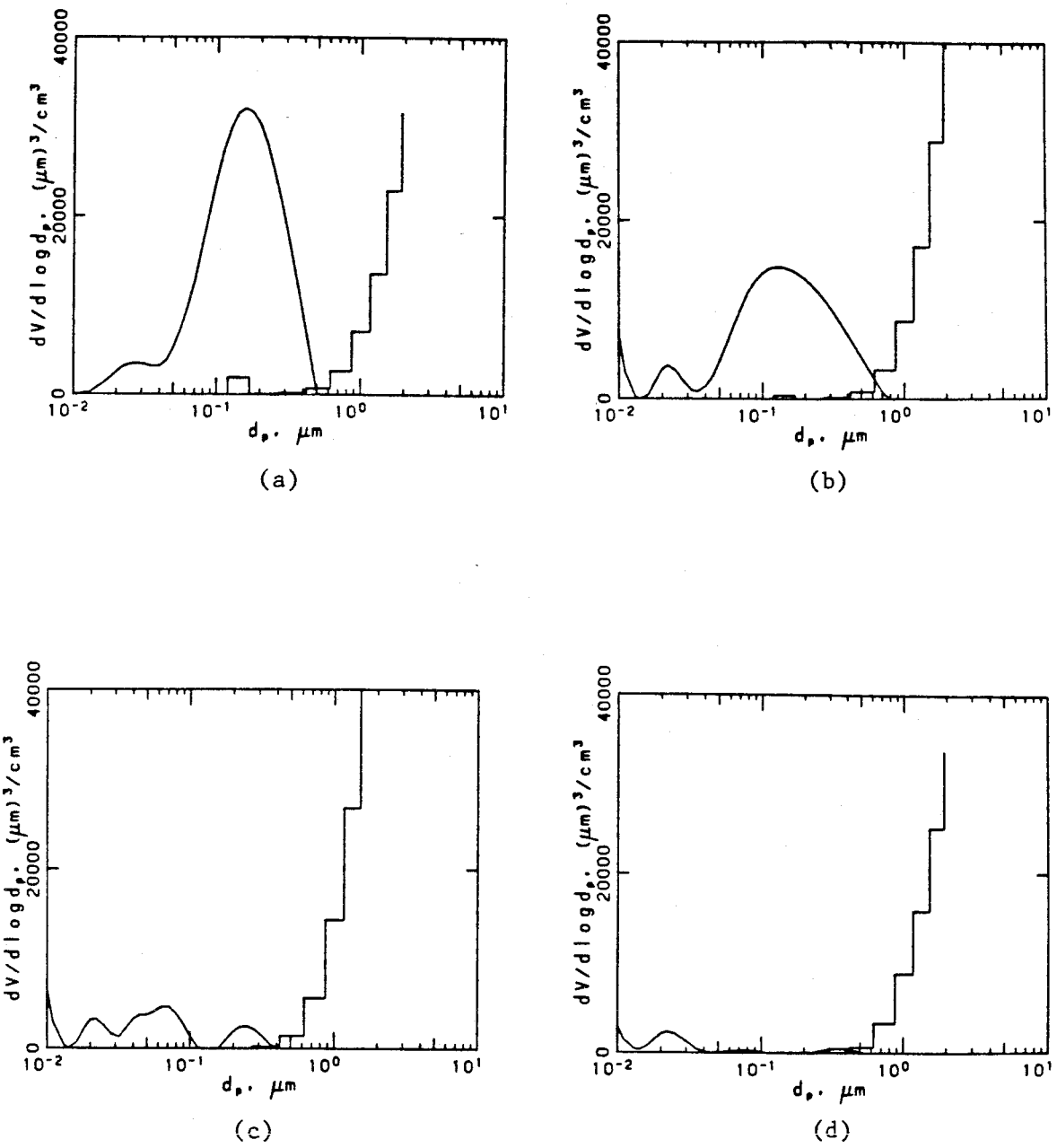

Figure 9.8 Effect of oxygen concentration on aerosol volume distributions for combustion of porous carbon at 1575 K.

(a) 100% O_2
(b) 80% O_2
(c) 61.4% O_2
(d) 39.8% O_2

there is a submicron mode associated with the combustion process that has an average size of 0.05 μm. As the oxygen concentration increases, this mode broadens until it encompasses the 0.2 μm mode. The former mode gives clear evidence of ash vaporization followed by condensation since the number and volume of the aerosol are such strong functions of local combustion conditions.

The effect of char structure on aerosol formation can be seen in Figure 9.9. Aerosol volume distributions for combustion of porous and non-porous carbon in pure oxygen are shown. First, the same volume peak at 0.02 μm occurs in both parts a and b. This is further evidence for the background aerosol. A comparison of parts a and b of Figure 9.9 indicates that combustion of porous carbon produces about five times as much submicron aerosol volume as does combustion of non-porous carbon. The porous char has been shown to contain many transitional pores which make a very large surface area available for reaction. The non-porous carbon, on the other hand, burns with no visible penetration of the carbon surface by pores. This means that the reaction rate for combustion on a volume basis may be much higher in the porous carbon than the non-porous carbon, implying that the latter has a higher temperature during combustion. The enormous difference in the amount of submicron aerosol that is produced when these two materials burn supports this hyothesis. Some vaporization occurs during combustion of non-porous carbon as evidenced in Figure 9.10. Increasing the oxygen concentration once again has the effect of increasing the amount of aerosol in the 0.05–0.5 μm size range.

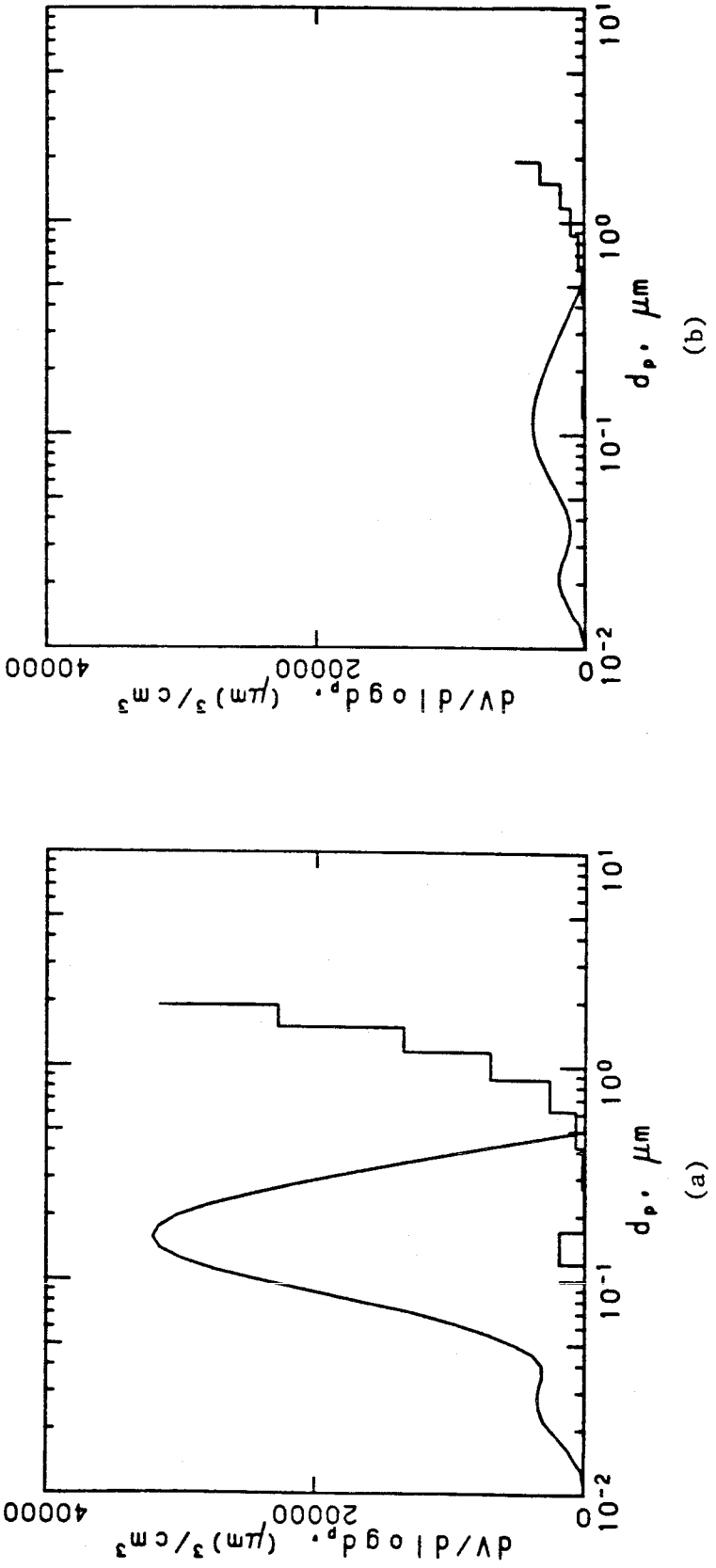

Figure 9.9 Effect of char structure on aerosol volume distributions for combustion at 1575 K in 100% oxygen.

(a) Porous carbon (b) Non-porous carbon

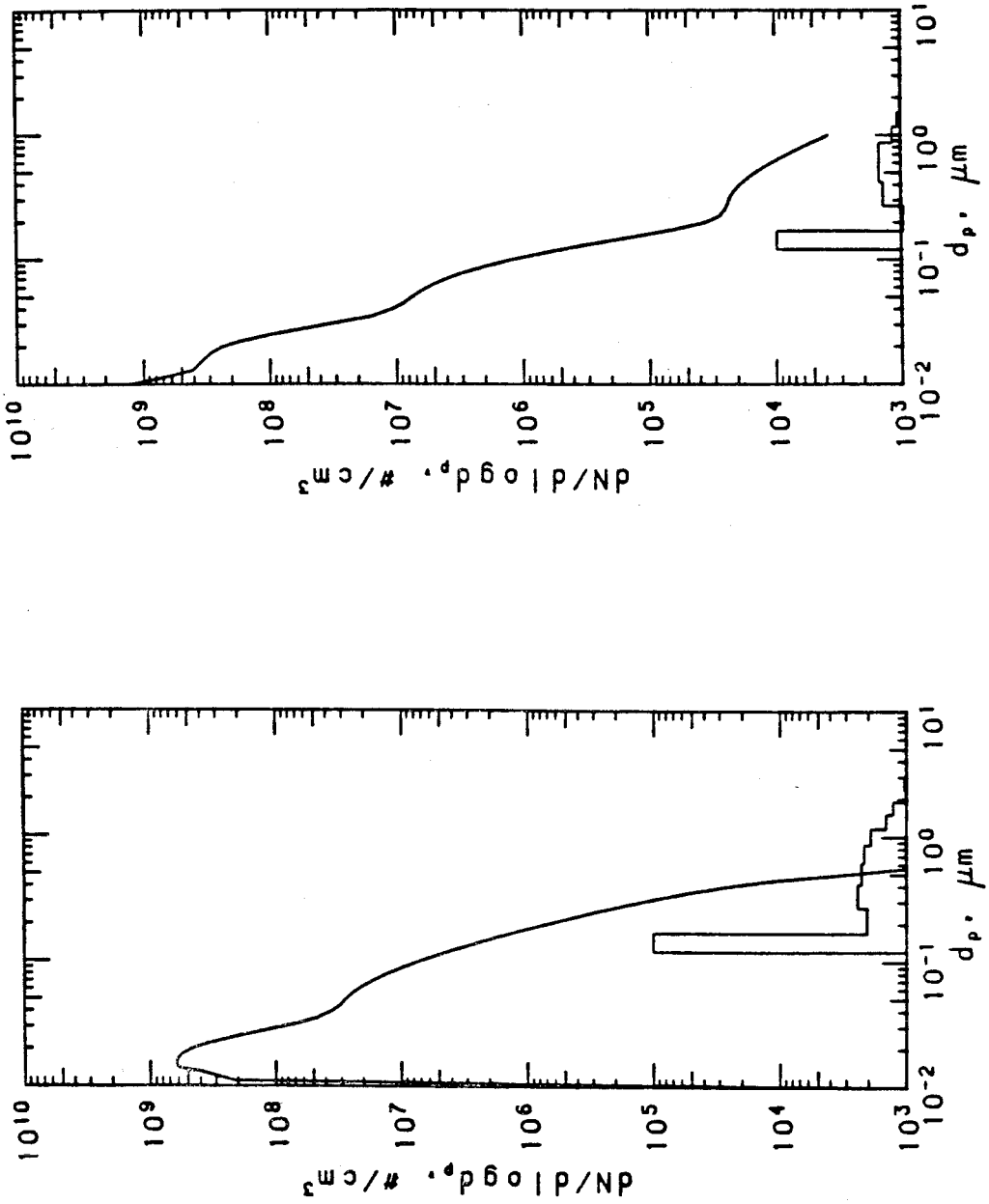

Figure 9.10 Effect of oxygen concentration on aerosol number distributions for combustion of non-porous carbon at 1575 K.

(a) 100% O_2 (b) 80% O_2

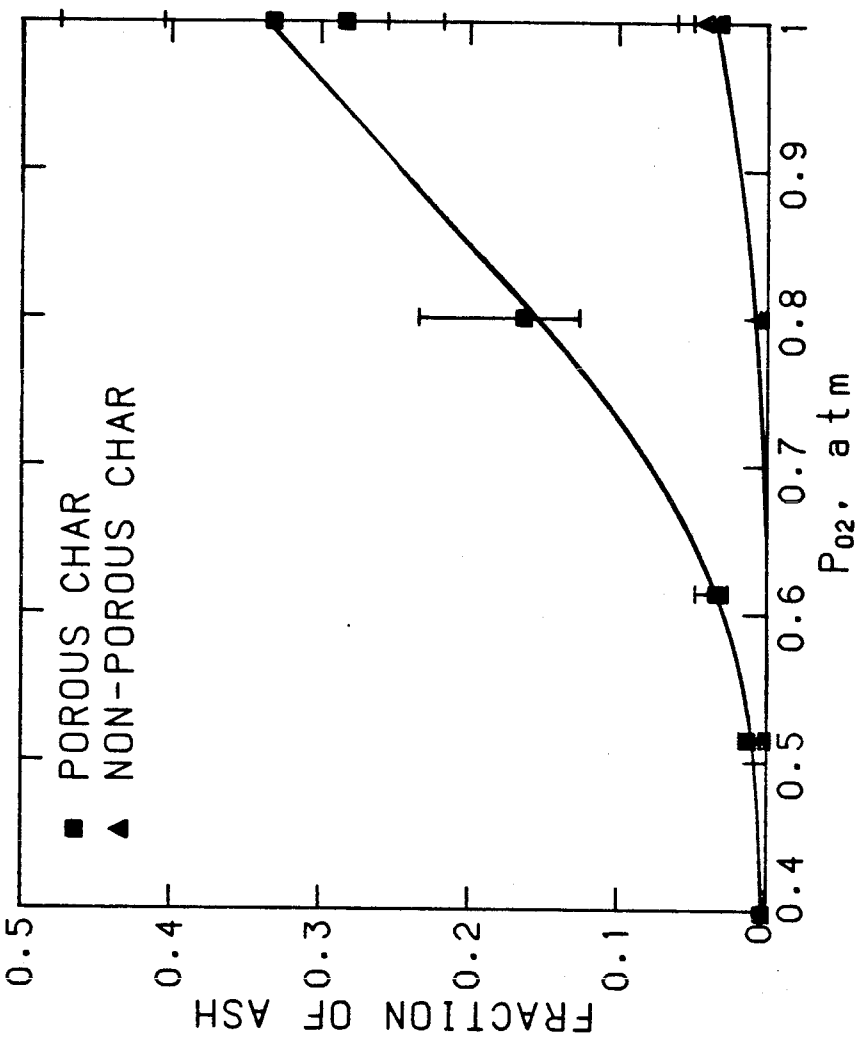

Figure 9.11 Fraction of ash appearing in submicron aerosol for combustion at 1575 K.

The results are summarized in Figure 9.11 where the fraction of the ash volume that resides in the submicron aerosol is shown as a function of oxygen concentration. The submicron volume does not include the 0.02 μm mode since it does not appear to be associated with the coal.

9.4 Conclusions

Two different materials have been produced to aid in the study of the formation of the submicron aerosol from pulverized coal combustion. One of these has quite low porosity during combustion and appears to burn only on its external surface. The other contains many fine pores which penetrate the particle during combustion. The latter material more closely resembles coal during combustion on a physical basis.

Combustion of these materials produces a submicron aerosol like the one observed from the combustion of coal. This aerosol is the result of vaporization of ash during combustion. Since the parent mineral matter does not contain such large numbers of submicron particles, this aerosol must be produced during the combustion process. In addition, the amount of ash in this submicron aerosol mode is a strong function of local combustion conditions. Particle temperature and the local gas composition have a very strong influence on vaporization and aerosol formation as Chapters 4 and 6 have demonstrated. Chapter 3 has illustrated that for combustion of coal, varying the oxygen partial pressure from 0.4 to 1 causes the particle temperature to vary by 500-600 K. Calculations have shown that this can lead to variations of

several orders of magnitude in the amount of ash vaporized during combustion. This has been observed in the experiments using the model compounds developed in this work.

The stated aims of the experimental program have been met. A system has been developed for studying aerosol formation during coal combustion. Char can be burned under well controlled conditions in a small-scale furnace. The chemistry of the mineral phase can also be controlled. This model system provides, for the first time, provides a means of understanding the details of the aerosol formation processes during combustion.

CHAPTER 10

SUMMARY

10.1 Submicron aerosol formation during combustion

This work represents the first detailed model of submicron aerosol formation during pulverized coal combustion. It combines a simulation of a single, burning coal particle with a description of the formation of aerosol by nucleation and its subsequent growth by coagulation.

To accomplish this, it has been necessary to develop a model for the combustion of a burning coal particle. No model was available to provide all the information needed to perform the aerosol calculation. Specifically, the local gas compostion and temperature around a burning coal particle are needed at each instant during combustion.

Vapor transport and aerosol formation processes occur on a much shorter time scale than char combustion. This allows the use of quasi-steady models for combustion and aerosol formation. That is, the steady-state problem is solved at each instant in combustion; this greatly simplifies the analysis.

The effect of thermophoresis of aerosol in the thermal boundary layer around a burning coal particle is included in the modeling effort. Thermophoresis has a minor effect on the aerosol transport in the system, but substantially influences the number and size of particles produced by nucleation.

Two very important conclusions arise from the aerosol modeling work. First, calculation of aerosol formation for vaporization of silica under pulverized coal combustion conditions shows that nucleation of vapor occurs entirely within 4-5 coal particle radii from the surface. At least for refractory species, nucleation is controlled by the combustion process and not by conditions in the bulk gas as previous models have assumed.

Second, the actual rate of vaporization is only weakly dependent on the presence of aerosol in the surrounding gas. Thus one can calculate the vaporization rate to a very good approximation without knowing the details of the aerosol formation that is occurring in the system.

Vaporization rates are estimated and compared with a very limited body of experimental data from coal combustion. The calculated rates are approximately an order of magnitude lower than the measured rates for two different chemical species of ash. This may indicate a need to consider some of the features not included in the present model, particularly vaporization of ash inside the pores during combustion.

An experimental system is developed in which to study aerosol formation under well-controlled and reproducible conditions. The complicated chemistry of coal ash clouds the study of ash vaporization and vapor condensation. Therefore a new material, artificial coal, is developed to aid in the understanding of some of the fundamental physics and chemistry. This material is designed to burn like coal but to contain mineral matter with precisely controlled composition and known chemistry.

Artificial coal is evaluated as a model system through combustion experiments in a laminar-flow furnace designed for this purpose. Combustion of artificial coal produces a submicron aerosol with a number-mean size of 0.05 μm. Since no particles this size have been added to the parent material, the aerosol is unambiguously the result of a vaporization-condensation mechanism. Thus the model system contains the processes of interest: ash vaporization and aerosol formation. Artificial coal shows promise in the study of ash chemistry and aerosol physics in the combustion process.

10.2 Suggestions for further work

The conclusions of the theoretical portion of this work open up many possibilities for the modeling of aerosol formation from coal combustion. The fact that the nucleation process is controlled by the local combustion conditions (at least for refractory species like silica), means that the aerosol formation process can be uncoupled from

the macro-scale combustion processes. The study of aerosol formation and growth in small laboratory furnaces has direct applicability to larger combustion systems.

Both the combustion and the aerosol modeling efforts point to a need for more detailed data about the systems of interest. The char pore structure is seen to be very important in determining the combustion behavior of coal particles; it may also prove important to the vaporization of mineral matter. Data on the structure of char are necessary to model combustion adequately. Details of the ash chemistry at high temperatures are also essential to the modeling effort.

The aerosol model developed in this work does not consider the influence of the porous char structure on ash vaporization. This would seem to be a fascinating and fruitful area for further study.

The artificial coal developed has tremendous potential in the study of aerosol formation and ash chemistry. It is clear that this work has only scratched the surface. The immediate need in this area is for better characterization of the materials. Characterization of the finer pores is necessary. Also, the development of the char structure as combustion proceeds must be studied in order to understand the conditions experienced by the ash during combustion. This line of research is very relevant to a fundamental understanding of the role of pore structure in the combustion process.

REFERENCES

Ayling, A.B. and Smith, I.W. (1972). Measured temperatures of burning pulverized-fuel particles, and the nature of the primary reaction product, Comb.Flame 18:173-184.

Baum, M.M. and Street, P.J. (1971). Predicting the combustion behaviour of coal particles, Comb.Sci.Tech. 3:231-243.

Biermann, A.H. and Ondov, J.M. (1980). Application of surface-deposition models to size-fractionated coal fly ash, Atm.Env. 14:289-295.

Brewer, L. (1953). The thermodynamic properties of the oxides and their vaporization processes, Chem.Rev. 52:1-75.

Caram, H.S. and Amundson, N.R. (1977). Diffusion and reaction in a stagnant boundary layer about a carbon particle, Ind.Eng.Chem.Fund. 16:171-181.

Conley, R.T. and Metil, I. (1963). An investigation of the structure of furfuryl alcohol polycondensates with infrared spectroscopy, J.Appl.Poly.Sci. 7:37-52.

Crump, J.G. (1983). Aerosol deposition, growth, and dynamics in a continuous stirred tank reactor, Ph.D. Thesis, California Institute of Technology.

Damle, A.S., Ensor, D.S., Ranade, M.B. (1982). Coal combustion aerosol formation mechanisms: a review, Aero.Sci.Tech. 1:119-133.

Davison, R.L., Natusch, D.F.S., and Wallace, J.R. (1974). Trace elements in fly ash-dependence of concentration on particle size, Env.Sci.Tech. 13:1107-1113.

Desrosiers, R.E., Riehl, J.W., Ulrich, G.D., and Chiu, A.S. (1978). Submicron fly-ash formation in coal-fired boilers, 17th Symp.(Int.) Comb. Combustion Institute, Pittsburg, pp 1395-1403.

Dobner, S. (1976). Modeling of entrained bed gasification: the issues, EPRI Memo, Electric Power Research Institute, Palo Alto, CA

Dollimore, D. and Heal, G.R. (1967). The degradation of selected polymers to carbons in an inert atmosphere, Carbon 5:65-72.

Dow Chemical Company, Thermal Research Laboratory. (1971). JANAF Tables (second edition) National Bureau of Standards, Washington, DC.

Dunlop, A.P. and Peters, F.N. (1953). The furans ACS Monograph Series, No. 119, American Chemical Society, Washington, DC.

Dutta, S. and Wen, C.Y. (1977). Reactivity of coal and char. 2. In oxygen-nitrogen atmosphere, Ind.Eng.Chem.Proc.Des.Dev. 16:31-37.

Ensor, D.S. (1980). Aerosol volatilization due to the combustion of coal. Symposium on Plumes and Visibility, Grand Canyon, Arizona.

Ensor, D.S., Cowen, S., Hooper, R., and Markowski, G. (1981). Evaluation of the George Neal No.6 electrostatic precipitation, EPRI Report FP-1145, Electric Power Research Institute, Palo Alto, CA.

Fehlberg, E. (1969). Low-order classical Runge-Kutta formulas with stepsize control, NASA Technical report R-315.

Feng, C. and Stewart, W.E. (1973). Practical models for isothermal diffusion and flow of gases in porous solids, Ind.Eng.Chem.Fund. 12:143-147.

Field, M.A. (1970). Measurements of the effect of rank on combustion rates of pulverized coal, Comb.Flame 14:237-248.

Field, M.A. (1969). Rate of combustion of size-graded fractions of char from a low-rank coal between 1200K and 2000K, Comb.Flame 13:237-252.

Field, M.A., Gill, D.W., Morgan, B.B., and Hawksley, P.G. (1967). Combustion of pulverized coal B.C.U.R.A., Leatherhead, Surrey.

Fisher, G.L., Chang, D.P.Y., and Brummer. M. (1976). Fly ash collected from electrostatic precipitators: microcrystalline structure and the mystery of the spheres, Science 192:553-555.

Fitzer, E. and Schaefer, W. (1970). The effect of crosslinking in the formation of glasslike carbons from thermosetting resins, Carbon 8:353-364.

Fitzer, E., Schaefer, W. and Yamada, S. (1969). The formation of glasslike carbon by pyrolysis of polyfurfuryl alcohol and phenolic resin, Carbon 7:643-648.

Flagan, R.C. and Friedlander, S.K. (1978). Particle formation in pulverized coal combustion-a review, in Recent developments in aerosol science (D.T.Shaw, ed.) Wiley, New York.

Flagan, R.C. and Taylor, D.D. (1981). Laboratory studies of submicron particles from coal combustion, 18th Symp.(Int.) Comb. Combustion Institute, Pittsburg, pp. 1227-1237.

Friedlander, S.K. (1977). Smoke, dust and haze. Fundamentals of aerosol behavior Wiley, New York.

Gan, H., Nandi, S.P. and Walker, P.L. (1972). Nature of the porosity of American coals, Fuel 51:272-277.

Gavalas, G.R. (1980). A random capillary model with application to char gasification at chemically controlled rates, AIChE Journal 26:577-585.

Gavalas, G.R. (1981). Analysis of char combustion including the effect of pore enlargement, Comb.Sci.Tech. 24:197-210.

Gelbard, F. (1978). The general dynamic equation for aerosols, Ph.D. Thesis, California Institute of Technology.

Given, P.H. (1960). The distribution of hydrogen in coals and its relation to coal structure, Fuel 39:147-154.

Gladney, E.S., Small, J.A., Gordon, G.E., and Zoller, W.H. (1976). Composition and distribution of in-stack particulate material at a coal-fired power plant, Atm.Env. 10:1071-1077.

Hamblen, D.G., Solomon, P.R., and Hobbs, R.H. (1980). Physical and chemical characterization of coal, EPA Report No. EPA-600/7-80-106.

Hamor, R.J., Smith, I.W., and Tyler, R.J. (1973). Kinetics of combustion of pulverized brown coal char between 630 and 2200 K, Comb.Flame 21:153-162.

Hamor, R.J. and Smith, I.W. (1971). Fluidizing feeders for providing fine particles at low, stable flows, Fuel 50:394-405.

Haynes, B.S., Neville, M., Quann, R.J., and Sarofim, A.F. (1982). Factors governing the surface enrichment of flyash in volatile trace species, J.Coll.Interf.Sci. 87:266-278.

Henderson, D. and Taylor, J. (1966). Thermodynamic properties in the $CaO-MgO-SiO_2$ and $MgO-Al_2O_3-SiO_2$ systems, J.Iron Steel Inst. (January), 39-43.

Hirsch, P.B. (1954). X-ray scattering from coals, Proc.Roy.Soc. (London) A226:286-297.

Hock, J.L. and Lichtman, D. (1982). Studies of surface layers on single particles of in-stack fly ash, Env.Sci.Tech. 16:423-427.

Huffman, G.P., Huggins, F.E., and Dunmyre, G.R. (1981). Investigation of the high-temperature behavior of coal ash in reducing and oxidizing atmospheres, Fuel 60:585-597.

Im, K.H .and Chung, P.M. (1980). Nucleation and evolution of slag droplets in coal combustion, AIChE Journal 26:655-663.

Jenkins, R.G., Nandi, S.P., and Walker, P.L. (1973). Reactivity of heat-treated coals in air at 500°C, Fuel 52:288-293.

Kaakinen, J.W., Jorden, R.M., Lawasani, M.H., and West, R.E. (1975). Trace element behavior in coal-fired power plant, Env.Sci.Tech. 9:862-869.

Kingery, W.D. (1959). Surface tension of some liquid oxides and their temperature coefficients, J.Amer.Ceram.Soc. 42:6-10.

Klein, D.H., Andren, A.W., Carter, J.A., Emery, J.F., Feldman, C., Fulkerson, W., Lyon, W.S., Ogle, J.C., Talmi, Y., van Hook, R.I, and Bolton, N. (1975). Pathways of thirty-seven trace elements through coal-fired power plant, Env.Sci.Tech. 9:973-979.

Kobayashi, H., Howard, J.B., and Sarofim, A.F. (1976) Coal devolatilization at high temperatures, 16th Symp.(Int.) Comb Combustion Institute, Pittsburg, pp.411-425.

Komanoff, C. (1980). Pollution control improvements in coal-fired electric generating plants: what they accomplish, what they cost, J.Air Poll.Control Assoc. 30:1051-1057.

Lawler, D.F. (1979). A particle approach to the thickening process, Ph.D. Thesis, The University of North Carolina at Chapel Hill.

Lee, S.H.D., Johnson, I., and Fischer, J. (1980). Volatility of selected minor and trace elements in the low-temperature ash of an Illinois No. 6 coal, Fuel 59:816-819.

Libby, P.A. and Blake, T.R. (1979). Theoretical study of burning carbon particles, Comb.Flame 36:139-169.

Littlejohn, R.F. (1966). Mineral matter and ash distribution in 'as-fired' samples of pulverized fuels, J.Inst.Fuel 39:59-67.

Lowell, S. (1979). Introduction to powder surface area Wiley, New York.

Markowski, G.R., Ensor, D.S., Hooper, R.G., and Carr, R.C. (1980). A submicron aerosol mode in flue gas from a pulverized coal utility boiler, Env.Sci.Tech. 14:1400-1402.

Marsh, H. and Campbell, H.G. (1971). The characterization of microporous carbons by adsorption from liquid and vapor phases, Carbon 9:489-498.

McCain, J.D., Gooch, J.P., and Smith, W.B. (1980). Results of field measurements of industrial particulate sources and electrical precipitator performance, J.Air Poll.Control Assoc. 25:117-121.

McNallan, M.J., Yurek, G.J. and Elliot, J.F. (1981). The formation of inorganic particulates by homogeneous nucleation in gases produced by the combustion of coal, Comb.Flame 42:45-60.

Mims, C.A., Neville, M., Quann, R.J., House, K., and Sarofim, A.F. (1980). Laboratory studies of trace element transformations during coal combustion, AIChE Symposium Series No. 201, Vol 76.

Mitchell, R.E. and McClean, W.J. (1982). On the temperature and reaction rate of burning pulverized fuels, presented at WSS/CI 1982 Spring meeting, Salt Lake City, Utah.

Mon, E. and Amundson, N.R. (1978). Diffusion and reaction in a stagnant boundary layer about a carbon particle. 2. An extension, Ind.Eng.Chem.Fund. 17:313-321.

Mulcahy, M.F.R. and Smith, I.W. (1969). Kinetics of combustion of pulverized fuel: A review of theory and experiment, Rev.Pure Appl.Chem. 18:81-108.

Murphy, P., Piker, J.D., and Schmansky, C.R. (1952). Fireside deposits on steam generators minimized through humidification of combustor air, Trans.ASME 73:821-843.

Nagle,J. and Strickland-Constable, R.F. (1962). Oxidation of carbon between 1000-2000°C, Proc.5th Carbon Conf. v. 1, Pergamon Press, Oxford, pp. 154-164.

Nakamura, H.H. and Atlas, L.M. (1960). Investigation of synthetic binders by differential thermal analysis and dilatometry, Proc.4th Conf.Carbon Pergamon Press, New York, pp. 625-637.

Neville, M., Quann, R.J., Haynes, B.S. and Sarofim, A.F. (1981). Vaporization and condensation of mineral matter during pulverized coal combustion, 18th Symp.(Int.) Comb Combustion Institute, Pittsburg, pp. 1267-1274.

O'Gorman, J.V. and Walker, P.L. (1973). Thermal behavior of mineral fractions from selected Americal coals, Fuel 52:71-79.

O'Gorman, J.V. and Walker, P.L. (1971). Mineral matter characteristics of some American coals, Fuel 50:135-151.

O'Neill, H.J., Putscher, R.E., Dynako, A. and Boquist, C. (1963). Pyrolysis studies of furfuryl alcohol resins by gas chromotography, J.Gas Chromatography 1:28-35.

Park, C. and Appleton, J.P. (1973). Shock-tube measurements of soot oxidation rates, Comb.Flame 20:369-379.

Quann, R.J. and Sarofim, A.F. 1982. Vaporization of refractory oxides during pulverized coal combustion, 19th Symp.(Int.) Comb Combustion Institute, Pittsburg, pp. 1429-1440.

Raask, E. (1969). Fusion of silicate particles in coal flames, Fuel 48:366-374.

Raask, E. (1968). Cenospheres in pulverized fuel ash, J.Inst.Fuel 38:255-262.

Raask, E. (1966). Slag-coal interface phenomena, J.Eng.Power (January), 40-44.

Raask, E. and Wilkins, D.M. (1965). Volatilization of silica in gasification and combustion processes, J.Inst.Fuel 38:255-262.

Ragaini, R.C. and Ondov, J.M. (1977). Trace-element emissions fromm western U.S. coal-fired power plants, J.Radioanal.Chem. 37:679-691.

Reid, W.T. (1971). External corrosion and deposits: boilers and gas turbines American Elsevier, New York.

Rein, R.H. and Chipman, J. (1965). Activities in the liquid solution SiO_2-CaO-MgO-Al_2O_3 at 1600°C, Trans.Metal.Soc.AIME 233:415-425.

Riesz, C.H. and Susman, S. (1960). Synthetic binders for carbon and graphite, Proc.4th Carbon Conf. Pergamon Press, New York, pp. 609-623.

Ruch, R.R., Gluskoter, H.J., and Skimp, N.F. (1974). Occurance and distribution of potentially volatile trace elements in coal, EPA Report EPA-650/2-74-054.

Sarofim, A.F., Howard, J.B., and Padia, A.S. (1977). The physical transformations of the mineral matter in pulverized coal under simulated combustion conditions, Comb.Sci.Tech. 16:187-204.

Schick, H.L. (1960). A thermodynamic analysis of the high-temperature vaporization properties of silica, Chem.Rev. 60:331-362.

Schlichting, H. (1960). Boundary layer theory (fourth edition) McGraw-Hill, New York.

Schmidt, E.W., Gieseke, J.A., and Allen, J.M. (1976). Size distributions of fine particulate emissions from a coal-fired power plant, Atm.Env. 10:1065-1069.

Schmitt, J.L. (1970). Carbon molecular sieves as selective catalyst supports, Ph.D. Thesis, The Pennsylvania State University.

Schmitt, J.L., Walker, P.L. and Castellion, G.A. (1976). Catalysts based on carbon supports, United States Patent 3,978,000.

Schultz, E.J., Engdahl, R.B., and Frankenberg, T.T. (1975). Submicron particles from a pulverized coal fired boiler, Atm.Env. 9:111-119.

Sergeant, G.D. and Smith, I.W. (1973). Combustion rate of bituminous coal char in the temperature range 800 to 1700 K, Fuel 52:52-57.

Simons, G.A. (1979). Char gasification: Part I. Transport model, Comb.Sci.Tech. 20:107-116.

Smith, I.W. (1978). The intrinsic reactivity of carbons to oxygen, Fuel 57:409-414.

Smith, I.W. and Tyler, R.J. (1972). Internal burning of pulverized semi-anthracite: the relation between particle structure and reactivity, Fuel 51:312-321.

Smith, I.W. (1971a). Kinetics of combustion of size-graded pulverized fuels in the temperature range 1200-2270 K, Comb.Flame 17:303-314.

Smith, I.W. (1971b). The kinetics of combustion of pulverized semi-anthracite in the temperature range 1400-2200 K, Comb.Flame 17:421-428.

Smithells, C.J. (1976). Metals reference handbook (fifth edition) Butterworths, London.

Stickler, D.B., Becker, F.E., and Ubhayakar, S.K. (1979). Combustion of pulverized coal in high temperature preheated air, presented at 17th Aerospace Sci.Meeting, New Orleans,LA.

Taylor, D.D. (1981). Laboratory studies of submicron particle formation in pulverized coal combustion, Ph.D. Thesis, California Institute of Technology.

Taylor, D.D. and Flagan, R.C. (1981). Aerosols from a laboratory pulverized coal combustor, ACS Symposium Series, No. 167, pp.157-172.

Thomas, J.M. (1970). Reactivity of carbon: some current problems and trends, Carbon 8:413-421.

Ubhayakar, S.K. and Williams, F.A. (1976). Burning and extinction of laser-ignited carbon particles in quiescent mixtures of oxygen and nitrogen, J.Electrochem.Soc. 123:747-756.

Wakeshima, H. (1954). Time lag in the self nucleation, J.Chem.Phys. 22:1614-1615.

Waldman, L. (1959). Uber die Kraft eines inhomogenen Gases auf kleine suspendierte Kugeln, Z.Naturf. A14:590-599.

Walls, J.R. and Strickland-Constable, R.F. (1964). Oxidation of carbon between 1000-2400°C, Carbon 1:333-338.

Watt, J.D. and Thorne, D.J. (1965). Composition and pozzolanic properties of pulverized fuel ashes. I. Composition of fly ashes from some British power stations and properties of the component particles, J.Appl.Chem. 15:585-594.

Wewerka, E.M., Walters, K.L. and Moore, R.H. (1969). Differential thermal analysis of furfuryl alcohol resin binders, Carbon 7:129-141.

Wood Smith, R.F. and Jenks, R.L. (1901). Arsenic in coal and coke, J.Soc.Chem.Ind. 20:437.

APPENDIX A: Coal Combustion and Aerosol Formation Programs

This appendix contains listing of the major programs used in this work. Briefly, these programs are

COAL	Coal combustion model using surface combustion kinetics
PRATE et al. J1 et al. PORE80 et al.	Subroutines used with the combustion model in the case of porous char combustion kinetics
PSHOOT	Aerosol formation and growth model

A sample session with PSHOOT is also included. This is followed by an output file from this program.

COAL.FTN

```
C   QUASI-STEADY COMBUSTION CALCULATION FOR A BURNING COAL
C   PARTICLE IN AN INFINITE QUIESCENT MEDIUM.
C   THIS CALCULATION DIFFERS FROM A STANDARD QUASI-STEADY ONE
C   LIKE THE ONE OF LIBBY AND BLAKE IN THAT IT ACCOUNTS FOR:
C      --VARIABLE GAS PROPERTIES
C      --VARIABLE PARTICLE DENSITY
C      --SURFACE ASH COVERAGE
C      --DEVOLATILIZATION
C
       external derivs
       dimension z(4),f(4),gb(4),gs(4),work(30),iwork(10)
C   work AND iwork ARE NEEDED FOR THE INTEGRATION ROUTINE
C   iwork MUST HAVE DIMENSION >=6.  work MUST HAVE
C   DIMENSION >=3+6*neq.  relerr AND abserr ARE NEEDED FOR
C   rkf, TOO, AND FOR THE pdp-11 SHOULD BE SET TO:
       data relerr,abserr,neq/1.E-3,1.E-15,4/
       data a11,a12,b1d,b2d/0.38,0.8,3.7E5,1.46E13/
       data ev1,ev2,pi/8861.,3.02E4,3.1415926/
       data bf1,bf0,ts0/2.106E4,247.,300./
       common ah,ap,at,ab,af1,bf1,af0,bf0
       common/gas/gb,gt1b,gt2b,gs,gt1s,gt2s,eb,tinf
       common/devol/a11,a12,b1,b2,ev1,ev2,hv1,hv2,vgroup
       common/deriv/tgroup,qgroup,egroup,rd0,fa1,fa0,fgroup,
     * rgroup,vol
C   INITIALIZATION FOR BURNING CALCULATION
       a12=8./11.
       a13=4./7.
       a22=3./11.
       a23=3./7.
       ah=a12/a22
       at=a13/a23
       ab=a22*(ah-at)
       ap=a23*(ah-at)
C
       call input(tinf,xo2inf,co2inf,ts0,a0,dinc,rha,fa,a11,dtau,dtaup)
C
C   COMBUSTION PARAMETER CALCULATIONS
       den=32.*xo2inf + 44.*co2inf + 28.*(1.-xo2inf-co2inf)
       gb(1)=xo2inf*32./den
       gb(2)=co2inf*44./den
       gb(3)=0.0
       gb(4)=1.-gb(1)-gb(2)
C
       gs(1)=gb(1)              !INITIALLIZE SURFACE M.F.
       gs(2)=gb(2)
       gs(3)=gb(3)
       gs(4)=gb(4)
       gt1b=gb(1) + a12*gb(2) + a13*gb(3)
       gt2b=a22*gb(2) + a23*gb(3)
       vol=fa*rha/2.5
       rhc=(1.-fa)/(1./rha - fa/2.5)
       rgroup=2.5*vol/rhc
       vgroup=0.28/0.48
       rd0=5.974E-6*(tinf**0.6575)
       dinc=dinc/(2.*a0)        !RATIO OF INCLUSION TO COAL RADIUS
       fa1=2.875*dinc*dinc - 0.79713*dinc + 9.3242E-2
       fa0=-0.75326*dinc*dinc + 0.37937*dinc - 7.7092E-2
C   fa'S ARE THE COEFFICIENTS FOR THE SURFACE COVERAGE
```

```
      fgroup=a0/rd0
      tauc=rhc*a0*a0/rd0
      b1=b1d*tauc
      b2=b2d*tauc
      tgroup=0.28/0.48   !CP/(CPS*LE); LE=1 ASSUMED
      egroup=0.48*tinf
      hv1=400./egroup                  !HEATS OF REACTION FOR
      hv2=200./egroup                  !DEVOLATILIZATION
      qgroup=1.35504E-12*a0*(tinf**4)/(rd0*egroup)
      eb=enth(tinf,gb)/egroup
C
C
      tau=0.0
      taupr=tau
      taup=tau
      z(1)=ts0/tinf
      z(2)=1.0
      z(3)=1.0
      z(4)=1.0
      iflag=1
300    continue
       call rkf(derivs,neq,z,tau,taup,relerr,abserr,iflag,work,iwork)
       if(iflag.ne.2) go to 500
       taup=taup+dtau
       if(tau.ge.taupr) call output(tau,taupr,dtaup,z,tauc,a0,rhc)
       brnout=1.-z(4)*z(2)**3
      if(brnout.lt.0.95) go to 300
499   stop
500   type 501,iflag
501   format(' iflag= ',i2)
      stop
      end
C
C
C  FUNCTION TO DO ENTHALPY CALCULATIONS FOR A GAS
C  MIXTURE.  iT'S SIMPLE HEAT CAPACITY FIT FROM
C  LIBBY & BLAKE'S PAPER.
C
      function enth(t,y)
      dimension y(4)
      enth=0.28*t -2172.*y(2)-956.*y(3)
C    IN CAL/G
      return
      end
C
      subroutine derivs(tau,z,f)
      dimension f(4),z(4),gb(4),gs(4)
      common ah,ap,at,ab,af1,bf1,af0,bf0
      common/gas/gb,gt1b,gt2b,gs,gt1s,gt2s,eb,tinf
      common/devol/a11,a12,b1,b2,ev1,ev2,hv1,hv2,vgroup
      common/deriv/tgroup,qgroup,egroup,rd0,fa1,fa0,fgroup,
     * rgroup,vol
      ts=z(1)*tinf
      vr=z(1)**(0.6575/2.)             !DIFFUSIVITY RATIO
C  ***COMBUSTION RATE CALCULATIONS***
      ash=1.-(fa1/z(2)+fa0)            !FRACTION OF AREA WHICH IS CARBON
      if(ash.gt.1.) ash=1.             !IF FRACTION ASH IS NEGATIVE
      af=ash*af0*z(2)*fgroup/vr
      bf=ash*bf0*z(2)*fgroup/vr
      yk=rate(ts,gb,gs,gt1b,gt2b,gt1s,gt2s,af,bf)
```

```
C  ***CALCULATION OF TERMS IN ENTHALPY BALANCE***
       rr=3.*z(2)/((1.-vol)*z(4)*(z(2)**3) + rgroup)
       qr=qgroup*(z(1)**4-1.)
       tr=tgroup*vr*(1.-z(1))
       if(z(3).le.0.0) go to 50          !CHECK TO SEE IF DEVOLATILIZATION
C                                         IS OVER
        vk1=b1*exp(-ev1/ts)
        vk2=b2*exp(-ev2/ts)
C  hgv IS THE HEAT OF REACTION FOR DEVOLATILIZATION (ENDOTHERMIC)
        esum=z(1)*(vgroup-1.) +140./egroup
        hgv=a11*vk1*(hv1+esum) + a12*vk2*(hv2+esum)
        f(1)=(-qr*z(2)+tr-(1.-vol)*z(3)*hgv/3.)*rr
        f(2)=0.0
        f(3)=-(vk1+vk2)*z(3)
        f(4)=-(a11*vk1 + a12*vk2)*z(3)
       return
C
50     continue                           !CHAR COMBUSTION
        es=surf(yk,ts,gb,gs,gt1b,gt2b,gt1s,gt2s,af,bf)/egroup
C   NOW CALCULATE HEAT GENERATION RATE, hg
        hr1=z(1)*(1.-tgroup) + 2090.67/egroup
        hr2=z(1)*(1.-tgroup) - 3642.67/egroup
        a=af*exp(-af1/ts)
        b=bf*exp(-bf1/ts)
        hg=a*gs(1)*hr1 + b*gs(2)*hr2
        f(1)=(-qr*z(2)+tr+hg*vr)*rr
        f(2)=-yk*vr/(z(4)*z(2)*(1.-vol))
        f(3)=0.0
        f(4)=0.0
       return
       end
C
       subroutine output(tau,taupr,dtaup,z,tauc,a0,rhc)
       dimension z(4),gb(4),gs(4)
       common ah,ap,at,ab,af1,bf1,af0,bf0
       common/gas/gb,gt1b,gt2b,gs,gt1s,gt2s,eb,tinf
       common/deriv/tgroup,qgroup,egroup,rd0,fa1,fa0,fgroup,
     * rgroup,vol
C
       taupr=taupr+dtaup
       ts=tinf*z(1)
       vr=z(1)**(0.6575/2.)              !DIFFUSIVITY RATIO
       ash=1.-(fa1/z(2)+fa0)             !FRACTION OF AREA WHICH IS CARBON
       if(ash.gt.1.) ash=1.              !IF FRACTION ASH IS NEGATIVE
       af=ash*af0*z(2)*fgroup/vr
       bf=ash*bf0*z(2)*fgroup/vr
       yk=rate(ts,gb,gs,gt1b,gt2b,gt1s,gt2s,af,bf)
       dummy=surf(yk,ts,gb,gs,gt1b,gt2b,gt1s,gt2s,af,bf)
       den=(gs(1)/32.+gs(2)/44.+(gs(3)+gs(4))/28.)
       po2=(gs(1)/32.)/den
       pco2=gs(2)/(44.*den)
       pco=gs(3)/(28.*den)
       r=a0*z(2)
       brnout=1.-z(4)*z(2)**3
C
       wtloss=100.*(1.-z(4))    !daf WT% LOSS DURING DEVOL.
       vtemp=(1.-vol)*z(2)**3
       rhot=(rhc*z(4)*vtemp+2.5*vol)/(vtemp+vol)        !TOTAL DENSITY
       t=tauc*tau
       type 350,t,ts,r,yk,po2,pco,wtloss,brnout
```

```
      write(2,350)t,ts,r,yk,po2,pco,rhot,brnout
350   format(1x,8(1pe12.3))
      return
      end
C
C
      subroutine input(tinf,xo2inf,co2inf,ts0,a0,dinc,rha,fa,
     * all,dtau,dtaup)
      common ah,ap,at,ab,af1,bf1,af0,bf0
      dimension ifile(20),d(3)
      data d(3)/'    '/
C
      type 1
1     format('$filename:',t40)
      accept 2,ifile
2     format(20a2)
      call assign(2,ifile)
      write(2,3)ifile
3     format(' filename:',t40,20a2)
      call date(d)
      write(2,4) d
4     format(' date:',t40,3a4)
C   **COMBUSTION CONDITIONS**
      type 5
5     format('$Tinf(K):',t40)
      accept 6,tinf
6     format(g14.7)
      type 7
7     format('$O2 mole fraction:',t40)
      accept 6,xo2inf
      type 8
8     format('$CO2 mole fraction:',t40)
      accept 6,co2inf
C   **COAL PROPERTIES**
      call getkin(af1,af0,rank)
      type 11
11    format('$coal radius(cm):',t40)
      accept 6,a0
      type 13
13    format('$inclusion diameter,cm:',t40)
      accept 6,dinc
      type 14
14    format('$weight fraction ash:',t40)
      accept 6,fa
      type 15
15    format('$apparent char density (g/cc):',t40)
      accept 6,rha
      type 16
16    format('$ASTM volatile matter (fraction):',t40)
      accept 6,all
      type 25
25    format('$dtau:',t40)
      accept 6,dtau
      type 26
26    format('$dtau (printout):',t40)
      accept 6,dtaup
C
      write (2,110) tinf
110   format(' Tinf(K):',t40,g14.7)
      write (2,111) xo2inf
```

```
111     format(' O2 mole fraction:',t40,g14.7)
        write(2,112)co2inf
112     format(' CO2 mole fraction:',t40,g14.7)
        write(2,113)ts0
113     format(' initial surface T (K):',t40,g14.7)
        write(2,123) rank
123     format(' coal type:',t40,a4)
        write (2,114) a0
114     format(' coal radius(cm):',t40,g14.7)
        write(2,115)dinc
115     format(' inclusion diameter,cm:',t40,g14.7)
        write(2,116)fa
116     format(' weight fraction ash:',t40,g14.7)
        write(2,117)rha
117     format(' apparent coal density (g/cc):',t40,g14.7)
        write(2,118) all
118     format(' ASTM volatile matter:',t40,g14.7)
        write (2,119) dtau
119     format(' dtau:',t40,g14.7)
        write(2,299)
299     format(' **')
        return
        end
C
C   SUBROUTINE TO GET KINETIC PARAMETERS FOR C + O2 -> 2CO
C
        subroutine getkin(af1,af0,rank)
        dimension af(4,2),coals(4),dummy(10)
        data coals/'ANTH','SEMI','BITU','COKE'/
        data af/10.,20.4,8.,20.,8405.,9562.,8052.,9160./
5       continue
        type 10
10      format('$coal type:',t40)
        accept 20,dummy
20      format(10a4)
        do 30 i=1,4
          n=i
          if(dummy(1).eq.coals(i)) go to 40
30        continue
        type 36
36      format(' never heard of it--try again')
        go to 5
40      continue
        af0=af(n,1)
        af1=af(n,2)
        rank=coals(n)
        return
        end
```

PRATE.FTN

```
C
C   tp IS THE PARTICLE TEMPERATURE
C   rp IS THE PARTICLE RADIUS
C   prate IS THE DIMENSIONLESS COMBUSTION RATE BASED ON EXTERNAL
C   SURFACE AREA...UNITS ARE CGS
C
      real function prate(tp,rp)
      external inrate
      double precision inrate,dx,dt
      real tp,rp,et0,pe,dpe
      real ah,ap,at,ab,a,rcoef,f,df,del,xs,rint
      real gb(4),gs(4),gt1b,gt2b,gt1s,gt2s,eb,tb
      integer j
      common ah,ap,at,ab,et0
      common/gas/gb,gt1b,gt2b,gs,gt1s,gt2s,eb,tb
C
      a=rcoef(tp,tb,rp,et0)
      xs=gs(1)                  !FIRST GUESS-LAST VALUE
      dt=dble(tp)
C
      j=0
10    continue
      dx=dble(xs)
      pe=a*rint(dx,dt)
      dpe=sngl(inrate(dx,dt))*0.5*a*a/pe
D     type 101,dx,dt,pe
D101  format(' xs,tp,pe', 2(1x,1pd12.4),1pe12.4)
      f=xs+at-(at+gb(1))*exp(-pe)
      df=1.+(gb(1)+at)*exp(-pe)*dpe
      del=-f/df
      test=abs(del/xs)
      xs=xs+del
      j=j+1
      if(j.gt.50)               go to 200
      if(test.ge.1.E-3)         go to 10
100   continue
      gs(1)=xs
      prate=a*rint(dx,dt)
      return
200   continue
      stop 'too many iterations in prate'
      end
C
      real function rcoef(t,tb,rp,et0)
      real t,rp,et0,diff,rho,ak,beta,j1,j
      real tb,rd
C
      rho=28.84/(82.056*t)
      diff=5.974E-6*(t**0.6575)/rho
      ak=9.7E3*sqrt(t/28.84)
      beta=ak/diff
      j=2.*j1(beta)/ak          !TORTUOSITY OF 2
      rd=5.974E-6*(sqrt(tb*t))**0.6575
      rcoef=(1.-et0)*sqrt(3.*rho/(4.*j))*rp/rd
C
D     type 99,t,r0
D99   format(' t,r0',2(1x,1pe11.4))
D     type 100,ak,beta,j
```

```
D100    format('   ak,beta,j',3(1x,1pe11.4))
        return
        end
C
C   COMPUTE THE SQUARE ROOT OF THE INTEGRAL OF REACTION RATE
C
        real function rint(x,t)
        external inrate
        double precision a,inrate,gaus8,t,x
        a=0.0D0
        rint=sngl(dsqrt(gaus8(inrate,a,x,t)))
        return
        end
C
C   TEST RATE
C
        double precision function inrate(x,t)
        double precision ka,kb,kz,kt,x,t
        kz=21.3D0*dexp(2060.D0/t)
        kt=1.51D5*dexp(-4.88D4/t)
        kb=4.46D-3*dexp(-8.5D3/t)
        ka=325.D0*dexp(-1.9D4/t)
        inrate=12.D0*x*(kt + ka*x/(1.+kz*x))/(x+kt/kb)
        return
        end
```

J1.FTN

```
C
C   CALCULATE J1 FOR A PORE SIZE DISTRIBUTION
C   REF:  GAVALAS, COMB.SCI.TECH. 24:197-210 (1981)
C
      real function j1(bta)
      external jint
      double precision et0,r(10),g(10),beta(10),qs,a,b
      double precision gaus8,jint
      real bta
      integer n,k
      common/pores/n,qs,et0,r,g,beta
C
      a=0D0
      b=qs
C
      do 10 k=1,n
              beta(k)=dble(bta)*r(k)
10            continue
      j1=sngl((1D0-et0)*gaus8(jint,a,b))
      return
      end
C
      double precision function jint(x)
      double precision et0,r(10),g(10),beta(10),qs,sum,pi,pisum
      double precision gam,term,x
      real ex
      integer j,k,n
      common/pores/n,qs,et0,r,g,beta
      pi=1D0
      sum=0D0
      do 20 j=1,n
              pisum=1D0
              gam=1D0 + x/r(j)
              ex=sngl(gam)
              term=g(j)**(ex*ex)
              if((j+1).gt.n)  go to 15
              do 10 k=j+1,n
                      ex=sngl(1D0 + x/r(k))
                      pisum=pisum*(g(k)**(ex*ex))
10                    continue
15            continue
              sum=sum+(1D0-term)*pisum*r(j)*gam/(1D0+beta(j)*gam)
              pi=pi*term
20            continue
      jint=(1D0 - pi/(1D0-et0))/sum
      return
      end
```

PORE80.FTN

```
C
C   FUNCTION TO COMPUTE PARAMETERS OF PORE SIZE DISTRIBUTION
C   FOR UP TO 10 PORE SIZES
C
      real function pores(e)
      double precision ets,det0,e(10),r(10),g(10),beta(10),qs
      double precision sum1,sum2,term,a,b
      integer j,n
      common/pores/n,qs,det0,r,g,beta
      ets=0.80D0
      det0=0D0
      do 5 j=1,n
            det0=det0+e(j)
5           continue
      pores=sngl(det0)
C
      sum1=det0
      sum2=det0-e(1)
      g(1)=(1D0-sum1)/(1D0-sum2)
      if(n.le.2) go to 15
      do 10 j=2,n-1
            sum1=sum1-e(j-1)
            sum2=sum2-e(j)
            g(j)=(1D0-sum1)/(1D0-sum2)
10          continue
15    continue
      g(n)=1D0-e(n)
C
      a=0D0
      b=0D0
      do 20 j=1,n
            term=dlog(g(j))/r(j)
            b=b+term
            a=a+term/r(j)
20          continue
      term=b*b - a*dlog((1D0-det0)/(1D0-ets))
      if(term.lt.0D0) stop 'negative sqrt'
      qs=(-b - dsqrt(term))/a
      return
      end
```

```
C  **                                                          **
C  **  ASH VAPORIZATION AROUND A BURNING COAL PARTICLE          **
C  **  INCLUDING AEROSOL FORMATION AND GROWTH                  **
C  **                                                          **
C      SOLUTION IS BY A SHOOTING METHOD WITH UNKNOWN
C      VAPORIZATION RATE AND EQUILIBRIUM SURFACE VAPOR
C      PRESSURE
C                                C. L. SENIOR 1983
C
       external derivs
       dimension gb(4),gs(4),ytest(3),ispec(3),prop(4,3),z(8)
       real*8 rtry,rtry0,rtest(3)
       data pi,boltz,rgas/3.1415926,1.38E-16,82.055/
       data prop/7.363E-6,9.11E-9,2.205,60.09,
     * 4.842E-6,6.763E-9,2.949,101.96,
     *  8.E-6,9.E-9,2.5,75./
       data ispec,nspec/'SI','AL','B-',3/
       common ah,ap,at,ab,et0,a0
       common/gas/gb,gtlb,gt2b,gs,gtls,gt2s,eb,tinf
       common/const/thetap,tc,yc,cc,rvor,dc,efact,gfact,rt
       common/out/wtmol,sc,cfact,detap,dmin
       common/prop/rgas,yref,evap,tref,xi,dcons,nvp,xiv,es
C
C                                          GET PARAMETERS FIRST:
       call input(tinf,xo2,ts,a,xi,di,vol,dets,detap,nvp,rtmlt,
     * ispec,nspec,prop,dcrit,srften)
       tmean=sqrt(ts*tinf)
       rd=5.974E-6*(tmean**0.6575)
       cdair=rd/28.97
C*************************************************************
C                    COAL COMBUSTION CONDITIONS
       al2=8./11.
       al3=4./7.
       a22=3./11.
       a23=3./7.
       ah=al2/a22
       at=al3/a23
       ab=a22*(ah-at)
       ap=a23*(ah-at)
C   KINETIC PARAMETERS FOR COMBUSTION
C   GAS MASS FRACTION AT BOUNDARY
       den=32.*xo2  + 28.*(1.-xo2)
       gb(1)=xo2*32./den
       gb(2)=0.0
       gb(3)=0.0
       gb(4)=1.-gb(1)
       gtlb=gb(1) + al2*gb(2) + al3*gb(3)
       gt2b=a22*gb(2) + a23*gb(3)
       eb=enth(tinf,gb)
C   xi IS THE DIMENSIONLESS COMBUSTION RATE AND ALSO
C   THE PECLET NUMBER AT THE PARTICLE SURFACE:
       es=psurf(xi,ts,gb,gs,gtlb,gt2b,gtls,gt2s)
       den=gs(1)/32.+gs(2)/44.+(gs(3)+gs(4))/28.
       po2=gs(1)/(32.*den)
       pco=gs(3)/(28.*den)
       ratep=4.*pi*a*cdair*xi  !COMBUSTION RATE IN MOLE/SEC
C
C*************************************************************
```

```
C
C   BEGIN ASH VAPORIZATION PARAMETER CALCULATION:
C         ASSIGN VAPOR SPECIES PROPERTIES
      cd1=prop(1,nvp)
      cd2=prop(2,nvp)
      rhop=prop(3,nvp)
      wtmol=prop(4,nvp)
C
      cd=cd1 + cd2*tmean
      xiv=xi*cdair/cd          !SPECIES PECLET NUMBER MUST BE
C                                CORRECTED FOR DIFFUSIVITY
      rtotal=ratep*(1.+ therm(jth,xi,ts,tinf))
D     type 100,ratep,rtotal
D100  format(' ratep,rtotal: ',2(1x,1pe11.3))
C   EVEN MORE PARAMETER CALCULATIONS...
      yc=vapor(nvp,ts,po2,pco,1.)
      dcm=(6.*wtmol/(pi*rhop*6.02E23))**(1./3.)
      cc=1./(rgas*ts)
      tc=ts
      dc=dcrit
      rk=3.812E10
      sc=sqrt(srften*wtmol)*5.541E31*yc*yc/(tc*tc*rhop)
      cfact=sc*a*a/(cd*xiv)
      dcons=4.*srften*wtmol/(rhop*boltz*6.02E23*tc)
      efact=4.*pi*a*a*a*7275.*((wtmol*tc)**0.5)*cc*cc*yc/(rtotal*
     1 dc*rhop)
      gfact=4.*pi*pi/6.*rk*dc*dc*dc*rk*a*a*a*rk*yc/(rtotal*tc*tc)*
     1 ((srften/wtmol)**0.5)
      thetap=17.57461*((wtmol/rhop)**2)*((srften/tc)**3)
C     SINCE THE VAPORIZATION RATE IS UNKNOWN, WE'LL MAKE TWO
C     GOOD GUESSES AND GET THE ITERATION ROLLING...
      rvoo=1./(1.-exp(-xiv))  !VAP. RATE IN THE ABSENCE OF AEROSOL
C                             NORMALIZED BY rtotal AND yc
      rtry0=dble(rtmlt)
      rtry=1.D0+0.9D0*(rtry0-1.D0)
C
C   ZEROTH PASS
            last=0
            dmin=0.0
            ipass=0
            rvor=rvoo*sngl(rtry0)
            call pass(derivs,z,deta,detap,yoo,last)
            rtest(2)=rtry0
            rtest(3)=rtry
            ytest(2)=yoo
            type 302,yoo
302         format(' yoo= ',1pe12.4)
            type 305,ipass,rtest(2)
305         format('  pass',i3,' completed,rtmlt=',1pd12.5)
            if(z(3).eq.0.0) go to 314
C
C   NEXT PASS ON INTEGRATION
313   continue
            dcnew=z(8)/z(3)          !NUMBER-AVERAGE CRITICAL DIAMETER
            if(dcnew.lt.dcm)dcnew=dcm
314         continue
            dmin=0.0
            ipass=ipass+1
            rtry=rtest(3)
            rvor=sngl(rtry)*rvoo
```

```
            call pass(derivs,z,deta,detap,yo,last)
            type 320,yo
320         format(' yo= ',1pe12.4)
            type 305,ipass,rtest(3)
            ytest(3)=yo
C   itest RETURNS A VALUE OF 1 IF THE SHOOTING METHOD IS DONE
C   OTHERWISE A VALUE OF 0 IS RETURNED
C   THE NEW VALUE OF THE RATE (DIVIDED BY rvoo)  IS RETURNED IN
C   rtest(3).
            if(itest(ipass,ytest,rtest).eq.0) go to 313
C
C   END OF SHOOTING METHOD CALCULATION
      ratev=rvor*ratep*yc
      last=1
      dmin=0.0
      call end(yo,ipass,rtest,dc,dcnew,ratev,jth)
C   REPEAT THE FINAL PASS, WRITING EACH STEP TO OUTPUT FILE
      call pass(derivs,z,deta,detap,yo,last)
900   stop
      end
C
C   SUBROUTINE end PRINTS OUT HEADER INFORMATION BEFORE FINAL PASS
C
      subroutine end(yo,ipass,rtest,dc,dcnew,ratev,jth)
      real*8 rtest(3)
      if(jth.ne.1) write(2,31)
      if(jth.eq.1) write(2,32)
31    format(' thermophoresis is not included')
32    format(' thermophoresis is included')
      write(2,5)yo
5     format(' yo= ',1pe12.4)
      write(2,10)ipass,rtest(3)
10    format(' finished after',i3,' passes. rtmlt=',1pd12.5)
      write(2,15)dc
15    format(' critical diameter (cm) = ',1pe12.4)
      type 20,ratev
      write(2,20) ratev
20    format(' --- final vaporization rate =',1pe12.4,' mole/sec')
      type 25,dcnew
      write(2,25)dcnew
25    format(' number average critical diameter (cm) = ',1pe12.4)
      write(2,30)
30    format(6x,'r/rp',4x,'tgas/tp',7x,'y/ys',7x,'s',6x,
     * 'i,/cc-sec',6x,'n,#/cc',2x,'davg/dcrit',2x,'ug/m**3')
      write(2,35)
35    format(' **')
      return
      end
C
C   SUBROUTINE pass DOES ONE INTEGRATION OF THE SOLUTION
C
      subroutine pass(derivs,z,deta,detap,yo,last)
      external derivs
      real*8 y1,y2,e1,e2
      dimension z(8),work(60),iwork(10)
C   work AND iwork ARE NEEDED FOR THE INTEGRATION ROUTINE.
C   iwork MUST HAVE DIMENSION >=6.
C   work MUST HAVE DIMENSION >=3 + 6*neq.  relerr AND abserr ARE
C   NEEDED, TOO AND FOR THE PDP-11 SHOULD BE GIVEN BY:
      data relerr,abserr,neq/1.E-3,1.E-15,8/
```

```
      iflag=1
      nstep=0
      ntotal=ifix(1./abs(deta)) + 1
c
      z(1)=1.
      z(2)=0.0
      z(3)=0.0
      z(4)=0.0
      z(5)=0.0
      z(6)=0.0
      z(7)=0.0
      z(8)=0.0
      eta=1.0
      etapr=1.
      etap=eta
405   continue
            call rkf(derivs,neq,z,eta,etap,relerr,abserr,iflag,
     *      work,iwork)
            if (iflag.ne.2) go to 420
            etap=etap+deta
            nstep=nstep+1
            y1=y2
            y2=z(1)
            e1=e2
            e2=eta
            if(last.eq.1)call final(eta,z,etapr)
            if(nstep.lt.ntotal) go to 405
C
      yo=z(1)
      etapr=1.
      if(last.eq.1)call final(eta,z,etapr)
      return
C
C  mAKE AN ESTIMATE OF z(1) AT eta=0:
420   continue
      yo=sngl(y1-e1*(y1-y2)/(e1-e2))
      return
      end
C
C   SUBROUTINE input GETS THE INPUT PARAMETERS AND SETS UP THE OUTPUT
C   FILE.  OUTPUT FILE IS OPENED AND THE INPUT PARAMETERS ARE WRITTEN.
C
      subroutine input(tinf,xo2inf,ts,a,xi,dinc,vol,deta,detap,
     * nvp,rtmlt,ispec,nspec,prop,dcrit,srften)
      dimension ifile(20),prop(1,1),ispec(1),d(3)
      data d(3)/'    '/
C
      type 1
1     format('$filename:',t40)
      accept 2,ifile
2     format(20a2)
      call assign(2,ifile)
      write(2,3)ifile
3     format(' filename:',t40,20a2)
      call date(d)
      write(2,4) d
4     format(' date:',t40,3a4)
C   **COMBUSTION CONDITIONS**
      type 5
5     format('$Tinf (K):',t40)
```

```
      accept 6,tinf
6     format(g14.7)
      type 7
7     format('$02 mole fraction:',t40)
      accept 6,xo2inf
      type 9
9     format('$surface T (K):',t40)
      accept 6,ts
C  **COAL PROPERTIES**
      type 11
11    format('$coal radius (cm):',t40)
      accept 6,a
      type 13
13    format('$inclusion diameter (cm):',t40)
      accept 6,dinc
      type 14
14    format('$volume fraction ash:',t40)
      accept 6,vol
      type 23
23    format('$dimensionless mass loss:',t40)
      accept 6,xi
      type 29
29    format('$deta:',t40)
      accept 6,deta
      deta=-abs(deta)
      type 30
30    format('$deta (printout):',t40)
      accept 6,detap
      detap=-abs(detap)
C   **VAPOR SPECIES PROPERTIES**
      type 51
51    format('$vapor species:',t40)
      accept 2,ifile
55    continue
      do 61 i=1,nspec
            nvp=i
            if(ifile(1).eq.ispec(i)) go to 65
61    continue
      type 62
62    format('$invalid species,enter vapor species:',t40)
      accept 2,ifile
      go to 55
65    continue
C  **ASSIGN VAPOR SPECIES PROPERTIES**
      cd1=prop(1,nvp)
      cd2=prop(2,nvp)
      rhop=prop(3,nvp)
      wtmol=prop(4,nvp)
      type 75
75    format('$surface tension (dyn/cm):',t40)
      accept 6,srften
      type 77
77    format('$rate multiplier:',t40)
      accept 6,rtmlt
C
      dcrit=(6.*wtmol/(3.1415926*rhop*6.02E23))**(1./3.)
      type 87,dcrit
87    format(' critical diameter  (cm) = ',1pe12.4)
      type 88
88    format(' you can change dcrit by entering a new value'/
```

```
     *  '$enter zero for no change: ',t40)
        accept 6,dcnew
        if(dcnew.ne.0.0) dcrit=dcnew
C    **WRITE OUT PARAMETERS**
        write (2,110) tinf
110     format(' Tinf (K):',t40,f12.4)
        write (2,111) xo2inf
111     format(' O2 mole fraction:',t40,f12.8)
        write(2,113)ts
113     format(' surface T (K):',t40,f12.4)
        write (2,114) a
114     format(' coal radius (cm):',t40,1pe12.4)
        write(2,115)dinc
115     format(' inclusion diameter (cm):',t40,1pe12.4)
        write(2,116)vol
116     format(' volume fraction ash:',t40,f12.6)
        write(2,124)xi
124     format(' dimensionless mass loss:',t40,1pe12.3)
        write (2,131) deta
131     format(' deta:',t40,1pe12.4)
        write (2,202) ifile
202     format(' vapor species:',t40,20a2)
        write (2,204) wtmol,rhop
204     format(' mole wt, density (g/mol, g/cc):',t40,f12.5,',',f12.5)
        write (2,206) srften
206     format(' surface tension (dyn/cm):',t40,f12.4)
        write(2,221) cd1,cd2
221     format('[cd=cd1 + cd2*t] cd1,cd2:',t40,1pe12.3,1pe12.3)
        return
        end
C
C
        subroutine derivs(eta,z,f)
        dimension z(8),f(8)
        common/const/thetap,tc,yc,cc,rvor,dc,efact,gfact,rt
        common/prop/rgas,yref,evap,tref,xi,dcons,nvp,xiv,es
        do 10 i=1,7
10              f(i)=0.0
        call props(eta,t,c,ye,xo2)
        t=t/tc
        ye=ye/yc
        c=c/cc
        y=z(1)
        b=1.-z(2)
        rm=z(7)
        f(1)=xiv*(rvor-y-rm*(1.+rt))
        if (b.le.0.0) return
C
        sat=y/ye
        s=0.0
        if (sat.gt.1.00001) s=y*y/(t*t)*exp(-thetap/((t**3)*
     1 (alog(sat)*alog(sat))))
        dcr=0.0
        if(sat.gt.1.00001) dcr=dcons/(t*alog(sat))
        f(2)=c*c*(t**0.5)*(y-ye)/(eta**4)*efact
        f(3)=-s/(eta**4)
        f(4)=f(3)*z(2)
        f(5)=f(4)*z(2)
        f(6)=f(5)*z(2)
        f(7)=gfact*((3.*b*b*z(3)+6.*b*z(4)+3.*z(5))*(-f(2))
```

```
     1 +b*b*b*f(3)+3.*b*b*f(4)+3.*b*f(5)+f(6))
       f(8)=f(3)*dcr
       return
       end
C
C  FINAL OUTPUT SUBROUTINE
C
       subroutine final(eta,z,etapr)
       common/const/thetap,tc,yc,cc,rvor,dc,efact,gfact,rt
       common/out/wtmol,sc,cfact,detap,dmin
       dimension z(8)
       if(eta.gt.etapr) go to 310
       etapr=etapr+detap
       y=z(1)
       r=1./eta
       if(dmin.ne.0.0) go to 100
               if(z(7).gt.1.E-30) dmin=-z(2)
               d=1.0
       go to 101
100    d=1.-z(2)-dmin
101    call props(eta,t,c,ye,xo2)
       rm=z(7)*1.E12*wtmol*yc/(82.056*t)        !MASS LOADING,UG/M**3
       tnum=cfact*z(3)/(82.056*t)               !#/CC
       davg=0.0
       if(z(3).ne.0.0) davg=z(4)/z(3)+1.-z(2)
C   NUMBER AVERAGE/CRITICAL DIAMETER
       t=t/tc
       ye=ye/yc
       sat=y/ye
       s=0.0
       if (sat.gt.1.00001) s=y*y/(t*t)*exp(-thetap/((t**3)*
     1 (alog(sat)*alog(sat))))
       s=s*sc                                   !NUCLEATION RATE,#/CC-SEC
       write (2,301)r,t,y,sat,s,tnum,davg,rm
301    format(' ',8(1pe11.3))
310    continue
       return
       end
C
C
       subroutine props(z,t,c,ye,xo2)
       dimension g(4),gs(4),gb(4)
       common ah,ap,at,ab,et0,a0
       common/gas/gb,gt1b,gt2b,gs,gt1s,gt2s,eb,tinf
       common/prop/rgas,yref,evap,tref,xi,dcons,nvp,xiv,es
       g(1)=profnc(xi,z,gb(1),gs(1))
       gt1=profnc(xi,z,gt1b,gt1s)
       gt2=profnc(xi,z,gt2b,gt2s)
       e=profnc(xi,z,eb,es)
       g(2)=(gt1-g(1)-at*gt2)/ab
       g(3)=(ah*gt2-gt1+g(1))/ap
       g(4)=1.-g(1)-g(2)-g(3)
       call zero(g)
       t=(e + 2172.*g(2) + 956.*g(3))/0.28
       c=1./(rgas*t)
       den=(g(1)/32. + g(2)/44. + g(3)/28. + g(4)/28.)
       xo2=(g(1)/32.)/den
       xco=(g(3)/28.)/den
       ye=vapor(nvp,t,xo2,xco,1.)
       return
```

```
      end
C
C
C  FUNCTION TO DO ENTHALPY CALCULATIONS FOR A GAS
C  MIXTURE.  IT'S SIMPLE HEAT CAPACITY FIT FROM
C  LIBBY & BLAKE'S PAPER.
C
      function enth(t,y)
      dimension y(4)
      enth=0.28*t -2172.*y(2)-956.*y(3)
C    IN CAL/G
      return
      end
C
      real function psurf(pe,ts,gb,gs,gt1b,gt2b,gt1s,gt2s)
      real pe,ts,gb(4),gs(4),gt1b,gt2b,gt1s,gt2s,enth,a0
      common ah,ap,at,ab,et0,a0
      gs(1)=(at+gb(1))*exp(-pe) - at
      gt1s=gt1b*exp(-pe)
      gt2s=1.-(1.-gt2b)*exp(-pe)
      gs(2)=(gt1s-gs(1)-at*gt2s)/ab
      gs(3)=(ah*gt2s-gt1s+gs(1))/ap
      gs(4)=1.-gs(1)-gs(2)-gs(3)
      call zero(gs)
      psurf=enth(ts,gs)
      return
      end
C
C  THIS VERSION OF VAPOR ONLY LOOKS AT THE RXNS. WITH CO
      function vapor(n,t,po2,pco,ac)
      th=1000./t
      vapor=0.0
      go to (10,20,30)n
10    continue
            eq=exp(-59.39*th+18.60)          !SIO2+CO->SIO+CO2
            vapor=sqrt(ac*eq*pco)
            return
20    continue
            eq=exp(-98.24*th+17.06)          !AL2O3+2CO->AL2O+2CO2
            vapor=(eq*ac*pco*pco)**(1./3.)
            return
30    continue        !PSUEDO-SPECIES b
            vapor=3.946E7*exp(-43.75*th)
            return
      end
C
C   TEST FOR END OF SHOOTING METHOD
C  INTERVAL BISECTION
      function itest(ip,y,r)
      dimension y(3)
      real*8 r(3),rtst,testv
      itest=1
      rtst=r(3)
      tst=y(3)
      if(abs(tst).lt.1.0E-3) return
      itest=0
      if(ip.gt.1) go to 200
C   FIRST PASS: JUST SHIFT
            r(1)=r(2)
            y(1)=y(2)
```

```
                r(2)=r(3)
                y(2)=y(3)
                go to 250
C
C   SUBSEQUENT PASSES:
200     continue
        if(y(3).gt.0.0.and.y(1).le.0.0) go to 210
        if(y(3).le.0.0.and.y(1).gt.0.0) go to 210
C  SAME SIGN:
                y(1)=y(3)
                r(1)=r(3)
                go to 250
C  OPPOSITE SIGN:
210             continue
                y(2)=y(3)
                r(2)=r(3)
C   CALCULATE A NEW RATE AND TEST IT
250     r(3)=r(1)+0.5D0*(r(2)-r(1))
        testv=(rtst-r(3))/rtst
        if(abs(testv).lt.1.D-6) itest=1
        return
        end
C
C   ON/OFF SWITCH FOR THERMOPHORESIS
C
        real function therm(jth,xi,ts,tinf)
        real xi,ts,tinf,sc,avg
        integer jth
        logical*1 yes,no,maybe
        data yes,no/'Y','N'/
        type 10
10      format('$include thermophoresis? (Y/N) ')
        accept 20,maybe
20      format(a1)
        if(maybe.eq.yes) go to 50
C
        therm=0.0
        jth=0
        return
C
50      continue
        jth=1
        sc=4.653/5.974          !SCHMIDT NUMBER BASED ON FITS FOR AIR
        avg=0.25*exp(-xi)+0.75*ts/tinf
        therm=-1.61*sc*(1.-ts/tinf)*avg/(3.*(1.-exp(-xi)))
D       type 100,therm
D100    format(' therm= ',1pe11.3)
        return
        end
```

filename: M2075.DAT
date: 07-JUL-83
Tinf (K): 1750.0000
O2 mole fraction: 0.20000000
surface T (K): 2282.0000
coal radius (cm): 2.5180E-03
inclusion diameter (cm): 2.0000E-04
volume fraction ash: 0.053300
dimensionless mass loss: 8.592E-02
deta: -1.0000E-02
vapor species: SILICA
mole wt, density (g/mol, g/cc): 60.09000, 2.20500
surface tension (dyn/cm): 305.0000
cd=cd1 + cd2*t] cd1,cd2: 7.363E-06 9.110E-09
thermophoresis is included
yo= -2.7456E-03
finished after 13 passes. rtmlt= 1.07504D+00
critical diameter (cm) = 4.4218E-08
--- final vaporization rate = 9.8493E-09 mole/sec
number average critical diameter (cm) = 4.4218E-08

r/rp	tgas/tp	y/ys	s	i,/cc-sec	n,#/cc	davg/dcrit	ug/m**3
1.000E+00	1.000E+00	1.000E+00	1.000E+00	0.000E-01	0.000E-01	0.000E-01	0.000E-01
1.020E+00	9.955E-01	9.794E-01	1.048E+00	0.000E-01	0.000E-01	0.000E-01	0.000E-01
1.042E+00	9.911E-01	9.588E-01	1.099E+00	0.000E-01	0.000E-01	0.000E-01	0.000E-01
1.064E+00	9.866E-01	9.381E-01	1.153E+00	0.000E-01	0.000E-01	0.000E-01	0.000E-01
1.087E+00	9.821E-01	9.174E-01	1.210E+00	0.000E-01	0.000E-01	0.000E-01	0.000E-01
1.111E+00	9.776E-01	8.966E-01	1.270E+00	0.000E-01	0.000E-01	0.000E-01	0.000E-01
1.136E+00	9.731E-01	8.758E-01	1.334E+00	0.000E-01	0.000E-01	0.000E-01	0.000E-01
1.163E+00	9.686E-01	8.550E-01	1.401E+00	0.000E-01	0.000E-01	0.000E-01	0.000E-01
1.190E+00	9.640E-01	8.341E-01	1.472E+00	0.000E-01	0.000E-01	0.000E-01	0.000E-01
1.220E+00	9.595E-01	8.131E-01	1.547E+00	0.000E-01	0.000E-01	0.000E-01	0.000E-01
1.250E+00	9.550E-01	7.922E-01	1.627E+00	0.000E-01	0.000E-01	0.000E-01	0.000E-01
1.282E+00	9.504E-01	7.711E-01	1.711E+00	0.000E-01	0.000E-01	0.000E-01	0.000E-01
1.316E+00	9.459E-01	7.501E-01	1.799E+00	0.000E-01	0.000E-01	0.000E-01	0.000E-01
1.351E+00	9.413E-01	7.290E-01	1.893E+00	0.000E-01	0.000E-01	0.000E-01	0.000E-01
1.389E+00	9.367E-01	7.078E-01	1.993E+00	9.983E-13	8.902E-20	1.022E+00	3.298E-30
1.429E+00	9.322E-01	6.866E-01	2.098E+00	1.465E-08	1.847E-15	1.028E+00	7.003E-26
1.471E+00	9.276E-01	6.654E-01	2.208E+00	3.768E-05	6.575E-12	1.037E+00	2.560E-22
1.515E+00	9.230E-01	6.441E-01	2.326E+00	2.518E-02	5.954E-09	1.049E+00	2.406E-19
1.562E+00	9.184E-01	6.228E-01	2.449E+00	5.822E+00	1.850E-06	1.065E+00	7.860E-17
1.613E+00	9.138E-01	6.014E-01	2.579E+00	5.769E+02	2.442E-04	1.086E+00	1.108E-14
1.667E+00	9.091E-01	5.800E-01	2.717E+00	2.885E+04	1.623E-02	1.113E+00	8.009E-13
1.724E+00	9.045E-01	5.586E-01	2.861E+00	8.229E+05	6.144E-01	1.147E+00	3.375E-11
1.786E+00	8.999E-01	5.371E-01	3.014E+00	1.476E+07	1.457E+01	1.191E+00	9.177E-10
1.852E+00	8.952E-01	5.155E-01	3.173E+00	1.796E+08	2.343E+02	1.246E+00	1.750E-08
1.923E+00	8.906E-01	4.939E-01	3.341E+00	1.574E+09	2.716E+03	1.317E+00	2.503E-07
2.000E+00	8.859E-01	4.723E-01	3.515E+00	1.043E+10	2.384E+04	1.406E+00	2.835E-06
2.128E+00	8.789E-01	4.398E-01	3.792E+00	1.143E+11	4.003E+05	1.587E+00	7.649E-05
2.222E+00	8.743E-01	4.180E-01	3.985E+00	4.384E+11	2.050E+06	1.750E+00	5.721E-04
2.326E+00	8.696E-01	3.962E-01	4.184E+00	1.412E+12	8.875E+06	1.957E+00	3.796E-03
2.439E+00	8.649E-01	3.744E-01	4.389E+00	3.885E+12	3.309E+07	2.224E+00	2.273E-02
2.564E+00	8.602E-01	3.525E-01	4.598E+00	9.273E+12	1.079E+08	2.569E+00	1.244E-01
2.703E+00	8.555E-01	3.306E-01	4.808E+00	1.936E+13	3.121E+08	3.018E+00	6.287E-01
2.857E+00	8.508E-01	3.087E-01	5.018E+00	3.563E+13	8.078E+08	3.609E+00	2.956E+00
3.030E+00	8.460E-01	2.866E-01	5.225E+00	5.802E+13	1.885E+09	4.395E+00	1.302E+01
3.226E+00	8.413E-01	2.646E-01	5.422E+00	8.345E+13	3.989E+09	5.458E+00	5.403E+01
3.448E+00	8.366E-01	2.425E-01	5.605E+00	1.055E+14	7.668E+09	6.920E+00	2.122E+02
3.704E+00	8.318E-01	2.203E-01	5.766E+00	1.157E+14	1.340E+10	8.977E+00	7.915E+02
4.000E+00	8.270E-01	1.981E-01	5.892E+00	1.079E+14	2.125E+10	1.195E+01	2.813E+03
4.348E+00	8.223E-01	1.759E-01	5.971E+00	8.243E+13	3.048E+10	1.636E+01	9.551E+03
4.762E+00	8.175E-01	1.536E-01	5.982E+00	4.850E+13	3.943E+10	2.311E+01	3.101E+04
5.263E+00	8.127E-01	1.313E-01	5.901E+00	1.971E+13	4.611E+10	3.359E+01	9.642E+04
5.882E+00	8.079E-01	1.090E-01	5.692E+00	4.509E+12	4.958E+10	4.970E+01	2.872E+05
6.667E+00	8.031E-01	8.686E-02	5.312E+00	3.788E+11	5.071E+10	7.309E+01	8.197E+05
7.692E+00	7.983E-01	6.507E-02	4.709E+00	4.194E+09	5.109E+10	1.047E+02	2.238E+06
9.091E+00	7.935E-01	4.433E-02	3.848E+00	2.876E+05	5.140E+10	1.454E+02	5.785E+06
1.111E+01	7.887E-01	2.613E-02	2.770E+00	2.251E-07	5.171E+10	1.947E+02	1.367E+07
1.429E+01	7.839E-01	1.292E-02	1.718E+00	0.000E-01	5.203E+10	2.455E+02	2.730E+07
2.000E+01	7.790E-01	6.356E-03	1.108E+00	0.000E-01	5.236E+10	2.805E+02	4.084E+07
3.333E+01	7.742E-01	2.971E-03	7.421E-01	0.000E-01	5.268E+10	2.560E+02	3.133E+07

APPENDIX B: Experimental Data

TABLE B.1 EAA and OPC data (averaged) for combustion of porous carbon at 1575 K.

	No Feed	Porous Carbon
% Oxygen	100.0	39.8
EAA Readings		
Channel 1	3.309	9.072
Channel 2	3.170	9.203
Channel 3	1.806	7.600
Channel 4	0.247	2.142
Channel 5	0.084	0.933
Channel 6	0.018	0.153
Channel 7	0.013	0.047
Channel 8	0.009	0.029
Channel 9	0.008	0.021
Channel 10	0.009	0.014
OPC Readings		
Channel 1	7275	31247
Channel 2	486	24714
Channel 3	71	40080
Channel 4	35	60631
Channel 5	21	75159
Channel 6	20	59096
Channel 7	9	37577
Channel 8	5	23738
Channel 9	4	13898
Channel 10	4	11507
Channel 11	1	7575
Channel 12	1	4880
Channel 13	1	4040
Channel 14	1	2951
Channel 15	0	105

TABLE B.2 EAA and OPC data (averaged) for combustion of porous carbon at 1575 K.

% Oxygen	100.0	100.0	80.0	61.4	61.4	51.5	39.8
EAA Readings							
Channel 1	8.501	8.953	8.080	5.564	6.471	4.536	3.379
Channel 2	9.368	9.094	7.718	5.357	6.132	4.568	3.222
Channel 3	8.360	8.443	6.045	3.682	4.191	2.925	1.839
Channel 4	5.426	6.040	3.338	1.455	1.543	0.637	0.156
Channel 5	4.396	4.949	2.706	0.953	0.929	0.313	0.046
Channel 6	2.354	2.729	1.335	0.350	0.295	0.073	0.015
Channel 7	0.768	0.883	0.429	0.094	0.075	0.024	0.010
Channel 8	0.225	0.269	0.137	0.035	0.030	0.012	0.009
Channel 9	0.094	0.109	0.066	0.020	0.015	0.011	0.008
Channel 10	0.049	0.057	0.034	0.016	0.012	0.010	0.009
OPC Readings							
Channel 1	421716	414113	87377	4381	4287	1044	438
Channel 2	5352	5539	2155	1147	1404	664	215
Channel 3	4049	4524	3497	3702	4404	2772	1002
Channel 4	3898	4202	4475	6695	7835	6382	3461
Channel 5	4244	4724	5262	7694	9081	7981	5342
Channel 6	3774	4210	4675	6621	7689	6641	4749
Channel 7	2722	3082	3439	4495	5395	4362	3199
Channel 8	1905	2112	2410	3034	3590	2946	2095
Channel 9	1177	1270	1501	1927	2278	1797	1256
Channel 10	970	1072	1258	1545	1868	1444	1038
Channel 11	615	678	840	998	1152	958	670
Channel 12	403	455	536	607	776	600	443
Channel 13	320	337	384	504	607	493	348
Channel 14	230	246	298	373	442	326	268
Channel 15	25	6	0	30	100	5	30

TABLE B.3 EAA and OPC data (averaged) for combustion of non-porous carbon at 1575 K.

% Oxygen	100.0	100.0	100.0	80.0	51.5
EAA Readings					
Channel 1	3.823	3.983	3.860	2.028	0.730
Channel 2	3.700	4.035	4.002	1.983	0.606
Channel 3	2.525	2.786	2.783	1.060	0.123
Channel 4	0.926	1.083	1.120	0.267	0.023
Channel 5	0.655	0.774	0.793	0.165	0.013
Channel 6	0.278	0.347	0.350	0.062	0.010
Channel 7	0.080	0.100	0.097	0.020	0.009
Channel 8	0.025	0.032	0.032	0.011	0.008
Channel 9	0.018	0.017	0.019	0.009	0.007
Channel 10	0.010	0.011	0.012	0.008	0.007
OPC Readings					
Channel 1	30553	29810	34456	3345	269
Channel 2	943	861	939	443	202
Channel 3	945	899	1073	609	278
Channel 4	705	687	875	577	363
Channel 5	572	569	721	496	331
Channel 6	458	431	551	336	306
Channel 7	336	306	363	265	240
Channel 8	230	243	277	181	175
Channel 9	157	134	190	113	120
Channel 10	144	141	170	124	122
Channel 11	103	101	119	82	91
Channel 12	75	70	90	66	56
Channel 13	68	53	85	54	57
Channel 14	52	47	64	36	47
Channel 15	0	28	0	4	13